Modelling Planar Cell Polarity in *Drosophila melanogaster*

Sabine Schamberg

Thesis submitted to The University of Nottingham
for the degree of Doctor of Philosophy

December 2009

Abstract

During development, polarity is a common feature of many cell types. One example is the polarisation of whole fields of epithelial cells within the plane of the epithelium, a phenomenon called planar cell polarity (PCP). It is widespread in nature and plays important roles in development and physiology. Prominent examples include the epithelial cells of external structures of insects like the fruit fly *Drosophila melanogaster*, polarised tissue morphogenesis in vertebrates and sensory hair cells in the vertebrate ear.

In this work we focus on the wing and the abdomen of *Drosophila*, where PCP becomes obvious in the alignment of hairs and bristles. The underlying dynamics are not fully understood yet, but two distinct protein networks centred around the transmembrane proteins Frizzled and Dachsous, respectively, have been shown to play essential roles. We will present and analyse five models for different aspects of the process of planar cell polarisation. The first two models assess the nature of PCP in a generic setting, ensuring that the results are valid for whole classes of PCP models. Models three and four are existing more complex models that include detailed assumptions about the underlying protein interactions of the Frizzled system in the *Drosophila* wing. Model five considers the Dachsous system in the *Drosophila* abdomen.

We describe the features of the different types of mechanisms and determine the conditions under which they can yield polarity. All five models can establish wild-type polarity for a wide range of parameter values. We find, however, that for model one, three and four an inhomogeneous pattern exists for the same parameter values as the polarised state. Therefore, in these cases either specific initial conditions, which are unlikely in nature, or a global bias are necessary to ensure correct polarisation. Furthermore, we present the effects of clonal clusters of cells on the polarity of the surrounding cells in our models and relate them to the phenotypes observed in experiments. Model one and five show the largest discrepance between the numerical and the experimental results. We discuss the biological relevance of these findings and indicate outstanding questions.

Acknowledgments

First of all I would like to thank my supervisors Markus Owen, Paul Houston and Nick Monk for their enthusiasm. Whenever I needed it they supported me with advice and encouragement. Talking to Peter Lawrence and José Casal from the University of Cambridge, I got the idea for the last chapter. I am grateful for that and the discussions which let me understand the biology a bit more. Thanks must also go to the EPSRC for providing the funding.

Doing a PhD would not have been as enjoyable without the people in the Department of Theoretical Mechanics. They helped me with computer problems, maths or language questions or fed me with sweets and cake.

Finally, my special thanks goes to my friends and family for their support, advice, patience and for always believing in me.

Contents

Appendices

Chapter 1

Introduction

Cell polarity is an important feature of development and critical for many organ functions. A cell is polarised if it is possible to distinguish different ends, e.g. by shape or by an asymmetric protein distribution within the cell. The phenomenon of a whole field of cells that is polarised within a plane is commonly referred to as planar cell polarity (PCP). PCP is involved in a variety of mechanisms in invertebrates as well as vertebrates. It contributes significantly to morphogenetic events in the developing embryo that shape e.g. tissues and organs (reviewed in [58]). Examples in vertebrates are gastrulation, the fundamental reconstruction of the morphology of the early embryo by cell migration, and neurulation, the formation of the neural tube, which later on becomes the central nervous system. Physiologically, PCP is important in adult tissues like the fallopian tubes, the trachea and the cochlea, organising cilia formation and polarised ciliary beating. Skin development and body hair orientation are further processes that require PCP signalling. Therefore, misfunction of the PCP pathway can lead to a wide range of diseases like congenital deafness syndromes, neural tube closure defects, respiratory diseases and polycystic kidneys (reviewed in [42]).

PCP falls at the interface between cellular and tissue level biology, giving a general framework for how the behaviour of individual cells is modified to achieve large scale organisation. It is fascinating how individual cells hundreds of cell diameters apart acquire the same polarity within a plane or how whole groups of cells establish a uniform polarisation during their intercalation.

In this chapter we present a history of the study of PCP, followed by a discussion about the proteins involved and their assumed interactions. Finally, we present existing models and an outline of this thesis.

1.1 History of research on planar cell polarity

The study of planar cell polarity started in the 1960s with work in insects like the milkweed bug (e.g. [25]). In those days the process was referred to as tissue polarity. About 25 years ago, the topic saw a rapid expansion because of genetic studies in the fruit fly *Drosophila melanogaster*. All external adult structures of the fruit fly show PCP features and they are especially obvious in the wings, the abdomen and the eyes as shown in Figure 1.1. In the wings, each of the approximately 30 000 cells orients itself along the axis from the hinge to the tip, elaborating a hair that points distally, i.e. towards the wing tip. The abdomen shows alignment of bristles and hairs with respect to the anterior-posterior (head to tail) axis, pointing towards the rear end. In the eye, PCP occurs as the regular arrangement of over 700 cell clusters, so called ommatidia, with respect to the two perpendicular axes, anterior-posterior and dorsal-ventral. The orientation of the hairs on the wings and the abdomen only requires the organisation of single cells, whereas the bristle formation and the ommatidia arrangement are based on the organisation of whole clusters of cells. Therefore, although it is believed that the same set of genes regulates PCP, every outcome seems to require a totally different response from the cells.

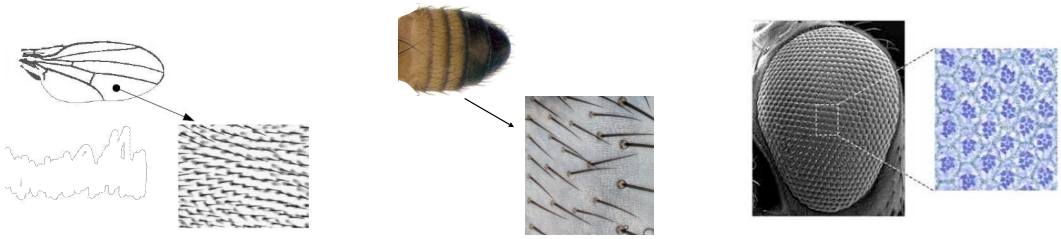

(a) (b) (c)

Figure 1.1: PCP features of the fruit fly *Drosophila melanogaster*; (a) Hairs on the wing, image from [48]; (b) bristles and hairs on the abdomen, image from [27]; (c) organisation of the ommatidia in the eye, image from http://cdbg.shef.ac.uk/research/strutt.

The study of PCP is now extended to many other organisms. Starting in *Xenopus* and zebrafish, PCP-related processes have been found to play a role in morphogenesis in vertebrates. The mammalian skin and inner ear are further examples of tissues with PCP features. Work by Guo *et al.* [15] has revealed that hair pattern defects in mice mutant for a key gene are very much reminiscent of hair pattern defects in flies mutant for the corresponding gene. This is an exciting finding, since it suggests that similar mechanisms are driving PCP in different organisms. In addition, it reinforces the use of *Drosophila* as a model organism for PCP studies. This choice has mostly practical reasons: First, many

PCP genes have several isoforms in vertebrates but only one in *Drosophila*. Hence, multiple knockouts are not needed as often. Tissues that typically display PCP features in *Drosophila* are external and therefore easy to access. In vertebrates, PCP mostly occurs during the development of the embryo, which is more difficult to analyse. In flies, many PCP mutations still produce viable animals, whereas corresponding mutations in mice are lethal. Finally, fruit flies are a popular laboratory animal in general, since they have a short life cycle (10-14 days) and it is easy and cheap to keep large numbers. Thus, most experimental data on PCP is available for *Drosophila*, which is why our theoretical studies will also focus on the fruit fly, in particular the wings and the abdomen. In the next section we give details of what is currently known about the mechanisms driving PCP in *Drosophila*.

1.2 Biological background

It is widely considered that there is a three-tiered mechanism controlling the generation of PCP in *Drosophila*. The first tier operates over the whole tissue and provides directional cues. The second tier interprets the directional signal and propagates it via a feedback loop. The third tier reads the information to shape the structure [48]. Little is known about the first and the third tier, apart from the third tier being tissue specific since it produces totally different outcomes in the different tissues. The second tier however is usually assumed to be common to all tissues.

PCP is based on the interactions of several proteins. A protein is a linear chain of amino acids that are arranged according to the sequence of the corresponding gene. For clarity, protein names are capitalised while gene names are non-capitalised and in italics. There are two systems of proteins that play key roles in the establishment of PCP. One protein group is centred around the transmembrane protein Frizzled (Fz). The other one consists of the transmembrane proteins Dachsous (Ds) and Fat (Ft) and the cytoplasmic protein Four-Jointed (Fj). The interactions and the relationship of these two protein networks are still unknown. There have been two proposals (reviewed in [4]). The first one is that the Ds system provides the directional cues for the Fz system, i.e., the Ds system acts in the first tier and the Fz system in the second tier [48]. A more recent approach claims that the two systems work in parallel in the second tier, both amplifying a global cue to establish PCP [7]. What provides the global cue however is still unknown. In this work we will follow the second approach and present models for the Fz system as well as the Ds system assuming they amplify an initial global cue.

Fz system

The proteins included in the Fz system are Dishevelled (Dsh), Van Gogh (Vang; also known as Strabismus), Prickle (Pk), Flamingo (Fmi; also known as Starry Night) and Diego (Dgo). Some of these protein names are derived from the appearance of the respective loss-of-function phenotypes, which display irregular hair orientations. Fz, Fmi and Vang are transmembrane proteins whereas Dsh, Pk and Dgo are cytoplasmic proteins. Loss of any of these leads to disruption of the polarisation. The properties presented here are mostly based on experimental findings in the wing. However, these proteins operate in all tissues in *Drosophila* in which PCP has been studied. Therefore, they are often referred to as core proteins.

It is known that during the first 18 h after puparium formation (APF) the proteins Fmi, Fz and Vang localise symmetrically in the membrane and that Dsh, Pk and Dgo are recruited from the cell interior to the membrane. Between 18 h APF and 32 h APF they become distributed asymmetrically [44]. Dsh, Fz and Dgo end up at the distal edge of the cell, Vang and Pk at the proximal edge and Fmi at both the proximal and the distal edge, but not anterior and posterior as shown in Figure 1.2. The localisation of these proteins is restricted to a circumferential ring in the apical (top) region of a cell [44]. Therefore, Figure 1.2 shows a two-dimensional view of the cells.

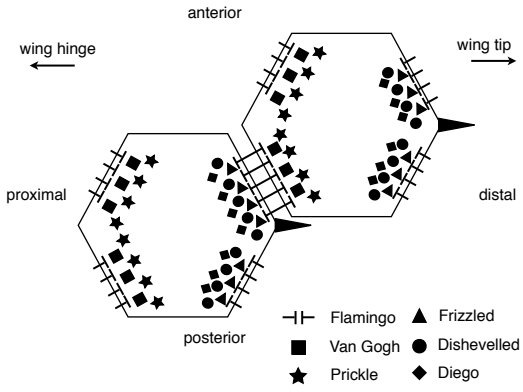

Figure 1.2: Localisation of the PCP core proteins at the cell edges and illustration of the hairs, which grow at the most distal tip of each cell.

The presented time course divides the second tier into two steps. For the first step ($0 - 18$ h APF) the presence of Fmi, Fz and Vang is necessary while Dsh, Pk and Dgo are irrelevant. Those last three proteins become important for the second step ($18 - 32$ h APF) [5]. The precise molecular interactions between the six proteins are still mostly unknown. The general idea is that polarisation is initiated by the directional cues from the first tier and amplified and stabilised by intercellular signalling. We know that Fz, Vang and Fmi are

necessary and sufficient for such intercellular communication [45]. Dsh, Pk and Dgo are most likely to propagate polarity by establishing intracellular asymmetries of proteins. In wing tissue lacking Pk there is no detectable asymmetry of Fz. Nonetheless, polarity becomes established and the hairs grow at the right time and the right position. It seems likely that protein asymmetry is not essential to PCP locally but increases the robustness of the coordination of polarity over longer ranges [45].

Usui *et al.* [50] found out that Fmi only accumulates at the membrane of two neighbouring cells if it is present in both. This suggests that Fmi forms homodimers bridging between adjacent cell membranes. So far, it is unclear whether those bridges act actively to amplify polarity or are more passive, e.g. supporting the binding of Fz and Vang (reviewed in [56]). Chen *et al.* [9] and Lawrence *et al.* [26] support the first theory by concluding that Fmi homodimers transfer information between the two cells they bridge. Wu and Mlodzik [55] as well as Strutt and Strutt [47] however find that Vang and Fz can bind directly across the membrane and suggest that the function of Fmi is to enhance this binding.

Pk, acting in complexes with Vang, ensures the asymmetric localisation of the core proteins [5]. This might be due to Pk inhibiting the recruitment of Dsh to the membrane [49]. Dgo counteracts this effect of Pk on Dsh, maybe by a direct competition of Dgo and Pk for Dsh binding [17].

To study PCP experimentally, clonal clusters in which a certain gene is either knocked out or overexpressed are induced in the tissue. The behaviour of the wild-type (not mutated) tissue around a clone gives insight into the interplay of the genes involved in the process. To verify a model it is therefore valuable to compare the results not only with the wild type but also with the results for clones. Figure 1.3 shows the experimental results for clones mutant for some PCP genes. Close to the clonal borders, fz^- and $vang^-$ clones influence the direction of the hairs in some cells outside the clone. This phenomenon is called domineering non-autonomy. The direction of the hairs in wild-type cells distal to a fz^- clone is disrupted while a $vang^-$ clone changes the direction of the hairs in the wild-type cells on its proximal side. The effects of a fmi^- clone and a dsh^- clone are restricted to the regions within the clones and for the case of a pk^- clone there is almost no disruption detectable. These results support the assumption that Fz and Vang are involved in mediating an intercellular signal while Dsh and Pk act cell-autonomously, stabilising polarity within a cell. Considering overexpression of a certain gene in a clonal cluster, we can divide the five genes into two groups. Overexpression of fz or dsh in a clone reorients the hairs in the wild-type cells proximal to the clone. A clone overexpressing $vang$, fmi or pk changes the hair direction on its distal side [29, 49, 50]. Thus, a clone overexpressing fmi, dsh or pk shows domineering non-autonomy, while a clone lacking one of these genes

does not effect the surrounding tissue.

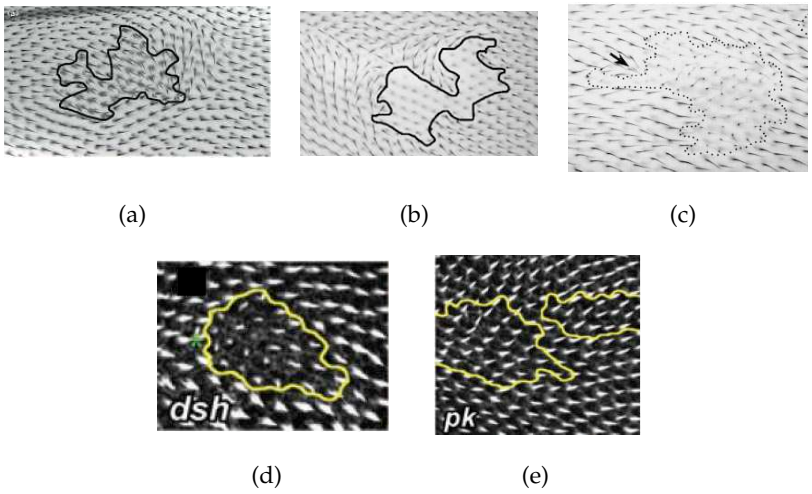

Figure 1.3: Results for knockout clones, proximal (wing hinge) is to the left, distal (wing tip) to the right; (a) Only the cells distal to the fz^- clone are affected, figure from [1]; (b) the $vang^-$ clone reorients the cells on its proximal and lateral sides, figure from [58]; (c) no disruption around the fmi^- clone can be detected apart from one cell with multiple hairs, indicated by the arrow, figure from [50]; (d) for the dsh^- clone disruptions are only detectable within the clone, figure from [3]; (e) for the pk^- clone we see almost no disruption, figure from [3].

Ds system

The adult abdomen of *Drosophila* is divided into several sections of which each comprises an anterior (A) and a posterior (P) compartment. The Ds system which includes Ds, Ft and Fj, has mostly been studied in the A compartment. Here, *fj* expression as well as Fj activity form a gradient that decreases from anterior to posterior, while *ds* expression and Ds activity occur as gradients that increase along the same axis. Ft activity is graded in the same way as Fj activity, decreasing from anterior to posterior. It is suggested that Fj influences the interactions of Ds and Ft through repression of Ds and promotion of Ft. Furthermore, there is evidence that Ds and Ft form trans-heterodimers, bridging between cells, and that Ds concentrates on edges adjacent to cells containing only Ft, while Ft concentrates on edges adjacent to cells containing only Ds [30, 46].

Hairs in the wild-type cells anterior to a ds^- clone point anterior, i.e. the wrong way. A clone overexpressing *ds* disrupts polarity behind the clone. Clones with abnormal levels of fj and ft give similar results but with opposite sign. Hence, ft^--clones and fj^--clones disrupt polarity behind the clone and ft^+-clones and fj^+-clones in front of the clone. The

amplitude of the repolarising signal from a clone seems to depend on the degree of discrepancy between Ft and Ds levels in the clone and the surrounding cells. E.g., a large difference in active Ft levels between the clone and the surrounding tissue would give a long-range effect, as observed in a ft^+ clone in a fj^- background, in which Ft activity is low, because there is not much Fj to activate Ft [7].
A further analysis of the gradients has revealed that in the *Drosophila* eye replacing either the Fj or the Ds gradient by ubiquitous expression has only a small effect on polarity, i.e. on average more than 92% of the ommatidia are correctly oriented. Replacement of both gradients with ubiquitous expression results in the complete loss of organised PCP. Reversing the direction of one of the two gradients reverses polarity [40].

1.3 Review of existing models

During the last few years several models studying aspects of the second tier of the PCP pathway have been developed. As mentioned above, direct interactions between adjacent cells are assumed to be an important feature of PCP. Therefore, we first review models which focus on intercellular signalling regardless of the biological context in which it occurs. Omitting the biological details keeps these approaches analytically tractable and widely applicable. They are based on the assumption that the signalling activity of one cell is responsive to signals received from neighbouring cells. It has been shown that these models exhibit patterning instabilities.

Models for juxtacrine intercellular signalling

A key approach has been established by Collier *et al.* [10]. They assume a cell is a point that is characterised by two parameters: the level of Notch activation, N, and the level of Delta activation, D. For the purpose of this model, the details of the biochemistry are not important. Hence, N and D can be interpreted in different ways, e.g. as the amount N of activated Notch protein and the amount D of activated Delta protein; or N could represent the quantity of Notch-Delta complexes, while D denotes the amount of the activated Delta protein. The model is based on five postulates: Cells interact only with cells right beside them; the production of N is activated by the level of D in the neighbouring cell; the production of D is inhibited by the level of N in the same cell; the production of N and D is balanced by decay; and the level of N determines the cell's fate. These yield two differential equations for each cell. Stability analysis and numerical simulations are applied to one and two-dimensional arrays of cells. The main result is that cells with a low level of Notch

activation are surrounded by cells with a high level. Hence, two neighbouring cells with low levels of Notch activation do not occur. This result matches the observations of similar patterns in early animal development.
In contrary to this idea of lateral inhibition, Owen *et al.* [35] showed that the opposite phenomenon, lateral induction, also leads to spatial patterns. They expressed their model in terms of the numbers of ligand molecules, free receptors and receptor-ligand complexes. Thus, one gets three differential equations including decay, association, dissociation and internalisation of the molecules and complexes, as well as the activating effect of the complexes on both ligand and receptor production. Again, the equations have been analysed and simulated and as a result patterns of different wavelengths occurred.
In [53], Webb and Owen extended this model to include induction and inhibition of ligand and receptor production. However, one of the main results is that lateral inhibition in ligand production can generate longer range patterns, whereas, the combination of lateral induction in ligand production and inhibition of receptor synthesis does not give rise to any patterning.
Until this point only homogeneous distributions of the involved proteins and receptors had been considered. In the following paper [54], Webb and Owen included inhomogeneous distributions and found out that in this case, intra-membrane ligand-diffusion is crucial for the generation of long wavelength patterns. Furthermore, they have studied the influence of different combinations of biased ligand and receptor production. An important discovery was that opposite bias for ligand and receptor can lead to regular polarity across a lattice, which is analogous to PCP in the *Drosophila* wing.

Models for the Fz system

The models presented in this section describe possible mechanisms for the interactions of the proteins of the Fz system.
One approach for polarity in the *Drosophila* wing was established by Amonlirdviman *et al.* ([3, 37]) based on an earlier idea in [49]; they assume there is a sustained global biasing signal that leads to higher Fz activity on the distal side of each cell. This asymmetry is amplified by a feedback loop specified by the four proteins Fz, Dsh, Pk and Vang and their interactions via binding to form complexes. The chemical reaction equations of these interactions yield ten reaction-diffusion equations for each cell which are subsequently solved numerically for a field of hexagonal cells. This work does not include a stability analysis or an investigation of the relative importance of the feedback loop and the permanent global bias for the establishment of PCP. Therefore, in Chapter 4 we will conduct a detailed anal-

ysis, focusing on these issues.

A different group of models considers a global initial gradient that is amplified. The one-dimensional averaging model for the *Drosophila* abdomen by Lawrence *et al.* [26] assumes a decreasing Fz activity gradient that is persistent during the whole process. Using Fmi, each cell compares its Fz value with its two neighbours and polarises toward the neighbour with the lowest Fz value. The Fz value of each cell is determined by two components, the average Fz value of the present cell and its two neighbours plus a contribution from the persistent gradient. Varying the ratio of these two components they analysed the behaviour for fz mutant and fz overexpression clones. If the influence of the averaging part dominates slightly over the influence of the persistent gradient they get the same range of domineering non-autonomy as seen in experiments.

An alternative idea has been presented by Le Garrec *et al.* [29], who developed a model for the polarisation in the *Drosophila* wing, which they later applied to the *Drosophila* eye [28]. They assume a global initial ligand gradient that leads to a gradient of active Fz which decreases from the proximal to distal end of the wing. The complexes forming in each cell are called Prox, consisting of Fmi, Vang and Pk, and Dist, containing Fmi, Fz and Dsh. Complexes facing each other in adjacent cells bind together through cell membranes by interaction between the two Fmi molecules. Thereby, only the formation of Prox-Dist is considered, because the authors assume it is more likely than Dist-Dist or Prox-Prox since the respective binding factors react more readily when joining distinct complexes. Another factor driving polarisation is Dist inhibiting the formation of Prox on its side of the cell. In [29] they conducted stochastic simulations for a field of roughly hexagonal cells. We will discuss this model in detail in Chapter 5.

Based on a similar idea Klein and Mlodzik proposed a model for the *Drosophila* wing [23]. They assume that an unspecified initial signal establishes a Fz activity gradient that decreases from the proximal to the distal side of the cell region. Then, two complexes form, which are A, containing Fmi, Fz and Dgo, and B, containing Fmi, Vang and Pk. During polarisation A and B stabilise each other across the cell membrane. This is due to interactions between the two Fmi proteins. Furthermore, complex A inhibits the formation of complex A across the cell membrane and B the formation of B. Within a cell each complex recruits itself but inhibits others. The authors present final distributions of the protein complexes for different initial conditions, but it is not mentioned how they are obtained. Although, at first glance, this model seems to be the same as the model by Le Garrec *at al.*, the interactions of the two protein complexes are slightly different.

1.4 Thesis outline

As mentioned before, we do not know the full biological details of the interactions in Tier two or the way in which Tier two depends on Tier one. The models described above test only specific assumptions about the nature of the interactions of the Fz system. All these models impose polarity on the system right from the start, either by including differences in the behaviour of PCP complexes at adjacent cell sides or via a global initial gradient. Focusing on the approaches by Amonlirdviman *et al.* [3] and Le Garrec *et al.* [29] we realise that they are the same type of model. In both cases the total amount of each protein in a cell is conserved. Polarity is established by a feedback loop coupled with a persistent global polarisation bias. Although the number of proteins involved, the assumed specific protein interactions forming the feedback loop and the type of global bias differ between the two models, both can reproduce wild-type polarity and the behaviour around clones. The relative importance of the different features of the models for ensuring these results was not analysed in the papers. Therefore, our aim is to investigate this question. We are interested in the generic features of such a conservative approach and whether other types of models can also establish planar cell polarity. Considering the details of the models by Amonlirdviman *et al.* and Le Garrec *et al.*, the aim is to map out the differences between the two feedback loops and to find out whether a global bias is necessary to yield PCP. In addition, we are also interested in the Ds system and its potential to establish PCP without the Fz system, an issue that has not been investigated mathematically so far.

In this thesis we address these questions in the following way. In Chapters 2 and 3 we present two models that aim to assess the nature of PCP in a generic setting - omitting details about the protein interactions and therefore encompassing a broad class of specific models. From our understanding of the biology we draw the conclusion that the basics of planar cell polarity are an initial global cue which is amplified by a feedback loop and intracellular diffusion. Initially, we will assume that every cell has a small imbalance or that the cell at the proximal end of the region is completely polarised. Unlike for an initial gradient, assuming our initial conditions the system can either polarise or adopt a state in which every cell is unpolarised. The first approach in Chapter 2 is the feedback and diffusion model, in which a negative feedback loop couples adjacent cell sides of neighbouring cells and the diffusion acts within a cell. The second approach in Chapter 3 is the conservative model. In this case we assume that movement within a cell depends on its neighbouring cells; this is also coupled with intracellular diffusion. The results of Chapter 2 and 3 are also included in [38].

As a next step we investigate whether the models developed by Amonlirdviman *et al.* and

Le Garrec *et al.* can give polarity from a temporary initial imbalance in every cell. In both cases we start by reducing the model to one spatial dimension and subsequently verifying our results in two spatial dimensions applying the finite element method. As mentioned in Section 1.2 the localisation of the PCP core proteins is restricted to a plane. Therefore, we do not consider three spatial dimensions. The analysis of the model by Amonlirdviman *et al.* is given in Chapter 4, while Chapter 5 contains the analysis of the model by Le Garrec *et al.*.

In Chapter 6 we cover the Ds system. We present a model for a possible mechanism based on the ideas by Casal *et al.* [7] and compare the results to experimental observations.

We conclude in Chapter 7 with a discussion of the results of the different chapters and their implications for the understanding of the biological system.

Chapter 2

Feedback and diffusion model

The model presented in this chapter is based on a positive feedback loop which couples adjacent cell sides of neighbouring cells, and diffusion that acts within a cell. We think that these two features are the essentials of the mechanism underlying the origin of planar cell polarity. In contrast to the existing models which are conservative, for the feedback and diffusion model we have chosen a non-conservative approach including regulated production and degradation of proteins. This yields a new class of PCP mechanisms and the aim is to find their generic features. To this end, and to make the mathematical analysis practicable, we have neglected biological details. Our main targets are to investigate the dependence of PCP emergence on the relative strength of the feedback and diffusion; analyse the model's potential to overcome anomalies in the initial conditions; and investigate the effects of induced clones – groups of cells that have a different amount of protein or a different strength of feedback than the rest of the cells. The focus is on modelling the behaviour of a field of cells, omitting the detailed intracellular processes; therefore, instead of treating the inside of the cell as a continuum we have chosen a discrete approach.

2.1 Analysis in one spatial dimension

We consider first a one-dimensional line of cells each having two sides, with r_j and l_j representing generic PCP activities on the right and left side of cell j, respectively. These activities can be regarded as accumulations or active states of certain PCP proteins. However, our aim is a generic analysis and therefore we continue to use the unspecific term. We assume that the activities on adjacent faces of neighbouring cells inhibit each other by juxtacrine intercellular signalling and that these interactions are described by the following system of equations:

$$\frac{\mathrm{d}l_j}{\mathrm{d}t} = -\delta l_j + F(r_{j-1}) + \frac{D}{\Delta x^2}(r_j - l_j),$$
$$\frac{\mathrm{d}r_j}{\mathrm{d}t} = -\delta r_j + F(l_{j+1}) + \frac{D}{\Delta x^2}(l_j - r_j),$$

where F is a decreasing positive function representing inhibition, with $F(0)$ finite and positive. The coefficient $\delta > 0$ represents the decay rate, Δx the spatial extension from left to right of a cell and D measures the rate of intracellular diffusion of PCP activity. This is summarised in Figure 2.1(a).

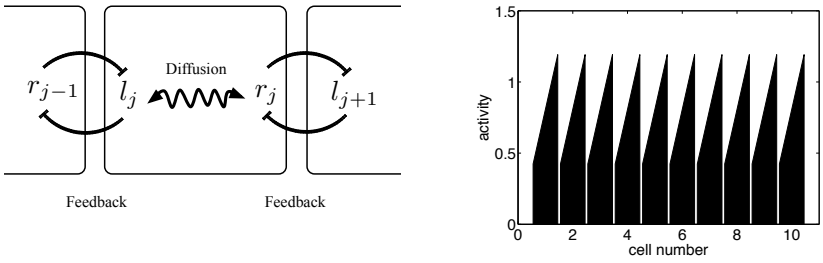

(a) (b)

Figure 2.1: Illustration of the feedback and diffusion model; (a) Mechanism of the feedback and diffusion model; (b) illustration of a homogeneous polarised steady state, each trapezium represents one cell, the two top vertices denote the values on the right and the left side of the cell, respectively.

The rescaling $\tau = \delta t$ gives the dimensionless system

$$\begin{aligned}\frac{\mathrm{d}l_j}{\mathrm{d}\tau} &= -l_j + f(r_{j-1}) + d(r_j - l_j),\\ \frac{\mathrm{d}r_j}{\mathrm{d}\tau} &= -r_j + f(l_{j+1}) + d(l_j - r_j),\end{aligned} \tag{2.1}$$

with $d = \frac{D}{\delta \Delta x^2}$, hence $d \geq 0$. In the following, we investigate the existence and stability of steady states in this model for a general positive decreasing function f. For the purpose of illustrative numerical examples, we use specific inhibition functions $f(x) = ce^{-x^2}$ or $f(x) = \frac{\alpha}{1+qx^k}$ with positive c, α, q and k, as representatives of typical families of inhibition functions.

Assuming that t corresponds to the time in experiments, its relationship to the time τ in our analysis and simulations is given by the the rescaling $\tau = \delta t$. According to [44] the polarisation of core proteins in cells of the pupal wing in *Drosophila* takes about 32 hours: 18 hours to recruit all the core proteins to the membrane and another 14 hours for

the proteins to polarise within the membrane. To achieve a time scale in our simulations that is comparable to 32 hours, we have to assume a decay rate of $\delta = \frac{1}{15}\,\mathrm{min}^{-1}$. This is relatively slow but still in a reasonable range [6].

Equation (2.1) encodes a system in which the feedback loop gives the potential for steady state patterns, such that at the interface between cells we have low activity on one cell side next to high activity in the adjacent side of the neighbouring cell; diffusion couples l_i and r_i within each cell. Our objective is to investigate this interplay quantitatively.

We refer to the case when all cells are the same at steady state, i.e., $l_j = L$ and $r_j = R$ for all j, as a homogeneous steady state of the system (2.1). If $L = R$ we call it a homogeneous unpolarised steady state and if $L \neq R$ a homogeneous polarised steady state. Figure 2.1(b) shows an illustration of a homogeneous polarised steady state.

In the following we conduct an analysis that allows us to map out existence and stability of unpolarised, polarised and spatially periodic steady state solutions of system (2.1). It is the second of these that is of particular interest in the context of planar cell polarity. For this analysis we assume that we have an infinite row of cells.

2.1.1 Existence of steady states

System (2.1) always has a unique homogeneous unpolarised steady state, $U = l_j = r_j$ for all j, because in this case the corresponding steady state equations reduce to $U = f(U)$ which has a unique solution since f is decreasing. Homogeneous polarised steady states (L, R) of (2.1) are given by solutions of

$$L = \frac{f(R) + dR}{1 + d}, \quad R = \frac{f(L) + dL}{1 + d}. \tag{2.2}$$

Setting $g(x) := \frac{f(x)+dx}{1+d}$, such steady states correspond to solutions of

$$x = g(g(x)). \tag{2.3}$$

We see that $g(0)$ is finite and positive, $g(U) = U$ and $g'(U) = \frac{f'(U)+d}{1+d} < 1$, since f is decreasing. Furthermore, $g(g(0))$ is finite and positive. Equation (2.3) has always at least one solution, which is U. If $g(g(U))' > 1$ there exist an additional pair (L, R) of solutions of (2.3). This condition can be reformulated as $g(g(U))' = g'(g(U)) \cdot g'(U) = g'(U) \cdot g'(U) > 1$, which is equivalent to $g'(U) < -1$, since $g'(U) < 1$. Furthermore, $g(L) = R$, $g(g(L)) = L$ and $g(g(L))' < 1$, which can be reformulated as $g'(g(L)) \cdot g'(L) = g'(R) \cdot g'(L) < 1$.

In summary, system (2.1) has a pair of homogeneous polarised steady states (L, R) if $g'(U) < -1$, i.e., $\frac{f'(U)+d}{1+d} < -1$. This implies $d < -\frac{f'(U)+1}{2}$. Since $d \geq 0$, this leads to the condition $f'(U) < -1$, which is necessary but not sufficient. Furthermore, $g'(R)g'(L) =$

$\left(\frac{f'(R)+d}{1+d}\right)\left(\frac{f'(L)+d}{1+d}\right) < 1$ holds, a condition we will need in the subsequent stability analysis.

Examples of graphs of (2.2) for systems with homogeneous polarised steady states are shown in Figure 2.2.

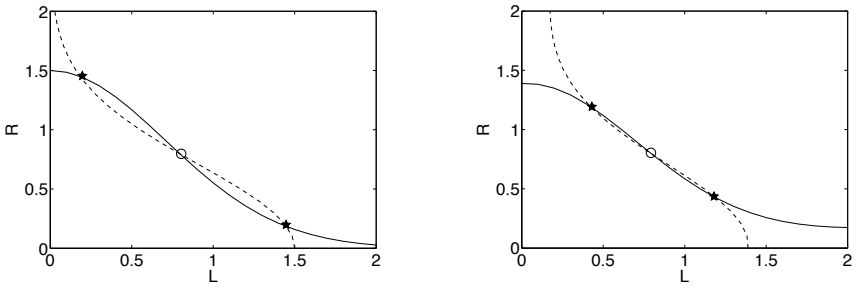

(a) (b)

Figure 2.2: Graphs of (2.2) for homogeneous steady states of (2.1) with $f(x) = 1.5e^{-x^2}$ and different choices of d; (a) $d = 0$; (b) $d = 0.08$. The solid lines are the graphs for the equation for R and the dashed lines the graphs for the equation for L, the homogeneous polarised steady states are indicated by stars, and the homogeneous unpolarised steady state by a circle.

We next investigate the existence of an unpolarised period two pattern, i.e., $l_j = r_j = V$ for j even and $l_j = r_j = W$ for j odd. Since $l_j = r_j$ for all j, this pattern is independent of intracellular diffusion and system (2.1) reduces to

$$\frac{\mathrm{d}W}{\mathrm{d}\tau} = -W + f(V),$$
$$\frac{\mathrm{d}V}{\mathrm{d}\tau} = -V + f(W),$$

which is essentially the same as the lateral inhibition system analysed in [10]. Similar to above, the period two pattern exists if $f'(U) < -1$ at the homogeneous unpolarised steady state U of (2.1) and $f'(V)f'(W) < 1$ whenever the period two pattern exists. We need the latter condition for the stability analysis.

2.1.2 Stability analysis

In this section we analyse the stability of the steady states of system (2.1) identified above to homogeneous and inhomogeneous perturbations. We start by linearising the system about a homogeneous steady state (L, R). Thus, with $l_j = L + \widetilde{l}_j$ and $r_j = R + \widetilde{r}_j$, neglecting

terms higher than first order, we get

$$\frac{\mathrm{d}\widetilde{l}_j}{\mathrm{d}\tau} = -\widetilde{l}_j + f'(R)\widetilde{r}_{j-1} + d(\widetilde{r}_j - \widetilde{l}_j),$$
$$\frac{\mathrm{d}\widetilde{r}_j}{\mathrm{d}\tau} = -\widetilde{r}_j + f'(L)\widetilde{l}_{j+1} + d(\widetilde{l}_j - \widetilde{r}_j),$$

where j indicates the cell number. Suppose the solutions of the above system are of the form $\widetilde{l}_j = L_0 e^{ikj+\lambda\tau}$ and $\widetilde{r}_j = R_0 e^{ikj+\lambda\tau}$, respectively, with $\lambda, k \in \mathbb{R}$ and where λ is the growth rate of perturbations with wave number k. Substituting into the linearised equations, dividing by $e^{ikj+\lambda\tau}$ yields

$$\begin{aligned} \lambda L_0 &= -L_0 + f'(R)R_0 e^{-ik} + d(R_0 - L_0), \\ \lambda R_0 &= -R_0 + f'(L)L_0 e^{ik} + d(L_0 - R_0). \end{aligned} \tag{2.4}$$

Nontrivial solutions of system (2.4) for (L_0, R_0) require

$$0 = \det\left[\begin{pmatrix} -1-d & f'(R)e^{-ik}+d \\ f'(L)e^{ik}+d & -1-d \end{pmatrix} - \lambda I\right] = \det(A - \lambda I). \tag{2.5}$$

If $\mathrm{Re}\lambda < 0$ for both solutions of (2.5), the homogeneous steady state is stable. Equivalently, for stability $\mathrm{tr}(A) < 0$ and $\det(A) > 0$ have to hold. The first condition ($\mathrm{tr}(A) < 0$) is always fulfilled. To investigate the second one, we consider the case where the homogeneous steady state is both stable to homogeneous perturbations (i.e., for $k = 0$) and unstable to inhomogeneous perturbations (i.e., for at least one $k \neq 0$). For this type of analysis it is important to ensure that the domain is large enough with respect to the admissible values of k. Here, we consider an infinite row of cells, as mentioned above.

Homogeneous unpolarised steady state

First we consider a homogeneous unpolarised steady state, $L = R = U$. Furthermore, assume $k = 0$, i.e., a homogeneous perturbation. Then, we get $\det(A) = 1 + 2d(1 - f'(U)) - f'(U)^2$, which is greater than 0 if $d > -\frac{f'(U)+1}{2}$ since $f'(U) < 0$. Hence, the homogeneous unpolarised steady state is stable to homogeneous perturbations if, relative to the feedback, the diffusion is strong enough.

Now consider $k \neq 0$. For the determinant we get $\det(A) = 1 + 2(1 - f'(U)\cos k)d - f'(U)^2$. If $d = 0$ the homogeneous steady state is unstable for all $k \neq 0$ if $f'(U) < -1$. If $d > 0$, it is unstable if

$$\cos k < -\frac{f'(U)^2 - 1 - 2d}{2df'(U)}, \quad \text{for some } k \neq 0.$$

Therefore, since $\cos k \geq -1$ for all k, the coefficient d has to satisfy

$$-1 < -\frac{f'(U)^2 - 1 - 2d}{2df'(U)}.$$

Since $f'(U) < 0$ and $d > 0$ we get

$$2d(f'(U) + 1) < f'(U)^2 - 1 = (f'(U) + 1)(f'(U) - 1).$$

Thus,

$$2d < f'(U) - 1, \text{ if } f'(U) > -1 \tag{2.6}$$

and

$$2d > f'(U) - 1, \text{ if } f'(U) < -1. \tag{2.7}$$

We see that equation (2.6) implies $d < 0$, which contradicts our assumptions, whereas (2.7) holds for all d. Hence, for $f'(U) < -1$ the homogeneous unpolarised steady state is unstable to inhomogeneous perturbations for any value of d.
Combining the results for $k = 0$ and $k \neq 0$ we conclude that if $f'(U) < -1$ and $d > -\frac{f'(U)+1}{2}$ hold, system (2.1) exhibits spatial instabilities. Since Reλ is maximal if det(A) is minimal and det(A) is minimal at $k = \pi$, the fastest growing mode is $k = \pi$. Hence, we expect to observe patterns of period two.

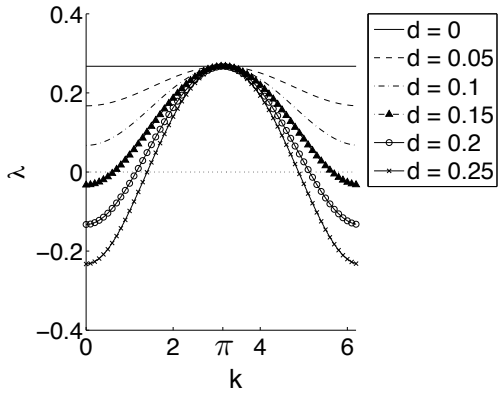

Figure 2.3: Dispersion relation for the homogeneous unpolarised steady state of (2.1) ($f(x) = 1.5e^{-x^2}$, different values of d); $d < 0.1336$, the homogeneous unpolarised steady state is unstable to homogeneous perturbations, the polarised steady state arises; $d > 0.1336$, the homogeneous unpolarised steady state is stable to homogeneous perturbations and unstable to inhomogeneous perturbations, we get period two patterns.

To clarify these results, Figure 2.3 shows the dispersion relation $\lambda(k)$ of the largest eigenvalue λ of system (2.1) for the inhibition function $f(x) = 1.5e^{-x^2}$ and different values of d.

In this case $f'(U) = -1.2672$ for the homogeneous unpolarised steady state U and therefore for all $d > 0.1336$ the system is stable to homogeneous perturbations and unstable to inhomogeneous perturbations.

Homogeneous polarised steady state

As a next step we investigate the case $L \neq R$. The corresponding matrix is

$$A = \begin{pmatrix} -1-d & f'(R)e^{-ik}+d \\ f'(L)e^{ik}+d & -1-d \end{pmatrix}$$

and its determinant is given by

$$\det(A) = 1 + 2d - f'(L)f'(R) - (f'(L)e^{ik} + f'(R)e^{-ik})d.$$

Hence, for $k = 0$ a polarised steady state of system (2.1) is stable if $d > \frac{f'(L)f'(R)-1}{2-(f'(L)+f'(R))}$. This is true for all $d \geq 0$, because f is decreasing and $f'(L)f'(R) < 1$ at a polarised steady state (see Section 2.1.1). The system is unstable for at least one $k \neq 0$ if $d < \frac{f'(L)f'(R)-1}{2-(f'(L)e^{ik}+f'(R)e^{-ik})} < 0$. This would be a contradiction since we chose $d \geq 0$. Thus, if homogeneous polarised steady states exist they are always stable to homogeneous and inhomogeneous perturbations.

Period two patterns

We continue by analysing the stability of period two patterns. We take every two cells together and label their sides with l_j, mr_j, ml_j, and r_j (derived from "left", "middle right", "middle left" and "right" side, respectively). We linearise about a steady state (V, W) using $l_j = V + \widetilde{l}_j, mr_j = V + \widetilde{mr}_j, ml_j = W + \widetilde{ml}_j$ and $r_j = W + \widetilde{r}_j$. Omitting terms of higher orders than one, this yields

$$\begin{aligned}
\frac{\mathrm{d}\widetilde{l}_j}{\mathrm{d}\tau} &= -\widetilde{l}_j + f'(W)\widetilde{r}_{j-1} + d(\widetilde{mr}_j - \widetilde{l}_j), \\
\frac{\mathrm{d}\widetilde{mr}_j}{\mathrm{d}\tau} &= -\widetilde{mr}_j + f'(W)\widetilde{ml}_j + d(\widetilde{l}_j - \widetilde{mr}_j), \\
\frac{\mathrm{d}\widetilde{ml}_j}{\mathrm{d}\tau} &= -\widetilde{ml}_j + f'(V)\widetilde{mr}_j + d(\widetilde{r}_j - \widetilde{ml}_j), \\
\frac{\mathrm{d}\widetilde{r}_j}{\mathrm{d}\tau} &= -\widetilde{r}_j + f'(V)\widetilde{l}_{j+1} + d(\widetilde{ml}_j - \widetilde{r}_j).
\end{aligned}$$

Now suppose $(\widetilde{l}_j, \widetilde{mr}_j, \widetilde{ml}_j, \widetilde{r}_j) = (A_0, B_0, C_0, D_0)e^{ikj+\lambda\tau}$, with $A_0, B_0, C_0, D_0, \lambda, k \in \mathbb{R}$. Therefore, we get

$$\begin{aligned}
\lambda A_0 &= -A_0 + f'(W)D_0e^{-ik} + d(B_0 - A_0),\\
\lambda B_0 &= -B_0 + f'(W)C_0 + d(A_0 - B_0),\\
\lambda C_0 &= -C_0 + f'(V)B_0 + d(D_0 - C_0),\\
\lambda D_0 &= -D_0 + f'(V)A_0e^{ik} + d(C_0 - D_0).
\end{aligned}$$

Hence, λ are eigenvalues of the matrix

$$\begin{pmatrix}
-1-d & d & 0 & f'(W)e^{-ik}\\
d & -1-d & f'(W) & 0\\
0 & f'(V) & -1-d & d\\
f'(V)e^{ik} & 0 & d & -1-d
\end{pmatrix}.$$

Let $k = 0$, i.e., assume a period two perturbation. The eigenvalues in this case are

$$\begin{aligned}
\lambda_1 &= -1 + \sqrt{f'(V)f'(W)},\\
\lambda_2 &= -1 - \sqrt{f'(V)f'(W)},\\
\lambda_3 &= -2d - 1 + \sqrt{f'(V)f'(W)},\\
\lambda_4 &= -2d - 1 - \sqrt{f'(V)f'(W)}.
\end{aligned}$$

As mentioned in Section 2.1.1, whenever the period two pattern exists $f'(W)f'(V) < 1$ holds. Therefore $\mathrm{Re}\lambda_i < 0$ for all $i = 1, ..., 4$. Hence, this state is always stable to perturbations of period two or less.

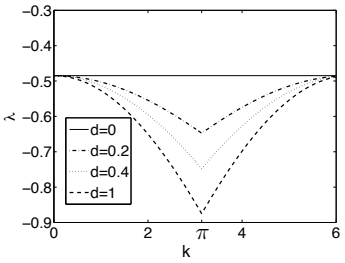

Figure 2.4: Dispersion relation for the growth rate of period two spatial perturbations ($f(x) = 1.5e^{-x^2}$, different values of d); the period two pattern is always stable.

Now consider $k \neq 0$. The eigenvalues in this case are too complex to study analytically, but numerical analysis suggests that this steady state is always stable to inhomogeneous perturbations. This result is supported by Figure 2.4, which shows the dispersion relation of the largest eigenvalue for a particular choice of f and different d. We see that the steady

state is stable for every $d > 0$ we have chosen.

The results of our linear stability analysis are summarised in Figure 2.5. There are three regions of interest. Region (a) is characterised by $0 > f'(U) > -1$. For values in this region, the homogeneous unpolarised steady state of system (2.1) is stable. Regions (b) and (c) are separated by the line $d = -\frac{f'(U)+1}{2}$ (see Section 2.1.1). The period two pattern is stable in both regions (b) and (c). The homogeneous polarised steady state is stable only in region (c).

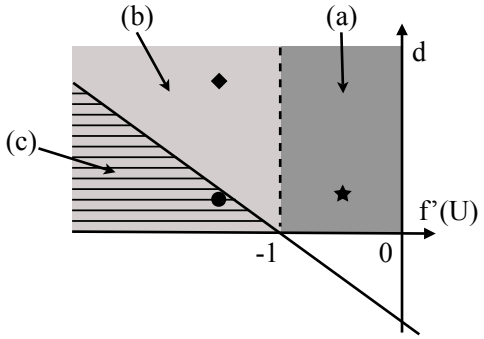

(a) Homogeneous unpolarised steady state is stable: both cell sides are equal

(b) Period two patterns are stable

(c) Period two patterns are stable; homogeneous polarised steady states are stable: polarisation

Figure 2.5: Summary of the dependence of the stability of steady states on $f'(U)$ and d. Rhombus, dot and star indicate the parameter values chosen for the simulations in Figure 2.6 in Section 2.1.3.

2.1.3 Numerical simulations

System (2.1) was simulated for a row of 100 cells, using the Matlab ODE solver ode45. At the boundaries we assumed $r_0 = r_1$ and $l_{101} = l_{100}$. Periodic boundary conditions gave similar results (results not shown). Both are compatible with the boundary condition chosen for the analysis of the homogeneous perturbations. For period two patterns the effects of the boundary conditions are restricted to the three cells closest to the boundaries as we can see in Figure 2.6.

The plots in Figures 2.6–2.10 were generated using $f(x) = ce^{-x^2}$ with different values for c, different values for d and different types of initial conditions. For clarity, not all the cells are shown in each figure, but the patterns continue in the obvious way. We have also considered $f(x) = \frac{\alpha}{1+qx^k}$ with positive α, q and k, but the results were similar, as expected from the analysis. For example, the simulations in Figure 2.6 can be qualitatively reproduced, choosing $f(x) = \frac{0.5}{x^6+1}$ and $f(x) = \frac{1.2}{x^6+1}$. In all figures in this section we have

presented the time to reach the polarised steady state, because this is the only one that has been observed in the *Drosophila* wing.

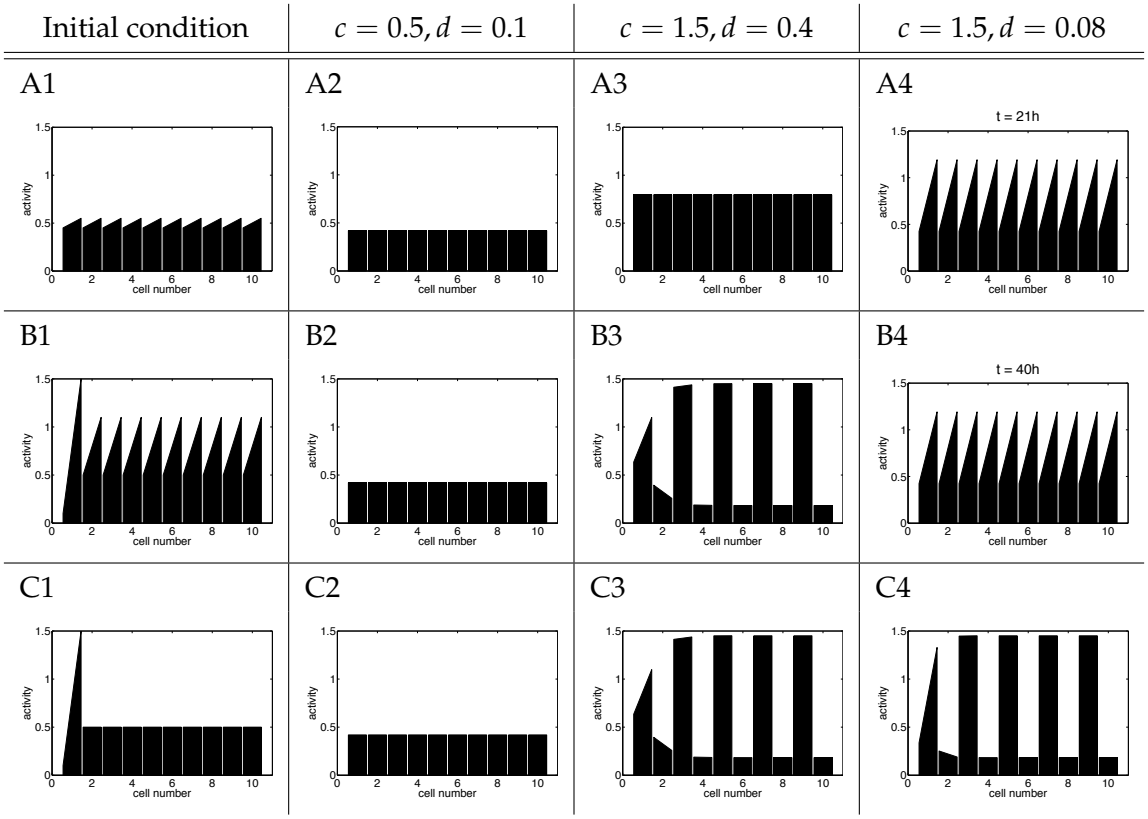

Figure 2.6: Steady state patterns of PCP activity for system (2.1) for different initial conditions, $f(x) = ce^{-x^2}$ with different c, and different choices of d. 100 cells were simulated, but only the first 10 are shown, for clarity. Patterns in the rest of the domain continue in the obvious way. For $c = 0.5$ and $d = 0.1$ we get the homogeneous unpolarised steady state irrespective of the initial condition. This parameter set corresponds to the star in Figure 2.5. For $c = 1.5$ and $d = 0.4$ the uniform initial conditions yield the homogeneous unpolarised steady state, whereas the two inhomogeneous initial conditions yield a period two pattern. This set of parameter values is represented by the rhombus in Figure 2.5. For $c = 1.5$ and $d = 0.08$ the final state for the first two initial conditions is the homogeneous polarised steady state, whereas for the last initial condition we get the period two pattern. This parameter set is indicated by the dot in Figure 2.5. Only the times to reach the homogeneous polarised steady state are presented, because this is the only state that has been observed in the biological system.

Figure 2.6 shows initial conditions and corresponding final states of system (2.1) for different values of c in $f(x) = ce^{-x^2}$ and different values of d. In column 2 we see that if $c = 0.5$ and $d = 0.1$, all cells evolve to the homogeneous unpolarised steady state irrespective of the initial conditions. This remains the case if d is increased. The result is consistent with

our analysis, because for this choice of parameter values $f'(U) > -1$ at the homogeneous unpolarised steady state U and therefore we are in region (a) of Figure 2.5, indicated by the star. Hence, by increasing d we do not cross any bifurcation lines.
The figures in column 3 of Figure 2.6 display the final states for $c = 1.5$, $d = 0.4$ and the different initial conditions shown in the first column of the figure. The parameter values for these simulations are represented by the rhombus in region (b) of Figure 2.5. Hence, the numerical results support the results from the analysis that the unpolarised steady state is stable to homogeneous perturbations. For inhomogeneous perturbations, period two patterns arise, spreading out as a wave. Similar waves have been investigated in [36]. As expected, the same patterns result if d is increased.
The results in column 4 of Figure 2.6 show the final states for $c = 1.5$ and $d = 0.08$. They do not change if d is decreased which will be further discussed below. Again this result is consistent with Figure 2.5 since we are now in region (c) as indicated by the dot. This column illustrates the fact that the homogeneous polarised steady state and the inhomogeneous period two pattern are both stable for the same parameter values. The final state achieved depends on the initial condition. Because of this we had a closer look at the initial conditions by moving gradually from the one in B1 of Figure 2.6 to the one in C1. Therefore we decreased the initial value $r_j(0)$ for $j \geq 2$ from 1.1 to 0.5 in 0.1 steps while $l_j(0) = 0.5$ for $j \geq 2$. The results are that down to $r_j(0) = 0.9$ the cells become stably polarised. For $r_j(0) = 0.8$ to $r_j(0) = 0.6$ the cells are polarised transiently, but subsequently a patterning wave arises from the left end of the row for the boundary conditions $r_0 = r_1$ and $l_{101} = l_{100}$ or from both ends for periodic boundary conditions. If $r_j(0) = 0.5$ the patterning wave starts immediately and no polarisation takes place. However, if we weaken the initial polarity in B1 of Figure 2.6 and increase c or decrease d we can still get the homogeneous polarised steady state.
These results show that apart from a small d and small $f'(U)$ we also need sufficiently uniform initial conditions to achieve polarity. Up to a certain degree, decreasing the diffusion coefficient or increasing the strength of the feedback can compensate for initial inhomogeneities. Otherwise, period two patterns will emerge, which always spread as a wave. Therefore, a small diffusion coefficient d is essential to overcome anomalies in initial conditions. This dependence is shown in Figure 2.7. If d is small enough the model can correct single cells that are initially polarised in the opposite direction to the surrounding cells (see Figure 2.7(b)). However, these single cells have to be more weakly polarised than their neighbours. If we increase d the cells pointing in the opposite direction give rise to an inhomogeneous pattern (shown in Figure 2.7(c)).

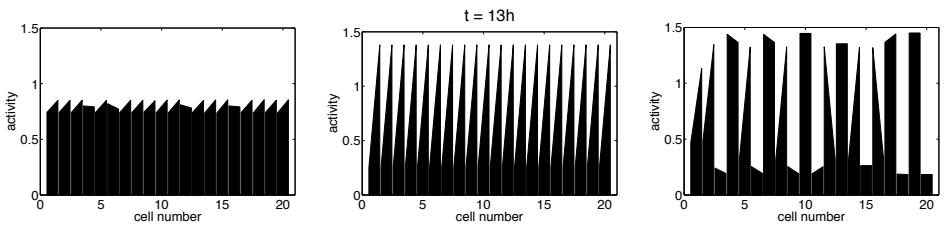

(a) (b) (c)

Figure 2.7: Initial condition with errors and the corresponding final states for system (2.1) with $f(x) = ce^{-x^2}$ and different values of c and d; (a) Initial condition, (b) result for $c = 1.5$ and $d = 0.02$; the time to reach this steady state is indicated; (c) result for $c = 1.5$ and $d = 0.08$.

The results for this section demonstrate that for the proposed mechanism a sufficiently small diffusion coefficient is necessary to get polarity, unless we have uniform initial conditions, which is unlikely in biological systems. As mentioned at the beginning of this chapter the diffusion coefficient D in experiments is related to the diffusion coefficient d in our simulations by $D = d\delta\Delta x^2$, where Δx is the spatial extension of a cell from left to right. Assuming $\Delta x = 8\,\mu\text{m}$ [19], a diffusion coefficient $d = 0.08$ would correspond to $D = \frac{0.08 \cdot 64}{15}\ \mu\text{m}^2/\text{min} = 0.006\ \mu\text{m}^2/\text{s}$. This value is small compared to diffusion coefficients measured in mammalian cell membranes, which are of the order of $0.1 - 0.01\ \mu\text{m}^2/\text{s}$ [22]. Experiments in yeast have revealed that the membrane diffusion coefficients of some proteins are also of the order of $0.001\ \mu\text{m}^2/\text{s}$ [14, 51].

Robustness of the model

In the previous section we have shown that system (2.1) can overcome irregularities in the initial conditions. Here, we will present a quantitative analysis of the robustness of the model. We choose initial conditions in which every cell has an initial polarity and add noise. Thus, initially we have

$$l_j = \frac{1}{2} - u + kU\left(-\frac{1}{2}, \frac{1}{2}\right),$$
$$r_j = 1 - l_j,$$

for all j, with a fixed $u \in [0, \frac{1}{2}]$, a fixed $k \in [0, 1-2u]$ and $U(-\frac{1}{2}, \frac{1}{2})$ denoting a uniform distribution on $[-\frac{1}{2}, \frac{1}{2}]$. This leaves us with two main cases: if $k < 2u$, then all cells have a right-pointing bias initially; if $k > 2u$, then we expect a fraction $f = \frac{1}{2} - \frac{u}{k}$ of cells to have a left-pointing bias initially. We varied u between 0 and $\frac{1}{2}$ in steps of 0.01 and k between 0 and $1 - 2u$ in steps of 0.01, and for each pair (u, k) we conducted 100 simulations for a row of 50 cells and calculated the mean ratio of cells in the final state pointing to the right. The

results for $f(x) = 1.5e^{-x^2}$ and $d = 0.02$ are presented in Figure 2.8. For pairs (u, k) in the area below the dashed line all the cells have a right-pointing bias initially and hence 100% of the cells in the final state point to the right. Increasing k above the dashed line increases the noise and in particular the number of cells initially pointing to the left. As shown, this decreases the percentage of cells in the final state pointing to the right. The continuous lines indicate the thresholds below which on average at least 95%, 75% and 50% of the cells in the final state point to the right. The average percentages of cells initially pointing to the right for parameter values on these lines are 93%, 75% and 58%. This shows that up to a certain noise level we get roughly the same percentage of cells pointing to the right in the final state as in the initial conditions. If half the cells initially point to the left, the fraction of cells in the final state pointing to the left is higher than in the initial conditions. Hence, up to a certain level of noise we get an improvement on the initial conditions. If we increase the noise further, considering the fraction of cells pointing to the right the final state is worse than the initial conditions.

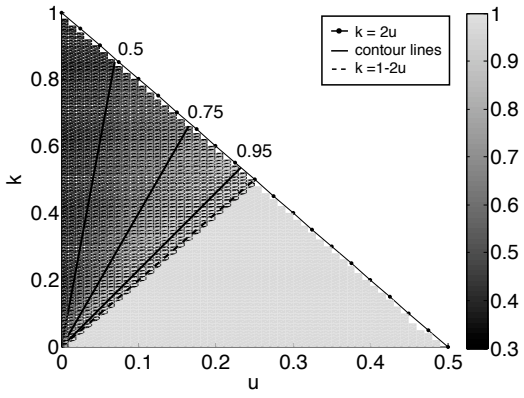

Figure 2.8: Results of the robustness analysis for system (2.1) for $f(x) = 1.5e^{-x^2}$ and $d = 0.02$. For every pair (u, k) with $0 \leq u \leq 0.5$ and $0 \leq k \leq 1 - 2u$ we conducted 100 simulations for a row of 50 cells and calculated the mean ratio of cells in the row that point to the right in the final state (indicated by the shading in the diagram). For values of (u, k) below the dashed line 100% of the cells in the final state point to the right. In addition we have included the contour lines for 95%, 75% and 50%. Increasing k increases the noise in the initial conditions and decreases the percentage of cells in the final state pointing to the right.

Analysis of clones

To study PCP experimentally, clonal clusters of cells in which a certain gene is either knocked out or overexpressed, are induced in the tissue [57]. The behaviour of the wild-type tissue around the clone gives insight into the interplay of the genes involved in the process.

We consider two different ways of representing clones in our model. In the first, we change the initial amount of activity in a group of cells in the row while having the same feedback in all cells. In the second, we alter the strength of the feedback in a group of cells while having the same initial amount of activity in every cell. The results of the first method (inclusion of a few cells in the row that have less initial activity than the rest) are shown in Figure 2.9.

We have considered clones comprising either an odd or an even number of cells, surrounded by wild-type cells each with an identical initial imbalance. We consider two different strengths of initial global cue. The initial difference between right and left in the wild-type cells in A1 and C1 of Figure 2.9 is 0.005 and in B1 it is 0.1. Columns 2, 3 and 4 of Figure 2.9 correspond to different strengths of the feedback and different values for the diffusion parameter. In all cases we observe a wave of period two pattern, which is initiated at the interface between the clone and the surrounding cells and moves in both directions. How far this wave spreads depends on the strength of the initial cue in the surrounding cells, the diffusion and the strength of the feedback. B2 shows that for a strong initial cue and small diffusion we get a short range of the effect of the clone. Increasing the diffusion (B3) or decreasing the strength of the initial global cue (A2) in the wild-type cells increases the range of the effect of the clone. Furthermore, increasing the diffusion increases the time to reach steady state. Comparing the third and fourth column of Figure 2.9 reveals that increasing the strength of the feedback decreases the range of the effect of the clone. In addition, it shortens the time to reach steady state. Similarly, decreasing c to 1.3 (corresponding to a weak feedback that still can give rise to the polarised steady state) increases the range of the effect of the clone and the time it takes to reach steady state (results not shown).

For a clone containing an even number of cells we get similar results, apart from a peak that occurs in the clone, because the number of cells in the clone is not compatible with the period of the pattern. The results for a weak initial global cue in the cells surrounding the clone are shown in row C of Figure 2.9. Results for a strong initial global cue are analogous (not shown). We get similar results if the initial activity in the cells in the clone is higher than in the rest of the cells (results not shown).

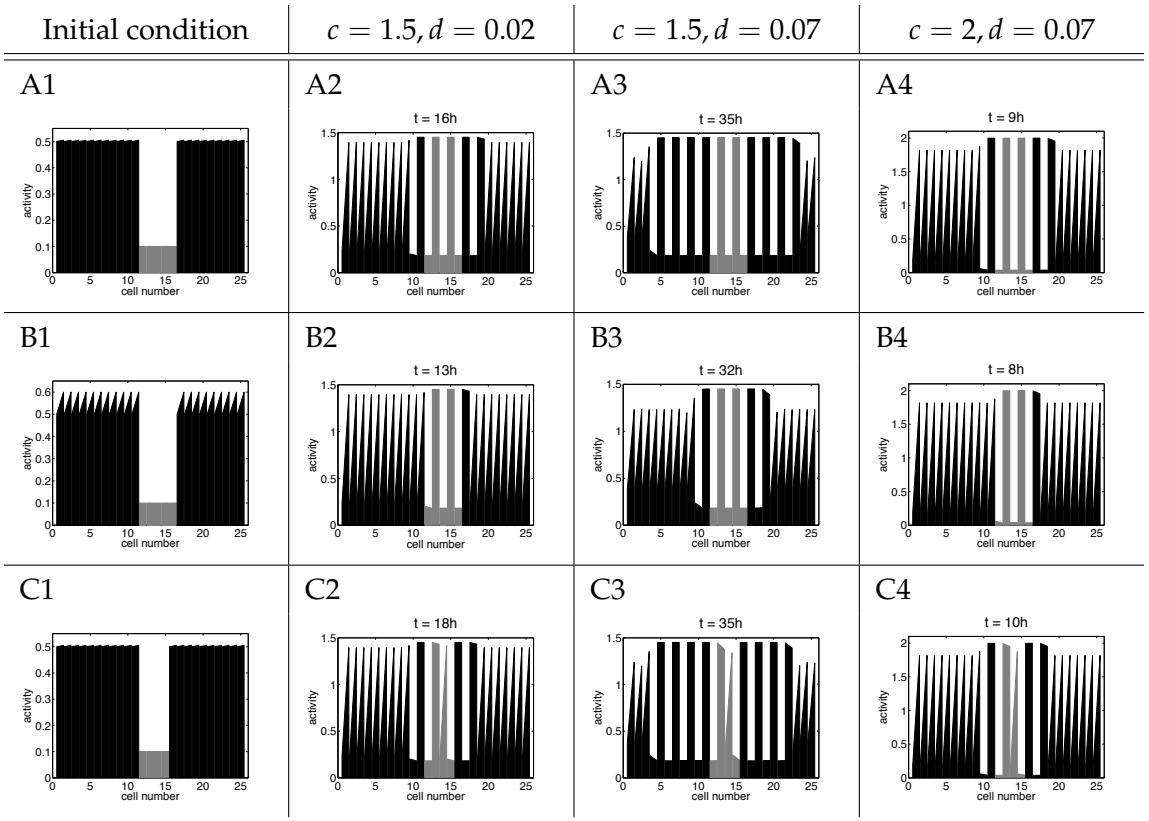

Figure 2.9: Column 1: initial conditions for clones (in grey) containing a number of cells that have less initial activity in each cell than the surrounding cells and different strength of initial global cue in the wild-type cells. The clones in A1 and B1 have an odd number of cells; the clone in C1 has an even number of cells. The difference between right and left side of each cell in A1 and C1 is 0.005 and in B1 it is 0.1; second, third and fourth column: the corresponding final states for system (2.1) for $c = 1.5$ and $c = 2$ and different diffusion parameters, there is a different scale in column 4. Furthermore, the times it takes to reach the steady states are shown.

Figure 2.10 shows the result for changing the strength of the feedback in a group of cells. The clones in rows A and B of Figure 2.10 have an odd and even number of cells, respectively. In the initial conditions in column 1 we chose a weak initial polarity in every cell as the global cue, with a difference of 0.005 between right and left sides. The diffusion parameter d is set to 0.02. Columns 2 and 3 of Figure 2.10 differ in the choice of feedback strength in the clone. In column 2 we chose $c = 1.4$ and in column 3 it is $c = 0.5$. The feedback in the surrounding cells is always set to $c = 1.5$. The two choices of feedback strength for the clonal cells represent two different cases of steady state behaviour. For $c = 1.4$ the homogeneous unpolarised steady state is unstable and period two patterns or polarisation can arise; for $c = 0.5$ the homogeneous unpolarised steady state is stable.

In row A of Figure 2.10 we see that the period two patterning wave which is initiated at the edges of the clone spreads in both directions for $c = 1.4$ (A2), but does not pattern the clone for $c = 0.5$ (A3). In this case the cells in the clone are unpolarised. Row B of Figure 2.10 shows that going from odd numbers of cells in the clone to even numbers only the result for $c = 1.4$ changes significantly (B2). Here again we see the peak arising in the clone. Increasing the feedback strength in the clone above $c = 1.5$ yields similar results to those for $c = 1.4$. Varying the diffusion parameter and the strength of the initial global cue gives a similar dependence (results not shown) to that shown in Figure 2.9 for a clone with a different amount of initial activity.

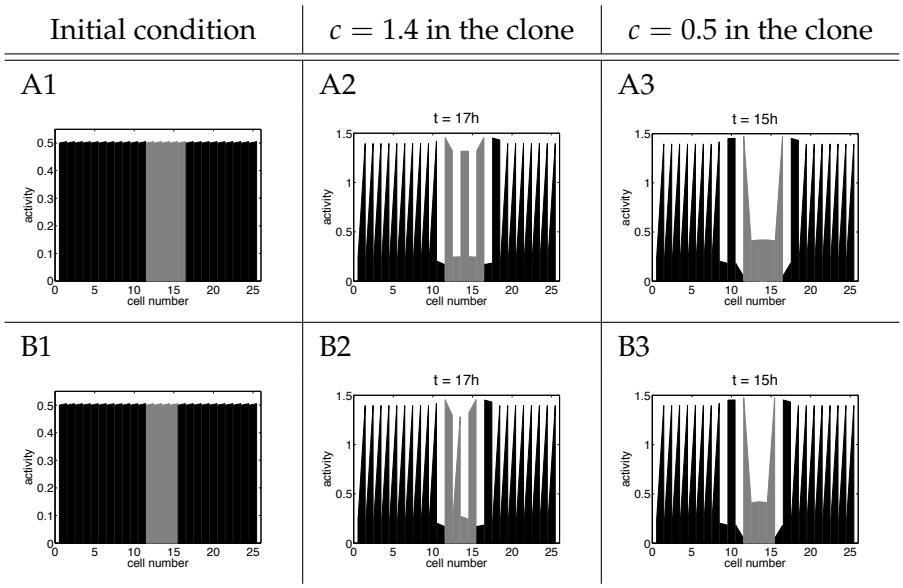

Figure 2.10: First column: initial conditions with clones (in grey) with different feedback strength, surrounded by cells with feedback $c = 1.5$. The clone in the first row has an odd number of cells, while the one in the second row contains an even number of cells. All cells have a weak initial bias – the difference between right and left is 0.005. Second and third columns: corresponding final states for system (2.1) for $c = 1.4$ and $c = 0.5$ in the clone and $d = 0.02$. In addition, the times to reach steady state are indicated.

In all cases a period two pattern is initiated at the clone boundaries and spreads into the surrounding cells with the range depending on the parameter values. The affected cells thus do not have an intracellular difference of activity, i.e., no polarity. This is different to the experimentally observed phenomenon of domineering non-autonomy as described in Section 1.2. Depending on which protein is lacking, i.e., which gene is knocked out in the clone, polarity can be disrupted in such a way that the hairs in a few cells on one side of the clone point in the opposite direction to the rest of the wild-type cells. Thus,

we conclude that this model does not account for the effects of clones observed in pupal wings in *Drosophila*.

2.2 Analysis in two spatial dimensions

We now consider a two dimensional array of square cells. The activity on the four sides of cell (i, j) is represented by $l_{i,j}, r_{i,j}, a_{i,j}$ and $b_{i,j}$ (see Figure 2.11).

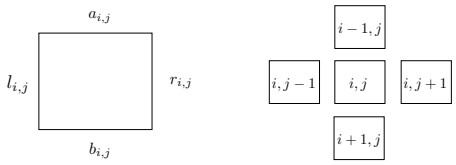

(a) (b)

Figure 2.11: (a) Labelling of the sides of a cell; (b) numbering of the cells in a two-dimensional array.

Again, adjacent cell sides inhibit each other by juxtacrine intercellular signalling. Diffusion takes place between the present side and its two abutting sides in the same cell. This gives the following system of equations

$$\begin{aligned}
\frac{\mathrm{d}l_{i,j}}{\mathrm{d}t} &= -\delta l_{i,j} + F(r_{i,j-1}) + \frac{D}{\Delta x^2}(a_{i,j} + b_{i,j} - 2l_{i,j}),\\
\frac{\mathrm{d}r_{i,j}}{\mathrm{d}t} &= -\delta r_{i,j} + F(l_{i,j+1}) + \frac{D}{\Delta x^2}(a_{i,j} + b_{i,j} - 2r_{i,j}),\\
\frac{\mathrm{d}a_{i,j}}{\mathrm{d}t} &= -\delta a_{i,j} + F(b_{i-1,j}) + \frac{D}{\Delta x^2}(l_{i,j} + r_{i,j} - 2a_{i,j}),\\
\frac{\mathrm{d}b_{i,j}}{\mathrm{d}t} &= -\delta b_{i,j} + F(a_{i+1,j}) + \frac{D}{\Delta x^2}(l_{i,j} + r_{i,j} - 2b_{i,j}),
\end{aligned}$$

where F is a decreasing positive function representing inhibition, with $F(0)$ finite and positive. The coefficient δ represents the decay rate, Δx the distance between two adjoining sides of a cell and D is the diffusion coefficient. The rescaling $\tau = \delta t$ yields

$$\begin{aligned}
\frac{\mathrm{d}l_{i,j}}{\mathrm{d}\tau} &= -l_{i,j} + f(r_{i,j-1}) + d(a_{i,j} + b_{i,j} - 2l_{i,j}),\\
\frac{\mathrm{d}r_{i,j}}{\mathrm{d}\tau} &= -r_{i,j} + f(l_{i,j+1}) + d(a_{i,j} + b_{i,j} - 2r_{i,j}),\\
\frac{\mathrm{d}a_{i,j}}{\mathrm{d}\tau} &= -a_{i,j} + f(b_{i-1,j}) + d(l_{i,j} + r_{i,j} - 2a_{i,j}),\\
\frac{\mathrm{d}b_{i,j}}{\mathrm{d}\tau} &= -b_{i,j} + f(a_{i+1,j}) + d(l_{i,j} + r_{i,j} - 2b_{i,j}),
\end{aligned} \tag{2.8}$$

with $d = \frac{D}{\delta \Delta x^2}$, hence $d \geq 0$. For the subsequent analysis we assume an infinite field of cells.

2.2.1 Existence of steady states and stability analysis

Let us assume we have a homogeneous steady state of system (2.8), i.e., $l_{i,j} = L, r_{i,j} = R, a_{i,j} = A$ and $b_{i,j} = B$ for all (i,j). Then there are seven different possibilities for the distribution of activity in the cell as shown in Figure 2.12.

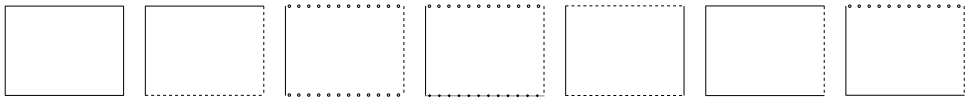

(a) (b) (c) (d) (e) (f) (g)

Figure 2.12: Illustration of possible distributions of activity in a four-sided cell; (a) $L = R = A = B$; (b) $L = A, R = B$; (c) $L \neq R, A = B$; (d) all cell sides are different; (e) $L = R, A = B$; (f) $L = A = B \neq R$; (g) $L = B, R \neq A$.

We investigated the existence of the different steady states and analysed their stability to homogeneous perturbations. Since we proceeded in the same manner as in Section 2.1, where possible, we just mention the results.

Homogeneous steady states

The homogeneous unpolarised steady state U ($U = L = R = A = B$) as shown in Figure 2.12(a) always exists and is stable to homogeneous perturbations if $d > -\frac{f'(U)+1}{2}$. The diagonally polarised steady state $L = A, R = B, L \neq R$ in Figure 2.12(b) exists if $\frac{f'(U)+d}{1+d} < -1$. We could only prove the stability analytically for $d = 0$. In this case it is stable to homogeneous perturbations if $f'(L)f'(R) < 1$, which holds as shown in Section 2.1.1. For $d > 0$ we simulated the system using Matlab and XPPaut, a tool for analysing dynamical systems [12]. This numerical analysis supports the notion that the steady state is stable to homogeneous perturbations whenever it exists, as shown in Figure 2.13(a).
The existence of $L \neq R, A = B$ (Figure 2.12(c)) could only be shown analytically for $d = 0$ in which case it exists if $f'(U) < -1$. Simulations using Matlab and XPPaut for $d \geq 0$ suggest that this steady state exists for $d < -\frac{f'(U)+1}{2}$. Figure 2.13(b) shows that it is unstable for $f(x) = 1.5e^{-x^2}$. Note that this bifurcation diagram shows only the stability of the homogeneous unpolarised steady state and the state $L \neq R, A = B$. Hence, although they are both unstable for small d there exists at least one other steady state that is stable for those parameter values as shown in Figure 2.13(a).
The stability of the steady state $L \neq R, A = B$ depends only on the derivative of f at U, L and R. Therefore, our result does not depend on our choice of f; we would expect it to hold for any f with a similar derivative at those points as $f(x) = 1.5e^{-x^2}$. We found

that for $d = 0$ for it to be stable an inhibition function with $f(U) = U$, $f'(U) > -1$ and $f(L) = R, f(R) = L, f'(L)f'(R) < 1$ is needed. Figure 2.14 shows an example of such a function. However, in absence of evidence of such a complex inhibition function, we omit further analysis of this case.

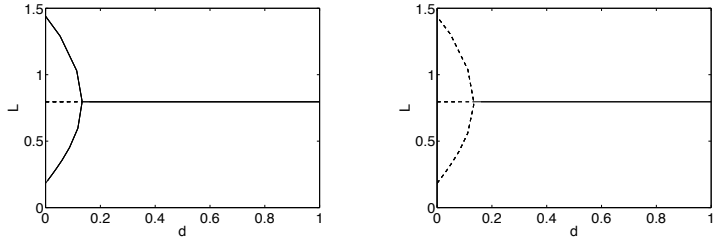

(a) (b)

Figure 2.13: Continuation of L versus d for the two homogeneous polarised steady states; (a) Diagonal polarity ($L = A, R = B, L \neq R$, Figure 2.12(b)); (b) polarity along the axis from left to right ($L \neq R, A = B$, Figure 2.12(c)). We chose $f(x) = 1.5e^{-x^2}$. In both cases the polarised steady state exist for sufficiently small d, but it is only stable in the diagonally polarised case. Note that in both bifurcation diagrams we have only considered two of the possible steady states.

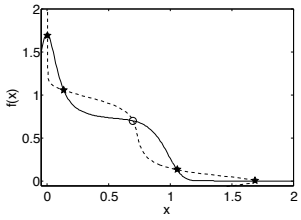

Figure 2.14: Example of a feedback function for which $f(u) = u, f(v) = w, f(w) = v, f(y) = z, f(z) = y$ and $f'(u) > -1, f'(v)f'(w) < 1$ for some $u, v, w, y, z \in \mathbb{R}^+$. The solid line indicates the function $f(x) = 0.7e^{-x^{10}} + \frac{1}{1+100x^2}$; the dashed line its inverse. The circle marks the unpolarised steady state and the stars the steady state for which all four sides of the cell are different.

An additional possible distribution would be that all sides of the cell are different (Figure 2.12(d)). This again would need an inhibition function like the one in Figure 2.14. Hence, we omit further analysis. There are three more possible allocations of the activity as shown in Figures 2.12(e)-(g). Substitution of the conditions for the three steady states into (2.8) combined with numerical analysis reveals that they are not steady states of system (2.8).

Period two pattern – "checkerboard"

Let us assume $l_{i,j} = r_{i,j} = a_{i,j} = b_{i,j} = V$ for all (i, j) where i and j are either both odd or both even ($i \bmod 2 = j \bmod 2$) and $l_{i,j} = r_{i,j} = a_{i,j} = b_{i,j} = W$ for all (i, j) where either i or j is odd and the other one even ($i \bmod 2 = (j+1) \bmod 2$). Substituting this into (2.8) yields $V = f(W)$ and $W = f(V)$, as for the existence of period two patterns in one spatial dimension. Hence, an unpolarised period two pattern exists if $f'(U) < -1$ at the homogeneous unpolarised steady state U. The stability analysis for this case would be very complex. However, the analysis in Section 2.1 and numerical simulations suggest that the period two pattern is stable whenever it exists.

Figure 2.15 summarises the results of our analysis of the stability of the steady states to homogeneous perturbations. We get the same three regions as in the one-dimensional case (see Figure 2.5). In region (I), which is characterised by $f'(U) > -1$, only the homogeneous unpolarised steady state is stable. In region (II) we have $f'(U) < -1$ and $d > \frac{-f'(U)+1}{2}$. Here, the homogeneous unpolarised steady state and the period two pattern are stable. In region (III) the diagonally polarised homogeneous steady state as well as the period two pattern are stable.

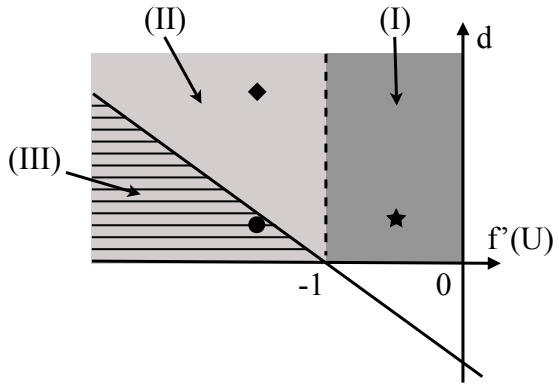

(I)+(II) Homogeneous unpolarised steady state is stable to homogeneous perturbations: all cell sides are equal

(II)+(III) Period two patterns are stable to homogeneous perturbations

(III) Homogeneous polarised steady state $L = A, R = B, L \neq R$ is stable to homogeneous perturbations

Figure 2.15: Summary of the results in this section for the dependence of the stability of steady states on $f'(U)$ and d; rhombus, dot and star indicate the parameter values chosen for the simulations in Figure 2.16 in Section 2.2.2.

Considering stability to inhomogeneous perturbations we expect the same results as in the one-dimensional case. The homogeneous unpolarised steady state is stable in region (I), the period two pattern is stable in region (II) and (III), and the diagonally polarised steady

state is stable in region (III).

2.2.2 Numerical simulations

We employed Matlab, in particular ode45, to simulate (2.8) and chose boundary conditions similar to those in one dimension, i.e., on each boundary of the array of cells we add another row or column of cells with the same activity values as the row or column of cells at the boundary. Applying periodic boundary conditions yields similar results (not shown). Both boundary conditions are compatible with our analysis for the homogeneous steady states. For the period two pattern we get an effect on the cells right at the boundary. A 10×10 array of cells is considered and our function f is of the form $f(x) = ce^{-x^2}$ with a positive parameter c. As expected from the analysis, simulations for $f(x) = \frac{\alpha}{1+qx^k}$ with positive α, q and k gave similar results.

Three different initial conditions and the corresponding final states of system (2.8) for different values of c and d are shown in Figure 2.16. We have indicated the time to reach the polarised steady state in A4, since this is the only state that has been observed in the biological system.

As expected from the stability analysis, the results in Figure 2.16 are similar to the ones in the one-dimensional case. Column 2 shows that for $c = 0.5$ and $d = 0.1$ we get the homogeneous unpolarised steady state irrespective of the initial conditions. Varying d does not change the final state. This matches our analysis as we can see from Figure 2.15, where this set of parameter values is indicated by the star. In Figure 2.16 column 3 we see that for $c = 1.5$ and $d = 0.4$ we get the homogeneous unpolarised steady state for the initial conditions A1 and B1 and the period two pattern for C1. The effect at the boundary in C3 is due to the boundary conditions we chose. For periodic boundary conditions the pattern spreads over the whole region. The same behaviour is obtained if d is increased, as expected. The choice of parameter values for column 3 is indicated by the rhombus in region (II) of Figure 2.15, where we found that the homogeneous unpolarised steady state is only stable to homogeneous perturbations, while we expect the period two pattern to be stable to both homogeneous and inhomogeneous perturbations. Decreasing the diffusion, we get into region (III) of Figure 2.15, where the dot represents the parameter values for column 4 in Figure 2.16. As expected from the analysis we get polarity as shown in Figure 2.16 A4. For the initial conditions in B1 and C1 we get inhomogeneous patterns (see B4 and C4). The boundary effects are due to the boundary conditions we chose; the patterns occur in the whole region for periodic boundary conditions. The distribution in C4 seems disordered. Decreasing the diffusion coefficient elucidates the underlying pattern as shown in

Figure 2.17. We see that the diagonally polarised steady state occurs along the diagonal from top left of the region to bottom right. The rest of the field mostly shows a period two pattern. As before, the effect at the boundaries is due to the boundary conditions. Hence, the disordered pattern is a result of the competition between polarisation and the period two pattern with extra freedom for propagation compared to the one-dimensional case.

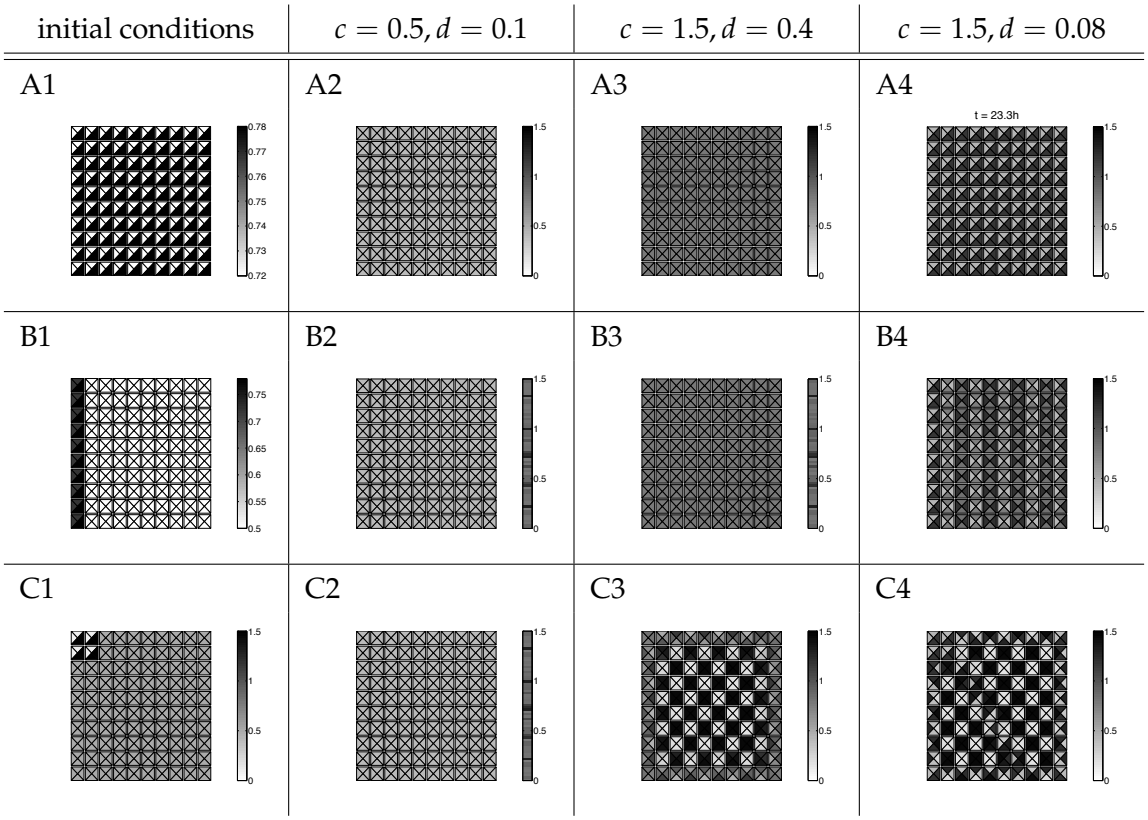

Figure 2.16: Final states for system (2.8) for different initial conditions and different choices of c and d, note the different scales in A1 and B1. We have indicated the time to reach the polarised steady state. Column 2: The parameter values are represented by the star in Figure 2.15. We get the unpolarised steady state irrespective of the initial conditions and the value of d. Column 3: We get either the unpolarised steady state or the period two pattern. This parameter set is indicated by the rhombus in Figure 2.15. Column 4: The parameter values correspond to the dot in Figure 2.15. Depending on the initial conditions we get the homogeneous polarised steady state or inhomogeneous steady states.

Like in the one-dimensional case in Section 2.1, uniform initial conditions yield polarity if the feedback is sufficiently strong and the diffusion sufficiently weak. Increasing the diffusion or weakening the feedback results in the homogeneous unpolarised steady state. Inhomogeneities in the initial conditions give rise to inhomogeneous steady states.

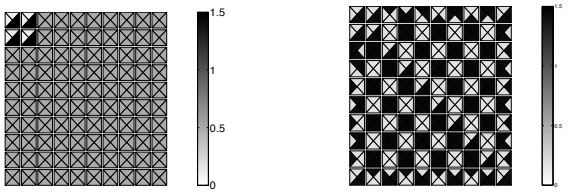

(a) (b)

Figure 2.17: The underlying pattern of Figure 2.16 C4; (a) Initial condition as in Figure 2.16 C1; (b) final state for $c = 1.5$ and $d = 0.01$; on the diagonal from top left to bottom right we get the diagonally polarised steady state, while the period two pattern arises in the rest of the region.

Simulations for initial conditions that include anomalies further support our results. We assume an initial condition like the one in Figure 2.16 A1 and add random noise such that there is still a bias to the bottom right corner of each cell but any two sides do not necessarily have the same amount of activity (see Figure 2.18(a)). For $c = 1.5$ and $d = 0.08$ we still get the polarised steady state (not shown). If we increase the diffusion to $d = 1$ we get the period two pattern (Figure 2.18(b)). This is different to the result in Figure 2.16 A3 for $d = 0.4$, which stays the same if d is increased as mentioned above. However, the result in Figure 2.18(b) is still consistent with our stability analysis since we are now in region (II) of Figure 2.15. There, the homogeneous unpolarised steady state is stable to homogeneous perturbations and the period two pattern is stable to both homogeneous and inhomogeneous perturbations.

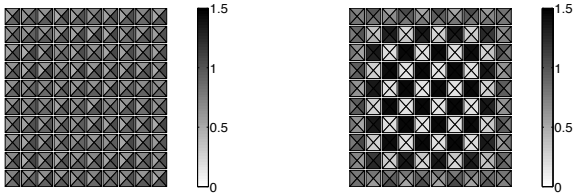

(a) (b)

Figure 2.18: Inhomogeneous initial conditions give rise to period two pattern; (a) Initial conditions with noise; (b) final state for $c = 1.5$ and $d = 1$.

As a next step, we included single cells that point the opposite way in the initial condition in Figure 2.18(a). As long as these incorrect cells are weakly polarised and not right next to each other they can be corrected if d is sufficiently small (not shown).

Analysis of clones

We now analyse the behaviour of system (2.8) for initial conditions with a clone in the middle of the field of cells. The initial conditions with a clone lacking activity and corresponding final states for different values of c and d are shown in Figure 2.19. In A1 the initial imbalance in the wild-type cells around the clone is weaker than in B1 (note the different scales). The results show that for the stronger initial imbalance in row B we get a shorter range of effect of the clone. Furthermore, a small diffusion parameter (column 2) or a strong feedback (column 4) also lead to a shorter range.

In our simulations the clones affect the cells all around them and we cannot detect a pattern of orientation for the affected cells. Especially in A3 and B3 patches of period two patterns occur, hence these cells do not have any orientation. We get similar results if the activity in the clone is higher than in the wild-type cells. This differs from experimental observations. There, the clones only affect cells on one side and the affected cells have a common orientation (see Section 1.2).

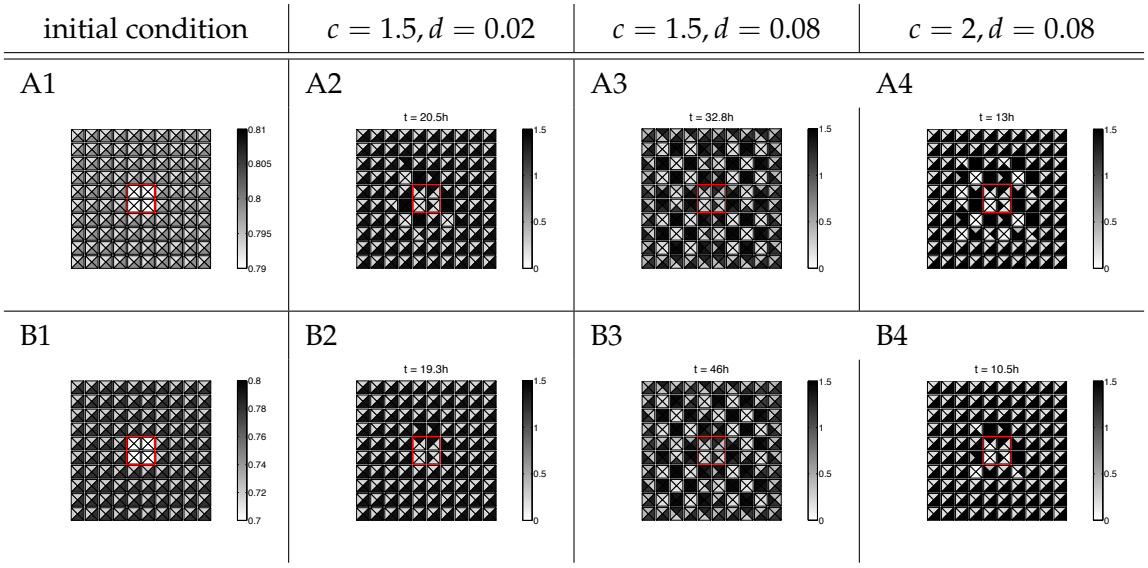

Figure 2.19: Simulations for a clone in the field of cells. In all figures the clone is circumscribed by a red rectangular. Row A: A1 shows an initial condition with a clone without activity, the intracellular difference in the wild-type cells is 0.006, A2-A4 display the corresponding final states of system (2.8) for different values of d and c; row B: B1 shows an initial condition with a clone without activity, the intracellular difference in the normal cells is 0.06, the corresponding final states for different values for c and d are shown in B2-B4.

2.3 Discussion

Based on the general consensus that the conserved second tier of PCP generation depends on a feedback loop that amplifies an initial global cue, we have developed the feedback and diffusion model that can generate polarity. To maximise the mathematical tractability of this model, we have used a simple system of equations that represents a wide range of more specific mechanistic models. We have employed a combination of linear stability analysis and numerical simulations in one and two spatial dimensions to investigate the patterns of cell polarity that this model can generate.

We found that both period two and polarised patterns can occur. To achieve polarisation, the intercellular feedback has to be sufficiently strong and the intracellular diffusion sufficiently weak. We have also shown that the model can overcome small anomalies in the initial conditions. Analysis of clones of cells that have a different amount of activity than the surrounding cells revealed that the range of the effect of these clones depends on both the strength of the initial global cue in the surrounding wild-type cells and on the value of the diffusion parameter. These results also hold for clones in which the strength of the feedback is different to that in the surrounding cells. The cells affected by the clones show either no polarity or a random distribution. This differs from experimental findings in the *Drosophila* wing, in which the cells surrounding the clone have a common orientation demonstrated by the direction of the hair growth (see Section 1.2).

Due to the bistability of the homogeneous polarised steady state and inhomogeneous patterns, for certain parameter values it depends only on the initial conditions which state will arise. Inhomogeneous initial conditions can give rise to inhomogeneous patterns, depending on the strength of the feedback and the rate of diffusion. Increasing the strength of the feedback or decreasing the diffusion coefficient increases the robustness of the model. It would be interesting to get an indication of these two parameters from experiments.

The feedback and diffusion model is not conservative — the PCP activity in a cell can be time-varying. However, if the activity in this model is interpreted as representing non-conserved protein complexes, the overall amounts of the proteins that combine to form complexes could be conserved in each cell. Furthermore, this type of non-conservative model can be derived by elimination of variables in a conservative model. As an example of this, assume that a cell is divided into three parts: a left, a right and a central compartment. Representing the activity in each compartment in cell j by l_j, r_j and c_j, respectively, a one-dimensional model corresponding to the system can be written as:

$$\begin{aligned} \dot{l}_j &= -l_j + f(r_{j-1}) + d(r_j - l_j), \\ \dot{r}_j &= -r_j + f(l_{j+1}) + d(l_j - r_j), \\ \dot{c}_j &= l_j + r_j - f(r_{j-1}) - f(l_{j+1}), \end{aligned} \tag{2.9}$$

for which $\dot{c}_j + \dot{l}_j + \dot{r}_j = 0$. Thus, although system (2.9) as a whole is conservative, the total activity on the left and right sides of a cell may not be conserved.

In the following chapter we will introduce an approach which is based on a feedback loop and diffusion and is conservative. We will investigate whether it has different properties than the feedback and diffusion model.

Chapter 3

Conservative model

The approach in this chapter is based on the idea that planar cell polarity is generated by a feedback loop that amplifies an initial cue. We propose a conservative model that describes the dynamic redistribution of conserved PCP activities within the membrane of each cell, depending on its neighbouring cells. This is coupled with intracellular diffusion. We have chosen a discrete approach since our main focus is on the intercellular interactions. By omitting biological details we ensure that the mathematical analysis is practicable and our results are valid for a whole class of models for PCP. Two specific models that belong to the class represented by the conservative model were proposed by Amonlirdviman *et al.* [3] and Le Garrec *et al.* [29]. We will discuss these approaches in Chapters 4 and 5. In the present chapter we introduce our conservative model and investigate its properties. To this end, we conduct linear stability analysis and numerical simulations to investigate which patterns the model can generate and their dependence on the strength of the feedback and the speed of diffusion. Furthermore, we analyse its robustness and the effects of clones.
We consider a row of two-sided cells with r_j representing PCP activity on the right side and l_j on the left side of cell j. These values may represent amounts of certain proteins. However, to ensure that our results are generally valid, we do not want to be more specific. The total amount of activity in each cell is identical and conserved, thus $l_j + r_j = Q$ for all j with a positive constant Q. In contrast to the feedback and diffusion model in the previous chapter, the amount of activity in a cell is not raised and lowered but redistributed within the cell, depending on the amount of activity in the adjacent sides of the neighbouring cell. The model is encoded by the following equations

$$\begin{aligned} \frac{\mathrm{d}l_j}{\mathrm{d}t} &= G(l_{j+1})r_j - G(r_{j-1})l_j + \frac{D}{\Delta x^2}(r_j - l_j), \\ \frac{\mathrm{d}r_j}{\mathrm{d}t} &= G(r_{j-1})l_j - G(l_{j+1})r_j + \frac{D}{\Delta x^2}(l_j - r_j), \end{aligned} \tag{3.1}$$

where G is an increasing non-negative function, representing the influence of the adjacent cells on the movement, $D \geq 0$ represents diffusion and Δx the spatial extension of a cell from left to right. The mechanism is a kind of lateral inhibition; if we look at a cell side and there is a large amount of activity in the adjacent side of the neighbouring cell then a large proportion of the PCP activity on the present cell side gets moved away from it. Similarly, if there is only a small amount of activity in the adjacent side of the neighbouring cell only a small proportion of the amount on the current side gets moved. The amount of activity at a cell side depends on the adjacent cell sides of both neighbours, because they together determine the net movement toward this cell side. An illustration of the proposed mechanism is presented in Figure 3.1.

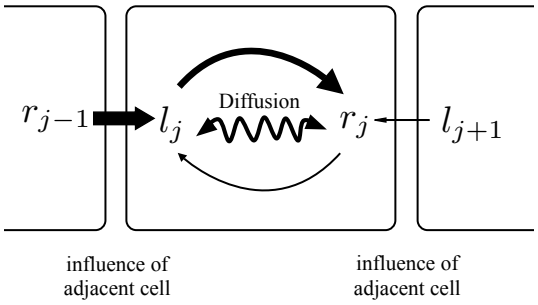

Figure 3.1: Schematic representation of the conservative polarisation model (3.1). A conserved PCP activity within each cell is redistributed in response to juxtacrine intercellular signalling and intracellular diffusion. The intracellular arrows indicate movement in response to inputs from adjacent cells (intercellular arrows). The thickness of the intercellular arrows represents the relative amount of input which in turn leads to different amounts of movement, indicated by the thicknesses of the intracellular arrows.

If T, D^{bio} and Δx^{bio} denote the time, the diffusion coefficient and the side length of a cell in the biological system, these parameters are related to the parameters in our model by $t = \kappa T, D = \frac{1}{\kappa} D^{bio}$ and $\Delta x = p\,\Delta x^{bio}$ with positive constants κ and p.
Rescaling (3.1) yields

$$\begin{aligned} \frac{\mathrm{d}l_j}{\mathrm{d}\tau} &= G(l_{j+1})r_j - G(r_{j-1})l_j + d(r_j - l_j), \\ \frac{\mathrm{d}r_j}{\mathrm{d}\tau} &= G(r_{j-1})l_j - G(l_{j+1})r_j + d(l_j - r_j), \end{aligned} \tag{3.2}$$

where $d = \frac{D}{\Delta x^2} = \frac{1}{\kappa p^2 (\Delta x^{bio})^2} D^{bio}$ and $\tau = dt$. Hence, the time τ in our analysis and our simulations is related to the time T in experiments by

$$T = \frac{1}{\kappa d}\tau = \frac{p^2 (\Delta x^{bio})^2}{D^{bio}}\tau. \tag{3.3}$$

We assume $\Delta x^{bio} = 8\ \mu m$ [19], $p = 1$ and $D^{bio} = 0.01\ \mu m^2/s$ [22]; then κ is determined by equation (3.3).
To investigate the properties of the conservative model (3.2) we apply a steady state analysis followed by numerical simulations. For the steady state analysis we assume an infinite row of cells.

3.1 Existence of steady states

Substitution of $r_j = Q - l_j$ into (3.2) and setting $L_j = \frac{l_j}{Q}$ yields

$$\frac{dL_j}{d\tau} = g(L_{j+1})(1 - L_j) - g(1 - L_{j-1})L_j + d(1 - 2L_j), \tag{3.4}$$

with $g(x) = G(Qx)$. Our rescaling implies $0 \leq L_j \leq 1$. The homogeneous unpolarised steady state is $L_j = \frac{1}{2}$ for all j, which always exists. A homogeneous polarised steady state $L_j = L \neq \frac{1}{2}$ for all j exists if and only if

$$d = \frac{g(1 - L)L - g(L)(1 - L)}{1 - 2L} =: \phi(L). \tag{3.5}$$

The function ϕ is not defined at $\frac{1}{2}$. Furthermore, we get $\phi(0) = \phi(1) = -g(0)$.
The completely polarised homogeneous steady states $L = 1$ or $L = 0$ exist if and only if $g(0) = 0$ and $d = 0$, since g is a non-negative function and d has to be non-negative. In our context the constraint $g(0) = 0$ is reasonable, since it states that if the activity on the adjacent cell side is 0 there is no influence from it on the present cell side. However, $d = 0$ is unlikely in biological systems.
Equation (3.5) yields that a steady state $L \in (0, \frac{1}{2})$ exists for some $d > 0$ if and only if

$$\frac{g(1 - L)}{g(L)} > \frac{1 - L}{L} \quad \text{for some} \quad L \in \left(0, \frac{1}{2}\right). \tag{3.6}$$

In the following we will show that for any Hill function

$$g(L) = \frac{bL^n}{\alpha^n + L^n}, \tag{3.7}$$

with $n \in \mathbb{N}, \alpha > 0$ and $b > 0$, inequality (3.6) holds for $n \geq 2$ for at least one $L \in (0, \frac{1}{2})$. Assume $g(L) = \frac{bL}{\alpha + L}$ with $0 < L < \frac{1}{2}$. Substituting into (3.6) yields

$$\frac{b(1 - L)(\alpha + L)}{(\alpha + 1 - L)bL} > \frac{1 - L}{L}.$$

A sequence of reformulations implies $L > \frac{1}{2}$, which contradicts our assumption. Hence, (3.6) does not hold for $n = 1$.

Let $n \geq 2$. Substituting (3.7) into (3.6) yields

$$\frac{b(1-L)^n(\alpha^n + L^n)}{[\alpha^n + (1-L)^n]bL^n} > \frac{1-L}{L}.$$

Rearranging implies

$$\alpha^n > \frac{L^{n-1}(1-2L)}{1-(\frac{L}{1-L})^{n-1}}. \tag{3.8}$$

For every α and $n \geq 2$ we can find an $L \in (0, \frac{1}{2})$ that satisfies this condition, since the right hand side of (3.8) tends to 0 as L tends to 0. Therefore, for every Hill function with $n \geq 2$, there exists a branch of polarised steady states connecting to $L = 0$. The existence of a branch of polarised steady states connecting to $L = 1$ can be shown in an analogous manner. This is due to the symmetry of (3.4).

We will now investigate the existence of polarised steady states near $L = \frac{1}{2}$. Equation (3.6) can be restated as

$$\frac{g(1-L)}{1-L} > \frac{g(L)}{L} \quad \text{for} \quad L \in \left(0, \frac{1}{2}\right). \tag{3.9}$$

Geometrically, this means that L and $1-L$ (with $0 < L < \frac{1}{2}$) are polarised steady states if the straight line through $(0,0)$ and $(1-L, g(1-L))$ is steeper than the straight line through $(0,0)$ and $(L, g(L))$ as illustrated in Figure 3.2.

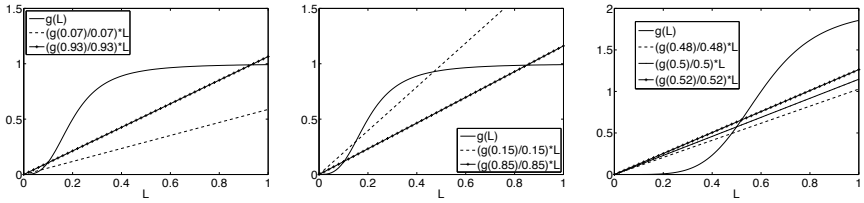

(a) (b) (c)

Figure 3.2: Illustration of the geometrical interpretation of condition (3.9) for the existence of a polarised steady state; (a) If $g(x) = \frac{L^3}{0.2^3+L^3}$ then $L = 0.07$ is a polarised steady state, since the dashed line $\frac{g(0.07)}{0.07}L$ is less steep than the line $\frac{g(1-0.07)}{1-0.07}L$; (b) if $g(x) = \frac{L^3}{0.2^3+L^3}$ then $L = 0.15$ is not a polarised steady state, since the dashed line $\frac{g(0.15)}{0.15}L$ is steeper than the line $\frac{g(1-0.15)}{1-0.15}L$; (c) if $g(x) = \frac{2x^5}{0.6^5+x^5}$ then $L = 0.48$ is a polarised steady state, since the dashed line $\frac{g(0.48)}{0.48}L$ is less steep than the line $\frac{g(1-0.48)}{1-0.48}L$; to illustrate equation (3.10) we also included the straight line $\frac{g(0.5)}{0.5}L$.

Figure 3.2(c) shows that a branch of steady states connecting to $L = \frac{1}{2}$ exists if

$$\frac{g(L)}{L} < \frac{g(\frac{1}{2})}{\frac{1}{2}} < \frac{g(1-L)}{1-L} \quad \text{for} \quad L \in \left(\frac{1}{2} - \epsilon, \frac{1}{2}\right), \tag{3.10}$$

with a sufficiently small $\epsilon > 0$. Inequality (3.10) can be restated as

$$\frac{\mathrm{d}}{\mathrm{d}L}\left(\frac{g(L)}{L}\right)\Big|_{L=\frac{1}{2}} > 0,$$

hence,

$$\frac{g'(L)L - g(L)}{L^2}\Big|_{L=\frac{1}{2}} > 0.$$

Reformulating we get

$$g'\left(\frac{1}{2}\right) > 2\, g\left(\frac{1}{2}\right). \tag{3.11}$$

Substituting (3.7) with $n \geq 2$ and rearranging yields that (3.11) is equivalent to

$$\alpha > \frac{1}{2\sqrt[n]{n-1}}. \tag{3.12}$$

This gives us restrictions on α and n. If $\alpha > \frac{1}{2\sqrt[n]{n-1}}$ we get a branch of polarised steady states connecting to $L = \frac{1}{2}$, if $\alpha < \frac{1}{2\sqrt[n]{n-1}}$ there is no such branch. It is $\frac{1}{2\sqrt[n]{n-1}} \leq \frac{1}{2}$ for general $n \geq 2$ and $\min_{n\geq 2} \frac{1}{2\sqrt[n]{n-1}} = 0.38$, which is the value at $n = 5$. Hence, for $\alpha > \frac{1}{2}$ we get a branch of polarised steady states connecting to $L = \frac{1}{2}$ for any $n \geq 2$ and for $\alpha < 0.38$ we do not get such a branch for any $n \geq 2$.

In summary, for every Hill function with $n \geq 2$ there exists a branch of polarised steady states connecting $L = 0$ and a branch connecting $L = 1$. In some cases, depending on α and n there exists also a branch connecting $L = \frac{1}{2}$. Note that all these results are independent of the coefficient b in the numerator of the Hill function (3.7). Considering the biological system we are especially interested in strongly polarised steady states, i.e. values of L close to 0 or 1. Our analysis shows that for a Hill function, which is a reasonable choice for the feedback function, these steady state exist always. We also expect our arguments to extend to more general feedback functions.

Now we will present examples of the existence of polarised steady states. Figures 3.3 and 3.4 show plots for $g(L)$, $\frac{g(1-L)}{g(L)}$, $\frac{1-L}{L}$ and $\phi(L)$ for $g(L) = g_1(L) = \frac{L^3}{0.2^3+L^3}$ and $g(L) = g_2(L) = \frac{2L^5}{0.6^5+L^5}$, respectively. For g_1 only values of L close to 0 and 1 are steady states as shown in Figure 3.3(b)-(d), whereas Figures 3.4(b) and (c) show that for g_2, every $0 < L < 1$ with $L \neq \frac{1}{2}$ is a possible steady state. It depends on the diffusion coefficient d which one will arise. For g_1 with $\alpha = 0.2$ and $n = 3$ the right hand side of (3.12) evaluates to $\frac{1}{2\sqrt[n]{n-1}} = \frac{1}{2\sqrt[3]{2}} = 0.4 > 0.2 = \alpha$ and for g_2 with $\alpha = 0.6$ and $n = 5$ to $\frac{1}{2\sqrt[n]{n-1}} = \frac{1}{2\sqrt[5]{4}} = 0.4 < 0.6 = \alpha$. This supports the finding that for g_1 we do not get polarised steady states near $\frac{1}{2}$, whereas for g_2 a branch of steady states connecting to $\frac{1}{2}$ does exist.

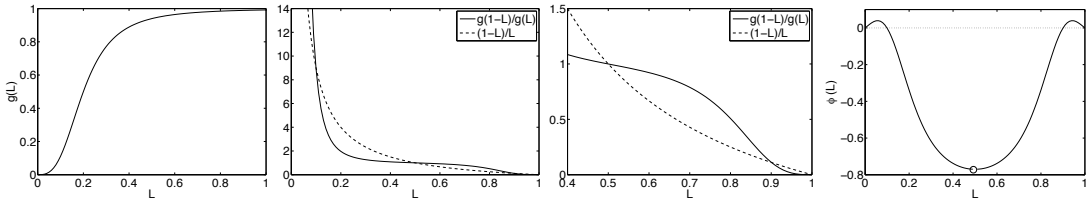

(a) (b) (c) (d)

Figure 3.3: Illustration of the existence of polarised steady states of (3.4) for $g_1(L) = \frac{L^3}{0.2^3+L^3}$; only values of L close to 0 and close to 1 are polarised steady states; (a) Plot of g_1; (b) plot of $\frac{g_1(1-L)}{g_1(L)}$ and $\frac{1-L}{L}$ (larger scale); (c) plot of $\frac{g_1(1-L)}{g_1(L)}$ and $\frac{1-L}{L}$ (zoomed in); (d) plot of $\phi(L)$, showing that it is only positive for values of L close to 0 and close to 1; the circle at $L = \frac{1}{2}$ indicates that $\phi(L)$ is not defined at this point.

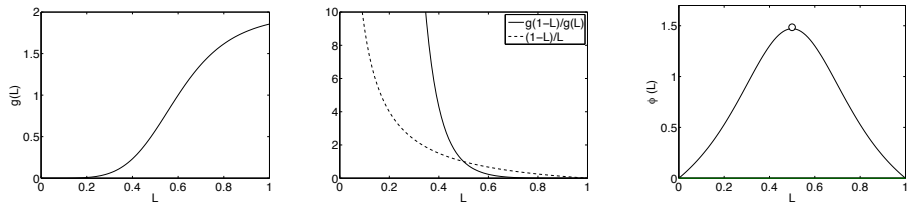

(a) (b) (c)

Figure 3.4: Illustration of the existence of polarised steady states of (3.4) for $g_2(L) = \frac{2L^5}{0.6^5+L^5}$. All $0 < L < 1$ with $L \neq \frac{1}{2}$ are polarised steady states; (a) Plot of $g_2(L)$; (b) plot of $\frac{g_2(1-L)}{g_2(L)}$ and $\frac{1-L}{L}$; the two curves intersect only at $L = \frac{1}{2}$, hence (3.6) is satisfied and therefore the polarised steady state exists for appropriate values of d; (c) plot of $\phi(L)$, it is positive for all L which we consider; the circle at $L = \frac{1}{2}$ indicates that $\phi(L)$ is not defined at this point.

Unpolarised period two patterns cannot arise for (3.4) because the initial amount of activity is the same in each cell and is conserved within a cell. In Section 3.2 we will show that there is no instability to polarised period two perturbations.

3.2 Stability analysis

Linearising (3.4) about a homogeneous steady state L by substituting $L_j = L + \tilde{l}_j$ yields

$$\begin{aligned}\frac{\mathrm{d}\tilde{l}_j}{\mathrm{d}\tau} &= g(L+\tilde{l}_{j+1})(1-L-\tilde{l}_j) - g(1-L-\tilde{l}_{j-1})(L+\tilde{l}_j) + d(1-2L-2\tilde{l}_j)\\ &\approx -g(L)\tilde{l}_j + g'(L)\tilde{l}_{j+1}(1-L) - g(1-L)\tilde{l}_j + g'(1-L)\tilde{l}_{j-1}L - 2d\tilde{l}_j.\end{aligned}$$

Substituting $\tilde{l}_j = L_0 e^{ikj+\lambda\tau}$ with $L_0, k, \lambda \in \mathbb{R}$ we get the dispersion relation

$$\lambda(k) = -g(L) + g'(L)e^{ik}(1-L) - g(1-L) + g'(1-L)e^{-ik}L - 2d, \tag{3.13}$$

which gives us the growth rate of perturbations as a function of their wave number. Figure 3.5 shows $\lambda(k)$ for the homogeneous unpolarised steady state with $g(x) = \frac{2x^5}{0.6^5+x^5}$ and different values of d. For $d \leq 1.47$ the growth rate $\lambda(k) > 0$ for certain k and the fastest growing mode is $k = 0$. Hence, the homogeneous unpolarised steady state of system (3.4) is unstable to homogeneous perturbations; we get polarity. For $d \geq 1.47$ we see $\lambda(k) < 0$ for all k, i.e. the homogeneous unpolarised steady state is stable to homogeneous and inhomogeneous perturbations; the cells remain unpolarised. Note, that $d = 1.47$ corresponds to the maximum value of $\phi(L)$ as shown in Figure 3.4(c).

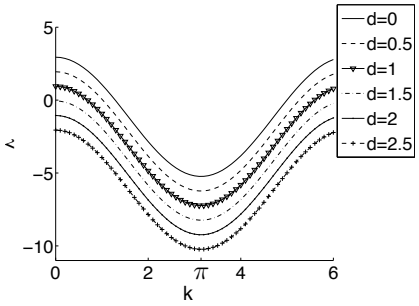

Figure 3.5: Dispersion relation (3.13) of the homogeneous unpolarised steady state $L = \frac{1}{2}$ of (3.4) for $g = \frac{2x^5}{0.6^5+x^5}$ and different values of d. For $d \leq 1.47$ the system is unstable to perturbations for certain k and the system polarises. For $d \geq 1.47$ the system is stable to homogeneous and inhomogeneous perturbations, all cells remain unpolarised.

Because of (3.13) the homogeneous unpolarised steady state $L = \frac{1}{2}$ is stable if $-g(\frac{1}{2}) + \frac{1}{2}g'(\frac{1}{2})\cos k < d$ for all k, i.e., if

$$-g\left(\frac{1}{2}\right) + \frac{1}{2}g'\left(\frac{1}{2}\right) < d, \tag{3.14}$$

since $g'(x) > 0$ for all x. Setting $h(L) := g(L)(1-L) - g(1-L)L + d(1-2L)$, the right hand side of (3.4) at a homogeneous steady state, we can rewrite (3.14) as $h'(\frac{1}{2}) < 0$.
The homogeneous polarised steady state $L \neq \frac{1}{2}$ is stable if

$$\frac{-g(L) + g'(L)\cos k(1-L) - g(1-L) + g'(1-L)L\cos k}{2} < d \qquad \text{for all } k, \tag{3.15}$$

since g is real. The left hand side of (3.15) is maximal for $\cos k = 1$. Thus, if (3.15) holds for $k = 0$ it holds for any k. Therefore, the stability condition (3.15) can be written as $h'(L) < 0$. The system cannot be simultaneously stable to homogeneous perturbations and unstable to inhomogeneous perturbations. Furthermore, the fastest growing mode is $k = 0$. Therefore, the system is also stable to polarised period two perturbations.
In summary, we get $h(0) \geq 0$, $h(1) \leq 0$, $h(0) = -h(1)$, $h(\frac{1}{2}) = 0$ and $h'(0) = h'(1)$. The

graph of h is rotationally symmetric about $(\frac{1}{2}, 0)$. The above stability analysis reveals that a homogeneous steady state L is stable if $h'(L) < 0$. Depending on the form of the function g and the value of d the function h has different forms, as illustrated in Figure 3.6. In Figure 3.6(a) there is a stable pair of homogeneous polarised steady states and the homogeneous unpolarised steady state is unstable. Figure 3.6(b) shows an example in which only the homogeneous unpolarised steady state is stable. We call these two cases monostable. The last two cases, in Figure 3.6(c) and (d), we refer to as a bistable cases because a pair of homogeneous polarised steady states as well as the homogeneous unpolarised steady state are stable. Furthermore, there exists a second pair of homogeneous polarised steady states, which are unstable. Although the graphs look essentially the same in these two figures we present both cases because the bifurcation diagrams corresponding to the two functions g are different as shown in Figure 3.7 (b) and (c).

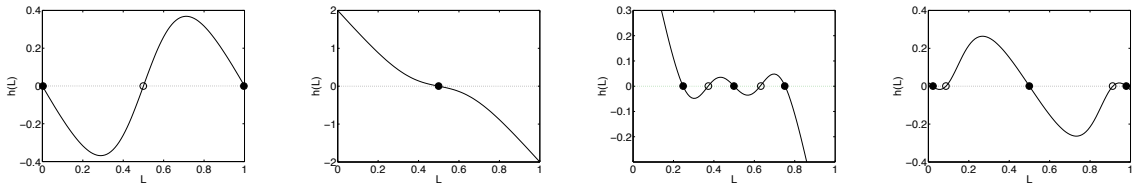

(a) (b) (c) (d)

Figure 3.6: Graphs of $h(L)$ for different forms of g and values of d, circles indicate unstable steady states, dots stable steady states; (a) Monostable case, $g(x) = \frac{2x^5}{0.6^5+x^5}$ and $d = 0$; (b) monostable case, $g(x) = \frac{2x^5}{0.6^5+x^5}$ and $d = 1.5$; (c) bistable case, $g(x) = \frac{2x^6}{0.4^6+x^6}$ and $d = 0.8$; (d) bistable case, $g(x) = \frac{x^3}{0.2^3+x^3}$ and $d = 0.02$.

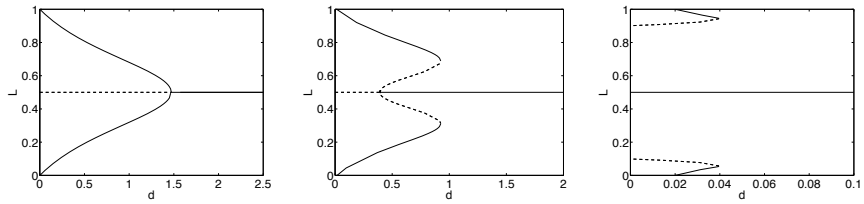

(a) (b) (c)

Figure 3.7: Bifurcation diagrams for (a) $g(x) = \frac{2x^5}{0.6^5+x^5}$, (b) $g(x) = \frac{2x^6}{0.4^6+x^6}$ and (c) $g(x) = \frac{x^3}{0.2^3+x^3}$; increasing d above a threshold disrupts polarity.

Figure 3.7 shows the bifurcation diagrams for $g(x) = \frac{2x^5}{0.6^5+x^5}$, $g(x) = \frac{2x^6}{0.4^6+x^6}$ and $g(x) = \frac{x^3}{0.2^3+x^3}$. In Figure 3.7(a) and (b) we see branches of polarised steady states connecting to $L = \frac{1}{2}$ as expected from our analysis in the previous section, since for the corresponding functions g equation (3.12) holds. In Figure 3.7(a) the branches are of stable polarised

steady states while in Figure 3.7(b) we have unstable branches. For g corresponding to Figure 3.7(c) equation (3.12) is not fulfilled and the branches of polarised steady states are not connected to $L = \frac{1}{2}$.

Combining the result in Figure 3.7(a) with the results in the previous section we see that for $g(x) = \frac{2x^5}{0.6^5+x^5}$ the polarised steady states are stable whenever they exist. Furthermore, 3.7(a) shows that as we increase d from zero the polarity gets weaker until the two branches for the two homogeneous polarised steady states merge with the branch for the homogeneous unpolarised steady state. However, for $g(x) = \frac{2x^6}{0.4^6+x^6}$ (Figure 3.7(b)) and $g(x) = \frac{x^3}{0.2^3+x^3}$ (Figure 3.7(c)) the branches for stable polarised steady states do not merge but stable and unstable polarised steady states disappear if d is increased above about 0.9 or 0.04, respectively. Hence, in this model, increasing the diffusion parameter d above a certain threshold, depending on g, disrupts polarity and results in only the homogeneous unpolarised steady state being stable. It would be interesting to test experimentally whether increasing the intracellular movement of components of the PCP pathway would lead to failure of polarisation. In experiments polarity is detected by the direction of the hair growth. So far there has not been a measure for the strength of polarisation. Therefore, it does not seem possible to distinguish the two different types of failure we have presented in Figure 3.7 in experiments.

3.3 Travelling wave solutions

If $h'(\frac{1}{2}) > 0$, system (3.4) has an unstable unpolarised steady state $L = \frac{1}{2}$ and a stable polarised steady state $L^* > \frac{1}{2}$, since $h(1) \leq 0$. Thus, we expect waves taking $L_j = \frac{1}{2}$ to $L_j = L^*$ similar to the travelling wave solutions of Fisher's equation [32], since the solutions are bounded between steady states and we expect a lower bound on the wave speed in some cases. Different to Fisher's equation, we consider a discrete system, which was previously done by a number of authors (see e.g. [11, 20, 34] and references therein). Introduction of the travelling wave coordinate $s = j - c\tau$ with $L_j(\tau) = f(j - c\tau) = f(s)$ yields

$$-c\frac{\mathrm{d}f}{\mathrm{d}s} = g(f(s+1))(1-f(s)) - g(1-f(s-1))f(s) + d(1-2f(s))$$

with

$$0 \leq f \leq 1, \lim_{s\to-\infty} f(s) = L^* \text{ and } \lim_{s\to+\infty} = \frac{1}{2}.$$

Linearising about a steady state F with $f(s) = F + \tilde{f}(s)$, we get

$$-c\frac{\mathrm{d}\tilde{f}}{\mathrm{d}s} \approx -g(F)\tilde{f}(s) + g'(F)\tilde{f}(s+1)(1-F) - g(1-F)\tilde{f}(s) + g'(1-F)\tilde{f}(s-1)F - 2d\tilde{f}(s).$$

Assuming $\tilde{f}(s) = F_0 e^{\lambda s}$ and dividing by $F_0 e^{\lambda s}$ yields

$$-c\lambda = -g(F) - g(1-F) + g'(F)e^{\lambda}(1-F) + g'(1-F)e^{-\lambda}F - 2d. \tag{3.16}$$

Provided that the initial amount $L_j(0) \in [\frac{1}{2}, L^*)$, the activity on the left side of the cell will never decrease below $\frac{1}{2}$; hence, there are no spatially oscillatory solutions. We will show this by contradiction. Let $L_j(0) \geq \frac{1}{2}$ for all j and assume $j = k$ is the first point at which L_j crosses through $\frac{1}{2}$ at time $\tau = \tau^*$. Hence, we would have $L_k(\tau^*) = \frac{1}{2}, L_{k+1}(\tau^*) \geq \frac{1}{2}$, $L_{k-1}(\tau^*) \geq \frac{1}{2}$ and $\frac{\mathrm{d}L_k}{\mathrm{d}\tau}(\tau^*) \leq 0$. However, substituting $L_k = \frac{1}{2}$ into (3.4) yields

$$\frac{\mathrm{d}L_k}{\mathrm{d}\tau}(\tau^*) = \frac{1}{2}(g(L_{k+1}) - g(1 - L_{k-1})) \geq 0,$$

with equality only if $L_{k+1} = L_{k-1} = \frac{1}{2}$, since g is increasing. Either $\frac{\mathrm{d}L_k}{\mathrm{d}\tau}(\tau^*) > 0$ and we have a contradiction or $\frac{\mathrm{d}L_k}{\mathrm{d}\tau}(\tau^*) = 0$. Applying the same argument to $L_{k\pm1}(\tau^*)$ we will eventually get the above contradiction or find that $L_j(\tau^*) = \frac{1}{2}$ for all j. Thus, there are no spatially oscillatory solutions about $L = \frac{1}{2}$ of system (3.4) given the above initial conditions. The wave speed c is therefore determined by the condition that there have to be real roots of equation (3.16). Substituting $F = \frac{1}{2}$, i.e., looking ahead of the wave, into (3.16) yields

$$-c\lambda = -2\left(g\left(\frac{1}{2}\right) + d\right) + g'\left(\frac{1}{2}\right)\cosh(\lambda), \tag{3.17}$$

with the two cases

$$-2\left(g\left(\frac{1}{2}\right) + d\right) + g'\left(\frac{1}{2}\right) < 0 \ (L = \tfrac{1}{2} \text{ is stable}): \text{ two real roots for all } c,$$
$$-2\left(g\left(\frac{1}{2}\right) + d\right) + g'\left(\frac{1}{2}\right) > 0 \ (L = \tfrac{1}{2} \text{ is unstable}): \text{ real roots only if } c \geq c_{min},$$

since $\min_{\lambda\in\mathbb{R}} \cosh(\lambda) = 1$. Figure 3.8 shows the plots of the two sides of (3.17) for $g(x) = \frac{2x^6}{0.4^6+x^6}$ and $d = 0.6$ as an example of the first case and for the same g and $d = 0.3$ as an example of the second case (see also Figure 3.7(b), for $d = 0.6$ we have bistability and for $d = 0.3$ monostability).

We can see that the right hand side of (3.17) is minimal at zero. In the first case, in Figure 3.8(a),the value at this minimum is less than zero, whereas in the second case it is greater than zero (see Figure 3.8(b)). Since all graphs for the left hand side of (3.17) go through the origin we get two real roots for all c in Figure 3.8(a) and only real roots for c above a certain minimum value in Figure 3.8(b). For our choice of g and d this minimum value is $c_{min} = 1.198$.

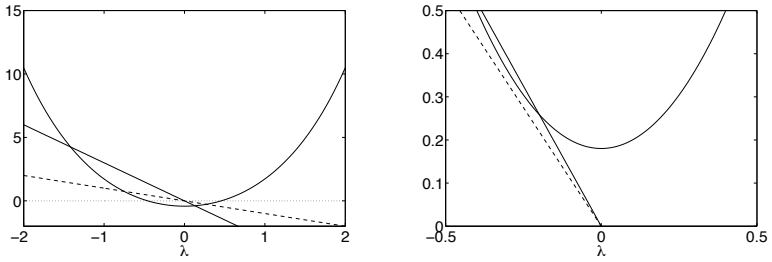

(a) (b)

Figure 3.8: Graphs of the two sides of equation (3.17) for $g(x) = \frac{2x^6}{0.4^6+x^6}$ and different d to determine the possible wave speeds c of the travelling wave solution of system (3.4); (a) $d = 0.6$, there are two real roots for all c, i.e. any c is a wave speed (solid straight line $c = 3$, dashed straight line $c = 1$); (b) $d = 0.3$, we only get real roots if $c \geq c_{min}$, i.e. a minimum wave speed c_{min} exists, in this case $c_{min} = 1.198$ (solid straight line $c = 1.3$, dashed straight line $c = 1.1$).

Now we want to investigate whether the speed of the wave depends on its direction. To this end, we assume that initially we have a single polarised cell (L_p, R_p) in the middle of a row of unpolarised cells as illustrated in Figure 3.9. For suitable choices of g and d, a polarising wave is initiated by cell p at $\tau = 0$ and spreads out in both directions into the unpolarised regions. We want to analyse the speed of this wave. Therefore, we assume (L_p, R_p) either equals $(L^*, 1 - L^*)$ or $(1 - L^*, L^*)$ for $L^* > \frac{1}{2}$. First, let $L_p = L^*$ in the initial conditions.

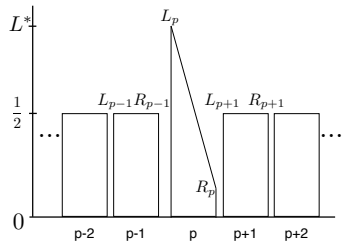

Figure 3.9: Initial conditions for system (3.4), which we use as an example to show that the speed of a wave may depend on its direction.

By substituting in (3.4) we get

$$\left.\frac{\mathrm{d}L_{p+1}}{\mathrm{d}\tau}\right|_{\tau=0} = \frac{1}{2}\left(g\left(\frac{1}{2}\right) - g(1-L^*)\right) \geq 0,$$
$$\left.\frac{\mathrm{d}L_{p-1}}{\mathrm{d}\tau}\right|_{\tau=0} = \frac{1}{2}\left(g(L^*) - g\left(\frac{1}{2}\right)\right) \geq 0,$$

since g is increasing. Therefore, if $g(\frac{1}{2}) - g(1-L^*) < g(L^*) - g(\frac{1}{2})$, the initial perturbation spreads faster to the left (decreasing indices). By symmetry, we conclude if $L_p = 1 - L^*$ initially and $g(\frac{1}{2}) - g(L^*) < g(1-L^*) - g(\frac{1}{2})$, the early perturbation spreads faster to the

right (increasing indices). This analysis suggests that the speed of the wave may depend on its direction.

3.4 Numerical simulations

We simulated the model (3.4) for a row of cells using the Matlab ODE solver ode45. The boundary conditions were $l_0 = l_1$ and $l_{101} = l_{100}$, which are compatible with the boundary conditions we chose for the analysis of the homogeneous perturbations. Moreover, we see in Figure 3.11 that the boundary conditions do not have a significant effect on the travelling wave solution as soon as the wave front has moved away from the boundary.
We state the times to reach the polarised steady state as this is the state that has been observed in the *Drosophila* wing. As mentioned before, according to [44], in experiments the polarisation of the wing cells takes about 32 hours, 18 hours for the recruitment of the core proteins to the membrane and 14 hours to establish their polarised distribution. We see that the times to reach the steady state in our simulations are in a reasonable range.

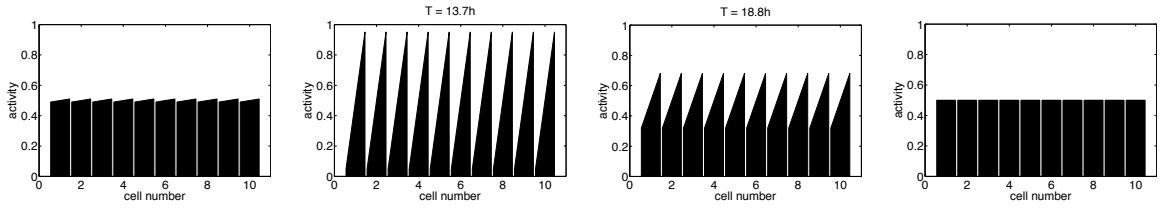

(a) (b) (c) (d)

Figure 3.10: Final states for system (3.4), with $g(x) = \frac{2x^5}{0.6^5+x^5}$ and different values for the diffusion parameter d; (a) Initial condition, $L_j = 0.49$ for all j; (b) final state for $d = 0.1$, strong polarity; (c) final state for $d = 1$, weaker polarity; (d) final state for $d = 1.9$, unpolarised steady state.

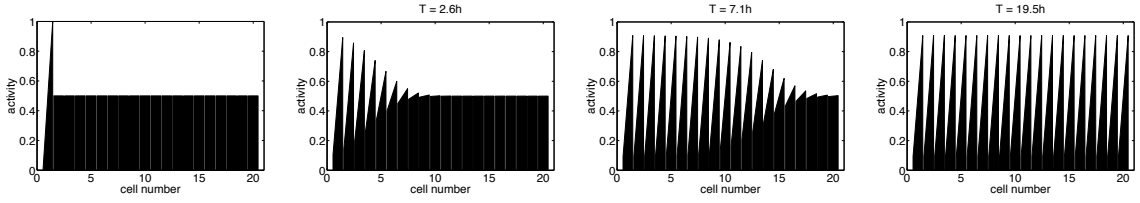

(a) (b) (c) (d)

Figure 3.11: Wave propagation; (a) Initial condition; (b)-(d) the state of system (3.4) at different points in time for $g(x) = \frac{2x^5}{0.6^5+x^5}$ and $d = 0.2$.

Figures 3.10 and 3.11 show the final states for two different initial conditions. In Figure 3.10(a) there is an initial imbalance in each cell for the whole row. The simulations were

performed using $g(x) = \frac{2x^5}{0.6^5+x^5}$, a function for which we analysed the properties of system (3.4) in Section 3.2. Consistent with our analysis we get a strongly polarised steady state for $d = 0.1$ (see Figure 3.10(b)), which gets weaker as we increase d (see Figure 3.10(c)) and disappears once d is greater than a certain threshold (see Figure 3.10(d)). These results match the corresponding bifurcation diagram in Figure 3.7(a). The direction of the polarisation of the homogeneous polarised steady state depends only on the direction of the initial conditions. For $g(x) = \frac{2x^6}{0.4^6+x^6}$ and $d = 0.5$, a bistable case (see Figure 3.7(b)), we need sufficiently strongly polarised initial conditions to get polarisation, otherwise solutions evolve toward the homogeneous unpolarised steady state (result not shown). This is not surprising as we know from the analysis that both states are stable for this choice of g and d.

With the initial condition depicted in Figure 3.11(a) only the first cell of the row is polarised while the rest remain unpolarised. For small values of d this results in the propagation of a wave with a speed that depends on g. The wave for $g(x) = \frac{2x^5}{0.6^5+x^5}$ and $d = 0.2$ is shown in Figure 3.11. Weakening the polarity in the first cell of the initial condition does not change the final state or the time to reach it (result not shown).

The analysis in Section 3.3 shows that, for $g(x) = \frac{2x^5}{0.6^5+x^5}$ and $d = 0.2$, there exists a minimum wave speed which is 4.76. The wave speed calculated from the simulations is 4.69, which matches the theoretical value reasonably well. A difference of the wave speed for different directions could not be detected. We have conducted the same calculations and simulations for other choices of g. The results are summarised in Table 3.1, which shows the theoretical value for the minimum wave speed and the numerical values for both directions of the wave.

	Wavespeed		
Function g, Diffusion d	**Theoretical minimum value**	**Numerical value First cell init. (0,1)**	**Numerical value First cell init. (1,0)**
$g(x) = \frac{x^3}{0.6^3+x^3}$, $d = 0.3$	0.41	0.4	0.4
$g(x) = \frac{3x^4}{0.7^4+x^4}$, $d = 0.1$	4.63	4.6	4.6
$g(x) = \frac{2x^6}{0.4^6+x^6}$, $d = 0.15$	1.96	**1.9**	**4.9**
$g(x) = \frac{4x^3}{0.5^3+x^3}$, $d = 0.5$	3.51	**3.4**	**4.3**

Table 3.1: Theoretical and numerical results of wave speed calculations for (3.4) for different choices of g and d and different initial conditions. In the first and the second row the speed of the wave does not depend on its direction. In the third and fourth row the wave moves faster if the first cell is initially polarised to the left.

The theoretical value of the minimum wave speed and the minimum of the numerical values of the wave speed agree well. In the first two cases the wave speed does not depend on the direction, whereas in the third and fourth case we get a significant difference. For these latter cases the wave is faster if the first cell in the initial conditions is polarised to the left, i.e., $(L_1, R_1) = (1, 0)$. For an initial condition as in Figure 3.9 this would mean that the wave moves faster to the right (increasing indices), which matches our earlier analysis since the inequality $g(0.5) - g(0) > g(1) - g(0.5)$ holds for the two choices of g in the third and fourth row of Table 3.1.

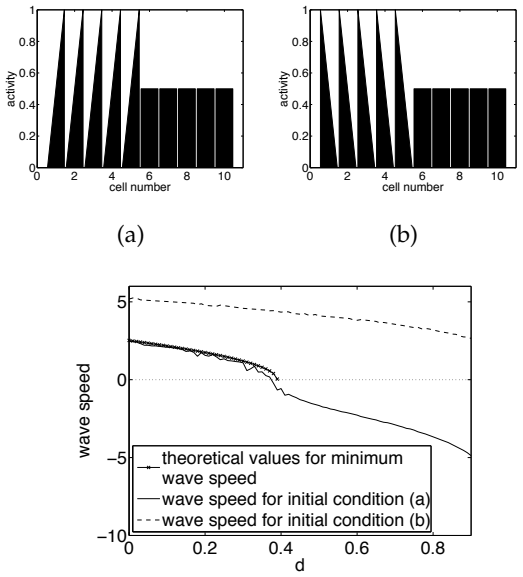

Figure 3.12: Analysis of the travelling wave solution of system (3.4) for $g(x) = \frac{2x^6}{0.4^6+x^6}$; (a) Initial condition which can give waves in both directions; (b) initial condition which only gives a wave to the right; (c) graphs of the theoretical value of the minimum wave speed and the wave speed for initial condition (a) and (b).

We analysed the travelling wave solution for $g(x) = \frac{2x^6}{0.4^6+x^6}$ in more detail, since it shows a strong difference in wave speeds for the different directions. In the corresponding bifurcation diagram (see Figure 3.7(b)) we can see that there is an interval (d_1, d_2) for which system (3.4) is bistable. Starting with the initial condition in which the first five cells are initially polarised to the right and the rest of the row is unpolarised (Figure 3.12(a)) we found that for $d < d_1$ the wave front moves to the right into the unpolarised region and for $d > d_1$ it moves to the left into the polarised region. Hence, we expect propagation failure at d_1. This is supported by Figure 3.12(c), which shows the speed of simulated waves as a function of the diffusion parameter d. The wave speed is positive up to a d close to 0.4 and then becomes negative. Where applicable the simulated speed agrees well with the the-

oretical values for the minimum wave speed. If we choose the initial condition in Figure 3.12(b), where the first five cells of the row are initially polarised to the left, we do not get propagation failure (see dashed line in Figure 3.12(c)). To obtain the data for the graphs in Figure 3.12(c) we repeat the calculation of the wave speed after fixed time steps for a fixed d until the change in the speed between one time step and the next is below a certain threshold. Due to this method and since the system is discrete, it is to be expected that the graphs are not entirely smooth.

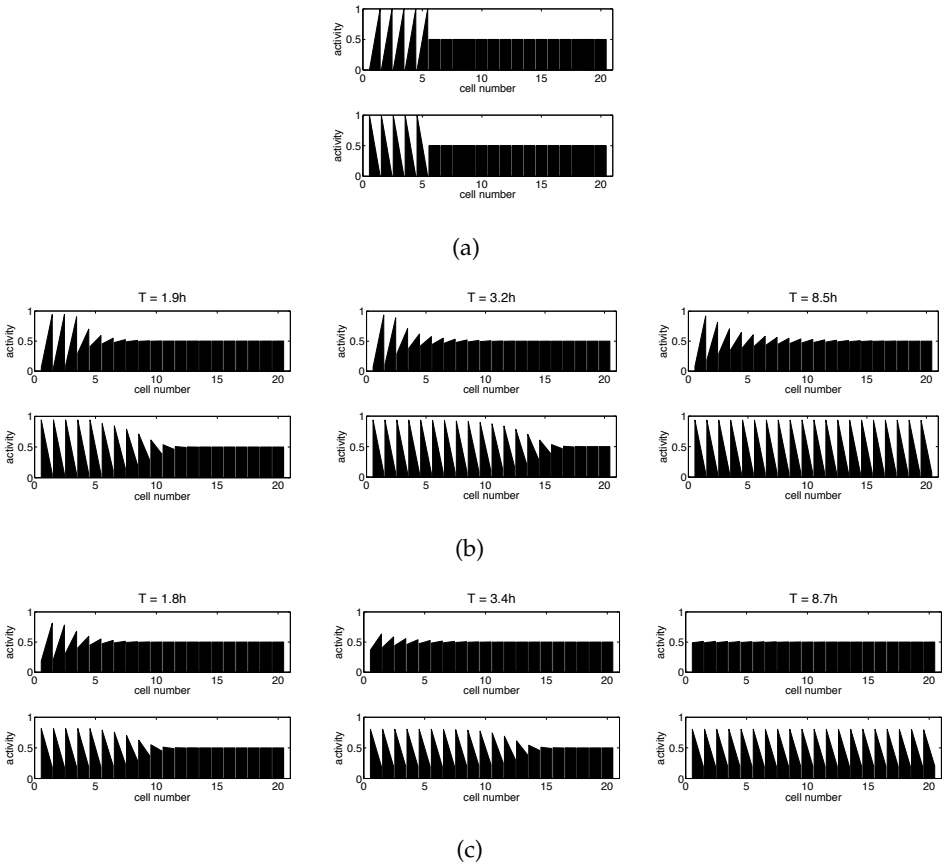

Figure 3.13: Snapshots of the travelling wave solution of system (3.4) for $g(x) = \frac{2x^6}{0.4^6+x^6}$; (a) Initial conditions as in Figures 3.12(a) and (b); (b) the states of system (3.4) at different points in time for $d = 0.15$ and the initial conditions in (a); (c) the states of system (3.4) at different points in time for $d = 0.6$ and the initial conditions in (a)

Figure 3.13 shows the travelling wave solution for the two initial conditions and different values of d at different points in time. For $d = 0.15$, Figure 3.13 (b) shows the difference in wave speed. For $d = 0.6$ the top row of Figure 3.13 (c) shows the wave reversal while the wave in the bottom row is not reversed but slower than the wave in the bottom row

for $d = 0.15$ in Figure 3.13 (b). We obtained similar results for other choices of g for which system (3.4) is bistable for some d.
The behaviour of the travelling wave solutions is fascinating. The different wave speeds in the different directions in some of the cases would suggest that the two steady states $(0,1)$ and $(1,0)$ are fundamentally different. This conclusion however is contradicted by the results for other travelling wave solutions which show the same speed in both directions. Further analysis is needed to improve the understanding of this matter.

Behaviour for irregularities in the initial conditions

To analyse the behaviour of the model when the initial conditions contain irregularities we distinguish between polarisation because of a global weak initial polarity as in Figure 3.10 and polarisation via a wave as in Figure 3.11. In the case of the global weak initial polarity we introduced a number of cells that are weakly polarised in the wrong direction (see Figure 3.14 (a)). We choose $g(x) = \frac{2x^5}{0.6^5+x^5}$, the function used to generate Figures 3.10 and 3.11. In Figure 3.14 we see that each cell in the row initiates a wave and the meeting of the wave fronts determines whether an irregularity is corrected. For our choice of parameter values and initial conditions, eventually we get correct polarity over the whole row.

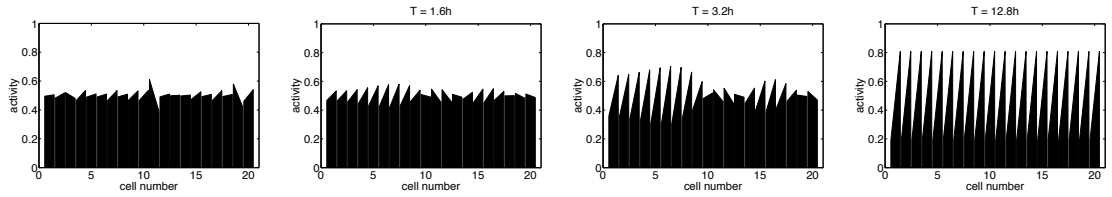

(a) (b) (c) (d)

Figure 3.14: Irregularities in the global initial polarity can be corrected by system (3.4); (a) Initial condition; (b)-(d) state of system (3.4) at different points in time for $g(x) = \frac{2x^5}{0.6^5+x^5}$ and $d = 0.5$.

To analyse the potential of a wave to overcome anomalies in the initial conditions we included one cell that points in the wrong direction (see Figures 3.15(a) and 3.16(a)). In Figure 3.15 we chose $g(x) = \frac{2x^6}{0.4^6+x^6}$ and $d = 0.1$. We see that the wave to the right initiated by cell 8 is faster than the one initiated by cell 1. Furthermore, the wave to the left initiated by cell 8 overcomes the wave from cell 1 to the right. As a result we get polarity in the wrong direction. For Figure 3.16 we chose $g(x) = \frac{x^8}{0.8^8+x^8}$ and $d = 0.1$, for which a wave to the right initiated by cell 1 in Figure 3.16(a) is faster than a wave to the right initiated by cell 8. We see in Figures 3.16(b)-(d) that the two waves meet and the one initiated by the first cell in the row overcomes the one initiated by the irregular cell. Hence, this wave can

correct single cells that initially point the wrong way.

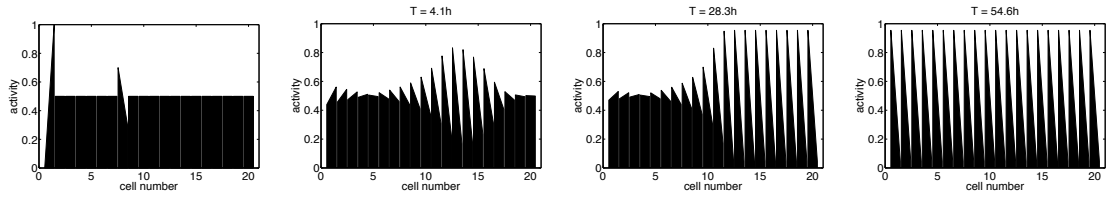

(a) (b) (c) (d)

Figure 3.15: Example of a travelling wave solution of (3.4) that cannot correct a single cell with incorrect polarity; (a) Initial condition, one cell is initially polarised the wrong way; (b)-(d) state of system (3.4) at different points in time for $g(x) = \frac{2x^6}{0.4^6+x^6}$ and $d = 0.1$.

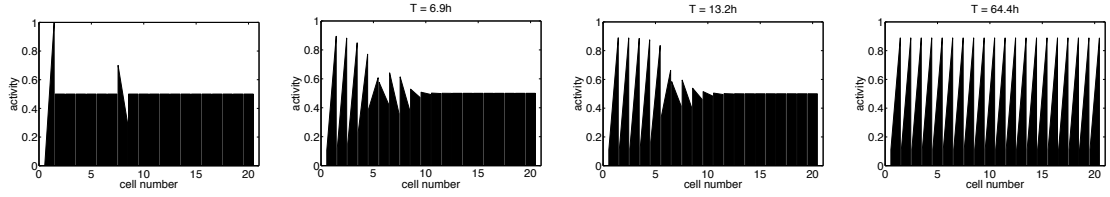

(a) (b) (c) (d)

Figure 3.16: Example of a travelling wave solutions of (3.4) that can correct single cells with incorrect polarity; (a) Initial condition, one cell is initially polarised in the wrong direction; (b)-(d) state of system (3.4) at different points in time for $g(x) = \frac{x^8}{0.8^8+x^8}$ and $d = 0.1$.

Most of the dynamics in a row of cells can be explained by the interactions of only two cells. These are summarised in the phase plane in Figure 3.17, for which we chose the same function $g(x)$ and diffusion coefficient d as in Figure 3.16. There are three steady states, indicated by crosses, two polarised steady states are stable and the unpolarised steady state is unstable. If we imagine the diagonal from $(0,1)$ to $(1,0)$, for every initial condition above this diagonal the system will tend to the left-pointing polarised steady state and from anywhere below the diagonal it will tend to the right-pointing polarised steady state. For example, if we start at $(0.39, 0.58)$, the values corresponding to cells 5 and 6 in Figure 3.16(b) the phase plane predicts these two cells will tend to the right-pointing steady state. An example of this behaviour is shown in Figure 3.16(c).

The analysis reveals that whether or not a wrongly polarised cell can be corrected by a polarising wave depends on the initial distance between this anomaly and the wave front and the strength of the anomaly. In addition we have to take into account that the wave might have a different speed depending on its direction. In Figure 3.16 we could get correct polarity, because the wave to the right initiated by cell 1 is faster than the wave in the same

direction initiated by cell 8. We present a quantitative analysis of the robustness of this model in the next section.

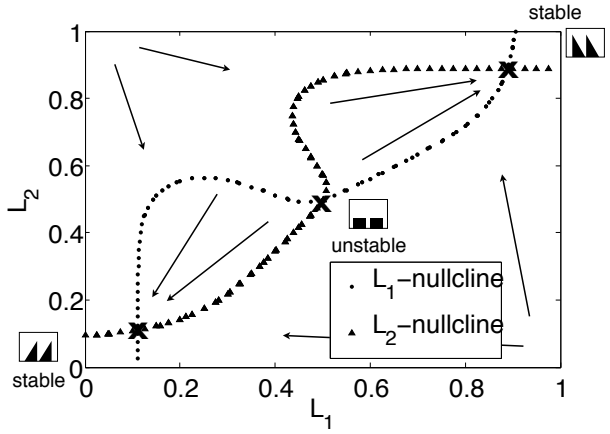

Figure 3.17: Phase plane for system (3.4) for two cells with $g(x) = \frac{x^8}{0.8^8+x^8}$ and $d = 0.1$. There are three steady states,indicated by crosses, two of which are stable. The diagonal from (0,1) to (1,0) is the separatrix; initial conditions above this diagonal yield the left-pointing polarised steady state and initial conditions below it give rise to the right-pointing polarised steady state.

Robustness of the model

To analyse the robustness of this model we use the same approach as for the feedback and diffusion model, presented in Section 2.1.3. Thus, as initial conditions we assume

$$l_i = \frac{1}{2} - u + kU\left(-\frac{1}{2}, \frac{1}{2}\right),$$

for all i, with a fixed $u \in [0, \frac{1}{2}]$, a fixed $k \in [0, 1-2u]$ and $U(-\frac{1}{2}, \frac{1}{2})$ denoting a uniform distribution on $[-\frac{1}{2}, \frac{1}{2}]$. Hence, if $k < 2u$, then all cells have a right-pointing bias initially; if $k > 2u$, then we expect a fraction $f = \frac{1}{2} - \frac{u}{k}$ of cells to have a left-pointing bias initially. Again, we choose $0 \leq u \leq \frac{1}{2}$ and $0 \leq k \leq 1-2u$ and vary the two parameters in steps of 0.01. For every parameter set (u, k) we conduct 100 simulations for a row of 50 cells and calculate the mean ratio of cells in the final state pointing to the right. Figure 3.18 shows the results for $g(x) = \frac{2x^5}{0.6^5+x^5}$ and $d = 0.2$. For pairs (u, k) in the area below the dashed line all the cells have a right-pointing bias initially and hence 100% of the cells in the final state point to the right. Increasing k above the dashed line increases the number of cells initially pointing to the left. As shown, this decreases the percentage of cells in the final state pointing to the right. The continuous lines indicate the thresholds below which on average at least 95% and 75% of the cells in the final state point to the right. The average

percentages of cells initially pointing to the right for parameter values on these lines are 56% and 50%. This indicates that a significant fraction of cells initially pointing the wrong way can be corrected. Even if almost half the cells have a wrong initial imbalance we can nearly get normal final polarity.

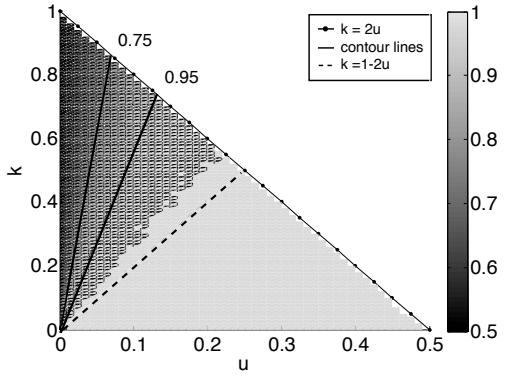

Figure 3.18: Robustness analysis of system (3.4) for $g(x) = \frac{2x^5}{0.6^5+x^5}$ and $d = 0.2$. The average ratio of cells in the final state pointing to the right is shown (indicated by the shading); it is calculated as the mean of the results of 100 simulations for a row of 50 cells. The parameter k is varied between 0 and $1-2u$ and u between 0 and $\frac{1}{2}$. For values (u,k) below the dashed line all cells point to the right in the initial conditions and hence also in the final state. Increasing k increases the noise in the system and the average percentage of cells pointing to the right in the final state is decreased. For parameter values below the continuous lines, on average at least 95% and 75% of the cells point to the right in the final state.

Analysis of clones

Similar to Section 2.1.3 we include clones in the row of cells and investigate their effects on the surrounding cells. Figure 3.19 shows the results for a clone in which the cells have less activity than the wild-type cells. Thus, the total amount of activity in each clonal cell is set to $q < 1$. As feedback function we have chosen $g_1(x) = \frac{2x^6}{0.4^6+x^6}$. The corresponding bifurcation diagram for this choice of g in Figure 3.7(b) shows that system (3.4) exhibits two bifurcations at $d_1 \approx 0.4$ and $d_2 \approx 0.9$. The initial conditions are shown in column 1 of Figure 3.19. The difference between the two initial conditions is the strength of the initial global cue in the surrounding wild-type cells. Columns 2-4 display the resulting final states for different values of d. At both boundaries of the clone a patterning wave is initiated which propagates away from the clone.

Domineering non-autonomy occurs in the direction of the initial global cue. As can be seen in Figure 3.19 its range depends both on the strength of the global cue in the surrounding cells and the diffusion parameter. Increasing the strength of the global cue decreases the range of domineering non-autonomy. Increasing d up to d_2 increases the range of the effect of the clone (exemplified by Figure 3.19, column 3). If $d > d_2$ the polarisation initiated at the clone boundaries spreads only a few cells into the surrounding region (see Figure 3.19, column 4). The rest of the wild-type cells are unpolarised. This is due to the fact that for this choice of $g(x)$ and d there exists no longer a polarised steady state of system (3.4). In this case, the unpolarised state is the only stable steady state (see also Figure 3.7(b)). Simulations using $g_2(x) = \frac{2x^5}{0.6^5+x^5}$ gave similar results. Considering the direction of the effect of the clone, the results in Figure 3.19 column 2 and 3 resemble the experimental results for clones lacking Fz as described in Section 1.2.

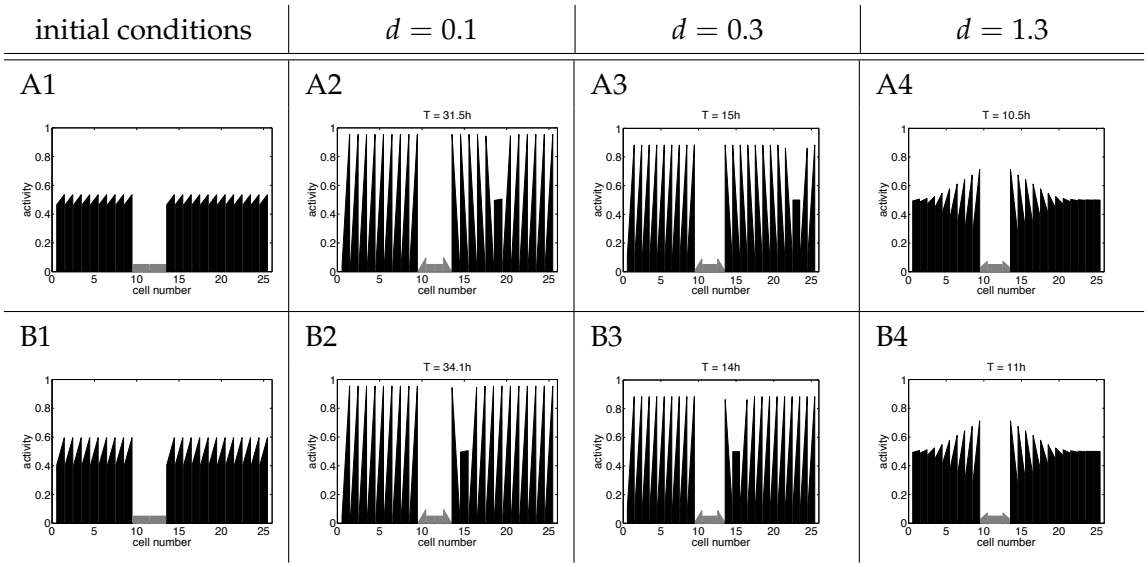

Figure 3.19: Final states of system (3.4) for a clone with low activity (shown in grey) and an initial polarisation in the surrounding cells. In the first row the difference between right and left side is initially 0.07, in the second row 0.19. Simulations were performed using $g_1(x) = \frac{2x^6}{0.4^6+x^6}$ and different values of d. Note that for $d = 1.3$ the polarised steady state is no longer stable.

As a next step, we set the activity in the clone to be higher than in the surrounding cells. For $g_1(x) = \frac{2x^6}{0.4^6+x^6}$, the clone does not affect polarity in surrounding cells for small d as shown in Figure 3.20(b). This is due to the difference in wave speed in different directions for this function (see Table 3.1). Any possible disruptions get corrected by a fast wave coming from the opposite side of the clone and moving through the clone. For $d = 0.5 > d_1$, the unpolarised steady state spreads as a wave from the clone in the direction opposite to the direction of the initial global cue. This is due to the bistability of the unpolarised

and the polarised steady state for this choice of d. If we decrease the strength of the initial global cue in the wild-type cells the polarisation of the cells on the other side of the clone fails as well. Increasing the diffusion coefficient to $d = 1.3 > d_2$ we get propagation failure on both sides of the clone.

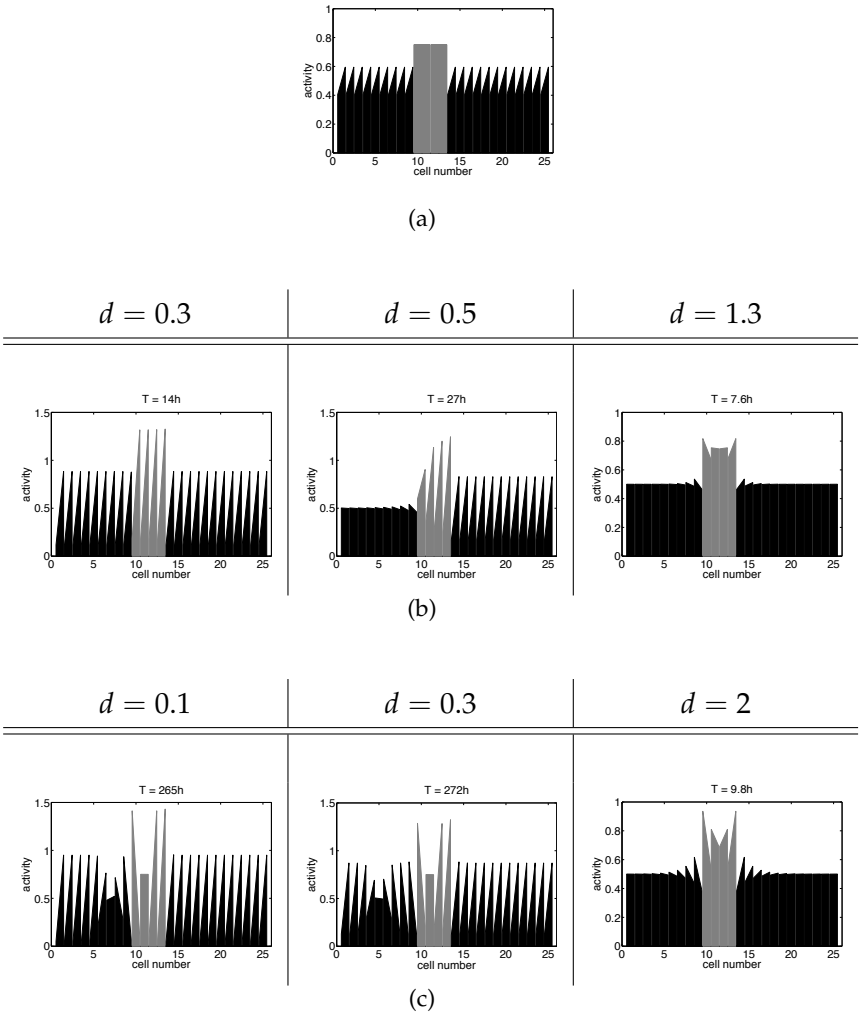

Figure 3.20: Final states of system (3.4) for a clone with high activity (shown in grey) and an initial polarisation in the surrounding cells; (a) Initial condition, in which the difference between right and left side in the wild-type cells is 0.19; (b) final states for $g_1(x) = \frac{2x^6}{0.4^6+x^6}$ and different values of d; (c) final states for $g_2(x) = \frac{2x^5}{0.6^5+x^5}$ and different values of d.

If we choose $g_2(x) = \frac{2x^5}{0.6^5+x^5}$ (see Figure 3.7(a) for corresponding bifurcation diagram), the disrupting effect of the clone spreads in the direction opposite to the direction of the initial global cue in the wild-type cells (see Figure 3.20(c)). As above, a weaker initial global cue yields a greater range of domineering non-autonomy. Furthermore, increasing d up to the

bifurcation point $d_3 \approx 1.4$ increases the range of the effect of the clone. For $d > d_3$ the polarisation initiated by the clone spreads only a short distance into the surrounding region. The rest of the wild-type cells are unpolarised. This is because the unpolarised state is the only stable steady state of system (3.4) for this choice of parameter values.

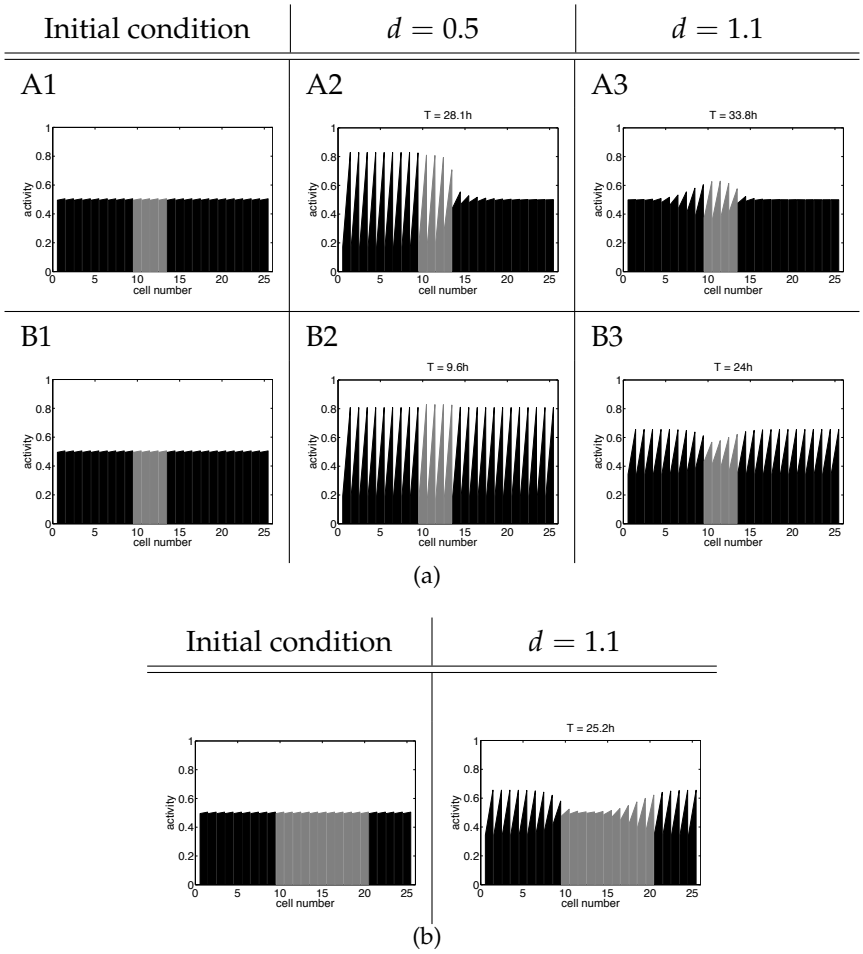

Figure 3.21: Effects of a clone of cells (shown in grey) with different strength of feedback than that in the surrounding cells; (a) Row A: feedback in the wild-type cells is represented by $g_1 = \frac{2x^6}{0.4^6+x^6}$, feedback in the clone by $g_2 = \frac{2x^5}{0.6^5+x^5}$; row B: g_2 represents the feedback in the wild-type cells and g_1 the feedback in the clone; (b) effect of a large clone; g_2 represents the feedback in the wild-type cells and g_1 the feedback in the clone; the polarising wave spreads from the wild-type cells into the clone.

Assigning a different feedback function to cells in the clone, compared to that in the surrounding cells, only yields an effect if for the chosen diffusion parameter d the stability of system (3.4) is different for the two feedback functions. Let $g_1(x) = \frac{2x^6}{0.4^6+x^6}$ represent the feedback function in the wild-type cells and $g_2(x) = \frac{2x^5}{0.6^5+x^5}$ the feedback in the clone. The

clone only affects surrounding cells if $0.4 \approx d_1 < d < d_3 \approx 1.4$, since for this choice of d the polarised state is the only stable steady state of system (3.4) for g_2 and for g_1 system (3.4) is bistable (see Figure 3.7) or only the unpolarised steady state is stable. If $d = 0.5$, system (3.4) is bistable for g_1. Figure 3.21(a) A2 shows that in this case polarisation spreads from the clone to the left. Increasing the initial global cue sufficiently will yield polarisation of the whole row. This is due to the bistability of system (3.4) for g_1 as mentioned at the beginning of Section 3.4.

If $d = 1.1$, for g_1 only the unpolarised steady state of system (3.4) is stable; for g_2 the polarised steady state is still stable. In Figure 3.21(a) A3 we see polarisation is initiated in the clone, spreading only a couple of cells into the surrounding region. It spreads a little further to the left. Reversing the initial polarity in Figure 3.21(a) A1, reverses the direction of the effect of the clone in A2 and A3.

If we choose g_1 as the feedback function in the clone and g_2 for the feedback in the surrounding cells we get the polarised steady state in the whole row for $d = 0.5$ (see Figure 3.21(a), B2). There is, however, a slight difference in the amount of activity between the clone and the surrounding cells, in that the peaks in the clone are slightly higher. For $d = 1.1$ a polarising wave spreads from both ends into the clone. Whether or not this wave can polarise the clone completely depends on the size of the clone, as shown in Figure 3.21(b). In Figure 3.21(b) the wave from the right side spreads further into the clone than from the left side because for our choice of g the wave is faster in that direction. Changing the strength of the initial global cue does not alter how far the waves spread into the clone (not shown).

3.5 Discussion

In this chapter we presented the conservative model, a mechanism that consists of amplification of an initial imbalance via a feedback loop. It is a generic approach representing a whole class of models, which also includes the more complex models by Amonlirdviman *et al.* [3] and Le Garrec *et al.* [29], that will be discussed in the following two chapters.

The conservative model can generate polarisation of a row of cells either as a result of a global weak initial polarisation of every cell or via a travelling wave emanating from a single cell or boundary. Both can be reasonable ways of spreading polarity over a whole region of cells. However, there are no experimental observations of the time course of the establishment of polarisation available, so far.

In addition to investigating the stability of steady states in this model, we also analysed

the behaviour of the travelling wave. We found that in some cases the speed of the wave depends on its direction of travel. For certain feedback functions the direction of the wave is determined by the diffusion coefficient. These features of the travelling wave solution might not be relevant for the understanding of the biological system. However, especially the difference of wave speed for different directions is mathematically interesting since this phenomenon is not common for travelling wave solutions. Exploring the factors determining this behaviour in more detail would be intriguing.

Including irregularities in the initial conditions, we demonstrated that the conservative model has the potential to overcome such anomalies and yield correct polarity for both a global initial polarity cue and under conditions that result in a travelling wave. We also analysed the effects of clones on the surrounding cells. For clones of cells having a different amount of PCP activity than that in surrounding cells, the strength of the initial global cue in the wild-type cells and the strength of the intracellular diffusion influence the range of the effect of the clone. Especially, for the clones with different strength of feedback compared to the surrounding cells, the effect of the clone was dependent on the stability behaviour of the model for the chosen parameters.

An analysis of the effects of noise in the initial conditions of this model revealed that for the parameter values considered it is more robust than the feedback and diffusion model in Chapter 2. Since this is due to the bistability of the homogeneous polarised steady state and the period two pattern in the feedback and diffusion model we expect similar results for different parameter sets.

We have restricted our analysis of the conservative model to one spatial dimension. However, it can be extended to fields of square or hexagonal cells in a similar manner as for the feedback and diffusion model in Section 2.2.

The main components determining polarity in the conservative model are the choice of the feedback function and the value of the diffusion coefficient. We mainly considered two types of feedback functions and found that in both cases, increasing the diffusion coefficient above a certain threshold disrupts polarity. The manner in which this occurred is what distinguishes the two feedback types. In one case polarity gets weaker until it disappears, whereas in the second case it disappears abruptly. It would be interesting to test this experimentally. To this end, it would first be necessary to determine what "strength of polarity" means in the context of the biological system. So far, polarity is determined by the direction of the hair growth in the wing and the abdomen or the orientation of the ommatidia in the eye. Therefore, only a direction but not a strength can be detected. Hence, it depends on what we mean by "activity" whether it is reasonable to speak of strength of polarity. Since the question of the interpretation of activity is similarly important for the

feedback and diffusion model, we further discuss this issue in Chapter 7.

Chapter 4

Analysis of the model by Amonlirdviman et al.

In the preceding chapters we developed two models that aim at describing the core of the PCP mechanism, while making minimal assumptions about the biological details. In this chapter, we consider a model that is centred around specific protein-protein interactions. The model we will discuss was introduced by Amonlirdviman *et al.* in [3]. It describes the amplification of an externally-imposed polarity in the pupal wings of the fruit fly *Drosophila melanogaster* as a result of interactions of the four proteins Dishevelled (Dsh), Frizzled (Fz), Van Gogh (Vang) and Prickle (Pk). The model aims at reproducing the experimentally observed asymmetric distribution of these core proteins shown in Figure 1.2. The mechanism consists of two main parts: a feedback loop and a persistent global bias. The readout is provided by the final distribution of total Dsh within each cell, i.e., the sum of the amount of Dsh in free form and bound in molecular complexes. The authors assume that the hair in each cell grows where the highest amount of total Dsh is accumulated. This is based on their observation that in clones lacking Dsh the hairs consistently emerge from the middle of the apical surface of each cell. The aim of this chapter is to investigate the relative importance of the feedback loop and the persistent global bias on the final distribution of total Dsh. To this end, we analyse the approach in one and two spatial dimensions.

The details of the model are presented in Figure 4.1. Fz is assumed to be located in the cell membrane. Fz recruits Dsh from the cytoplasm to its cell side and Vang to the membrane of the adjacent cell. Vang for its part causes Pk to colocalise at the cell edge. Feedback is included by Vang and Pk inhibiting the recruitment of Dsh. Furthermore, a persistent global bias is introduced that ensures that more Fz and Dsh colocalise at the distal end of

each cell than at the proximal end. There is no protein production or degradation.

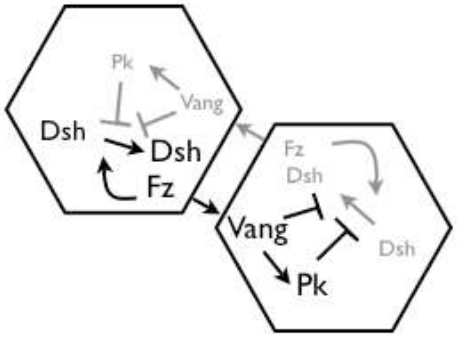

Figure 4.1: Proposed feedback loop. The amounts of proteins in black are higher than the amounts of proteins in grey. Arrows represent recruitment of proteins, T-signs inhibition.

Assuming that the proteins colocalise by forming complexes, the model can be summarised by the following reactions.

$$Dsh + Fz \underset{AB\lambda_1}{\overset{R_1}{\rightleftharpoons}} DshFz \tag{4.1}$$

$$Fz^+ + Vang \underset{\lambda_2}{\overset{R_2}{\rightleftharpoons}} FzVang \tag{4.2}$$

$$Vang + Pk \underset{\lambda_3}{\overset{R_3}{\rightleftharpoons}} VangPk \tag{4.3}$$

$$DshFz^+ + Vang \underset{\lambda_4}{\overset{R_4}{\rightleftharpoons}} DshFzVang \tag{4.4}$$

$$Dsh^+ + FzVang \underset{A^+B^+\lambda_5}{\overset{R_5}{\rightleftharpoons}} DshFzVang \tag{4.5}$$

$$Fz^+ + VangPk \underset{\lambda_6}{\overset{R_6}{\rightleftharpoons}} FzVangPk \tag{4.6}$$

$$FzVang + Pk \underset{\lambda_7}{\overset{R_7}{\rightleftharpoons}} FzVangPk \tag{4.7}$$

$$Dsh^+ + FzVangPk \underset{A^+B^+\lambda_8}{\overset{R_8}{\rightleftharpoons}} DshFzVangPk \tag{4.8}$$

$$DshFz^+ + VangPk \underset{\lambda_9}{\overset{R_9}{\rightleftharpoons}} DshFzVangPk \tag{4.9}$$

$$DshFzVang + Pk \underset{\lambda_{10}}{\overset{R_{10}}{\rightleftharpoons}} DshFzVangPk. \tag{4.10}$$

For each equation (4.i) there is a forward reaction rate R_i and a backward reaction rate λ_i. The superscript $+$ indicates that the two reactants are in different cells, binding over the cell membrane to form a cell bridging complex. Similarly, A^+ and B^+ indicate that these scaling factors depend on the protein values in the neighbouring cell. We assume

that the cell bridging complexes belong to the same cell as their Vang part. The different proteins and complexes have different regions in which they can move. Dsh and Pk occur in the cytoplasm. Fz, Vang, DshFz and VangPk can move along the whole membrane of a cell while the cell bridging complexes are restricted to the part of the membrane that is common to the two cells they connect.

The persistent global bias is built into the equations by decreasing the rate of dissociation of Dsh from Fz and Fz complexes at the distal side, so that the backward reaction rates of equations (4.1), (4.5) and (4.8) are multiplied by $A \leq 1$ with

$$A = \begin{cases} M_1, & \text{distal region of the cell,} \\ 1, & \text{otherwise,} \end{cases}$$

and $M_1 < 1$.

The feedback loop that consists of Vang and its complexes inhibiting the recruitment of Dsh is represented by an increase of the backward reaction rates of all the reactions in which Dsh binds to Fz or Fz complexes, namely (4.1), (4.5) and (4.8). To this end, those backward reaction rates are multiplied by a factor $B \geq 1$ with

$$\begin{aligned} B = 1 + K_b(K_{pk}[Pk] + [VangPk] + [FzVangPk] + [DshFzVangPk] \\ + K_{va}([Vang] + [FzVang] + [DshFzVang]))^{K_p} \end{aligned}$$

and constants K_b, K_{pk}, K_{va} and K_p. We see that B depends on the concentrations of Pk, Vang and their complexes, indicated by the square brackets. In [3] Amonlirdviman *et al.* applied the law of mass action to reactions (4.1)-(4.10) to obtain the corresponding system of PDEs, which they discretised applying the finite volume method and integrated numerically using the semi-implicit Euler method. They assumed a field of hexagonal cells, each of which is subdivided by a triangular mesh. The parameter values were determined by parameter optimisation applying the Nelder-Mead method, such that the wild-type polarity was achieved. Furthermore, experimental observations for the behaviour around clones could be reproduced. What remains unclear is whether both the feedback loop and the persistent global bias are necessary for the establishment of stable coherent patterns of cell polarity. We are aiming at analysing their relative importance for the generation of PCP. The full model in two spatial dimensions is rather complex and does not lend itself to analysis very easily. Therefore, as a first step we reduce the model to one spatial dimension.

4.1 Analysis in one spatial dimension

We assume a row of two-sided cells, similar to Chapters 2 and 3. On each side of a cell there are certain concentrations of the four proteins Dsh, Fz, Vang and Pk. Furthermore,

we assume that intracellular diffusion takes place, i.e. exchange of proteins between the two sides of a cell. Applying reaction kinetics, equations (4.1)-(4.10) yield a system of ODEs for cell i, which describes the protein interactions taking place. Here we present two sample equations. The complete system of equations can be found in Section B.1 of the appendix.

$$\begin{aligned}
\frac{\mathrm{d}[Dsh]_i^l}{\mathrm{d}t} &= -R_1\,[Dsh]_i^l\,[Fz]_i^l + \lambda_1 B_i^l\,[DshFz]_i^l - R_5\,[Dsh]_i^l\,[FzVang]_{i-1}^r \\
&\quad + \lambda_5 B_i^l\,[DshFzVang]_{i-1}^r - R_8\,[Dsh]_i^l\,[FzVangPk]_{i-1}^r \\
&\quad + \lambda_8 B_i^l\,[DshFzVangPk]_{i-1}^r + \mu_1 \frac{([Dsh]_i^r - [Dsh]_i^l)}{\Delta x^2}, \\
\frac{\mathrm{d}[Dsh]_i^r}{\mathrm{d}t} &= -R_1\,[Dsh]_i^r\,[Fz]_i^r + M_1\lambda_1 B_i^r\,[DshFz]_i^r - R_5\,[Dsh]_i^r\,[FzVang]_{i+1}^l \\
&\quad + M_1\lambda_5 B_i^r\,[DshFzVang]_{i+1}^l - R_8\,[Dsh]_i^r\,[FzVangPk]_{i+1}^l \\
&\quad + M_1\lambda_8 B_i^r\,[DshFzVangPk]_{i+1}^l + \mu_1 \frac{([Dsh]_i^l - [Dsh]_i^r)}{\Delta x^2},
\end{aligned} \tag{4.11}$$

with

$$\begin{aligned}
B_i^l &= 1 + K_b(K_{pk}\,[Pk]_i^l + [VangPk]_i^l + [FzVangPk]_i^l + [DshFzVangPk]_i^l \\
&\quad + K_{va}([Vang]_i^l + [FzVang]_i^l + [DshFzVang]_i^l))^{K_p}, \\
B_i^r &= 1 + K_b(K_{pk}\,[Pk]_i^r + [VangPk]_i^r + [FzVangPk]_i^r + [DshFzVangPk]_i^r \\
&\quad + K_{va}([Vang]_i^r + [FzVang]_i^r + [DshFzVang]_i^r))^{K_p}
\end{aligned}$$

and

$$M_1 < 1.$$

The superscripts l and r refer to the cell sides, left and right, the subscripts to the number of the cell. The square brackets indicate that we are dealing with concentrations. Bridging complexes are always counted as if they belong to the cell in which their Vang-part is located. The parameter μ_1 represents diffusion and Δx the spatial extension of a cell in our model from left to right. Let T, μ_1^{bio} and Δx^{bio} be the time, the diffusion coefficient and the side length of a cell in the biological system. They relate to the parameters in our model by $t = kT$, $\mu_1 = \frac{1}{k}\mu_1^{bio}$ and $\Delta x = p\,\Delta x^{bio}$, with positive constants k and p.
Upon rescaling, (4.11) can be stated in the general form

$$\begin{aligned}
\frac{\mathrm{d}[Dsh]_i^l}{\mathrm{d}\tau} &= F + \mu_1^{sim}([Dsh]_i^r - [Dsh]_i^l), \\
\frac{\mathrm{d}[Dsh]_i^r}{\mathrm{d}\tau} &= F + \mu_1^{sim}([Dsh]_i^l - [Dsh]_i^r),
\end{aligned} \tag{4.12}$$

where F represents the reaction terms, $\tau = \mu_1^{sim} t$ and $\mu_1^{sim} = \frac{1}{\Delta x^2}\mu_1 = \frac{1}{kp^2(\Delta x^{bio})^2}\mu_1^{bio}$. Therefore, the relation between the time T in experiments and the time τ in our analysis and simulations is given by

$$T = \frac{1}{k\mu_1^{sim}}\tau = \frac{p^2(\Delta x^{bio})^2}{\mu_1^{bio}}\tau. \tag{4.13}$$

We assume $p = 1$, $\Delta x^{bio} = 8\,\mu$m [19] and $\mu_1^{bio} = 1\,\mu\text{m}^2/\text{s}$ [22], since Dsh is a cytoplasmic protein. The parameter k can be determined from equation (4.13).

The system exemplified by (4.12) shows that the proposed mechanism relies on intracellular protein movement. Protein movement between the cells and production or degradation of proteins are not considered. Hence, the model is conservative. There are four conservation laws, one for each protein. But since using these laws to reformulate the equations does not give us more insight into the model, we omit it. Although we have simplified things considerably, this system of ODEs is still too complex to analyse by hand. Hence we decided to simulate it in Matlab.

4.1.1 Numerical simulations

We simulated the system of equations exemplified by (4.12) for a row of ten cells using the Matlab ODE solver ode45 and applying periodic boundary conditions. As results we will present the final distributions of total Dsh and total Vang in each cell, which are the sum of Dsh and all Dsh containing complexes and the sum of Vang and all Vang containing complexes, respectively.

K_b	10
K_p	2.2
K_{pk}	0.5
K_{va}	0.5
μ	$(0.1, 0.1, 0.1, 0.1, 0.001, 0.1)$
λ	$(0.1, 0.1, 0.1, 0.1, 0.01, 0.1, 0.1, 0.1, 0.1, 0.1)$
R	$(10, 5, 5, 5, 10, 5, 5, 10, 5, 5)$

Table 4.1: Set of parameter values for which the system exemplified by (4.12) polarises with and without the global bias. We used these parameter values for the simulations shown in Figures 4.2-4.5

Effect of the persistent global bias

We start our analysis by investigating the effect of the persistent global bias on the final distributions of total Dsh and total Vang as shown in Figure 4.2. The parameter values in [3] vary in orders of magnitude between 10^{-5} and 10^{5}, which would considerably slow down our simulations. Furthermore, these values are not based on experimental estimates. Therefore, we chose different parameter values as show in Table 4.1. However, Amonlirdviman *et al.* conducted a sensitivity analysis which gave them a range for each parameter value in which it could vary such that the model still yields wild-type polarity. Except for μ_5 and λ_5 all our parameter values lie within the respective ranges.

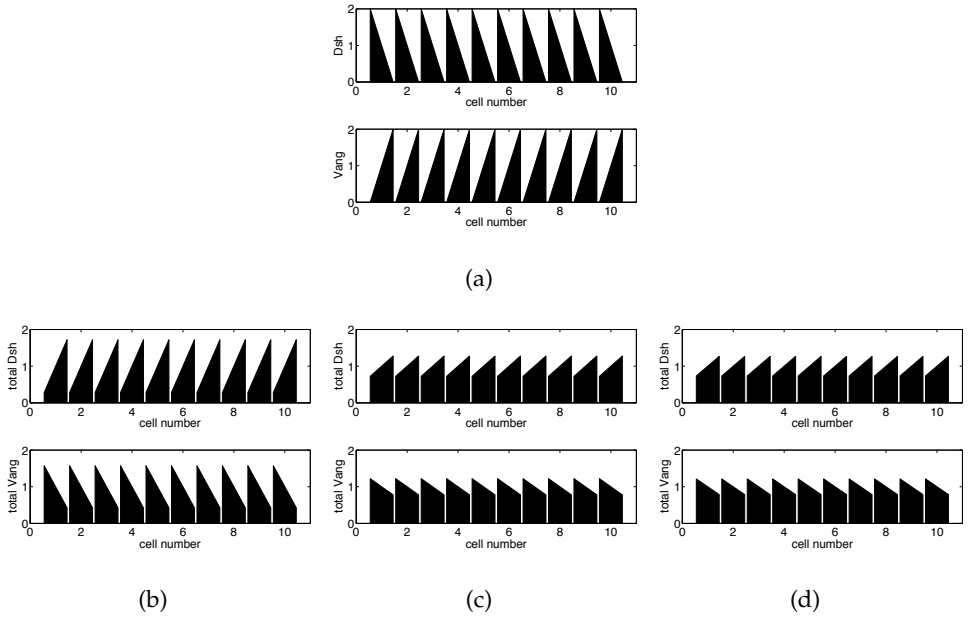

Figure 4.2: Results for simulations of the system exemplified by (4.12) for different values of M_1; (a) Initial condition with a strong polarity in the direction opposite to the direction of the final state observed in experiments, initially, Pk and Fz are distributed homogeneously; (b) final state for $M_1 = 0.2$; (c) final state for $M_1 = 0.8$; (d) final state for $M_1 = 0.2$ and no feedback, i.e. $K_b = 0$.

For the initial conditions in Figure 4.2(a) we chose a strong global polarity for Dsh and Vang opposite to the distribution presented in Figure 1.2. Pk and Fz are initially distributed homogeneously in every cell and initially, there are no complexes. Figures 4.2(b) and (c) show the final states for different values for M_1. As we can see the polarity of the final state is reversed compared to the polarity of the initial conditions and $M_1 = 0.2$ yields a stronger polarity than $M_1 = 0.8$. To generate Figure 4.2(d) we chose the same initial condition and the same value for M_1 as in (b) ($M_1 = 0.2$), but we set $K_b = 0$. Hence,

there is no feedback loop and the final state of the simulation relies only on the persistent global bias. In this case the polarity is a bit weaker than in Figure 4.2(b) but its direction is still reversed compared to the direction of the initial condition in Figure 4.2(a). Thus, the persistent global bias has a very strong impact.

Behaviour without a persistent global bias

As a next step we are interested in the behaviour of the system if there is no persistent global bias. Hence, we set $M_1 = 1$. Figure 4.3 shows the results for different strengths of feedback. In the previous section we chose an initial condition with imbalances in Dsh and Vang to emphasize the effect of the persistent global bias. In the following we assume an initial imbalance in Fz, based on a general consensus that the global cue of the first tier of the PCP mechanism affects Fz. Figure 4.3(a) presents the initial Fz distribution, which has a small imbalance in every cell. Initially, the other proteins are distributed homogeneously. A similar initial imbalance in any of the other three proteins gives the same results. The total amount of each protein in a cell is 2. The results for the parameter values in Table 4.1 are displayed in Figure 4.3(b). They demonstrate that the persistent global bias is not needed to get polarity. The small initial imbalance is necessary and the direction of the polarity of the final state depends on the direction of the imbalance in the initial conditions (not shown). Increasing the strength of the feedback increases the polarity of the final state and accelerates the process as shown in Figure 4.3(c). As mentioned in Section 1.2, in the *Drosophila* pupal wing, polarisation of the cells takes about 32 h. Therefore, the time to reach the steady state in Figure 4.3(c) is in a reasonable range.

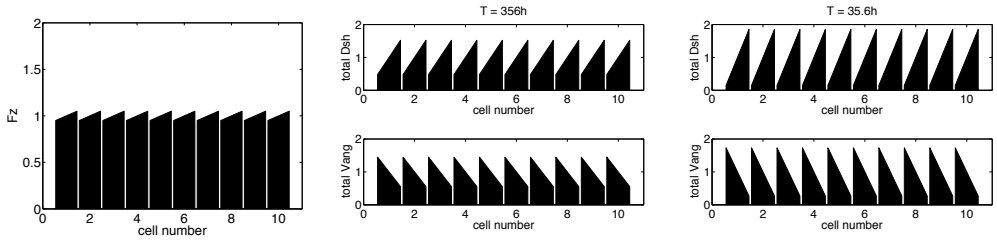

(a) (b) (c)

Figure 4.3: Final states for the system exemplified by (4.12) for $M_1 = 1$, the parameter values in Table 4.1 and different strengths of feedback; (a) Initial condition, an imbalance in Fz with a difference of 0.1 between right and left side; initially, the other proteins are distributed homogeneously; (b) final distribution of total Dsh and total Vang for $K_b = 10$ and $K_p = 2.2$, (c) final distribution of total Dsh and total Vang for $K_b = 20$ and $K_p = 5$.

Propagation as a wave

As a next step we chose a different type of initial condition in which the cell at the left end of the row has a strongly polarised Fz distribution. The other proteins are initially distributed homogeneously in all cells. Again, the total amount of each protein in a cell is 2. For this simulation we had to apply different boundary conditions. On both ends of the row we assumed another half a cell next to the boundary cell with its initial protein values set according to the protein values in the boundary cell. We ensured that these end-cells are only half by setting the diffusion in these cells to zero. Furthermore, we now consider 20 cells instead of 10 to minimise the boundary effects. Figure 4.4 shows that for the chosen initial condition, the stronger feedback $K_b = 20$ and $K_p = 5$, $M_1 = 1$ and the remaining parameter values from Table 4.1, a polarising wave is initiated that spreads over the whole row of cells. The same is true for the weaker feedback $K_b = 10$ and $K_p = 2.2$ (not shown). In this case it takes longer to reach the final state and the resulting polarity is weaker, as expected from Figure 4.3(b). The effect at both ends of the row in Figure 4.4(d) is due to the boundary conditions.

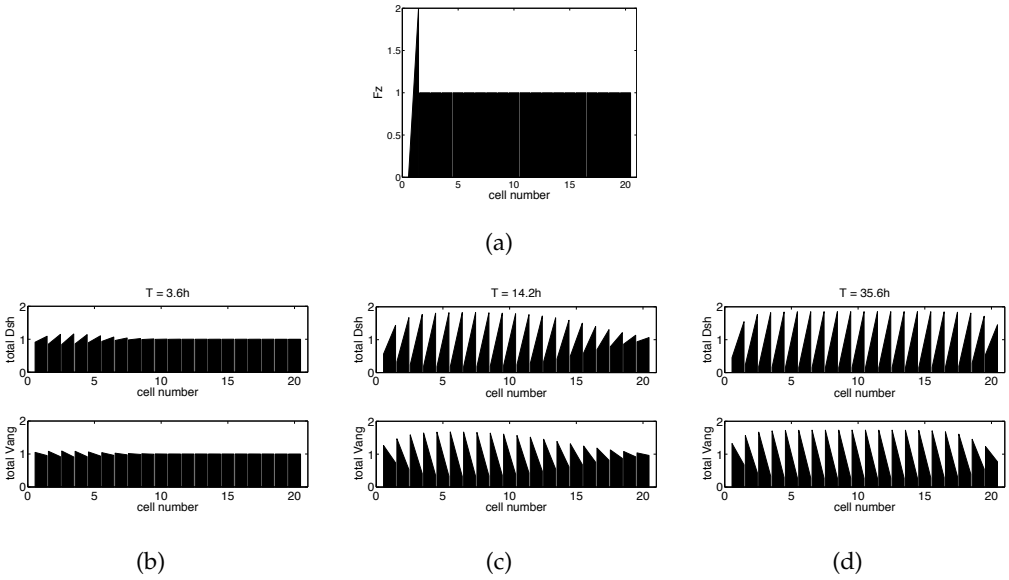

Figure 4.4: Propagation as a wave for the system exemplified by (4.12) for $M_1 = 1, K_b = 20, K_p = 5$ and the rest of the parameter values from Table 4.1; (a) Initial condition for Fz, all other proteins are initially distributed homogeneously in every cell; (b)-(d) results at different points in time; the weaker polarity in the boundary cells is due to our choice of boundary conditions.

Like the conservative model in Chapter 3 this model can generate polarity from an initial imbalance in every cell or via a wave. Furthermore, coherent patterns of cell polarity can be generated in the absence of a persistent global bias, provided there is an initial imbalance

that can be amplified. In the following we will show that this result is consistent with what would be expected from linear stability analysis and that it does not depend strongly on our choice of parameter values.

4.1.2 Comparison with linear stability analysis

The numerical results in Figures 4.3 and 4.4 show cases in which the mechanism presented in this chapter does not need a persistent global bias to polarise a row of cells. To support these numerical simulations we check whether the solution behaves as predicted by linear stability analysis. We get the homogeneous unpolarised steady state by simulating the system exemplified by (4.12) for the parameter values in Table 4.1, $M_1 = 1$ and the initial conditions $[Dsh]_i^l = [Dsh]_i^r = [Pk]_i^l = [Pk]_i^r = [Fz]_i^l = [Fz]_i^r = [Vang]_i^l = [Vang]_i^r = 1$ for all i. Calculating the eigenvalues of the matrix of the corresponding eigenvalue problem yields $\lambda = 5.68 \cdot 10^{-4}$ as the greatest real part of any of them. We expect that a small perturbation of the homogeneous unpolarised steady state would grow with growth rate λ. Therefore, we use 0.99 times the left sides of the homogeneous unpolarised steady state and 1.01 times the right sides as initial left and right sides for a new simulation. This results in a polarised steady state. Tracking the solutions for $[DshFzVangPk]^l$ for one cell and plotting $\ln([DshFzVangPk]^l - [DshFzVangPk]^{l^*})$, with * indicating the value at the homogeneous unpolarised steady state, we get the graph in Figure 4.5 with a slope of approximately 0.0005 at its straight part, which is in good agreement with λ.

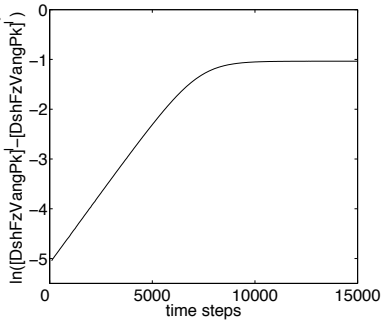

Figure 4.5: Graph of $\ln([DshFzVangPk]^l - [DshFzVangPk]^{l^*})$; it verifies that our simulations are consistent with linear stability analysis as explained in the text.

The entries of the eigenvector corresponding to λ are given in Table 4.2. We applied the conservation laws for the four proteins to calculate the eigenvalues and this eigenvector. Therefore, we did not obtain entries of the eigenvector corresponding to $[Dsh]^l$, $[Pk]^l$, $[Fz]^l$ and $[Vang]^l$. Since the entries for left and right of every protein complex have opposite sign and the same absolute value, the eigenvector confirms that we get a polarised distribution of the protein complexes.

	Dsh	Pk	Fz	Vang	DshFz
left	–	–	–	–	0.12217
right	0.0038063	-6.276e-16	0.0037239	-0.00028455	-0.12217
	VangPk	FzVang	DshFzVang	FzVangPk	DshFzVangPk
left	0.0018748	0.002217	-0.10261	0.026886	-0.68833
right	-0.0018748	-0.002217	0.10261	-0.026886	0.68833

Table 4.2: Entries of the eigenvector corresponding to the eigenvalue λ for the homogeneous unpolarised steady state of the system exemplified by (4.12). The parameter values we chose are given in Table 4.1. Because we applied the conservation laws for the four proteins there are no entries corresponding to $[Dsh]^l$, $[Pk]^l$, $[Fz]^l$ and $[Vang]^l$. This eigenvector confirms that we get polarised distributions of the protein complexes.

These results show that our simulations are consistent with linear stability analysis. Applying the same method for different values of the total amount of each protein in a cell yield similar results (not shown). This analysis supports the findings in the last section that the persistent global bias is not needed for our choice of parameter values.

4.1.3 Parameter search

So far we have shown that in one spatial dimension, for the parameter values in Table 4.1, the persistent global bias is not necessary to amplify polarity provided there is an imbalance in the initial conditions. Now we want to show that this result is not unique to our initial choice of parameter values, but rather that it holds for significant regions of parameter space. Therefore, we search for alternative sets of parameter values that give polarity. The idea is to calculate the homogeneous unpolarised steady state and the corresponding eigenvalue with the largest real part for a given parameter set. Then, the real part of the eigenvalue is increased applying a search step based on the Nelder-Mead algorithm [24, 33]. If we reach a positive result, the corresponding set of parameter values will yield polarity.

We have based our search algorithm on the Nelder-Mead method since it requires only function values but no information about the derivative. The original version by Nelder and Mead was developed to solve unconstrained problems. Our parameters however can only take positive values. Therefore, we had to adapt the method to take into account this constraint. The algorithm can be found in Chapter A in the appendix. The difference to the version for unconstrained problems is that whenever a newly calculated point is outside

the domain it gets projected to the domain boundary, namely in (S.2), (S.4) and (S.5)(b) of Algorithm A.1. In our specific case, components of the new point with a negative value are set to 10^{-6}. During our calculations, this happened only for one or two parameters.
A start vector x_0 and the corresponding parameter set x_b with the best eigenvalue after 430 steps are shown in Table 4.3. During this calculation λ was increasing and therefore always positive. Hence, the maximum number of steps of 430 was chosen arbitrarily and stopping earlier would have provided a different parameter set that ensures polarisation of the system exemplified by (4.12). Different starting vectors x_0 gave similar results (not shown). Hence, there exist many other parameter sets for which the persistent global bias is not needed to polarise the cells. Therefore, our results do not depend on a specific choice of parameter values.

	x_0	x_b after 430 search steps
K_b	20	1.1050
K_p	5	23.7627
K_{pk}	0.5	1.0504
K_{va}	0.5	0.0857
μ	$(0.1, 0.1, 0.1, 0.1, 0.001, 0.1)$	$(6.4009, 4.4087, 13.2970, 0.1723, 10^{-6}, 7.5585)$
λ	$(0.1, 0.1, 0.1, 0.1, 0.01,$ $0.1, 0.1, 0.1, 0.1, 0.1)$	$(1.3304, 3.4353, 0.1764, 0.0210, 2.6999,$ $6.9145, 4.8676, 0.5371, 0.0879, 0.0300)$
R	$(10, 5, 5, 5, 10,$ $5, 5, 10, 5, 5)$	$(11.8722, 0.1962, 0.2583, 11.5766, 11.6367,$ $5.9838, 10^{-6}, 5.4359, 3.6203, 8.9815)$
λ	0.0078	4.56

Table 4.3: Starting vector x_0 and corresponding parameter set x_b with the best eigenvalue after 430 search steps applying a method based on the Nelder-Mead algorithm. The last row shows the largest real parts of the eigenvectors corresponding to the two parameter sets.

A possible alternative approach to analysing the sensitivity of a system to variations of the parameter values was applied by von Dassow *et al.* [52]. The idea is to take an initial parameter set that yields the desired result, in our case the set in Table 4.1, and vary one parameter while holding all others fixed. Amonlirdviman *et al.* used this method for their sensitivity analysis in [3].
A next step would be to analyse the behaviour of the system exemplified by (4.12) for anomalies in the initial conditions and clones in the row of cells. We defer this and first extend our analysis to two spatial dimensions.

4.2 Analysis in two spatial dimensions for compartmentalised cells

In this section we analyse the model proposed by Amonlirdviman *et al.* [3] in two spatial dimensions. We assume that we have a field of hexagonal cells and each cell is divided into six compartments. Applying reaction kinetics to Equations (4.1)-(4.10) and omitting the persistent global bias, we get a system of ODEs describing the change of a protein or protein complex in compartment j of cell i. As an example, we present the equation for the change of $[Dsh]$ in compartment $j \pmod 6$ of cell i represented by $[Dsh]_{i,j}$. We have

$$\begin{aligned}\frac{\mathrm{d}[Dsh]_{i,j}}{\mathrm{d}t} = &-R_1\,[Dsh]_{i,j}\,[Fz]_{i,j} + \lambda_1 B_{i,j}\,[DshFz]_{i,j} - R_5\,[Dsh]_{i,j}\,[FzVang]^+_{i,j} \\ &+ \lambda_5 B_{i,j}\,[DshFzVang]^+_{i,j} - R_8\,[Dsh]_{i,j}\,[FzVangPk]^+_{i,j} \\ &+ \lambda_8 B_{i,j}\,[DshFzVangPk]^+_{i,j} + \mu_1 \frac{([Dsh]_{i,j+1} + [Dsh]_{i,j-1} - 2[Dsh]_{i,j})}{\Delta x^2}\end{aligned} \tag{4.14}$$

with

$$\begin{aligned}B_{i,j} = 1 + K_b(&K_{pk}[Pk]_{i,j} + [VangPk]_{i,j} + [FzVangPk]_{i,j} + [DshFzVangPk]_{i,j} \\ &+ K_{va}([Vang]_{i,j} + [FzVang]_{i,j} + [DshFzVang]_{i,j}))^{K_p},\end{aligned}$$

where + indicates that the reactants are in adjacent compartments of neighbouring cells, μ_1 represents diffusion and Δx the distance between two neighbouring compartments within a cell. The complete system can be found in Section B.2 of the appendix. If T, μ_1^{bio} and Δx^{bio} denote the time, the diffusion coefficient and the length of a cell side in the biological system, these parameters can be related to the parameters in our model by $t = kT$, $\mu_1 = \frac{1}{k}\mu_1^{bio}$ and $\Delta x = p\,\Delta x^{bio}$ with positive constants k and p.
Rescaling (4.14) yields

$$\frac{\mathrm{d}[Dsh]_{i,j}}{\mathrm{d}\tau} = F + \mu_1^{sim}([Dsh]_{i,j+1} + [Dsh]_{i,j-1} - 2[Dsh]_{i,j}), \tag{4.15}$$

where $\mu_1^{sim} = \frac{1}{\Delta x^2}\mu_1 = \frac{1}{kp^2(\Delta x^{bio})^2}\mu_1^{bio}$ denotes diffusion and F represents the reaction terms. Furthermore, $\tau = \mu_1^{sim} t$. Hence, the simulation time τ is related to the time T in experiments by

$$T = \frac{1}{k\mu_1^{sim}}\tau = \frac{p^2(\Delta x^{bio})^2}{\mu_1^{bio}}\tau. \tag{4.16}$$

For the parameter values we assume $p = \frac{1}{4}$, $\Delta x^{bio} = 8\,\mu\mathrm{m}$ [19] and $\mu_1^{bio} = 1\,\mu\mathrm{m}^2/\mathrm{s}$ [22]. Hence, Δx^{bio} and μ_1^{bio} are the same as in the one-dimensional case, while p is smaller, since it now determines the distance between two compartments of a cell instead of the size of a whole cell as in the one-dimensional case. The parameter k is determined by (4.16). We

are interested in the types of steady states this system can generate, in particular whether the polarised steady state is one of them. To this end, we perform a numerical analysis in the next section.

4.2.1 Numerical simulations

We simulated the system exemplified by (4.15) in Matlab for a hexagonal cell applying periodic boundary conditions for the intercellular binding. Hence, our domain represents an infinite field of hexagonal cells with the same initial conditions. The aim is to gain insight into the different steady states the system can reach. We assume two different kinds of initial conditions, a symmetric one and an asymmetric one, referring to symmetry with respect to the horizontal line dividing the cell into three top compartments and three bottom compartments.

K_b	20
K_p	5
K_{pk}	0.5
K_{va}	0.5
μ	$m \cdot (0.1, 0.1, 0.1, 0.1, 0.001, 0.1)$
λ	$(0.1, 0.1, 0.1, 0.1, 0.01, 0.1, 0.1, 0.1, 0.1, 0.1)$
R	$(10, 5, 5, 5, 10, 5, 5, 10, 5, 5)$

Table 4.4: Set of parameter values which were used for the simulations in Section 4.2.1. The diffusion depends on a parameter m that was varied to gain insight into the effect of the speed of diffusion on the final state.

Figures 4.6 and 4.7 show the initial conditions for Fz and the corresponding final distributions of total Dsh. In Figure 4.6(a) we chose an initial distribution of Fz which is symmetric with respect to the horizontal axis and has a slight imbalance to the right. Initially, the other proteins are distributed homogeneously. The parameter values are given in Table 4.4 where the speed of the diffusion depends on a parameter m. Figures 4.6(b)-(d) show the final distribution of total Dsh for different values of m. Note the different scales in the different figures. For $m = 16$ we get a polarised steady state that is symmetric with respect to the horizontal axis as shown in Figure 4.6(b). Note that, assuming a cell in the one-dimensional simulations is 8 μm long and the distance between two compartments in a cell in our simulations here is 2 μm, the set of parameter values corresponding to Figure 4.6(b) is, after scaling of the diffusion coefficient, the same as the one corresponding to Figure 4.3(c). Increasing m, the polarity gets weaker and for m sufficiently large we get the

unpolarised steady state (see Figures 4.6(c) and (d)). We have indicated the times it takes to reach the polarised steady states. Considering that it takes about 32 h in the *Drosophila* wing to polarise the cells, the time T is very small. If the diffusion in the biological system was slower than our assumed 1 $\mu m^2/s$ we would obtain a greater T.

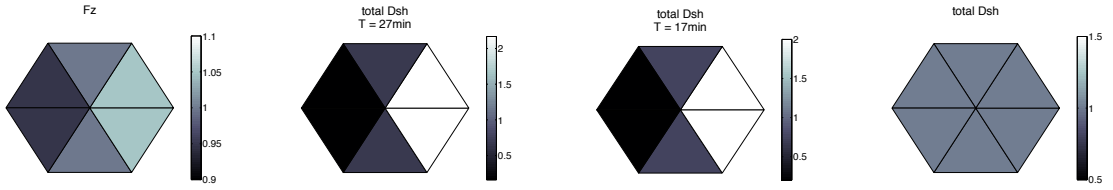

(a) (b) (c) (d)

Figure 4.6: Results for a single hexagonal cell with six compartments for the system exemplified by (4.15), initial conditions that are symmetric with respect to the horizontal axis, the parameter values in Table 4.4 and different values for m. The results show the distribution of total Dsh which is assumed to determine the direction of hair growth. For clarity the compartments are divided by black lines. Note that the scales are different in the different figures. (a) Symmetric initial condition with an imbalance for Fz, the difference between the right and the left end of the cell is 0.1; initially, the other proteins are distributed homogeneously; (b) final state for $m = 16$, polarised steady state; (c) final state for $m = 160$, polarised steady state; (d) final state for $m = 5000$, unpolarised steady state.

Figure 4.7(a) shows an initial condition with an asymmetric distribution of Fz. The bottom three compartments have a slightly higher value of Fz than the top three. Initially, the remaining proteins are distributed homogeneously within the cell. The parameter values are given in Table 4.4. Figures 4.7(b)-(d) show the final distribution of total Dsh for different values of m. For $m = 16$ we get a distinct asymmetric state as displayed in Figure 4.7(b). Increasing m to 160 in Figure 4.7(c) yields a state in which the cell is divided into halves along its horizontal axis and in each half the middle compartment has a different value than the two others (see illustration). Increasing m further, we get the unpolarised steady state in Figure 4.7(d).

The analysis shows that the system can polarise without the persistent global bias. We also discovered that the steady states in Figures 4.7(b) and (c), which are asymmetric with respect to the horizontal axis, exist for the same parameter values as the polarised steady states in Figures 4.6(b) and (c). Analysing the existence and stability of the steady states for the system exemplified by (4.15) is very complex. Therefore, we conducted a numerical investigation. We found that, in addition to the steady states shown in Figures 4.6 and 4.7, there exist at least five more steady states. Similar to the one in 4.7(c), which is

polarised towards the bottom middle compartment, we can get steady states which are polarised toward any of the six compartments of the cell. To test the stability of the different steady states we used perturbations of the steady states as initial conditions. We considered two types of perturbations; one that is symmetric with respect to the horizontal axis and another one that is asymmetric with respect to the same axis. Our results indicate that the polarised steady states that are symmetric with respect to the horizontal axis (Figures 4.6(b) and (c)) are only stable to perturbations which are symmetric with respect to the horizontal axis. The states that are asymmetric with respect to the horizontal axis seem stable to both kinds of perturbations. This suggests that only initial conditions which are symmetric with respect to the horizontal axis can yield the desired polarised steady state. Irregularities in the initial conditions will lead to disturbance of correct polarity. Fluctuations or clones introduce such irregularities.

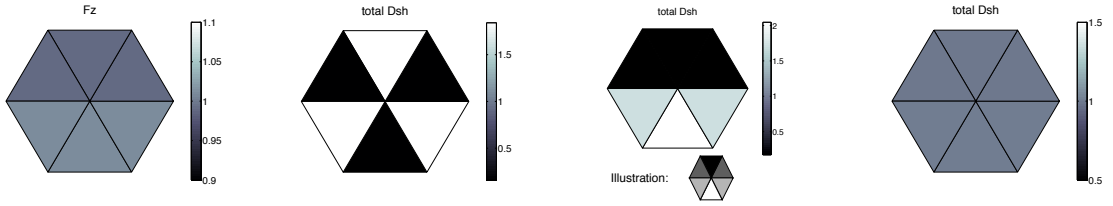

(a) (b) (c) (d)

Figure 4.7: Results for a single hexagonal cell with six compartments for the system exemplified by (4.15), an initial condition that is asymmetric with respect to the horizontal axis, the parameter values in Table 4.4 and different values for m. The results show the distribution of total Dsh which is assumed to determine the direction of hair growth. For clarity the compartments are divided by black lines. Note that the axes are different in the different figures. (a) Initial condition for Fz that is asymmetric with respect to the horizontal axis, the difference between the bottom and the top compartments is 0.02, other proteins are initially distributed homogeneously; (b) final state for $m = 16$; (c) final state for $m = 160$, the bottom middle compartment has a higher value than the two next to it and the top middle compartment has a lower value than the two next to it, as shown in the illustration; (d) final state for $m = 5000$, unpolarised steady state.

Figure 4.8 and 4.9 show the results for a field of hexagonal cells with and without a clone. For the top and bottom boundary of the 10×10 field of cells we applied periodic boundary conditions while at the left and right boundary there was half a row of cells, with their initial values corresponding to the initial values in the cells right next to the boundaries. In Figure 4.8(a) we assume an initial imbalance in Fz in every cell while the other proteins are

initially distributed homogeneously. The corresponding final state in Figure 4.8(b) shows polarity over the whole region. The difference in strength of polarity between the different rows of the field are due to the boundary conditions at the left and right boundary.

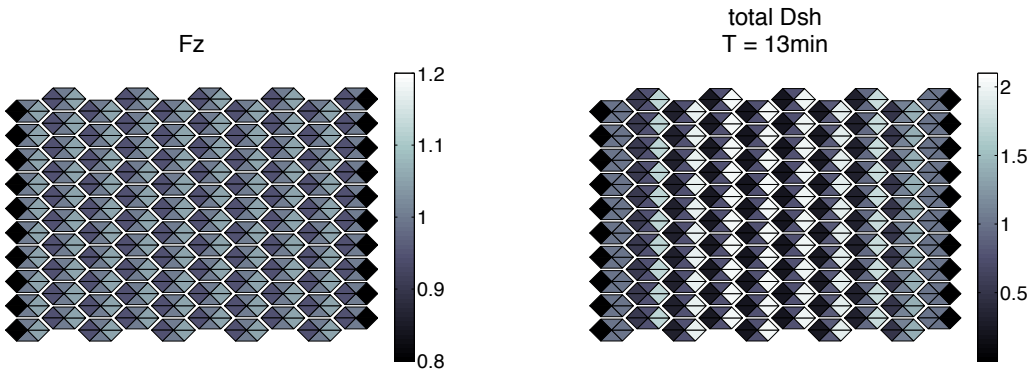

(a) (b)

Figure 4.8: Result for a 10×10 field of cells for an initial Fz imbalance in every cell for the system exemplified by (4.15), the parameter values in Table 4.4 and $m = 160$; note the different scales in the two figures; (a) Initial condition for Fz, the other proteins are distributed homogeneously; (b) final state of total Dsh, the weaker polarisation in the columns near the boundary are due to the boundary conditions.

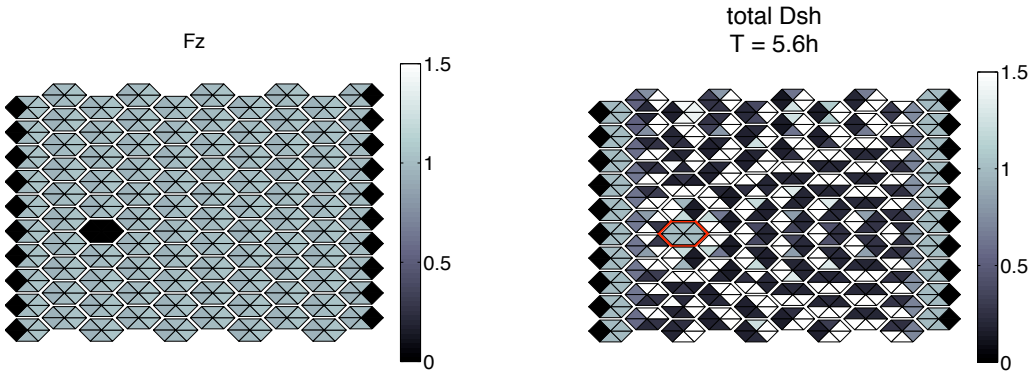

(a) (b)

Figure 4.9: Result for a 10×10 field of cells including one cell with no Fz for the system exemplified by (4.15), the parameter values in Table 4.4 and $m = 160$; (a) Initial condition for Fz, the other proteins are distributed homogeneously; (b) final state of total Dsh; the cells in the same row as the clonal cell (framed in red) show an orientation toward the left.

In Figure 4.9(b) we present the final distribution of total Dsh in a field of cells for which

initially every cell has a small imbalance in Fz pointing to the right except for one cell that has no Fz as shown in Figure 4.9(a). The other proteins are initially distributed homogeneously in every cell. Figure 4.9(b) shows that the cells in the same row as the Fz-null cell are polarised toward the left while the rest of the cells in the field show a disordered distribution of total Dsh. This result differs from the experimental finding shown in Figure 1.3(a) in which the hairs of the cells closest to the clone point toward the clone and the cells further away show normal polarity.

4.3 Analysis of the full spatial model

In this section we investigate the behaviour of the full spatial version of the model on a hexagonal domain. Instead of compartmentalising the cell like in the previous section we now approximate the full system of partial differential equations for diffusion within the cell and the membrane. Applying reaction kinetics to equations (4.1)-(4.10) omitting the persistent global bias, we obtain the desired system of partial differential equations. Here, we present the equation for $[Dsh]$ as an example; the complete system can be found in the Appendix B.3. To this end, we have

$$\begin{aligned}\frac{\partial\,[Dsh]}{\partial t} = &-R_1\;[Dsh][Fz] + \lambda_1 B\;[DshFz] - R_5\;[Dsh][FzVang]^+ \\ &+ \lambda_5 B\;[DshFzVang]^+ - R_8\;[Dsh][FzVangPk]^+ \\ &+ \lambda_8 B\;[DshFzVangPk]^+ + \mu_1\;\nabla^2[Dsh],\end{aligned} \tag{4.17}$$

where

$$\begin{aligned}B = 1 + K_b(K_{pk}[Pk] + [VangPk] + [FzVangPk] + [DshFzVangPk] \\ + K_{va}([Vang] + [FzVang] + [DshFzVang]))^{K_p}.\end{aligned} \tag{4.18}$$

The superscript + indicates that the reactants are in different cells and μ_1 is the diffusion coefficient. Different to the previous sections we now assume the protein concentrations to be continuously varying.

Let Δx denote the side length of the hexagonal domain. If the time, the diffusion coefficient and the side length of a cell in the biological system are given by T, μ_1^{bio} and Δx^{bio}, they relate to the parameters in our model by $t = kT$, $\mu_1 = \frac{1}{k}\mu_1^{bio}$ and $\Delta x = p\,\Delta x^{bio}$ for positive k and p.

Upon rescaling, equation (4.17) can be written in the generic form

$$\frac{\partial[Dsh]}{\partial\tau} = F + \mu_1^{sim}\nabla^2[Dsh], \tag{4.19}$$

where F represents the reaction terms. The diffusion coefficient $\mu_1^{sim} = p^2\mu_1 = \frac{1}{k}p^2\mu_1^{bio}$. In addition, $\tau = \mu_1^{sim}t$. Therefore, the simulation time τ is related to the time T in experiments by

$$T = \frac{1}{k\mu_1^{sim}}\tau = \frac{1}{p^2\mu_1^{bio}}\tau. \tag{4.20}$$

We assume $p = \frac{1}{4}$, $\Delta x^{bio} = 8\,\mu\text{m}$ [19] and $\mu_1^{bio} = 1\,\mu\text{m}^2/\text{s}$ [22]. The parameter k is determined by equation (4.20). As initial conditions we assume certain distributions for Dsh, Fz, Vang and Pk, which we will specify in Section 4.3.3. There are no protein complexes initially.
In the following we will construct a numerical approximation of the system exemplified by (4.19) based on the application of the finite element method.

4.3.1 Development of the finite element code

In this section we describe the development of the finite element code employed for the numerical approximation of our underlying system of partial differential equations. To this end, we first specify the generation of the mesh. This will be followed by details about the theoretical background and the implementation. Finally, we present a convergence analysis study in order to validate our code.

Mesh generation

The computational domain is hexagonal with side length two; to save computing time we apply periodic boundary conditions for the intercellular interactions. The coarsest mesh we use is a uniform triangulation of the domain of mesh size one as depicted in Figure 4.10. To refine the mesh we isotropically subdivide every triangle into four uniform new subtriangles, which leads to a finer uniform triangulation with granularity half of that in the previous refinement step. This process is iterated until the desired mesh size is attained.

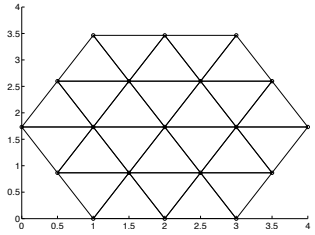

Figure 4.10: Uniform triangulation with mesh size one

Theoretical background

To address the theory underlying our finite element simulations we first have to examine the model in more detail. It is based on the interactions of the four proteins Dsh, Pk, Fz and Vang and their complexes DshFz, VangPk, FzVang, DshFzVang, FzVangPk and DshFzVangPk. These ten proteins and complexes can be divided into three groups depending on where they occur in the biological cell. Dsh and Pk have been observed in the cytoplasm, i.e., in the whole hexagonal domain in our simulations; they are freely diffusible in this regime. Therefore, we simulate the partial differential equations corresponding to these proteins on the whole of the two dimensional hexagonal domain, based on applying Neumann boundary conditions for the intracellular interactions with membrane located proteins. The components Fz, Vang, DshFz and VangPk are found in the cell membrane, diffusing within these constraints. The corresponding partial differential equations for these quantities are therefore simulated on a one-dimensional domain with periodic boundary conditions. The cell bridging complexes FzVang, DshFzVang, FzVangPk and DshFzVangPk occupy only the part of the membrane which is common to the two cells they connect. They can diffuse in this part but cannot move past a vertex of the biological cell. Therefore, the corresponding partial differential equations for these complexes are simulated on six one-dimensional domains, one for every edge of the biological cell, together with homogeneous Neumann boundary conditions.
In all cases the application of the finite element method includes three key steps. First, the equivalent weak formulation to the given problem has to be determined. The weak formulation is then discretised, which leads to a finite dimensional system of equations – the finite element approximation – that has to be solved. In the following we describe the details of these steps for the three different cases introduced above.

Diffusible in the whole domain - 2-D Problem with Neumann boundary conditions
This section describes the derivation of the finite element approximation for Dsh and Pk. We give a general description of the theory, following the steps mentioned above, and then relate it to our special case. Let Ω be the hexagonal domain and consider the problem: find $u(x,t)$ such that

$$\begin{aligned} \frac{\partial u}{\partial t} &= \mu \Delta u \quad \text{in } \Omega, \\ \mu \frac{\partial u}{\partial n} &= g(u) \quad \text{on } \partial\Omega, \\ u(\,\cdot\,,0) &= u_0, \end{aligned} \tag{4.21}$$

where μ is a positive constant, representing the diffusion coefficient. The reaction terms of the equations for Dsh and Pk describe the exchange of proteins between the two-dimensional representation of the whole cell and the one-dimensional representation of the membrane. It is unclear from [3] how Amonlirdviman *et al.* implemented this aspect. We include it as Neumann boundary conditions. Therefore, the function g is given by the reaction terms of the equations for Dsh and Pk, respectively.

Let $H^1(\Omega)$ be the Sobolov space of order 1. The weak formulation of (4.21) is derived by multiplying the problem with a test function $v \in H^1(\Omega)$ and integrating by parts. Thereby, we have the following variational formulation: find $u(\,\cdot\,,t) \in H^1(\Omega)$ such that

$$\int_\Omega \frac{\partial u}{\partial t} v \,\mathrm{d}x + \mu \int_\Omega \nabla u \cdot \nabla v \,\mathrm{d}x - \int_{\partial\Omega} g(u) v \,\mathrm{d}s = 0 \quad \text{for all } v \in H^1(\Omega),$$
$$\int_\Omega u(\,\cdot\,,0) v \,\mathrm{d}x = \int_\Omega u_0 v \,\mathrm{d}x \quad \text{for all } v \in H^1(\Omega).$$

Before formulating the finite element method, we first introduce some notation. To this end, let $T_h = \{K\}$ be a conforming shape regular triangulation of Ω, which is obtained by subdividing Ω into a set of non-overlapping triangles K, with $\Omega = \cup_{K \in T_h} K$. Here we consider arbitrary triangulations as e.g. in Figure 4.11(a). For our simulations we will use a uniform mesh. We introduce the mesh parameter $h = \max_{K \in T_h} \mathrm{diam}(K)$. For a given mesh of granularity h with nodes x_i, let N be the number of nodes and $\{\phi_1, ..., \phi_N\}$ the set of continuous piecewise linear basis functions defined on T_h such that $\phi_i(x_j) = \delta_{ij}$, where δ_{ij} denotes the Kronecker delta, i.e., $\delta_{ij} = 1$ if $i = j$ and $\delta_{ij} = 0$, otherwise. An example of such a basis function is shown in Figure 4.11(b).

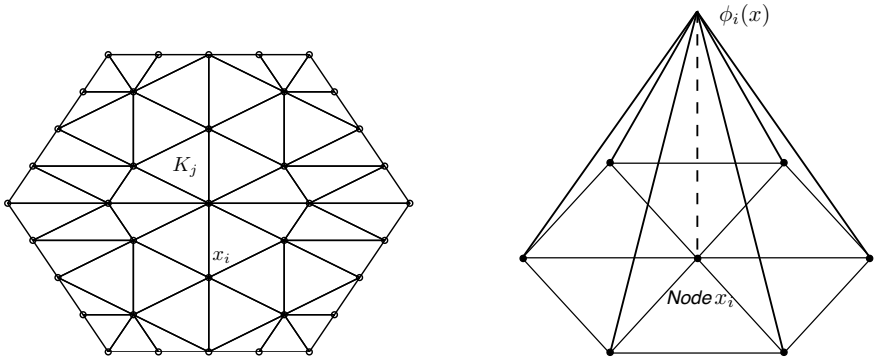

(a) (b)

Figure 4.11: Examples of a triangulation and a basis function; (a) Arbitrary finite element triangulation of a hexagonal domain with triangles K_j and nodes x_i, in our simulations we will use a uniform mesh, (b) node x_i with basis function ϕ_i.

We choose the finite element space $V_h \subset H^1(\Omega)$ to be $V_h = \text{span}\{\phi_1, ..., \phi_N\}$. Hence, the semidiscrete finite element approximation is given by: find $u_h(\cdot, t) \in V_h$ such that

$$\int_\Omega \frac{\partial u_h}{\partial t} v_h \, \mathrm{d}x + \mu \int_\Omega \nabla u_h \cdot \nabla v_h \, \mathrm{d}x - \int_{\partial\Omega} g(u_h) v_h \, \mathrm{d}s = 0 \quad \text{for all } v_h \in V_h,$$
$$\int_\Omega u_h(\cdot, 0) v_h \, \mathrm{d}x = \int_\Omega u_0 v_h \, \mathrm{d}x \quad \text{for all } v_h \in V_h.$$

In order to discretise in time, we apply the Backward-Euler method for the diffusion terms, and time lag g, i.e., the value of g at the previous time step is used as the boundary condition. To this end, let $0 = t^0 < t^1 < \ldots < t^M = T$ be a uniform subdivision of the time interval $[0, T]$, with time step Δt. Writing $u_{h,n}$ with $0 \leq n \leq M$, to denote the finite element approximation at time level t^n, we have: find $u_{h,n} \in V_h$ such that

$$\begin{aligned} \int_\Omega \frac{u_{h,n} - u_{h,n-1}}{\Delta t} v_h \, \mathrm{d}x + \mu \int_\Omega \nabla u_{h,n} \cdot \nabla v_h \, \mathrm{d}x - \int_{\partial\Omega} g_{n-1} v_h \, \mathrm{d}s = 0 \\ \text{for all } v_h \in V_h, n = 1, \ldots, M, \\ \int_\Omega u_{h,0} v_h \, \mathrm{d}x = \int_\Omega u_0 v_h \, \mathrm{d}x \quad \text{for all } v_h \in V_h, \end{aligned} \tag{4.22}$$

where $g_{n-1} = g(u_{h,n-1})$. Rearranging the first equation of (4.22) leads to

$$\int_\Omega u_{h,n} v_h \, \mathrm{d}x + \Delta t \mu \int_\Omega \nabla u_{h,n} \cdot \nabla v_h \, \mathrm{d}x = \Delta t \int_{\partial\Omega} g_{n-1} v_h \, \mathrm{d}s + \int_\Omega u_{h,n-1} v_h \, \mathrm{d}x$$
$$\text{for all } v_h \in V_h, n = 1, \ldots, M.$$

Writing

$$u_{h,n}(x) = \sum_{j=1}^{N} U_{n,j} \phi_j(x)$$

with appropriate coefficients $U_{n,j}$, system (4.22) is equivalent to

$$(Z + \Delta t \mu Y) U_n = \Delta t b + Z U_{n-1},$$
$$Z U_0 = c,$$

with $Y, Z \in \mathbb{R}^{N \times N}$ and $b, c \in \mathbb{R}^N$ such that

$$Y_{j,k} = \int_\Omega \nabla \phi_j \cdot \nabla \phi_k \, \mathrm{d}x,$$
$$Z_{j,k} = \int_\Omega \phi_j \phi_k \, \mathrm{d}x,$$
$$b_j = \int_{\partial\Omega} g_{n-1} \phi_j \, \mathrm{d}s,$$
$$c_j = \int_\Omega u_0 \phi_j \, \mathrm{d}x.$$

The matrices Y and Z are sparse since $Y_{j,k} \neq 0$ and $Z_{j,k} \neq 0$ if and only if nodes j and k belong to the same triangle. Furthermore, Y and Z are symmetric and non-singular.

Matrix Y is usually referred to as the stiffness matrix while Z is called the mass matrix and b the load vector. This terminology derives from early applications of the finite element method in structural mechanics.

To compute the stiffness and the mass matrices we calculate so called element stiffness and mass matrices, respectively, for every triangle in the mesh. Subsequently, we assemble them to obtain the global matrices. To this end, a connectivity array which stores the vertex numbers of each element in the mesh is employed. Let K_i be the triangular element with the vertices x_1, x_2, x_3 with $|K_i|$ denoting the area of K_i. For the element stiffness matrix we follow the approach from [16], which yields

$$Y^{K_i} = \frac{1}{4|K_i|} \begin{pmatrix} |x_2 - x_3|^2 & (x_2 - x_3) \cdot (x_3 - x_1) & (x_2 - x_3) \cdot (x_1 - x_2) \\ & |x_3 - x_1|^2 & (x_3 - x_1) \cdot (x_1 - x_2) \\ \text{symm.} & & |x_1 - x_2|^2 \end{pmatrix}. \tag{4.23}$$

The formula to calculate the element mass matrix is given in [2], namely, we have

$$Z^{K_i} = \frac{|K_i|}{12} \begin{pmatrix} 2 & 1 & 1 \\ 1 & 2 & 1 \\ 1 & 1 & 2 \end{pmatrix}. \tag{4.24}$$

The load vector b is also calculated elementwise. The integral $\int_{\partial\Omega} g_{n-1}\phi_j \, \mathrm{d}s$ is approximated using the value of g_{n-1} in the centre (x_m, y_m) of the boundary element E with length H by

$$\int_E g(u_{h,n-1})\phi_j \, \mathrm{d}s \approx \frac{H}{2} g(u_{h,n-1}(x_m, y_m)). \tag{4.25}$$

Substituting the details of the model into Equations (4.23)-(4.25) leads to the finite element approximations for the PDEs for Dsh and Pk. The properties of the triangulation are provided by the mesh generation, the functions ϕ_j are defined in this section and, as mentioned above, the function g is given by the reaction terms of the equations for Dsh and Pk. The vector u_0 is given by the initial distributions of Dsh and Pk, which we specify in Section 4.3.3. This leaves us with two linear systems, which need to be solved numerically at each time step.

Diffusible in the domain border - 1-D Problem with periodic boundary conditions

In this section we derive the linear systems employed for the numerical approximation of Fz, Vang, DshFz and VangPk. These proteins and complexes only occur on the membrane of the biological cell. We will proceed in a similar fashion as in the last section. Consider

the problem: find $u(x,t)$ such that

$$\begin{aligned} \frac{\partial u}{\partial t} &= \mu \frac{\partial^2 u}{\partial x^2} + f(u) \quad \text{in } [0,1), \\ u(1,\cdot) &= u(0,\cdot), \\ u(\cdot,0) &= u_0, \end{aligned} \tag{4.26}$$

where $\mu > 0$ is diffusion and f represents the reaction terms. Define $H^1_{per}(0,1) := \{v \in H^1(0,1) \,|\, v(0) = v(1)\}$. Multiplying problem (4.26) with a test function $v \in H^1_{per}(0,1)$ and integrating by parts yields its weak formulation: find $u(\cdot,t) \in H^1_{per}(0,1)$ such that

$$\begin{aligned} \int_0^1 \frac{\partial u}{\partial t} v \,\mathrm{d}x + \mu \int_0^1 \frac{\partial u}{\partial x}\frac{\partial v}{\partial x}\,\mathrm{d}x &= \int_0^1 f(u)v \,\mathrm{d}x \quad \text{for all } v \in H^1_{per}(0,1), \\ \int_0^1 u(\cdot,0)v \,\mathrm{d}x &= \int_0^1 u_0 v \,\mathrm{d}x \qquad \text{for all } v \in H^1_{per}(0,1). \end{aligned}$$

We now introduce some additional notation before formulating the finite element approximation. Let $T_h = \{x_1, \ldots, x_N\}$ with $0 = x_1 < x_2 < ... < x_N = 1$ be a partition of the interval $[0,1]$ into subintervals of length $h_j = x_{j+1} - x_j$ for $j = 1, ..., N-1$. Let $h := \max_{1 \le j \le N-1} h_j$ and define $\{\phi_1, ..., \phi_N\}$ as the set of continuous piecewise linear basis functions on T_h such that $\phi_i(x_j) = \delta_{ij}$ (see Figure 4.12).

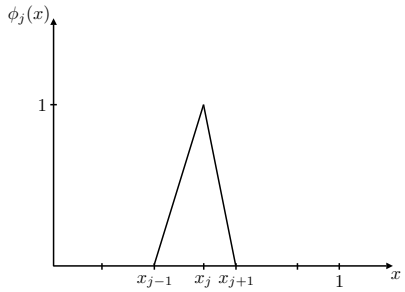

Figure 4.12: A partition of the interval $[0,1]$ and the basis function ϕ_j.

Due to the periodic boundary conditions we get $\phi_1 = \phi_N$. Therefore, as finite element space $V_h \subset H^1_{per}(0,1)$ we choose $V_h = \text{span}\{\phi_1, ..., \phi_{N-1}\}$. This gives us the semidiscrete finite element approximation: find $u_h(\cdot,t) \in V_h$ such that

$$\begin{aligned} \int_0^1 \frac{\partial u_h}{\partial t} v_h \,\mathrm{d}x + \mu \int_0^1 \frac{\partial u_h}{\partial x}\frac{\partial v_h}{\partial x}\,\mathrm{d}x &= \int_0^1 f(u_h)v_h \,\mathrm{d}x \quad \text{for all } v_h \in V_h, \\ \int_0^1 u_h(\cdot,0)v_h \,\mathrm{d}x &= \int_0^1 u_0 v_h \,\mathrm{d}x \qquad \text{for all } v_h \in V_h. \end{aligned}$$

We now discretise in time applying the Backward-Euler method for the diffusion terms and time lag f. To this end, we choose $0 = t^0 < t^1 < \ldots < t^M = T$ to be a uniform subdivision of the time interval $[0,T]$ with time step Δt. Furthermore, we represent the

finite element approximation at time level t^n by $u_{h,n}$ with $0 \leq n \leq M$. This implies: find $u_{h,n} \in V_h$ such that

$$\int_0^1 \frac{u_{h,n} - u_{h,n-1}}{\Delta t} v_h \,\mathrm{d}x + \mu \int_0^1 \frac{\partial u_{h,n}}{\partial x} \frac{\partial v_h}{\partial x} \,\mathrm{d}x = \int_0^1 f_{n-1} v_h \,\mathrm{d}x$$
$$\text{for all } v_h \in V_h, n = 1, \ldots, M, \tag{4.27}$$
$$\int_0^1 u_{h,0} v_h \,\mathrm{d}x = \int_0^1 u_0 v_h \,\mathrm{d}x \quad \text{for all } v_h \in V_h,$$

where $f_{n-1} = f(u_{h,n-1})$. Rearranging the first equation of (4.27) yields

$$\int_0^1 u_{h,n} v_h \,\mathrm{d}x + \Delta t \mu \int_0^1 \frac{\partial u_{h,n}}{\partial x} \frac{\partial v_h}{\partial x} \,\mathrm{d}x = \Delta t \int_0^1 f_{n-1} v_h \,\mathrm{d}x + \int_0^1 u_{h,n-1} v_h \,\mathrm{d}x$$
$$\text{for all } v_h \in V_h, n = 1, \ldots, M.$$

Writing

$$u_{h,n}(x) = \sum_{j=1}^{N-1} U_{n,j} \phi_j(x)$$

with appropriate coefficients $U_{n,j}$, the finite element approximation (4.27) can be restated as

$$(Z + \Delta t \mu Y) U_n = \Delta t b + Z U_{n-1},$$
$$Z U_0 = c,$$

with $Y, Z \in \mathbb{R}^{N-1 \times N-1}$ and $b, c \in \mathbb{R}^{N-1}$ such that

$$Y_{j,k} = \int_0^1 \frac{\mathrm{d}\phi_j}{\mathrm{d}x} \frac{\mathrm{d}\phi_k}{\mathrm{d}x} \,\mathrm{d}x,$$
$$Z_{j,k} = \int_0^1 \phi_j \phi_k \,\mathrm{d}x,$$
$$b_j = \int_0^1 f_{n-1} \phi_j \,\mathrm{d}x,$$
$$c_j = \int_0^1 u_0 \phi_j \,\mathrm{d}x.$$

The stiffness matrix Y and the mass matrix Z are non-singular, symmetric, positive definite tridiagonal matrices with additional non-zero entries in the top right and the bottom left corner, which account for the periodic boundary conditions.
Calculating the entries of the stiffness matrix and the mass matrix yields

$$Y = \frac{1}{h} \begin{pmatrix} 2 & -1 & 0 & \cdots & & -1 \\ -1 & 2 & -1 & 0 & \cdots & 0 \\ 0 & \ddots & \ddots & \ddots & & 0 \\ \vdots & & \ddots & \ddots & \ddots & \vdots \\ 0 & \cdots & 0 & -1 & 2 & -1 \\ -1 & \cdots & & 0 & -1 & 2 \end{pmatrix}$$

and

$$Z = h \begin{pmatrix} \frac{2}{3} & \frac{1}{6} & 0 & \cdots & & \frac{1}{6} \\ \frac{1}{6} & \frac{2}{3} & \frac{1}{6} & 0 & \cdots & 0 \\ 0 & \ddots & \ddots & \ddots & & 0 \\ \vdots & & \ddots & \ddots & \ddots & \vdots \\ 0 & \cdots & 0 & \frac{1}{6} & \frac{2}{3} & \frac{1}{6} \\ \frac{1}{6} & \cdots & & 0 & \frac{1}{6} & \frac{2}{3} \end{pmatrix}.$$

The load vector b is again calculated elementwise. To calculate the integral, f_{n-1} is approximated on (x_j, x_{j+1}) by $f\left(\frac{u_{h,n-1}(x_j)+u_{h,n-1}(x_{j+1})}{2}\right)$. We get

$$\begin{aligned} b_1 &= \int_{x_1}^{x_2} f_{n-1}\phi_1 \,\mathrm{d}x = \frac{h_1}{2} f\left(\frac{u_{h,n-1}(x_1) + u_{h,n-1}(x_2)}{2}\right), \\ b_j &= \int_{x_{j-1}}^{x_j} f_{n-1}\phi_j \,\mathrm{d}x + \int_{x_j}^{x_{j+1}} f_{n-1}\phi_j \,\mathrm{d}x \\ &= \frac{h_{j-1}}{2} f\left(\frac{u_{h,n-1}(x_{j-1}) + u_{h,n-1}(x_j)}{2}\right) + \frac{h_j}{2} f\left(\frac{u_{h,n-1}(x_j) + u_{h,n-1}(x_{j+1})}{2}\right) \\ &\qquad\qquad \text{for } j = 2, ..., N-1, \end{aligned}$$

where f is given by the reaction terms. The initial distributions for Fz and Vang are specified in Section 4.3.3. Initially, there are no complexes. Therefore, the entries of u_0 corresponding to DshFz and VangPk are zero.

This provides us with the necessary details for the linear systems corresponding to the PDEs for Fz, Vang, DshFz and VangPk, which are subsequently solved numerically.

Diffusible in one edge of the domain border - 1-D Problem with zero Neumann boundary conditions

As a last step we have to form the linear systems for the cell bridging complexes FzVang, DshFzVang, FzVangPk and DshFzVangPk. As mentioned above, in this model, initially there are no complexes. Hence, we consider the problem: find $u(x,t)$ such that

$$\begin{aligned} \frac{\partial u}{\partial t} &= \mu \frac{\partial^2 u}{\partial x^2} + f(u) \quad \text{in } (0,1), \\ -\frac{\partial u}{\partial x}(0,\cdot) &= \frac{\partial u}{\partial x}(1,\cdot) = 0, \\ u(\cdot,0) &= 0, \end{aligned} \tag{4.28}$$

where $\mu > 0$ represents diffusion and f the reaction terms. Multiplying (4.28) with a test function $v \in H^1(0,1)$, integrating by parts, and exploiting the homogeneous Neumann boundary conditions yields the corresponding weak formulation: find $u(\cdot,t) \in H^1(0,1)$

such that

$$\int_0^1 \frac{\partial u}{\partial t} v \,\mathrm{d}x + \mu \int_0^1 \frac{\partial u}{\partial x}\frac{\partial v}{\partial x}\,\mathrm{d}x = \int_0^1 f(u)v\,\mathrm{d}x \quad \text{for all } v \in H^1(0,1).$$

Similar to the previous sections we need further notation to be able to formulate the finite element approximation. Let $T_h = \{x_1, \ldots, x_N\}$ with $0 = x_1 < x_2 < ... < x_{N-1} < x_N = 1$ be a partition of the interval $[0,1]$ into subintervals of length $h_j = x_{j+1} - x_j$ for $j = 1, ..., N-1$. Define the granularity h of the mesh as $h := \max_{1\le j\le N} h_j$ and $\phi_1, ..., \phi_N$ as above with $\phi_i(x_j) = \delta_{ij}$ (see Figure 4.12). As finite element space $V_h \subset H^1(0,1)$ we choose $V_h = \operatorname{span}\{\phi_1, ..., \phi_N\}$. This gives the semidiscrete finite element approximation: find $u_h(\,\cdot\,, t) \in V_h$ such that

$$\int_0^1 \frac{\partial u_h}{\partial t} v_h \,\mathrm{d}x + \mu \int_0^1 \frac{\partial u_h}{\partial x}\frac{\partial v_h}{\partial x}\,\mathrm{d}x = \int_0^1 f(u_h)v_h\,\mathrm{d}x \quad \text{for all } v_h \in V_h.$$

In order to discretise in time we apply the Backward-Euler method for the diffusion terms and time lag f. To this end, we uniformly subdivide the time interval $[0,T]$ into $0 = t^0 < t^1 < \ldots < t^M = T$ with time step Δt. Writing $u_{h,n}$ with $0 \le n \le M$ to represent the finite element approximation at time level t^n, we get: find $u_{h,n} \in V_h$ such that

$$\int_0^1 \frac{u_{h,n} - u_{h,n-1}}{\Delta t} v_h \,\mathrm{d}x + \mu \int_0^1 \frac{\partial u_{h,n}}{\partial x}\frac{\partial v_{h,n}}{\partial x}\,\mathrm{d}x = \int_0^1 f_{n-1} v_h \,\mathrm{d}x \qquad \text{for all } v_h \in V_h, n = 1, \ldots, M,$$

where $f_{n-1} = f(u_{h,n-1})$. Rearranging yields

$$\int_0^1 u_{h,n} v_h \,\mathrm{d}x + \Delta t\mu \int_0^1 \frac{\partial u_{h,n}}{\partial x}\frac{\partial v_{h,n}}{\partial x}\,\mathrm{d}x = \Delta t \int_0^1 f_{n-1} v_h \,\mathrm{d}x + \int_0^1 u_{h,n-1} v_h \,\mathrm{d}x \qquad \text{for all } v_h \in V_h, n = 1, \ldots, M. \tag{4.29}$$

Writing

$$u_{h,n}(x) = \sum_{j=1}^{N} U_{n,j}\phi_j(x)$$

with appropriate coefficients $U_{n,j}$, we can restate the finite element approximation (4.29) as

$$(Z + \Delta t\mu Y)U_n = \Delta t b + ZU_{n-1},$$

with $Y, Z \in \mathbb{R}^{N\times N}$ and $b, c \in \mathbb{R}^N$ such that

$$\begin{aligned} Y_{j,k} &= \int_0^1 \frac{\mathrm{d}\phi_j}{\mathrm{d}x}\frac{\mathrm{d}\phi_k}{\mathrm{d}x}\,\mathrm{d}x, \\ Z_{j,k} &= \int_0^1 \phi_j\phi_k\,\mathrm{d}x, \\ b_j &= \int_0^1 f_{n-1}\phi_j\,\mathrm{d}x. \end{aligned}$$

The matrices Y and Z are symmetric, positive definite and tridiagonal.
Calculating the entries of Y and Z yields

$$Y = \frac{1}{h}\begin{pmatrix} 1 & -1 & 0 & \cdots & & 0 \\ -1 & 2 & -1 & 0 & \cdots & 0 \\ 0 & \ddots & \ddots & \ddots & & 0 \\ \vdots & & \ddots & \ddots & \ddots & \vdots \\ 0 & \cdots & 0 & -1 & 2 & -1 \\ 0 & \cdots & & 0 & -1 & 1 \end{pmatrix}$$

and

$$Z = h\begin{pmatrix} \frac{1}{3} & \frac{1}{6} & 0 & \cdots & & 0 \\ \frac{1}{6} & \frac{2}{3} & \frac{1}{6} & 0 & \cdots & 0 \\ 0 & \ddots & \ddots & \ddots & & 0 \\ \vdots & & \ddots & \ddots & \ddots & \vdots \\ 0 & \cdots & 0 & \frac{1}{6} & \frac{2}{3} & \frac{1}{6} \\ 0 & \cdots & & 0 & \frac{1}{6} & \frac{1}{3} \end{pmatrix}.$$

The load vector b is calculated elementwise. To calculate the integral, we approximate f_{n-1} on the interval (x_j, x_{j+1}) by $f\left(\frac{u_{h,n-1}(x_j)+u_{h,n-1}(x_{j+1})}{2}\right)$. We get

$$\begin{aligned} b_1 &= \int_{x_1}^{x_2} f_{n-1}\phi_1 \,\mathrm{d}x = \frac{h_1}{2} f\left(\frac{u_{h,n-1}(x_1) + u_{h,n-1}(x_2)}{2}\right), \\ b_j &= \int_{x_{j-1}}^{x_j} f_{n-1}\phi_j \,\mathrm{d}x + \int_{x_j}^{x_{j+1}} f_{n-1}\phi_j \,\mathrm{d}x \\ &= \frac{h_{j-1}}{2} f\left(\frac{u_{h,n-1}(x_{j-1}) + u_{h,n-1}(x_j)}{2}\right) + \frac{h_j}{2} f\left(\frac{u_{h,n-1}(x_j) + u_{h,n-1}(x_{j+1})}{2}\right) \\ &\qquad\qquad \text{for } j = 2, ..., N-1, \\ b_N &= \int_{x_{N-1}}^{x_N} f_{n-1}\phi_1 \,\mathrm{d}x = \frac{h_{N-1}}{2} f\left(\frac{u_{h,n-1}(x_{N-1}) + u_{h,n-1}(x_N)}{2}\right), \end{aligned}$$

where f represents the reaction terms.
Thus, we can compute the linear systems for the cell-bridging complexes FzVang, DshFzVang, FzVangPk and DshFzVangPk, which we then solve numerically.

Implementation

In the previous section we have derived the finite element approximations and their equivalent representation as linear systems for the PDEs of the system exemplified by equation

(4.19). In this section we demonstrate how we combine the approaches to simulate the whole system. The simulations are undertaken in Matlab for one hexagonal shaped domain. We apply periodic boundary conditions for the intercellular complex formation. Therefore, our setup represents a whole field of cells with identical initial conditions. A uniform mesh of granularity h is employed. The linear systems for Dsh and Pk are solved for all points in the two-dimensional mesh. The linear systems for Fz, Vang, DshFz and VangPk are only solved for the mesh points on the boundary of the domain. To compute the load vectors we have to calculate the reaction terms as described in the previous section. The size of the time step is adaptively chosen to ensure stability. The simulation stops once the system has reached a steady state, i.e., the change of the sum of the Dsh complexes at each mesh point is below a certain threshold.

Error convergence analysis

To validate our code we compared solutions for the system exemplified by equation (4.19) for different mesh sizes to a reference solution. We chose the parameter values given in Table 4.5.

K_{pk}	0.5
K_{va}	0.5
K_b	500
K_p	5
μ	$(100, 100, 0.1, 0.1, 0.01, 0.1, 0.1, 0.1, 0.1, 0.1)$
λ	$(50, 25, 0.001, 25, 50, 25, 25, 50, 25, 25)$
R	$(100, 50, 1000, 50, 100, 50, 50, 100, 50, 50)$

Table 4.5: Set of parameter values for simulations for Figures 4.13 and 4.15.

As initial condition we assumed an imbalance in Vang, since this yields a smoother reference solution than an initial imbalance in Fz as shown in Section 4.3.3. Initially, the other proteins were distributed homogeneously and there were no protein complexes. As reference solution u_r we simulated the system on a uniform mesh with mesh size $h = 0.0312$, which corresponds to 12481 nodes and 24576 elements.
Figure 4.13 shows the error of solutions u_h on coarser meshes compared to the reference solution. We plotted $\log(\|u_r - u_h\|_2)$ against $\log(h)$. All four figures show straight lines with slopes of approximately 2; hence the error decreases quadratically as we refine the mesh, which is indeed the optimal rate we would expect to observe [18].

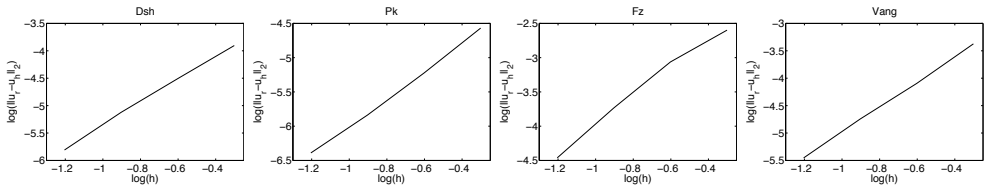

(a) (b) (c) (d)

Figure 4.13: Errors of solutions for Dsh, Pk, Fz and Vang of the system exemplified by (4.19) for different mesh sizes compared to a reference solution. We chose the parameter values in Table 4.5. Initially, there was an imbalance in Vang while the other proteins were distributed homogeneously and the complexes were zero.

4.3.2 Relationship between the full two-dimensional and the compartmentalised version of the model

To further clarify the setup of the full spatial representation of the model, we discuss its relationship to the compartmentalised representation in Section 4.2. For the latter, a cell is subdivided into six compartments, hence, it is essentially represented by six points and diffusion is the exchange of proteins or protein complexes between neighbouring points that belong to the same cell. The transition from this representation of the cell to the full spatial representation has to be explained separately for the three different groups of proteins and complexes, which are distinguished by the domain in which they are diffusing in the full spatial model.

The bridging complexes are only diffusing in the part of the membrane that is common to the two cells they connect. Let $A_j(t)$ denote the state variable for the bridging complexes in compartment $j \pmod 6$ then $\tilde{A}_j(x,t)$ represents the continuous function for the bridging complexes on piece $j \pmod 6$ of the membrane in the full spatial model as shown in the illustration in Figure 4.14. The transition of $\tilde{A}_j(x,t)$ to $\tilde{A}_{j\pm1}(x,t)$ at the vertices is not necessarily continuous.

Now we consider the proteins and protein complexes that diffuse in the whole membrane. If the state variable $B_j(t)$ represent these proteins and complexes in compartment $j \pmod 6$, then it corresponds to the continuous function $\tilde{B}_j(x,t)$ in the full spatial model, where $j \pmod 6$ denotes the jth piece of the membrane. The transition of $\tilde{B}_j(x,t)$ to $\tilde{B}_{j\pm1}(x,t)$ at the vertices has to be continuous.

The remaining proteins diffuse in the cytoplasm. This is unrelated to the compartmentalised representation of a cell, since the cell interior is not considered in that approach. However, in the full spatial model we apply flux boundary conditions for the interactions of these proteins with proteins and protein complexes in the membrane. Hence, the bound-

ary conditions can be related to the state variables $\tilde{A}_j(x,t)$ and $\tilde{B}_j(x,t)$.

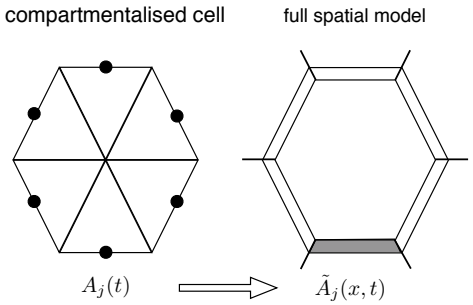

Figure 4.14: Illustration of the relationship between the compartmentalised version of the model and the full spatial representation. In the compartmentalised cell on the left, each compartment can be represented by a dot; in the full spatial model on the right, the membrane is divided into six pieces, each piece corresponding to one dot in the compartmentalised model. The variable $A_j(t)$ denotes the state of the bridging complexes in compartment $j \pmod 6$ of the compartmentalised cell and $\tilde{A}_j(x,t)$ the continuous function representing the bridging complexes in piece $j \pmod 6$ of the membrane in the full spatial model.

4.3.3 Numerical simulations

We simulated the system exemplified by equation (4.19) in Matlab for a hexagonal domain, applying the finite element method as described in the previous section. The parameter values we used are presented in Table 4.5. Figure 4.15 shows the four initial conditions we have chosen and the corresponding final states for the sum of the Dsh complexes. All the proteins and protein complexes considered in this figure only occur on the membrane. For clarity, we show a line plot and a two dimensional plot in each case.

The initial conditions in row A and B of Figure 4.15 are symmetric with respect to the horizontal axis whereas in row C and D they are asymmetric with respect to the same axis. For the initial condition in A1 and A2 we assume that Fz has an imbalance towards the right of the cell. All the other proteins are initially distributed homogeneously and there are no protein complexes initially. The final state in A3 and A4 shows that for this initial condition we do not get a significant polarity. The effects at mesh points 1 and 3 occur because there are discontinuities in the cell bridging complexes at these points. Refining the mesh to a granularity of $h = 0.008$, we get the same final distribution of the Dsh complexes.

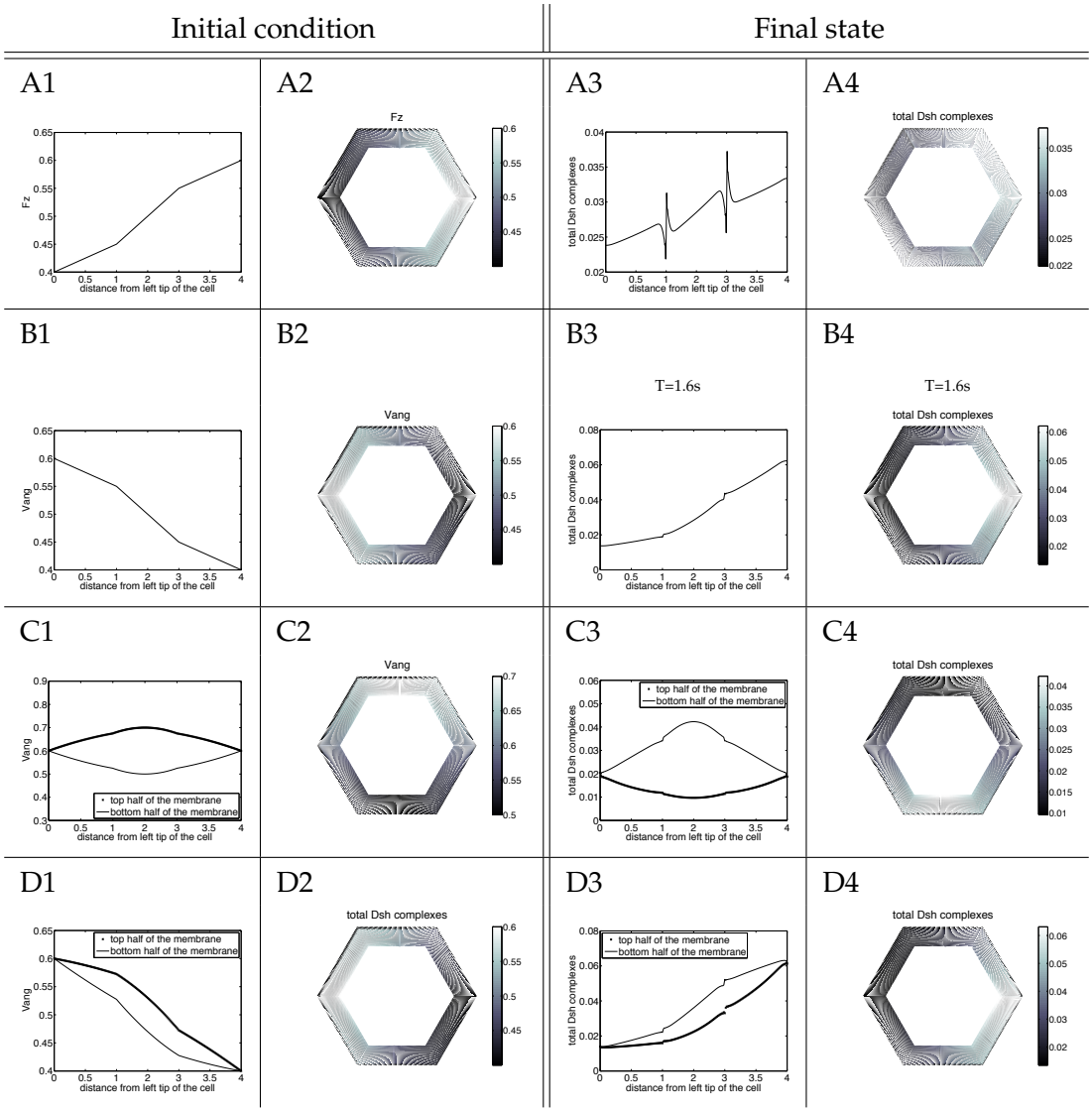

Figure 4.15: Initial conditions and final states for simulations of the system exemplified by (4.19) with the parameter values in Table 4.5. All the proteins and protein complexes represented occur only on the membrane. In each case a line plot and a two dimensional plot are shown. Row A: an initial imbalance in Fz does not give significant polarity for the parameter values in Table 4.5; the mesh size is $h = 0.016$; row B: an initial imbalance in Vang yields polarity; the mesh is of size $h = 0.031$; row C: initial conditions that are asymmetric with respect to the horizontal axis give rise to an asymmetric final state; the line plots show top and bottom half of the membrane separately; the mesh is of size $h = 0.031$; row D: initial condition in row B with an asymmetry with respect to the horizontal axis yields an asymmetric final state; the line plots show top and bottom half of the membrane separately; the mesh size is $h = 0.031$.

Row B shows that an initial imbalance in the Vang concentration yields polarity. We present the time to reach the state in B3 and B4 because this is the one that has been observed in the *Drosophila* pupal wings. In the biological system it takes about 32 h to polarise the cells. Therefore, the time T to reach steady state in our simulations is very small. Considering the relationship between our simulation time and the time in experiments, a possible explanation could be that the value of the diffusion coefficient μ_1^{bio} is less than the assumed 1 $\mu m^2/s$.

The difference in behaviour between row A and B is surprising. Comparing the final distributions for the individual proteins and protein complexes, we see that the two steady states represented by A3/A4 and B3/B4 are qualitatively different (not shown). A possible explanation might be that initially the mechanism of the model works different for the different initial conditions. The amplification of the initial imbalance is driven by the feedback loop. The way the inhibition is implemented in the model, building of most of the Dsh complexes is inhibited by themselves. Therefore, to get the amplification of the polarity Vang, Pk and VangPk have to dominate over the other terms in equation (4.18). For an initial imbalance in Fz the bridging complexes including Vang and Pk have first to be formed to transfer the initial imbalance in Fz into a biased inhibition. For the initial imbalance in Vang the inhibition is biased right from the start and therefore helps to generate stronger polarity. However, to verify this theory, further analysis is necessary.

Figures 4.15 C1 and C2 show an initial imbalance in Vang that is asymmetric with respect to the horizontal axis. The other proteins are initially distributed homogeneously. The final state in C3 and C4 shows that the asymmetry remains throughout the simulations. The same is true in row D. As initial condition we chose the imbalance in Vang in row B and added a small asymmetry with respect to the horizontal axis. We see in D3 and D4 that the corresponding final distribution of the total Dsh complexes is asymmetric with respect to the same axis.

If we increase the diffusion in Figure 4.15 row B and C, the difference between the different parts of the cell becomes weaker and for a sufficiently large diffusion we get the unpolarised steady state (not shown).

The results in this section support the findings in the previous sections that the persistent global bias is not needed to get polarity if there is an initial imbalance which is symmetric with respect to the horizontal axis. Furthermore, we found that there has to be an initial imbalance in Vang to get a significant polarity.

4.4 Discussion

In this chapter we presented an analysis of the model proposed by Amonlirdviman *et al.* [3]. While in [3] the model was simulated for a field of hexagonal cells we started our investigations by reducing it to a row of cells in one spatial dimension. The model consists of two main parts, a persistent global bias and an inhibition loop. Our first result was that the persistent global bias has a very strong impact, since it can reverse an initial polarity even when the inhibition loop is switched off. However, it is also possible to get polarity without the persistent global bias in one spatial dimension provided there is an initial imbalance that can be amplified. Our analysis showed that this result is consistent with linear stability analysis and does not depend on the parameter values. Similar to the conservative model in Chapter 3, the model in this chapter can amplify polarity from an initial imbalance in every cell or via a wave.

Extending the system to two spatial dimensions, assuming a hexagonal cell with six compartments gave further insight into the model. Again the persistent global bias is not needed to amplify an initial imbalance. However, to get correct polarity the initial conditions have to be symmetric with respect to the horizontal axis. Initial conditions that are asymmetric with respect to the horizontal axis give rise to asymmetric final states, which exist for the same parameter values as the desired polarised steady state and seem more robust against fluctuations in the initial conditions. The analysis of the full spatial model supports these findings. We numerically approximated the full spatial model in a hexagonal cell applying the finite element method. To this end, we considered three different domains since this model includes proteins that diffuse in the whole cell, proteins and complexes that only diffuse in the membrane and cell bridging complexes that are restrained to the edge of the membrane common to the cells they link together. The results of these simulations show that the persistent global bias is not needed provided there is an initial imbalance in the cell that is symmetric with respect to the horizontal axis. We further found out that an initial imbalance in Fz is not sufficient to polarise the cells significantly; an initial imbalance in Vang gave polarity. Possibly, the feedback loop is more suitable to amplify an initial imbalance in Vang than in Fz. So far, it is more common to assume a global cue that affects Fz, but there is no biological evidence for that.

Concerning the persistent global bias our analysis shows that it is not needed to amplify an initial imbalance. However, it is necessary to ensure correct polarisation if there is an asymmetry with respect to the horizontal axis. Such an asymmetry can be introduced by anomalies in the initial conditions or a clone. Therefore, we need to include the persistent global bias in the model to get the behaviour observed in experiments.

In all sections we have indicated the time it takes to reach the polarised steady state. Compared with the time it takes to polarise the cells in experiments, our simulation time was in a reasonable range in one spatial dimension, but too small for both two-dimensional representations. This result indicates that under our assumptions the value we used for the diffusion in the biological system is too large. This conclusion is supported by findings in yeast [51], which show that membrane diffusion for some of the proteins involved in cell polarisation is 1-2 orders of magnitude slower than the values given in [22] for membrane diffusion in mammalian cells.

Chapter 5

The effect of the initial conditions in the model by Le Garrec et al.

In [29] Le Garrec *et al.* proposed a model for PCP in the *Drosophila* wings. It is based on interactions of six proteins, a ligand (Ld), Fz, Dsh, Vang, Pk and Fmi, assuming they bind together to form complexes.

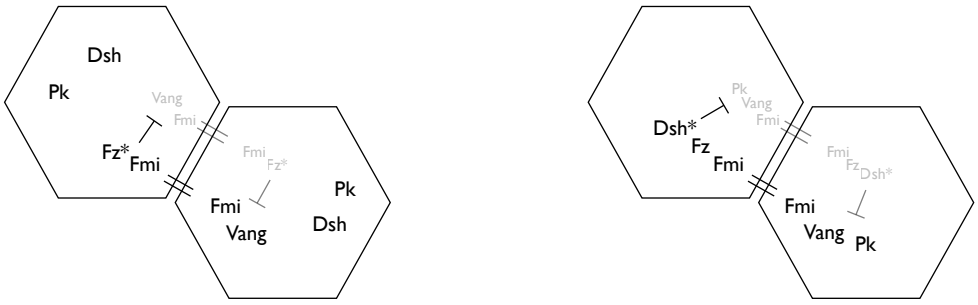

(a) (b)

Figure 5.1: Proposed mechanism for the model by Le Garrec *et al.*; light grey represents less protein than black; = indicates binding over the cell membrane and T inhibition; (a) First feedback loop: Fz* (active Fz) and its complexes inhibit the binding of Vang to Fmi, (b) second feedback loop: the Dsh* complexes inhibit the binding of Pk to Vang complexes (Dsh is phosphorylated when binding to the Fz*-ends of the cell bridging complexes, becoming Dsh*).

The idea of the mechanism is as follows (see also Figure 5.1). Initially there is an exponential Ld gradient decreasing from the proximal to the distal side of the region of cells. It is used up very quickly by binding to Fz, generating a gradient of active Fz (Fz*). Since Fz*

and Vang are both supposed to bind to Fmi, this competition for Fmi leads to two opposite gradients, a Fz*Fmi gradient decreasing from the proximal end of the cell region and a FmiVang gradient decreasing from the distal end. Formation of the cell bridging complex Fz*Fmi=FmiVang combined with the shallow Fz*Fmi and FmiVang gradients favours accumulation of slightly more Fz*-containing complexes on the distal sides of the cells. This is amplified by Fz* and its complexes inhibiting Vang from binding to Fmi, which is presented in Figure 5.1(a). To stabilise the cell bridging complexes Dsh binds to their Fz*-ends and is phosphorylated (Dsh*), whereas Pk binds to their Vang-ends. The asymmetry is further amplified by another feedback loop; Dsh* inhibits the binding of Pk as shown in Figure 5.1(b). These interactions are described by the following reactions.

$$Fz + Ld \xrightarrow{Kf_1} Fz^* \tag{5.1}$$

$$Fz^* + Fmi \underset{Kd_2}{\overset{Kf_2}{\rightleftharpoons}} Fz^*Fmi \tag{5.2}$$

$$Vang + Fmi \underset{en3\ Kd_3}{\overset{inh3\ Kf_3}{\rightleftharpoons}} FmiVang \tag{5.3}$$

$$Fz^*Fmi + FmiVang \underset{Kd_4}{\overset{Kf_4}{\rightleftharpoons}} Fz^*Fmi = FmiVang \tag{5.4}$$

$$Fz^*Fmi = FmiVang + Pk \underset{en5\ Kd_5}{\overset{inh5\ Kf_5}{\rightleftharpoons}} Fz^*Fmi = FmiVangPk \tag{5.5}$$

$$Dsh + Fz^*Fmi = FmiVang \underset{Kd_6}{\overset{Kf_6}{\rightleftharpoons}} Dsh^*FzFmi = FmiVang \tag{5.6}$$

$$Dsh + Fz^*Fmi = FmiVangPk \underset{Kd_7}{\overset{Kf_7}{\rightleftharpoons}} Dsh^*FzFmi = FmiVangPk \tag{5.7}$$

$$Dsh^*FzFmi = FmiVang + Pk \underset{en8\ Kd_8}{\overset{inh8\ Kf_8}{\rightleftharpoons}} Dsh^*FzFmi = FmiVangPk \tag{5.8}$$

The symbol = indicates complexes that bridge the membranes of two neighbouring cells. The forward reaction rate for equation (5.i) is Kf_i and the backward reaction rate is Kd_i. The two feedback loops are implemented by decreasing the forward reaction rates and increasing the backward reaction rates of equations (5.3), (5.5) and (5.8). They are multiplied by

$$inhi = \frac{1}{1 + A_i[\text{inhibitor}]},$$

and

$$eni = 1 + B_i[\text{inhibitor}],$$

respectively. The parameters A_i and B_i are positive. For $inh3$ and $en3$ the inhibitor is the sum of Fz* and its complexes, for $inh5, en5, inh8$ and $en8$ it is the sum of the Dsh* complexes.

In [29] these reactions are simulated in two spatial dimensions applying stochastic processes. Their approach is similar to the Cellular Potts model and was first introduced in [21]. A tissue is represented on a two-dimensional screen by a set of hexagonal pixels, which are coloured depending on their function, e.g. as part of the membrane, the extracellular matrix or the cytoplasm. They consider approximately 150 cells that are roughly hexagonal. Each pixel can contain proteins or protein complexes. Diffusion and intercellular as well as extracellular reactions are considered. The dynamics are noisy and described by stochastic difference equations. The reaction rates are assumed to fluctuate and intracellular diffusion is introduced by comparison of the concentration of a certain protein between two pixels of the same cell combined with a probability to move. Furthermore, thermodynamic fluctuations are introduced in the diffusion process. In contrast to the approach by Amonlirdviman *et al.* [3] in the previous chapter, diffusion is restricted to the membrane. Tests revealed that in this model cytoplasmic diffusion of Pk and Dsh does not significantly alter polarisation, provided that initial concentrations are similar throughout the cell. Ligand diffusion through the extracellular matrix also has a minimal effect on polarity in this model, since the ligand is rapidly depleted. Cell division was omitted. The choice of complexes results from experimental observations of interactions of the PCP proteins. To determine the feedback loops Le Garrec *et al.* tested different regulations. The loops chosen were the only ones that could reproduce the wild-type polarity for reasonably weak inhibition. Considering the parameter values, correct polarity is dependent on the four dissociation rates Kd_5 to Kd_8 being significantly smaller than the other reaction parameters, i.e. the fully built complexes have to be more stable than the intermediate ones. With this setup, the authors are able to reproduce wild-type polarity and the behaviour seen in experiments around clones lacking Fz, Fmi, Vang or Dsh as well as clones with higher levels of Fz, Fmi, Pk or Dsh. Furthermore, they find that the model is robust against noise and boundary effects.

Our aim is to analyse the proposed mechanism mathematically, focusing on the role of the initial global cue. To this end, we choose a deterministic approach, applying the law of mass action to (5.1)-(5.8). We expect our approach to give similar results to the stochastic simulations by Le Garrec *et al.*. To facilitate the analysis we first consider one spatial dimension.

5.1 Analysis in one spatial dimension

We assume a row of two-sided cells. On each side of a cell there are certain concentrations of the six proteins and their complexes. Applying the law of mass action, reactions (5.1)-(5.8) yield a system of ODEs for the rates of change of the protein and protein complex concentrations in cell i. We present two sample equations. The full system can be found in Appendix C.1. Here, we have

$$\begin{aligned}
\frac{\mathrm{d}[Pk]_i^l}{\mathrm{d}t} &= -inh5_i^l Kf_5\ [Fz^*FmiFmiVang]_{i-1}^r \cdot [Pk]_i^l + en5_i^l Kd_5\ [Fz^*FmiFmiVangPk]_{i-1}^r \\
&\quad - inh8_i^l Kf_8\ [Dsh^*FzFmiFmiVang]_{i-1}^r \cdot [Pk]_i^l \\
&\quad + en8_i^l Kd_8\ [Dsh^*FzFmiFmiVangPk]_{i-1}^r \\
&\quad + \mu_7\ \frac{([Pk]_i^r - [Pk]_i^l)}{\Delta x^2} \\
\frac{\mathrm{d}[Pk]_i^r}{\mathrm{d}t} &= -inh5_i^r Kf_5\ [Fz^*FmiFmiVang]_{i+1}^l \cdot [Pk]_i^r + en5_i^r Kd_5\ [Fz^*FmiFmiVangPk]_{i+1}^l \\
&\quad - inh8_i^r Kf_8\ [Dsh^*FzFmiFmiVang]_{i+1}^l \cdot [Pk]_i^r \\
&\quad + en8_i^r Kd_8\ [Dsh^*FzFmiFmiVangPk]_{i+1}^l \\
&\quad + \mu_7\ \frac{([Pk]_i^l - [Pk]_i^r)}{\Delta x^2}
\end{aligned} \tag{5.9}$$

where

$$\begin{aligned}
inh5_i^l &= \frac{1}{1 + A_5([Dsh^*FzFmiFmiVang]_i^l + [Dsh^*FzFmiFmiVangPk]_i^l)}, \\
inh5_i^r &= \frac{1}{1 + A_5([Dsh^*FzFmiFmiVang]_i^r + [Dsh^*FzFmiFmiVangPk]_i^r)}, \\
en5_i^l &= 1 + B_5([Dsh^*FzFmiFmiVang]_i^l + [Dsh^*FzFmiFmiVangPk]_i^l), \\
en5_i^r &= 1 + B_5([Dsh^*FzFmiFmiVang]_i^r + [Dsh^*FzFmiFmiVangPk]_i^r),
\end{aligned}$$

and $inh8$ and $en8$ are defined analogously. The parameter μ_7 represents diffusion and Δx the spatial extension of a cell from left to right. The equations describe the variation of the protein concentrations, indicated by the square brackets. Subscripts refer to the cell number, superscripts to the cell side, left or right. Bridging complexes are not allowed to diffuse and they are counted as if they belong to the same cell as their Fz part. If T, μ_7^{bio} and Δx^{bio} denote the time, the diffusion coefficient and the side length of a cell in the biological system they are related to the parameters in our model by $t = kT, \mu_7 = \frac{1}{k}\mu_7^{bio}$ and $\Delta x = p\Delta x^{bio}$ with positive constants k and p.

After rescaling, (5.9) can be stated in the general form

$$\begin{aligned} \frac{\mathrm{d}[Pk]_i^l}{\mathrm{d}\tau} &= F + \mu_7^{sim}\ ([Pk]_i^r - [Pk]_i^l), \\ \frac{\mathrm{d}[Pk]_i^r}{\mathrm{d}\tau} &= F + \mu_7^{sim}\ ([Pk]_i^l - [Pk]_i^r), \end{aligned} \tag{5.10}$$

where F represents the reaction terms, $\mu_7^{sim} = \frac{1}{\Delta x^2}\mu_7 = \frac{1}{kp^2(\Delta x^{bio})^2}\mu_7^{bio}$ and $\tau = \mu_7^{sim}t$. Hence, the time in experiments T is related to the time in our analysis and simulations τ by

$$T = \frac{1}{k\mu_7^{sim}}\tau = \frac{p^2(\Delta x^{bio})^2}{\mu_7^{bio}}\tau. \tag{5.11}$$

We assume $p = 1$, $\mu_7^{bio} = 0.1\,\mu\mathrm{m/s}$ [22] and $\Delta x^{bio} = 8\,\mu\mathrm{m}$ [19]; then k is determined by equation (5.11). We chose a smaller value for μ_7^{bio} than in Section 4.1, because membrane diffusion, which we consider here, is slower than cytoplasmic diffusion [22]. The values for p and Δx are the same as in Section 4.1. The system exemplified by (5.10) conserves the total concentration of each protein in a cell. However, reformulating the equations using these laws would not simplify the system significantly. Considering that the system is very complex we do not study it analytically, but conduct a computational analysis.

5.1.1 Numerical simulations

We commence our analysis by investigating the behaviour of the system exemplified by (5.10) for the parameter values given in [29]. To this end, we have to find the appropriate scaling for the diffusion coefficient. In [29] they consider 150 roughly hexagonal cells on a screen of 175 by 175 pixels, whereby each pixel has a size of 1 µm. Hence, the side length Δx^{hex} of one cell is about 9 µm. Let μ^{hex} denote the rescaled diffusion coefficient for the hexagonal cells in [29] and μ the rescaled diffusion coefficient for our one-dimensional analysis. We get

$$\begin{aligned} \mu^{hex} &= \mu^{bio}\frac{(\Delta x^{hex})^2}{(\Delta x^{bio})^2}, \\ \mu &= \frac{1}{\Delta x^2}\mu^{bio}, \end{aligned}$$

and therefore substituting the values from above $\mu = \frac{1}{81}\mu_{hex}$. The parameter values are shown in Table 5.1.

A_3	1.5
A_5	1.5
A_8	1.5
B_3	3
B_5	3
B_8	3
Kf	$(0.01, 0.01, 0.01, 0.015, 0.03, 0.03, 0.003, 0.003)$
Kd	$(0, 0.04, 0.04, 0.04, 0.001, 0.001, 0.0005, 0.0005)$
μ	$\frac{1}{81}(0.02, 0.02, 0.02, 0.02, 0.02, 0.02, 0.02, 0.02, 0.02)$

Table 5.1: Set of parameter values from [29] after rescaling of the diffusion coefficients. We used these values for the simulations in Figures 5.2- 5.4.

Behaviour for initial ligand gradient

We simulated the system exemplified by (5.10) using Matlab's ODE solver ode15s, which is faster than the previously used ode45. Initially Fz, Fmi, Vang, Dsh and Pk are distributed homogeneously in every cell, with $[Fz]_i^l = [Fz]_i^r = 4, [Fmi]_i^l = [Fmi]_i^r = 4, [Vang]_i^l = [Vang]_i^r = 2, [Dsh]_i^l = [Dsh]_i^r = 2$ and $[Pk]_i^l = [Pk]_i^r = 2$ for all i. These numbers are the concentrations of the proteins in each membrane pixel in [29]. We choose different initial ligand gradients to gain insight into their effect on the final state of the system. As boundary conditions we assume that at both ends of the row we have another half cell which has its initial ligand concentration according to the one in the cell next to the boundary and the initial concentrations of the other proteins equal to the ones in the rest of the cells. We ensure these two cells are only half by setting all their intracellular diffusion coefficients to zero; the remaining interactions in these cells are governed by the same equations as for the rest of the cells. In [29] there are roughly 13 cells in each row. At the boundaries they assume that no material escapes or enters the domain. We simulate the system for 11 cells plus 2 half boundary cells. We assume that the system has reached a final state if the change of the protein and protein complex concentrations is below 10^{-4}.

Different initial ligand gradients and the corresponding final states of the system exemplified by (5.10) are shown in Figures 5.2 and 5.3. We present the final distributions of the sum of the Dsh* complexes, because in [29] this is assumed to determine the direction of the hair growth; the hairs are assumed to grow at the end of the cell with the highest Dsh* concentration.

In Figure 5.2 A1 we assume a decreasing exponential ligand gradient similar to the initial condition in [29]. In the corresponding final state in B1 every cell is polarised to the

right. Due to the boundary conditions the polarity of the cells at the two ends of the row is weaker. The cells in the left half of the row are more weakly polarised than in the right half of the row. This is because in cells 1-3 the total amount of ligand is greater than the total amount of Dsh, Vang and Pk. Assuming an initial gradient with a lower level of Ld gives a more uniform distribution of the polarity (not shown). Figures 5.2 B2 and B3 show that the final distribution does not depend strongly on the type of gradient. An initial linear ligand gradient gives similar polarity and so does an initial condition in which the initial amount of ligand is the same on both sides of the cell. The direction of the final polarity depends on the direction of the gradient. Increasing gradients lead to polarity to the left (not shown). In all cases in Figure 5.2 the total amount of ligand in each cell is less than the total amount of Fz. If we choose $[Ld]_{total} > [Fz]_{total}$ within each cell, we do not get polarity (not shown), because in this case there would not be a Fz* gradient which initiates polarity.

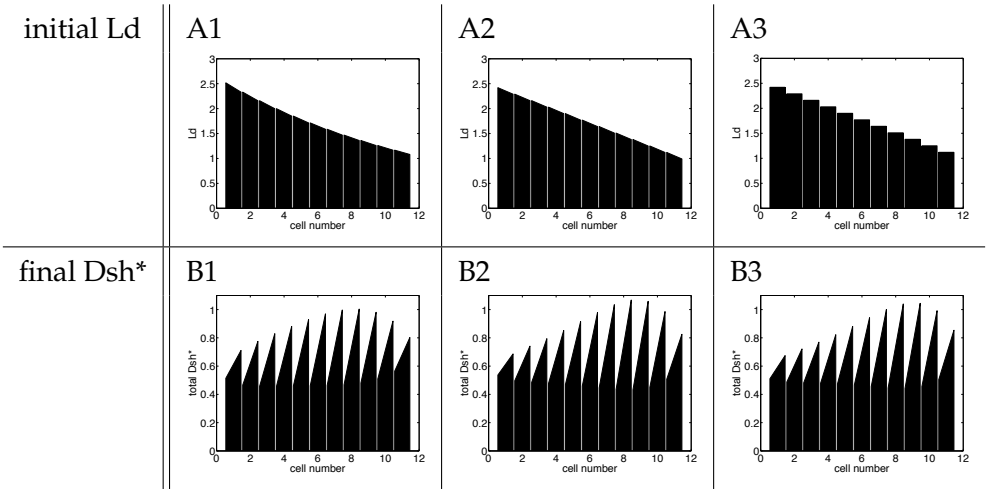

Figure 5.2: Different initial ligand gradients and the corresponding final Dsh* distributions for the system exemplified by (5.10). The gradient in A1 is similar to the one in [29]. The weaker polarity in the first and the last cell of the row in B1-B3 is due to the boundary conditions. The polarity in the left half of the row in B1-B3 is weaker because in cell 1-3 there is more ligand than Dsh, Vang and Pk. We see that the final polarity is not strongly dependent on the type of initial ligand gradient.

Figure 5.3 shows the final distribution of the sum of the Dsh* complexes for gradients with different slopes and different total amounts of Ld. Column 1 shows that a shallower gradient yields weaker polarity. The initial ligand gradient in Figure 5.3 A2 only leads to significant polarity on the left end of the row. On the right end, there is not enough Ld to form a significant amount of Dsh* complexes. In Figure 5.3 column 3 we see the opposite effect. On the left end of the row of Figure 5.3 A3, the total amount of Ld in each cell is

greater than the total amount of Fz. Hence, we do not get polarity. On the right end of the row the level of Ld is low enough and the gradient is steep. Therefore, we get strong polarity.

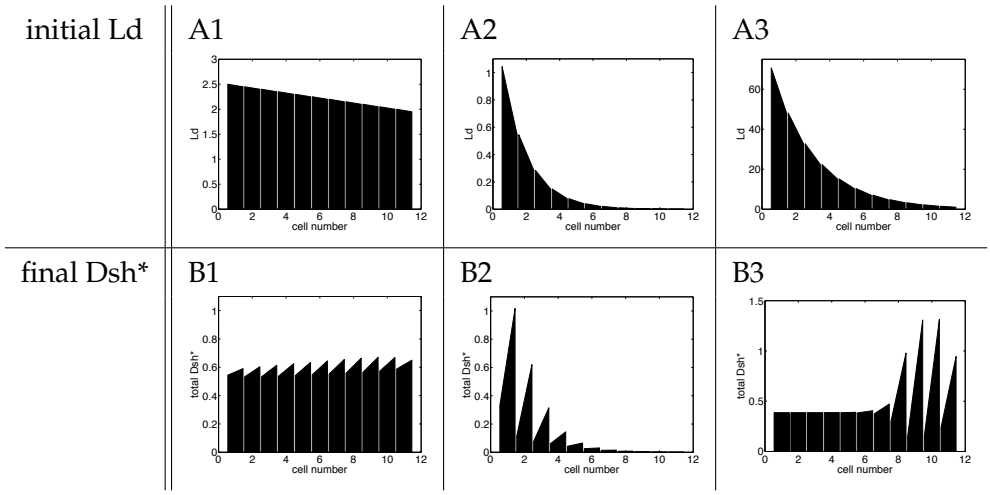

Figure 5.3: Different initial ligand gradients and the corresponding final Dsh* distributions for the system exemplified by (5.10); Column 1: a shallow gradient gives weak polarity; column 2: if the ligand concentration is not sufficient we do not get polarity; column 3: too much ligand hinders polarity.

These results show that as long as there is a sufficient amount of ligand, but less than Fz in each cell, polarity occurs in the direction opposite to the direction of the initial ligand gradient. The strength of the polarity is dependent on the slope of the initial ligand gradient.

Behaviour for an initial ligand imbalance in every cell

An initial gradient has a similar effect to the persistent global bias in the model by Amonlirdviman *et al.* (see Chapter 4, [3]); it gives the system a bias that lasts for the whole process, preventing any homogeneous unpolarised steady states. Our aim is to investigate whether an initial ligand distribution with a small imbalance in every cell can also yield polarity. The initial condition and the corresponding final state for a row of ten cells and the parameter set in Table 5.1 are presented in Figure 5.4. Note, that we chose the total amount of ligand in each cell to be less than the total amount of any other protein to ensure that the ligand is the limiting factor and we do not get effects on the polarity caused by excessive amounts of Ld. We apply periodic boundary conditions. Hence, our simulations represent an infinite line of cells and the results do not depend on the number of cells chosen. Figure 5.4 shows that even for a strong initial cue the system exemplified by

(5.10) cannot generate polarity with this parameter set. This is supported by linear stability analysis. We calculate the homogeneous unpolarised steady state for the given total amounts of the proteins and the parameter set in Table 5.1. Subsequently, we evaluate the eigenvalue with the greatest real part λ. In this case it is $\lambda = -1.4 \cdot 10^{-4} < 0$. Hence, linear stability analysis does not predict instabilities for this set of parameter values.

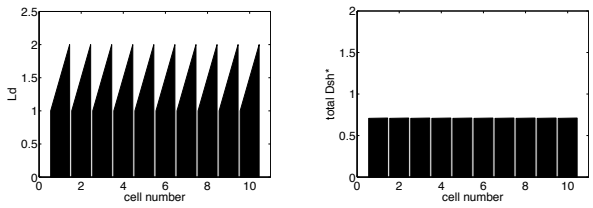

(a) (b)

Figure 5.4: The system exemplified by (5.10) does not polarise for an initial ligand imbalance in every cell and the parameter values in Table 5.1. (a) Initial ligand distribution with a strong polarity; (b) final Dsh* distribution for the parameter values in Table 5.1.

The aim now is to find a parameter set for which the system polarises for a small initial ligand imbalance in every cell. To this end, we use the parameter search method that was introduced in Section 4.1.3, applying search steps based on the Nelder-Mead method to increase the largest real part of the eigenvalues of the system (see Appendix A). Two resulting parameter sets are shown in Table 5.2. For these parameter sets the largest real part λ of the eigenvalues of the system exemplified by (5.10) is positive. Hence, we expect polarisation.

To test this, we simulated the system exemplified by (5.10) for the parameter values in Table 5.2, applying periodic boundary conditions. The total amount of each protein in every cell is the same as above. As initial condition we assumed a small imbalance of the ligand concentration in every cell. Figure 5.5 shows that we get polarity for both parameter sets in Table 5.2. The polarity for parameter set 1 in Figure 5.5(b) is stronger than the polarity for parameter set 2 in Figure 5.5(c). Furthermore, it takes longer to establish.

These results show that in one spatial dimension a small ligand imbalance in every cell can give rise to polarity. Before investigating the behaviour of the model for anomalies in the initial conditions and clones we will first extend the model to two spatial dimensions.

	Parameter Set 1	Parameter Set 2
A_3	2.9577	3.3885
A_5	8.1077	8.5385
A_8	0.3692	0.8
B_3	5.6271	6.0579
B_5	10.3692	10.8
B_8	0.1077	0.5385
Kf	$(858.8877, 398.1077, 86.6077, 57.9227,$ $12.3716, 1.405, 10.1077, 10.9574)$	$(10.3185, 5.5385, 6.0385, 2.3535,$ $13.5095, 1.8358, 10.5385, 11.3882)$
Kd	$(0, 0.5657, 0.6713, 0.3533,$ $0.2045, 0.001114, 0.9148, 0.001177)$	$(0, 0.9965, 1.1021, 1.4912,$ $0.6353, 0.4319, 2.7598, 0.4319)$
μ	$(0.7519, 0.4829, 0.1695, 0.7507,$ $2.6369, 1.4969, 1.5244, 2.4982, 0.0269)$	$(0.0625, 0.0625, 0.0019, 0.0625,$ $0.1250, 0.0625, 0.0625, 0.1250, 0.0019)$
λ	0.0072	0.0081

Table 5.2: Two parameter sets resulting from a parameter search applying the method in Section 4.1.3 and Appendix A. The parameter λ represents the maximal real part of the eigenvalues of the system exemplified by equations (5.10).

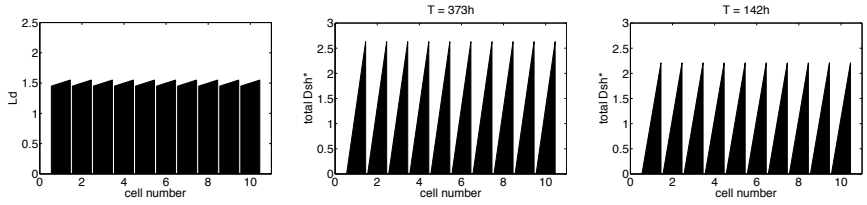

(a) (b) (c)

Figure 5.5: Results of simulations for the system exemplified by (5.10); (a) Initial ligand distribution with a small imbalance in every cell, the difference between right and left in each cell is 0.1; initially, the other proteins are distributed homogeneously and there are no protein complexes; (b) final state of total Dsh* for parameter set 1 in Table 5.2; (c) final state of total Dsh* for parameter set 2 in Table 5.2.

5.2 Analysis in two spatial dimensions for compartmentalised cells

In this section we extend our analysis to two spatial dimensions. We assume hexagonal cells with six compartments. Applying reaction kinetics to equations (5.1)-(5.8) we get the system of equations, which can be found in Appendix C.2. We present one sample equation.

$$\begin{aligned}\frac{\mathrm{d}[Pk]_{i,j}}{\mathrm{d}t} = &-inh5_{i,j}Kf_5\ [Fz^*FmiFmiVang]^+_{i,j}\cdot[Pk]_{i,j}\\ &+ en5_{i,j}Kd_5\ [Fz^*FmiFmiVangPk]^+_{i,j}\\ &- inh8_{i,j}Kf_8\ [Dsh^*FzFmiFmiVang]^+_{i,j}\cdot[Pk]_{i,j}\\ &+ en8_{i,j}Kd_8\ [Dsh^*FzFmiFmiVangPk]^+_{i,j}\\ &+ \mu_7\frac{[Pk]_{i,j+1}+[Pk]_{i,j-1}-2[Pk]_{i,j}}{\Delta x^2},\end{aligned} \tag{5.12}$$

where

$$\begin{aligned}inh5_{i,j} &= \frac{1}{1+A_5([Dsh^*FzFmiFmiVang]_{i,j}+[Dsh^*FzFmiFmiVangPk]_{i,j})},\\ en5_{i,j} &= 1+B_5([Dsh^*FzFmiFmiVang]_{i,j}+[Dsh^*FzFmiFmiVangPk]_{i,j})\end{aligned}$$

and $inh8$ and $en8$ analogue. The superscript + indicates binding over the cell membrane, i is the cell number and j (mod 6) the number of the compartment. The diffusion is represented by μ_7 and Δx describes the distance between two neighbouring compartments within a cell. Let T, μ_7^{bio} and Δx^{bio} denote the time, the diffusion coefficient and the side length of a cell in the biological system. Then, these parameters are related to the parameters in our model by $t = kT, \mu_7 = \frac{1}{k}\mu_7^{bio}$ and $\Delta x = p\,\Delta x^{bio}$ with positive constants p and k. Rescaling (5.12) yields

$$\frac{\mathrm{d}[Pk]_{i,j}}{\mathrm{d}\tau} = F + \mu_7^{sim}\ ([Pk]_{i,j+1}+[Pk]_{i,j-1}-2[Pk]_{i,j}), \tag{5.13}$$

where $\mu_7^{sim} = \frac{1}{\Delta x^2}\mu_7 = \frac{1}{kp^2(\Delta x^{bio})^2}\mu_7^{bio}$ is the diffusion parameter, F represents the reaction terms and $\tau = \mu_7^{sim}t$. Hence, the relation between the time T in experiments and our simulation time τ is

$$T = \frac{1}{k\mu_7^{sim}}\tau = \frac{p^2(\Delta x^{bio})^2}{\mu_7^{bio}}\tau. \tag{5.14}$$

We assume $p = \frac{1}{4}$, $\Delta x^{bio} = 8\,\mu\mathrm{m}$ [19] and $\mu_7^{bio} = 0.1\,\mu\mathrm{m}^2/\mathrm{s}$ [22]; then the parameter k is determined by equation (5.14). In the following we will investigate whether a ligand imbalance is sufficient to get polarity.

5.2.1 Numerical simulations

We simulated the system exemplified by equation (5.13) for a hexagonal cell with six compartments in Matlab using the ODE solver ode15s. For the intercellular interactions we apply periodic boundary conditions. Thereby, we ensure that our results are valid for an array of hexagonal cells with identical initial conditions. For the parameter values we choose parameter set 2 in Table 5.2 including a factor m to vary the diffusion as shown in Table 5.3. After scaling of the diffusion coefficient, the parameter set in Table 5.3 corresponds to parameter set 2 in Table 5.2 if $m = 16$. The total amount of each protein in a cell is the same as in the previous section.

A_3	3.3885
A_5	8.5385
A_8	0.8
B_3	6.0579
B_5	10.8
B_8	0.5385
Kf	$(10.3185, 5.5385, 6.0385, 2.3535, 13.5095, 1.8358, 10.5385, 11.3882)$
Kd	$(0, 0.9965, 1.1021, 1.4912, 0.6353, 0.4319, 2.7598, 0.4319)$
μ	$m \cdot (0.0625, 0.0625, 0.0019, 0.0625, 0.1250, 0.0625, 0.0625, 0.1250, 0.0019)$

Table 5.3: Parameter set 2 with a variable diffusion coefficient. We used these parameter values for the simulations of the system exemplified by (5.13) in Figures 5.6-5.8.

Figures 5.6 and 5.7 show two initial conditions and the corresponding final states for different values of m. In Figure 5.6(a) we assume an initial ligand imbalance that is symmetric with respect to the horizontal axis while the other proteins are initially distributed homogeneously and there are no complexes initially. For $m = 16$ this leads to a polarised final distribution of total Dsh* that is symmetric with respect to the horizontal axis as shown in Figure 5.6(b). For $m = 320$ we get a weaker polarised steady state (see Figure 5.6(c)). If we increase m above a certain threshold, Figure 5.6(d) shows that we get the homogeneous unpolarised steady state. We only show the times to reach the polarised steady states, since this is the only type of steady state that has been observed in the *Drosophila* wing.
The initial ligand distribution in Figure 5.7(a) is asymmetric with respect to the horizontal axis. The top three compartments have less ligand than the bottom three. This gives rise to asymmetric final distributions of total Dsh* for sufficiently small m and we get the homogeneous unpolarised steady state for m above a certain threshold as shown in Figures 5.7(b)-(d). In Figure 5.7(c) total Dsh* is higher in the bottom middle compartment than in

the two next to it and it is lower in the top middle compartment than in the two next to it as shown in the illustration. We refer to this state as polarised toward the bottom middle compartment. It exists for the same parameter values as the polarised steady state that is symmetric with respect to the horizontal axis in Figure 5.6(c). Numerical analysis suggests that there exist at least five other polarised steady states that are asymmetric with respect to the horizontal axis; the states that are polarised toward each of the remaining five compartments in the cell.

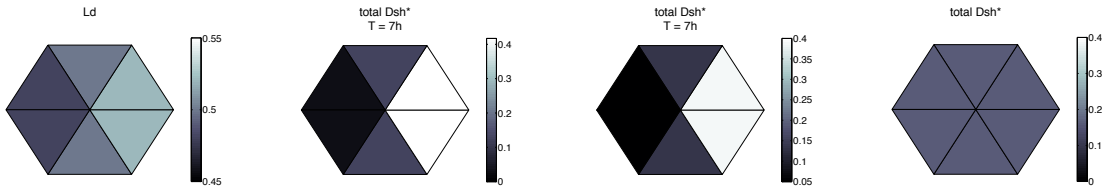

(a) (b) (c) (d)

Figure 5.6: Final states for a single hexagonal cell with six compartments for the system exemplified by (5.13). Due to the periodic boundary conditions this cell represents an array of identical cells with the same initial conditions. We used the parameter values in Table 5.3 and different values of m. For clarity the compartments are divided by black lines. Note the different scales in the different figures. (a) Initial ligand distribution, which is symmetric with respect to the horizontal axis; initially, the other proteins are distributed homogeneously; (b) final distribution of total Dsh* for $m = 16$; polarised steady state; these parameter values correspond after scaling of the diffusion coefficient to parameter set 2 in the one-dimensional case in Section 5.1; (c) final distribution of total Dsh* for $m = 320$, polarised steady state, the polarity of this state is slightly weaker than of the state in (b); (d) final distribution of total Dsh* for $m = 4800$, unpolarised steady state.

Analysing the existence and stability of the system exemplified by (5.13) would be very complex. Therefore, we conducted a numerical analysis. To this end, we simulated the system exemplified by equation (5.13) for the parameter values in Table 5.3 and $m = 320$. As initial conditions we perturbed the steady states in two different ways. We chose a symmetric perturbation and an asymmetric perturbation with respect to the horizontal axis. The results suggest that the polarised steady state that is symmetric with respect to the horizontal axis is stable to perturbations that are symmetric with respect to the same axis but unstable to perturbation that are asymmetric with respect to the horizontal axis. The steady states that are asymmetric with respect to the horizontal axis seem to be stable to both types of perturbations. Hence, introducing an asymmetry with respect to the hor-

izontal axis hinders correct polarisation. Including a clone or fluctuations in the field of cells would yield such an asymmetry.

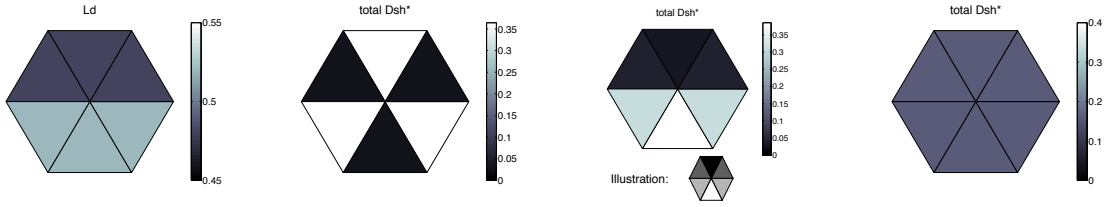

(a) (b) (c) (d)

Figure 5.7: Final states for a single hexagonal cell – representing a whole array of cells – with six compartments for the system exemplified by (5.13), initial conditions that are asymmetric with respect to the horizontal axis, the parameter values in Table 5.4 and different values of m. For clarity the compartments are divided by black lines; note the different scales in the different figures; (a) Initial ligand distribution, which is asymmetric with respect to the horizontal axis; initially, the other proteins are distributed homogeneously; (b) final distribution of total Dsh* for $m = 1.6$; (c) final distribution of total Dsh* for $m = 320$, the amount of total Dsh* is higher in the bottom middle compartment than in the two neighbouring compartments, the amount in the top middle compartment is lower than in the two neighbouring compartments as shown in the illustration; (d) final distribution of total Dsh* for $m = 3200$, unpolarised steady state.

Figure 5.8 shows the result for a clone lacking Fz. As initial condition we assume an initial ligand imbalance in every cell, while the other proteins are distributed homogeneously. Furthermore, we include one cell that has no Fz as shown in Figure 5.8(a). On the left and right boundaries of the 10×10 field of cells we assumed that all the cells are only half with their properties corresponding to the boundary cells. For the top and bottom boundaries we applied periodic boundary conditions. The final state of the system exemplified by (5.13) for the parameter values in Table 5.3 and $m = 320$ is shown in Figure 5.8(b). The clone is indicated by the red border. The cells in the same row as the clonal cell show polarity but the rest of the cells in the field show a disordered distribution of total Dsh*. This differs from experimental findings in the *Drosophila* wing in which the cells close to the clone show reorientation but the rest of the wing cells are polarised normally (see Figure 1.3(a)).

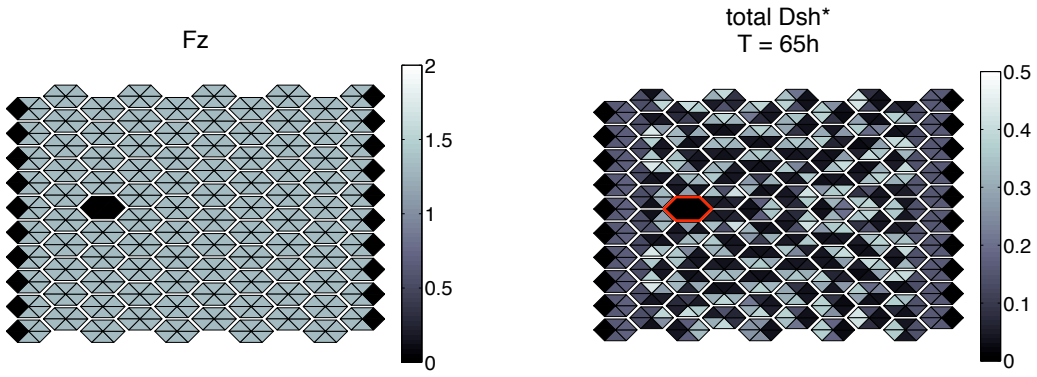

(a) (b)

Figure 5.8: Result for a 10×10 field of cells with a Fz-null cell. At the top and bottom boundary we apply periodic boundary conditions, while at the left and right boundary we assume we have a column of half a cell with the same properties as the boundary cells; we chose the parameter values in Table 5.3 with $m = 320$. (a) Initial Fz distribution with one cell without Fz; initially there is a symmetric (with respect to the horizontal axis) Ld imbalance in every cell, the remaining proteins are distributed homogeneously; (b) distribution of total Dsh*, the clonal cell is indicated by the red border, the cells in the same row as the clone show an orientation.

5.3 Analysis of the full spatial model

In this section we consider the full spatial model on a hexagonal domain. Different to the previous section we do not consider a coarse compartmentalisation of the cells but approximate the full partial differential model for diffusion within the cell membrane. Applying the law of mass action to reactions (5.1)-(5.8) we get the system of equations. Here we present the equation for $[Pk]$ as an example. The full system of equations can be found in Appendix C.3.

We get

$$\begin{aligned}\frac{\partial [Pk]}{\partial t} = &-inh5\, Kf_5\, [Fz^*FmiFmiVang]^+\, [Pk] + en5\, Kd_5\, [Fz^*FmiFmiVangPk]^+ \\ &- inh8\, Kf_8\, [Dsh^*FzFmiFmiVang]^+\, [Pk] \\ &+ en8\, Kd_8\, [Dsh^*FzFmiFmiVangPk]^+ + \mu_7 \nabla^2 [Pk],\end{aligned} \tag{5.15}$$

where

$$inh5 = \frac{1}{1 + A_5([Dsh^*FzFmiFmiVang] + [Dsh^*FzFmiFmiVangPk])},$$
$$inh8 = \frac{1}{1 + A_8([Dsh^*FzFmiFmiVang] + [Dsh^*FzFmiFmiVangPk])},$$

$$en5 = 1 + B_5([Dsh^*FzFmiFmiVang] + [Dsh^*FzFmiFmiVangPk]),$$
$$en8 = 1 + B_8([Dsh^*FzFmiFmiVang] + [Dsh^*FzFmiFmiVangPk]).$$

The superscript + indicates binding over the cell membrane and μ_7 is the diffusion coefficient. In contrast to the previous sections we now assume continuous distributions of the protein concentrations. The side length of the domain in our model is given by Δx. If T, μ_7^{bio} and Δx^{bio} denote the time, the diffusion coefficient and the side length of a cell in the biological system, they are related to the parameters in our model by $t = kT$, $\mu_7 = \frac{1}{k}\mu_7^{bio}$ and $\Delta x = p\,\Delta x^{bio}$ with positive k and p.
After rescaling, (5.15) can be written in the general form

$$\frac{\partial\,[Pk]}{\partial\tau} = F + \mu_7^{sim}\nabla^2[Pk], \tag{5.16}$$

where F represents the reaction terms. The parameter μ_7^{sim} is a diffusion coefficient, with $\mu_7^{sim} = p^2\mu_7 = \frac{1}{k}p^2\mu_7^{bio}$. Furthermore, $\tau = \mu_7^{sim}t$. Hence, the simulation time τ is related to time T in experiments by

$$T = \frac{1}{k\mu_7^{sim}}\tau = \frac{1}{p^2\mu_7^{bio}}\tau \tag{5.17}$$

We assume $\mu_7^{bio} = 0.01\ \mu m^2/s$ [22], $\Delta x^{bio} = 8\ \mu m$ [19] and $p = \frac{1}{4}$. Then, the parameter k is determined by (5.17).
In [29] Le Garrec *et al.* assume that the cell bridging complexes cannot diffuse. Furthermore, they found out that in this model cytoplasmic diffusion does not significantly alter the polarisation. Therefore, we assume that all proteins and complexes occur in the membrane and diffuse within this domain unless they are bridging complexes. Hence, the Laplacian in (5.15) and (5.16) is only applied within the membrane.

5.3.1 Numerical simulations

We numerically approximated the system exemplified by equation (5.16) in Matlab, applying the finite element method introduced in Section 4.3. Since in this model all proteins and protein complexes that diffuse do so in the whole membrane, our problem is essentially one-dimensional. Hence, the finite element code derived in Section 4.3 can be reduced to the case " Diffusible in the domain boundary - 1-D Problem with periodic boundary conditions".
In Section 5.2 we had six compartments, i.e. essentially six dots representing a cell. Here, the cell consists of six pieces of membrane and the proteins and protein complexes are represented by functions that are continuous on these membrane pieces. For the cell bridging

complexes the transition at the vertices is not necessarily continuous, for the rest of the proteins and protein complexes it has to be.
We simulated the system for one cell, applying periodic boundary conditions for the cell bridging complex formation. Therefore, our setup represents a whole field of cells with identical initial conditions. The total amounts of the proteins are the same as in the previous sections, i.e. $[Ld]_{total} = 3, [Fz]_{total} = 8, [Fmi]_{total} = 8, [Vang]_{total} = 4, [Dsh]_{total} = 4$ and $[Pk]_{total} = 4$. Our choice of parameter values is presented in Table 5.4. After scaling the diffusion coefficients they correspond to parameter set 1 in the one-dimensional case in Section 5.1.

A_3	2.9577
A_5	8.1077
A_8	0.3692
B_3	5.6271
B_5	10.3692
B_8	0.1077
Kf	$(858.8877, 398.1077, 86.6077, 57.9227, 12.3716, 1.405, 10.1077, 10.9574)$
Kd	$(0, 0.5657, 0.6713, 0.3533, 0.2045, 0.001114, 0.9148, 0.001177)$
μ	$4 \cdot (0.7519, 0.4829, 0.1695, 0.7507, 2.6369, 1.4969, 1.5244, 2.4982, 0.0269)$

Table 5.4: Parameter values we used for the simulations of the system exemplified by (5.16) in Figures 5.9 and 5.10. They correspond to parameter set 1 in Table 5.2. The factor 4 is derived by the scaling of the diffusion coefficient.

To validate our code we conduct an error convergence study similar to Section 4.3.1. We calculated a reference solution u_r for a uniform mesh with mesh size $h = 0.0312$ (384 nodes and elements) and the parameter values in Table 5.4. Initially, we assume a ligand gradient in the cell, increasing from left to right. The other proteins are initially distributed homogeneously and there are no complexes initially. We then compare solutions u_h on coarser meshes to the reference solution. We plotted $\log(\|u_r - u_h\|_2)$ against $\log(h)$ in Figure 5.9. It shows that the error decreases if the mesh is refined, which is what we expect. We do not expect quadratic convergence, since the finite element solutions for the cell bridging complexes are not necessarily continuous.

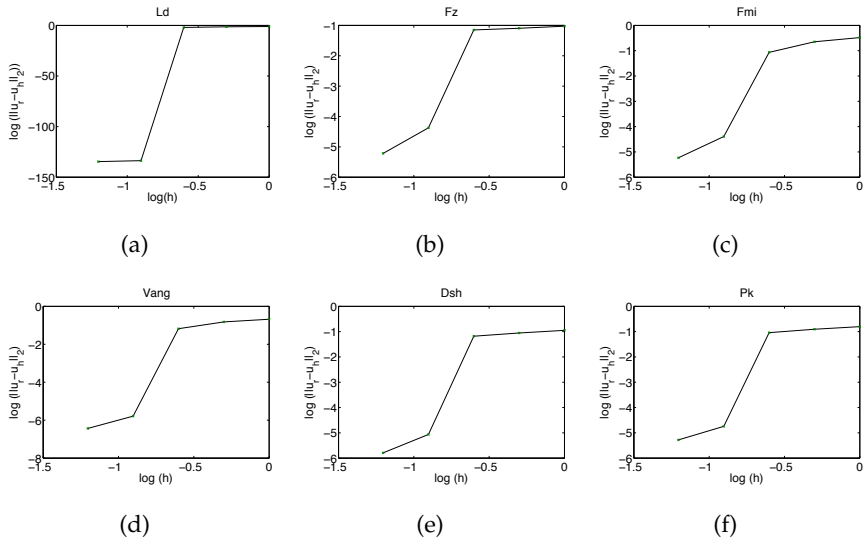

Figure 5.9: Error convergence study to validate our finite element code for the system exemplified by (5.16). As reference solution u_r we chose the solution for mesh size $h = 0.0312$, an initial ligand imbalance and the parameter values in Table 5.4; (a)-(f) Plots of the error of the solution u_h for certain mesh sizes h compared to the reference solution for the six proteins involve in the mechanism. They show that the error decreases if the mesh is refined.

Figure 5.10 shows different initial conditions and the corresponding final distributions of total Dsh* for the system exemplified by (5.16) and the parameter values in Table 5.4. In each case we show a line plot and a two-dimensional image. In Figure 5.10 row A both the initial condition and the final state are symmetric with respect to the horizontal axis. We see that an initial ligand imbalance in the cell, which is effectively an initial imbalance in Fz*, can lead to polarisation of the Dsh* distribution. Figure 5.10 row B shows that an initial ligand distribution that is asymmetric with respect to the horizontal axis yields an asymmetric distribution of total Dsh*, which has it's maximum on one side of the membrane. Note that the line plots in B1 and B3 show the distributions on the top and bottom half of the cell separately. Increasing the diffusion in row A and B weakens the difference of total Dsh* between the different parts of the cell. If the diffusion is sufficiently large we get the unpolarised steady state.

These results support our findings in the previous sections. We can get polarity of a whole field of cells from an initial ligand imbalance in every cell. However, this imbalance has to be symmetric with respect to the horizontal axis. Otherwise it will give rise to asymmetric Dsh* distributions.

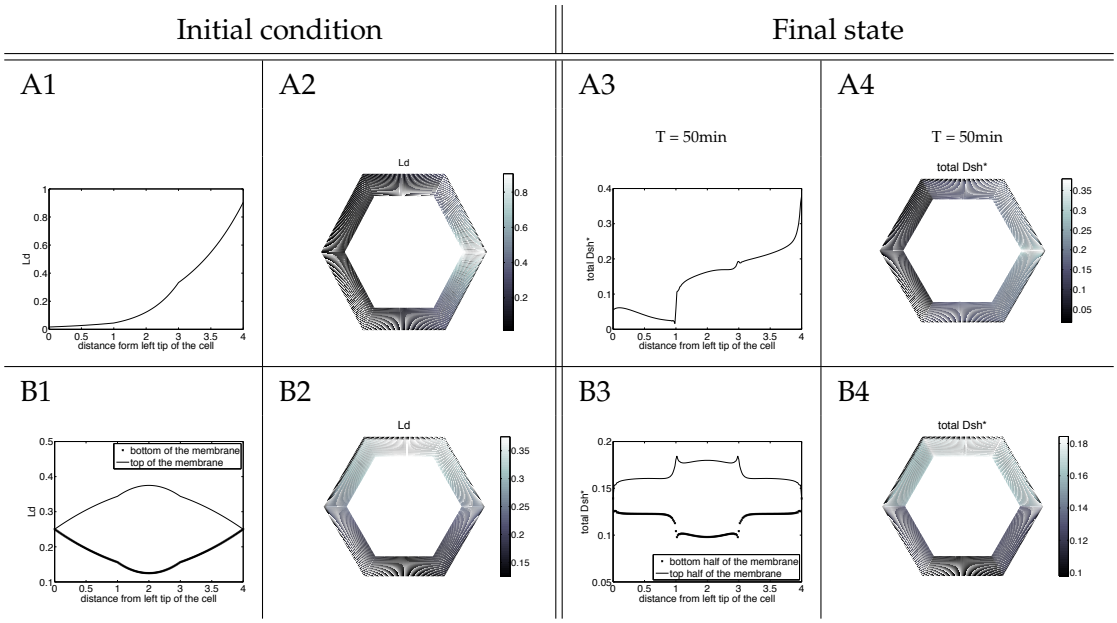

Figure 5.10: Final distribution of total Dsh* for the system exemplified by (5.16) the parameter values in Table 5.4 and different initial conditions. All protein and protein complex distributions occur on the membrane. In every case a line plot and a two-dimensional plot are shown. Row A: An initial ligand imbalance which is symmetric with respect to the horizontal axis yields a polarised final state of total Dsh* that is symmetric with respect to the horizontal axis; row B: an initial ligand distribution that is asymmetric with respect to the horizontal axis leads to an asymmetric final distribution of total Dsh*; the line plots show top and bottom half of the membrane separately.

5.4 Discussion

In this chapter the model for PCP in the *Drosophila* wing was proposed by Le Garrec *et al.* [29]. It is based on the interactions of the five core proteins Fz, Dsh, Fmi, Pk and Vang which establish polarity from a global initial ligand gradient. To this end, the proteins are assumed to act in two negative feedback loops. Our aim was to investigate whether this mechanism would also polarise the cells for an initial local ligand imbalance instead of a global gradient. We commenced our analysis in one spatial dimension for a row of cells. Applying a parameter search method based on the Nelder-Mead algorithm we found parameter sets that yield polarity from an initial ligand imbalance in every cell. Extending our investigations to two spatial dimensions, assuming a hexagonal cell which consists of six compartments, we could confirm these results for certain initial conditions. For an initial ligand imbalance that is symmetric with respect to the horizontal axis the desired polarised steady state can arise. Choosing an initial ligand distribution that is asymmetric

with respect to the horizontal axis, we found that a steady state which is asymmetric with respect to the horizontal axis exists for the same parameter values as the polarised steady state that is symmetric with respect to the horizontal axis. Furthermore, numerical analysis suggests that the state that is asymmetric with respect to the horizontal axis is stable, while the polarised steady state which is symmetric with respect to the horizontal axis is unstable to perturbations that are asymmetric with respect to the same axis. Our analysis of the full spatial model supports the need for symmetric initial conditions. We numerically approximated the system for a hexagonal cell, applying the finite element method. The proteins and protein complexes were restricted to the membrane. Cell bridging complexes were not allowed to diffuse, while all other proteins and protein complexes could diffuse in the whole membrane. Simulations revealed that an initial ligand imbalance that is symmetric with respect to the horizontal axis can give correct polarity, but for the same parameter values an initial condition that is asymmetric with respect to the horizontal axis can yield a steady state that is asymmetric with respect to the same axis. We cannot rule out the possibility that a parameter set does exist for which the state that is symmetric with respect to the horizontal axis is stable. However, extensive numerical investigations and our understanding from previous chapters suggests that such a parameter set does not exist.

Introducing a clone in a field of compartmentalised hexagonal cells yields an asymmetric initial condition that results in a final state with a disordered distribution of total Dsh*. Therefore, we were not able to reproduce the experimental results for effects of clones. In experiments only the cells near the clone are affected while the ones further away polarise normally.

We conclude that this mechanism does not need a gradient to initiate cell polarisation, an initial imbalance in every cell also yields polarity. However, the gradient is necessary to overcome asymmetries with respect to the horizontal axis in the field of cells, which can be introduced by anomalies in the initial conditions. Since biological systems always include a certain rate of fluctuations, an initial gradient is essential for this model to reproduce experimental results.

Considering the time to establish polarity we found great discrepancies between our simulation times and the time measured in experiments. In the one-dimensional case the simulation time was far too long while for both two-dimensional representations it was too short. Experimental results in yeast suggest a second explanation for the short times in the two-dimensional cases. Due to the relationship in our model between the simulation time and the time in experiments, assuming a smaller diffusion coefficient for the biological system would also increase the time calculated for the simulations. This seems reasonable

since polarity in yeast has been shown to rely on slow membrane diffusion of the proteins involved [51].

Chapter 6

Modelling the Dachsous system in the Drosophila *abdomen*

The models by Amonlirdviman *et al.* and Le Garrec *et al.*, which we presented in the previous two chapters focus on the polarising mechanism of the Fz system in the *Drosophila* wings. In this chapter we concentrate on the Dachsous (Ds) system in the *Drosophila* abdomen.

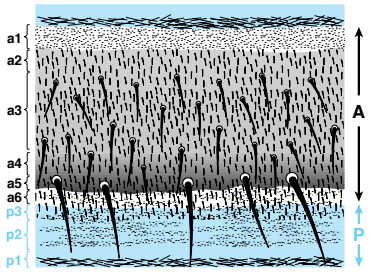

Figure 6.1: Compartments and cell types of a typical abdominal segment. Anterior is at the top and posterior at the bottom of the figure. The cuticle of the A compartment (black) consists of six different stripes distinguished by pigmentation and decoration, a1: unpigmented, without hairs; a2: lightly pigmented with hairs; a3: lightly pigmented with hairs and bristles of moderate size; a4: darkly pigmented with hairs and bristles of moderate size; a5: darkly pigmented with hairs and bristles of large size; a6: unpigmented with hairs but no bristles. The P compartment (grey) can be divided into three stripes. p3: unpigmented with hairs; p2: unpigmented without hairs; p1: unpigmented but tessellated. Note that several hairs are secreted per cell and that all hairs and bristles point posteriorly. The p2, p1 and a1 cuticles can only be seen in well-stretched preparations. They are normally folded under the remainder of the segment. Figure from [43].

The dorsal epidermis of the adult abdomen is divided into several segments. Each segment is assigned an anterior (A) and a posterior (P) compartment. An illustration of a typical segment is shown in Figure 6.1. We see that the A and P compartments consist of different types of cuticle distinguished by pigmentation and decoration and that most of the surface is covered with hairs and bristles that all point posteriorly.
As mentioned in Section 1.2 the Ds system includes the proteins Ds, Fat (Ft) and Four-Jointed (Fj). All three are distributed in gradients. Ds forms an increasing gradient in the A compartments and a decreasing gradient in the P compartments. The Ft and Fj gradients decrease in the A compartments and increase in the P compartments. Figure 6.2 shows an illustration of the Ds and Ft gradients.

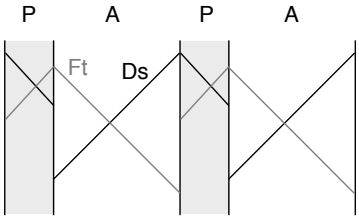

Figure 6.2: Illustration of the Ds and Ft gradients in the A and P compartments. Apart from the sign of the slope all features of the gradients are chosen arbitrarily since so far they are unknown.

In [7] Casal *et al.* have found evidence in the *Drosophila* abdomen that the Ds system acts in parallel to the Fz system to generate planar cell polarity. Their studies focus on the A compartment. Hence, the idea of the mechanism is based on a Ds gradient that increases from anterior to posterior and Fj and Ft gradients that decrease along the same axis. Fj is assumed to inhibit Ds and activate Ft. Furthermore, Ds and Ft form complexes over the cell membrane. The authors assume a row of cells in which each cell has a right and a left side. The polarity of a cell is determined by the difference of cell bridging complexes between its two ends. The cell will polarise towards the end with the lower number of complexes.
Figure 6.3 shows an illustration of the mechanism. In this figure as well as in the rest of this chapter we omit Fj for simplicity. We assume that we have a Ds and a Ft gradient. In Figure 6.3 the protein names in italics represent the gradients while the abbreviated protein names illustrate the formation of the cell bridging complexes. We do not specify the number of cell bridging complexes in each cell.

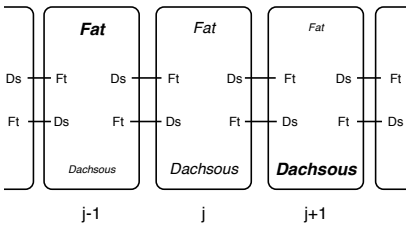

Figure 6.3: Illustrations of the mechanism for the Ds system. The protein names in italics represent the protein gradients and the abbreviated protein names illustrate the formation of the DsFt complexes, which form over the cell membrane.

Figure 6.4 is taken from [7]. It illustrates the authors' ideas of the mechanism of the Ds system and an expected outcome. Omitting the role of Fj and focusing on Ds and Ft we see that they assume Ds and Ft gradients and indicate that Ds and Ft bind over the cell membrane. Finally, the number of bridging complexes determines the polarity of each cell. To this end, they count bound Ds and bound Ft on every cell side and compare the two. Each cell has a higher amount of bridging complexes on its left side. Furthermore, the amount of bound Ds on the right side of cell j is the same as on the left side of cell $j+1$ and the same is true for bound Ft.

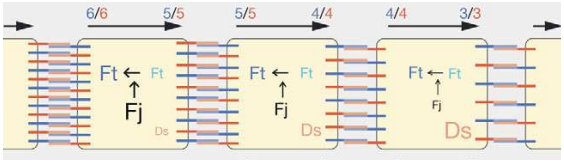

Figure 6.4: Figure from Casal *et al.* [7]. The Ds, Ft and Fj gradients are indicated by different font sizes. Fj is assumed to mainly act on Ft. More recent results have shown that Fj acts on both Ds and Ft (correspondence with Peter Lawrence). Ds (in red) binds to Ft (in blue) over the cell membrane. In each cell the number of bound Ds and bound Ft are counted which is indicated by the numbers above the cells. The arrows above the cells depict the direction of polarity of each cell, pointing from the higher to the lower number of cell bridging complexes.

Based on these ideas we formulate a mathematical model. We assume a row of cells and each cell has a left and a right side. On each cell side there are certain amounts of Ds (Ft) which can bind to Ft (Ds) in the adjacent cell side of the neighbouring cell forming a cell bridging complex DsFt. The chemical reaction underlying this model is given by

$$Ds + Ft^{+} \underset{\lambda}{\overset{R}{\rightleftharpoons}} DsFt,$$

with the forward reaction rate R and the backward reaction rate λ. The superscript + indicates that the two reactants are in different cells. Furthermore, we include intracellular diffusion in the model.

It is unclear whether it is more reasonable to use a model which includes constant protein production and degradation throughout the polarising process or to choose a conservative approach that relies purely on intracellular protein movement. Therefore, we consider both cases and compare their results. This gives us two possibilities to include the observed gradients in the model. For the conservative version, we include the gradients via the initial conditions; in the version with production and degradation we include the gradients via the production terms.

The production and degradation term is based on the idea that the rate of production depends on the position of a cell in the row but is the same everywhere in that cell. We define the production rate of Ds in cell j as $\bar{D}s_j = \bar{D}_1 + a_j$ with a positive constant $\bar{D}_1$ which describes the production rate in cell 1 and a_j represents the difference in Ds production between cell j and cell 1. Similarly, the production rate of Ft in cell j is given by $\bar{F}t_j = \bar{F}_1 + b_j$ where $\bar{F}_1 > 0$ is the production rate in cell 1 and b_j represents the difference between cell j and cell 1. We choose a_j as an increasing sequence with non-negative elements and b_j as a decreasing sequence with non-positive elements. Thereby, we ensure an increasing Ds gradient and a decreasing Ft gradient. These ideas yield the following system of equations

$$\begin{aligned}
\frac{\mathrm{d}Ds_j^l}{\mathrm{d}t} &= \delta(\bar{D}_1 + a_j - Ds_j^l) - R\, Ds_j^l \cdot Ft_{j-1}^r + \lambda\, DsFt_j^l + \mu_1(Ds_j^r - Ds_j^l),\\
\frac{\mathrm{d}Ds_j^r}{\mathrm{d}t} &= \delta(\bar{D}_1 + a_j - Ds_j^r) - R\, Ds_j^r \cdot Ft_{j+1}^l + \lambda\, DsFt_j^r + \mu_1(Ds_j^l - Ds_j^r),\\
\frac{\mathrm{d}Ft_j^l}{\mathrm{d}t} &= \delta(\bar{F}_1 + b_j - Ft_j^l) - R\, Ds_{j-1}^r \cdot Ft_j^l + \lambda\, DsFt_{j-1}^r + \mu_2(Ft_j^r - Ft_j^l),\\
\frac{\mathrm{d}Ft_j^r}{\mathrm{d}t} &= \delta(\bar{F}_1 + b_j - Ft_j^r) - R\, Ds_{j+1}^l \cdot Ft_j^r + \lambda\, DsFt_{j+1}^l + \mu_2(Ft_j^l - Ft_j^r),\\
\frac{\mathrm{d}DsFt_j^l}{\mathrm{d}t} &= R\, Ds_j^l \cdot Ft_{j-1}^r - \lambda\, DsFt_j^l,\\
\frac{\mathrm{d}DsFt_j^r}{\mathrm{d}t} &= R\, Ds_j^r \cdot Ft_{j+1}^l - \lambda\, DsFt_j^r,
\end{aligned} \tag{6.1}$$

where the subscripts give the number of the cell. The superscripts are l for the left side of the cell and r for the right side. Assuming a suitable rescaling, the degradation rate is included by δ, and μ_1 and μ_2 represent diffusion.

The aim of this chapter is to gain insight into the interactions of the Ds system by analysing system (6.1) and comparing our results to experimental observations. We are interested in the emergence of polarity depending on the parameter values and the initial conditions. Furthermore, we investigate the potential of the model to overcome anomalies in the initial

conditions and study its behaviour around clones. We commence in Section 6.1 with the conservative approach, i.e. $\delta = 0$. Section 6.2 contains the analysis for $\delta > 0$, i.e. the case which includes protein production and degradation.

6.1 Conservative form of the Ds model

Steady states

In this section we determine conditions for steady states of system (6.1), assuming $\delta = 0$, i.e. the total amounts of proteins are conserved in each cell.
At steady state, for $\mu_1, \mu_2 > 0$, system (6.1) yields

$$Ds_j^r = Ds_j^l \text{ and } Ft_j^r = Ft_j^l, \tag{6.2}$$

as well as

$$\begin{aligned} DsFt_j^l &= \frac{R}{\lambda} Ds_j^l Ft_{j-1}^r, \\ DsFt_j^r &= \frac{R}{\lambda} Ds_j^r Ft_{j+1}^l. \end{aligned} \tag{6.3}$$

This gives us a relationship between the final distributions of DsFt, and Ds and Ft. Initially, we assume there is no DsFt. The initial conditions for Ds and Ft as well as the parameter values of R and λ determine the final distributions of Ds and Ft. They are independent of the diffusion parameters μ_1 and μ_2. The only homogeneous final distribution for DsFt we can get is the unpolarised one. To identify conditions for an inhomogeneous polarised steady state we consider three different ways of determining polarity in a cell. The cell could detect the difference in bound Ds between its two sides or the difference in bound Ft or the difference in the sum of bound Ds and bound Ft.
Counting bound Ds and using (6.2) and (6.3) we get

$$\begin{aligned} DsFt_j^l - DsFt_j^r &= \frac{R}{\lambda}(Ds_j^l Ft_{j-1}^r - Ds_j^r Ft_{j+1}^r) \\ &= \frac{R}{\lambda} Ds_j^l (Ft_{j-1}^l - Ft_{j+1}^l). \end{aligned} \tag{6.4}$$

Equation (6.4) implies a relation between the final distributions of Ft and DsFt. If the final state of Ft is decreasing over the row of cells, we get polarisation of DsFt to the left. If it is increasing, DsFt polarises to the right. If the steady state of Ft is flat, DsFt does not polarise. The ratio $\frac{R}{\lambda}$ influences the strength of the polarity.
Now we assume the cell polarises according to its distribution of bound Ft. Using (6.2)

and (6.3) yields

$$\begin{aligned} DsFt^r_{j-1} - DsFt^l_{j+1} &= \frac{R}{\lambda}[Ds^r_{j-1}Ft^l_j - Ds^l_{j+1}Ft^r_j] \\ &= \frac{R}{\lambda}Ft^l_j[Ds^r_{j-1} - Ds^l_{j+1}] \end{aligned}$$

Hence, if the final distribution of Ds is increasing we get a distribution that is polarised to the right and if it is decreasing we get polarity to the left. The strength of the polarity depends on the ratio of R and λ.

If the cell detects the sum of bound Ds and bound Ft, using (6.2) and (6.3) we get

$$\begin{aligned} (DsFt^l_j + DsFt^r_{j-1}) - (DsFt^r_j + DsFt^l_{j+1}) &= \frac{R}{\lambda}[Ds^l_jFt^r_{j-1} + Ds^r_{j-1}Ft^l_j - Ds^r_jFt^l_{j+1} - Ds^l_{j+1}Ft^r_j] \\ &= \frac{R}{\lambda}[Ds^l_j(Ft^l_{j-1} - Ft^l_{j+1}) + Ft^l_j(Ds^l_{j-1} - Ds^l_{j+1})]. \end{aligned}$$

Assuming a decreasing final distribution of Ft and an increasing final distribution of Ds we see that a sufficient condition for polarity to the left is that Ds^l_j is sufficiently larger than Ft^l_j for all j. The strength of polarity depends on the ratio $\frac{R}{\lambda}$.

The final distribution proposed by Casal *et al.*

The final DsFt distribution proposed by Casal *et al.* [7] is shown in Figure 6.4. We see that the total amounts of cell bridging complexes as well as bound Ds and bound Ft in adjacent sides of neighbouring cells are the same. In this section we want to investigate whether system (6.1) can reproduce this distribution. First we calculate the difference of the total amount of cell bridging complexes between adjacent cell sides of neighbouring cells. With (6.3) we get

$$(DsFt^r_j + DsFt^l_{j+1}) - (DsFt^l_{j+1} + DsFt^r_j) = 0.$$

Hence, at steady state the total amount of cell bridging complexes on the right side of cell j is the same as on the left side of cell $j+1$.

We now consider bound Ds. The condition that we have the same amount of bound Ds on adjacent sides of neighbouring cells can be written as $DsFt^r_j = DsFt^l_{j+1}$, which yields $Ds^r_jFt^l_{j+1} = Ds^l_{j+1}Ft^r_j$, hence $\frac{Ds^r_j}{Ds^l_{j+1}} = \frac{Ft^r_j}{Ft^l_{j+1}}$. Therefore, the final distributions of the two proteins have to be the same or the two ratios have to be 1. The first case is not possible because the slopes of the initial gradients have opposite sign and the proteins get both used up in the same way. The second case would imply that all the final distributions are homogeneous, because of (6.2) and (6.4). Thus, this model cannot generate the proposed distribution of bound Ds if we include diffusion.

If $\mu_1 = \mu_2 = 0$ equation (6.2) does not hold. Hence, the ratio could be 1 if $Ds^r_j = Ds^l_{j+1}$

and $Ft_j^r = Ft_{j+1}^l$. A final state like this can only be reached if the initial distributions already fulfil these conditions, because the binding rates are the same on each side of the cell and there is no diffusion. However, this would imply that the cells are already polarised initially and the whole system might only strengthen this initial polarity. Furthermore, no diffusion is unlikely in biological systems.
For the same reasons, for $\delta = 0$ we cannot get a final state in which the amount of bound Ft is the same in adjacent sides of neighbouring cells.
Hence, for $\delta = 0$ system (6.1) cannot reproduce the final distribution proposed by Casal *et al.* in [7].

Numerical simulations

We simulated systems (6.1) for $\delta = 0$ for a row of 20 cells using the Matlab ODE solver ode15s. For the parameter values we chose $R = 5, \lambda = 0.1$ and $\mu_1 = \mu_2 = 0.5$. At each boundary we assume another half a cell in which the initial protein distributions continue in the obvious way. We ensure that the cell is only half by setting its diffusion coefficients to zero. To calculate the time to reach the steady states we need to relate the parameters in our model to the corresponding parameters in the biological system. Similar to previous chapters, it is $\mu_1 = \frac{1}{\Delta x^2}\tilde{\mu}_1 = \frac{1}{p^2(\Delta x^{bio})^2}\mu_1^{bio}$, where Δx denotes the spatial extension of a cell in our model from left to right, Δx^{bio} the side length of a biological cell in the *Drosophila* wing, μ_1 the diffusion coefficient in our simulations and μ_1^{bio} the diffusion coefficient in the biological system. The parameter p is a positive constant. The time t in our simulations is related to the time T in the experiments by

$$T = \frac{1}{k\mu_1}t = \frac{p^2(\Delta x^{bio})^2}{\mu_1^{bio}}t. \tag{6.5}$$

We assume $\Delta x^{bio} = 8\,\mu\text{m}$ [19], $\mu_1^{bio} = 0.1\,\mu\text{m}^2/\text{s}$ [22] and $p = 1$; then the constant k is determined by (6.5). As mentioned in Section 1.2, in the *Drosophila* wing it takes 32 h to polarise the cells. Assuming the time scale for polarisation in the *Drosophila* abdomen is similar, the times we get from our simulations are in a reasonable range.
We assume an increasing initial Ds gradient and a decreasing initial Ft gradient as shown in Figure 6.5(a). Figure 6.5(b) shows the corresponding final distributions of free Ds and free Ft. The final distributions of the complexes for system (6.1) are shown in Figure 6.5(c)-(e). In Figure 6.5(c) the bridging complex is assumed to contribute to polarity of the same cell as its Ds part. We see that in all cells the DsFt distribution is polarised to the left. Figure 6.5(d) shows the results if each cell counts its bound Ft. We get polarity to the right. If we reverse the initial gradients the distribution of bound Ft polarises to the left (not shown).

If each cell counts both its bound Ft and bound Ds we get the result in Figure 6.5(e). The cells in the left half of the row for which the final value of Ds is less than their final Ft value are polarised to the right; the cells in the right half of the row, with a higher final Ds than Ft value are polarised to the left. Furthermore, the amount of bridging complexes on the right of cell j is the same as on the left of cell $j+1$.
In all three cases the overall slope of the distribution of the bridging complex seems to depend on the Ft to Ds ratio; positive if there is more Ft than Ds in the cell and negative if there is more Ds than Ft.

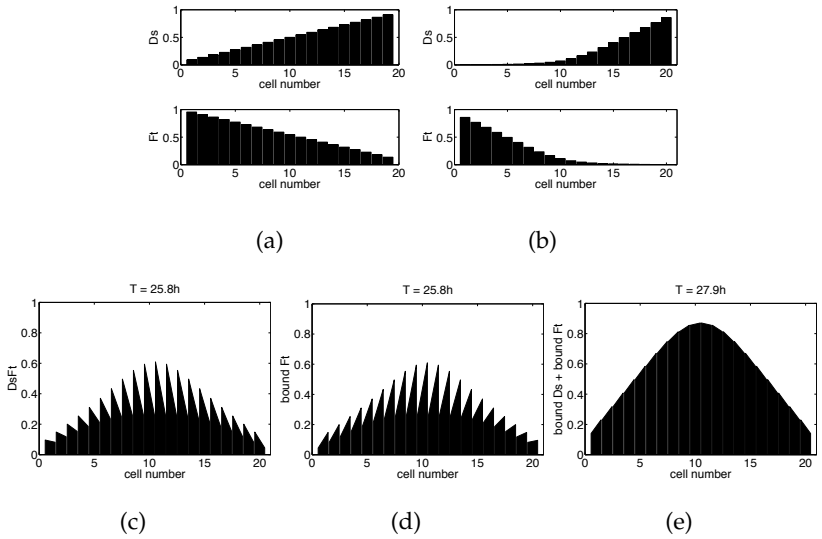

Figure 6.5: Simulations for system (6.1) and the parameter values $\delta = 0, R = 5, \lambda = 0.1$ and $\mu_1 = \mu_2 = 0.5$; (a) Initial condition, (b) final distribution for Ds and Ft for system (6.1), (c) final distribution of bound Ds which we refer to as DsFt, (d) final distribution of bound Ft, (e) final distribution of the sum of bound Ds and bound Ft.

An interesting feature of the *Drosophila* abdomen is that the Ds and Ft gradients in the P compartment have opposite slopes than in the A compartment. Nonetheless, the hairs in both compartments point posteriorly indicating that all the cells are polarised the same way. The results in Figure 6.5 suggest two hypotheses for solutions of this problem. One possibility is that the readout differs between the A and the P compartment. The cells in the A compartment compare the number of bound Ds on their cell membrane to determine their polarity while the cells in the P compartment use the number of bound Ft (see Figures 6.5(c) and (d)). The second possibility is that the cells in both compartments count the sum of bound Ds and bound Ft but the ratio between Ds and Ft is different in the different compartments. In the A compartment the amount of Ds in each cell is greater than the

amount of Ft while in the P compartment there is more Ft in each cell than Ds (see Figure 6.5(e)). Since in [7] Casal *et al.* focus on the A compartment we do not further analyse the case in which each cell counts its bound Ft.

Assuming that every cell counts its bound Ds, equation (6.4) shows that the final DsFt distribution depends on the final Ft distribution. Therefore, we want to investigate how the final Ft distribution depends on the initial conditions and the parameter values.

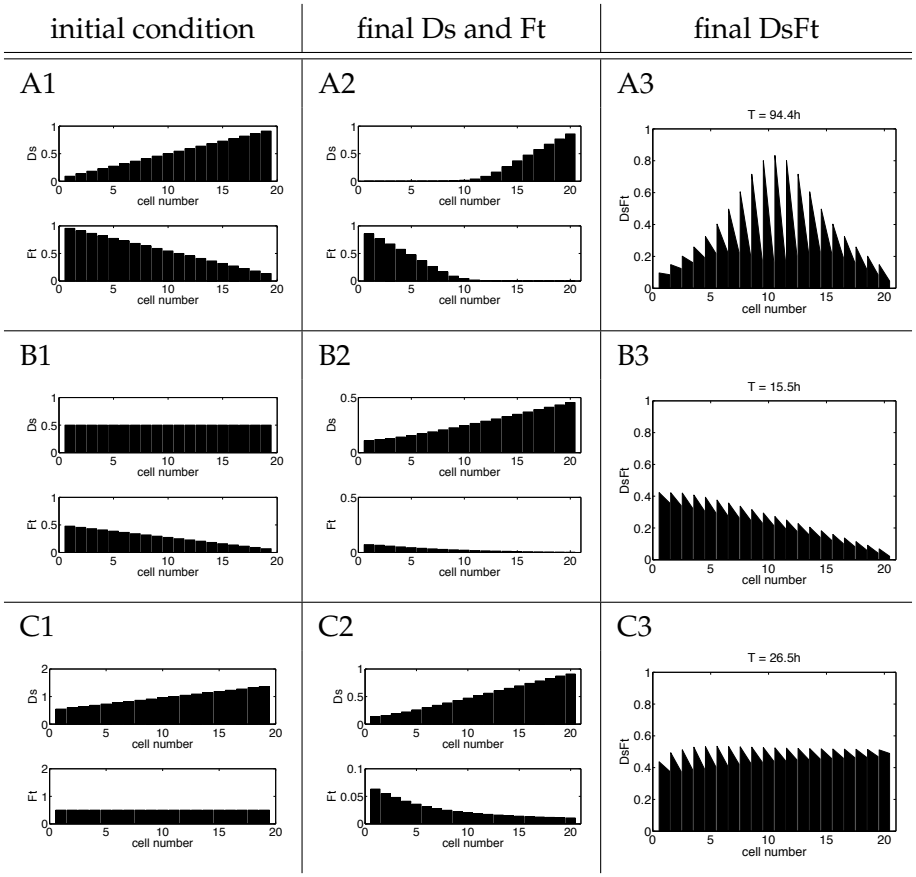

Figure 6.6: Different initial Ft and Ds distributions and the corresponding final states for system (6.1), if each cell counts its bound Ds; the value of R varies, the remaining parameter values are $\delta = 0, \lambda = 0.1$ and $\mu_1 = \mu_2 = 0.5$; Row A: same initial condition as Figure 6.5, different forward reaction rate, $R = 50$, stronger polarity, row B: initially Ds is distributed uniformly, $R = 5$, we get a decreasing final Ft distribution and DsFt polarity to the left, row C: Ft is initially distributed uniformly, $R = 5$, the final Ft distribution is decreasing and DsFt is polarised to the left.

Figure 6.6 shows different initial distributions for Ds and Ft and the corresponding final states. The initial gradients shown in Figure 6.6 A1 are the same as in Figure 6.5(a). For the final states in Figure 6.6 A2 and A3 we chose $R = 50$ instead of $R = 5$ and the other parameter values as above. We see that it takes longer to reach the steady state and that the

Ds and Ft gradients are slightly steeper than in Figure 6.5(b). Furthermore, the strength of DsFt polarity is increased as expected from equation (6.4). Increasing the diffusion does not change the final distribution but reduces the time to reach steady state (not shown). Figure 6.6, rows B and C show the final distribution of Ds, Ft and DsFt if there is either no Ds gradient (row B) or no Ft gradient (row C). The parameter values are the same as for Figure 6.5. Figures 6.6 B2 and C2 show that both initial conditions can give a decreasing final Ft gradient. Thus, in both cases we get a polarised distribution of DsFt as we see in Figures 6.6 B3 and C3. If both Ft and Ds are initially distributed uniformly in the row of cells their final distributions are also flat and we do not get DsFt polarity (not shown). Reversing the initial gradients yields reversed final gradients for Ds and Ft and DsFt polarity to the right (not shown). This analysis suggests that if either Ds or Ft are initially distributed in a gradient we get a final Ft gradient and the sign of its slope depends on the initial conditions but not the parameter values.

A similar analysis is shown in Figure 6.7 for the case in which every cell counts the sum of bound Ds and bound Ft. In Figure 6.7 A1 the initial amount of Ds in every cell is greater than the initial amount of Ft. This yields polarity to the left for every cell as shown in A3. Increasing the ratio $\frac{R}{\lambda}$ does not change the steady state significantly but increases the time to reach it (row B). Increasing the diffusion decreases the time to reach the steady state (not shown) and the final distributions are the same as in Figure 6.7 row A. If we assume that there is no Ds gradient we can still get polarity as shown in row C. For a flat Ft distribution however we get a slight polarity to the right (see D3). The effects on the boundary cells in D3 are due to the boundary conditions. Decreasing the initial level of Ft affects the total amount of final cell bridging complexes and the strength of the polarity. It does not alter the direction of polarisation. Both in row C and D the final distributions of Ds and Ft are increasing and decreasing gradients, respectively. The final Ds gradient in C2 is less steep than D2, the final Ft gradient in C2 is steeper than in D2. If the initial distributions for Ft and Ds are both uniform we do not get polarity (not shown). Assuming an initial Ds gradient that decreases, an initial Ft gradient that increases and that the initial amount of Ds is higher in each cell than the initial Ft amount, we get reversed polarity (not shown).

These results suggest that the Ds model is more sensitive to the initial conditions if the cells polarise according to the sum of bound Ds and bound Ft than if they only count bound Ds.

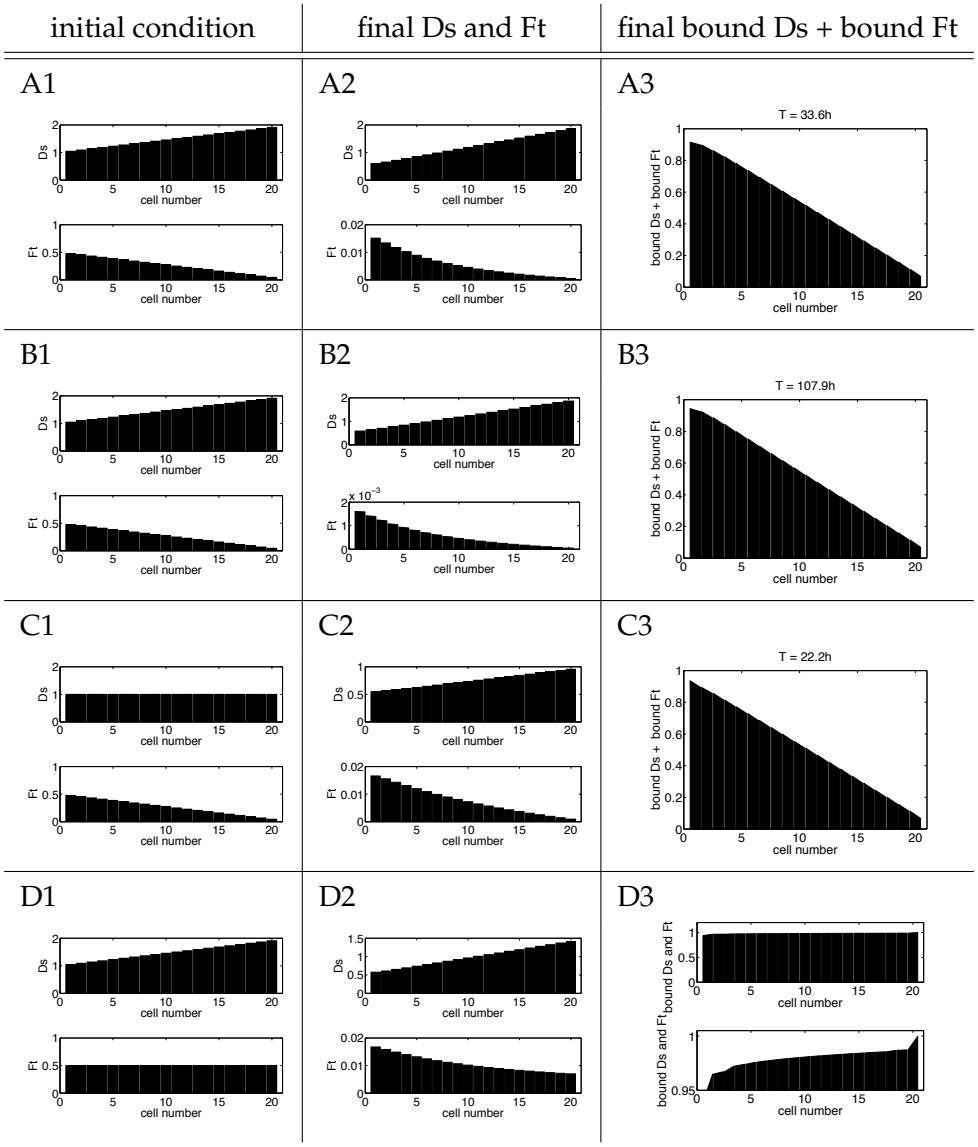

Figure 6.7: Different initial Ft and Ds distributions and the corresponding final states for system (6.1), each cell counts both its bound Ds and bound Ft; we assume different values for R; the remaining parameter values are $\delta = 0, \lambda = 0.1$ and $\mu_1 = \mu_2 = 0.5$; Row A: initial gradients for which the amount of Ds is higher in each cell than the amount of Ft, $R = 5$, we get polarity to the left; row B: same initial conditions as in row A, $R = 50$, the total amount of cell bridging complexes is slightly higher than in row A, row C: the initial Ds distribution is uniform, $R = 5$, we get polarity to the left, row D: the initial Ft distribution is uniform, $R = 5$, both figures in D3 show the final distribution of the cell bridging complexes, the bottom figure shows an enlargement, we get a weak polarity to the right.

Anomalies in the initial conditions

As a next step we include anomalies in the initial conditions and investigate the behaviour of the model.

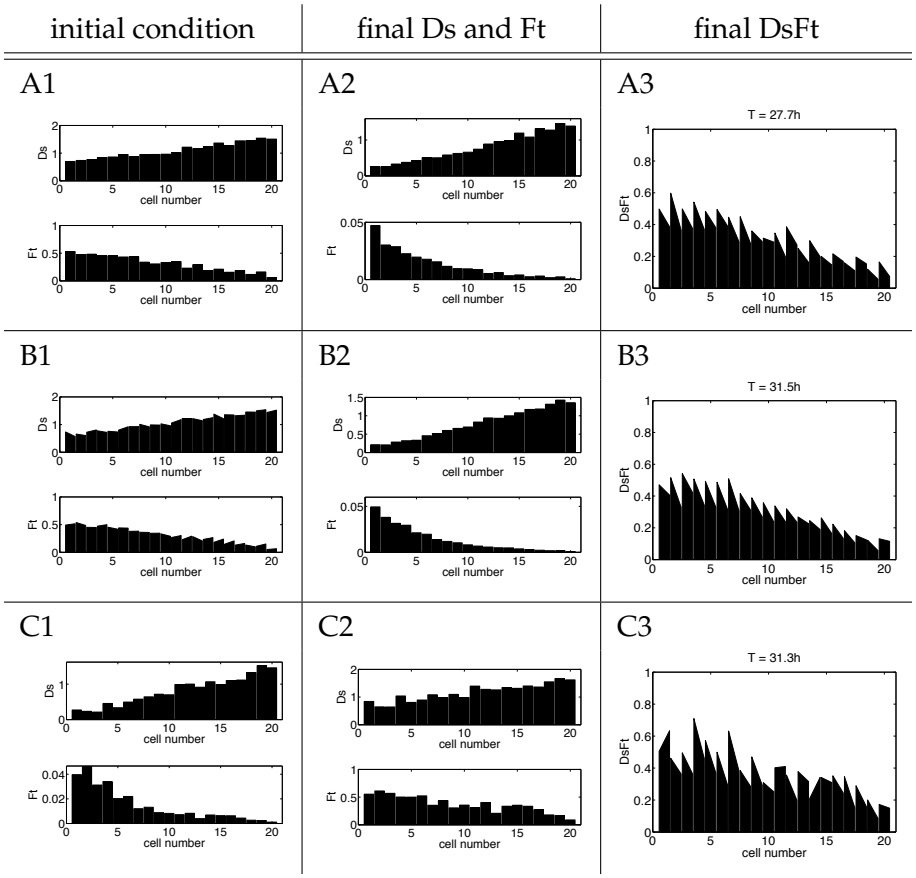

Figure 6.8: Behaviour of system (6.1) for anomalies in the initial conditions; cells polarise according to their distribution of bound Ds; we chose $\delta = 0, R = 5, \lambda = 0.1$ and $\mu_1 = \mu_2 = 0.5$; Row A: initially we assume an increasing Ds gradient and a decreasing Ft gradient and add random values in [0,0.2] and [0,0.1], respectively, left and right side of each cell have the same amounts of proteins, in the final state the strength of polarity is affected but not the direction; row B: initially we choose an increasing Ds gradient and a decreasing Ft gradient and add random values in [0,0.2] and [0,0.1], respectively, left and right side of each cell have different amounts of proteins; the anomalies can be corrected; row C: initial conditions with a higher level of noise, we assume an increasing Ds gradient and a decreasing Ft gradient and add random values in [0,0.4] and [0,0.2], respectively, left and right side of each cell have the same amounts of proteins, in the final state the strength as well as the direction of polarity is affected, cells 1, 11 and 14 point to the right.

Assuming that the cell polarises according to is distribution of bound Ds, Figure 6.8 shows two initial conditions with different kinds of anomalies and the corresponding final distributions for Ds, Ft and DsFt. In both initial conditions the gradients are no longer monotone. We added random values in [0,0.2] to the Ds gradient and random values in [0,0.1] to the Ft gradient. In Figure 6.8 A1 the left and right side of each cell have the same value. In B1 there are differences between the left and the right sides. The final DsFt distributions in A3 and B3 show that the anomalies affect the strength of polarisation but not its direction. These results depend on the initial conditions but are independent of R, λ and the diffusion parameters. Increasing the strength of the anomalies in the initial conditions will eventually disrupt polarity as shown in row C of Figure 6.8.

Now we investigate the behaviour of the model for anomalies in the initial conditions if the polarity of each cell is determined by the sum of bound Ds and bound Ft. Figure 6.9 shows the initial conditions and the corresponding final states.

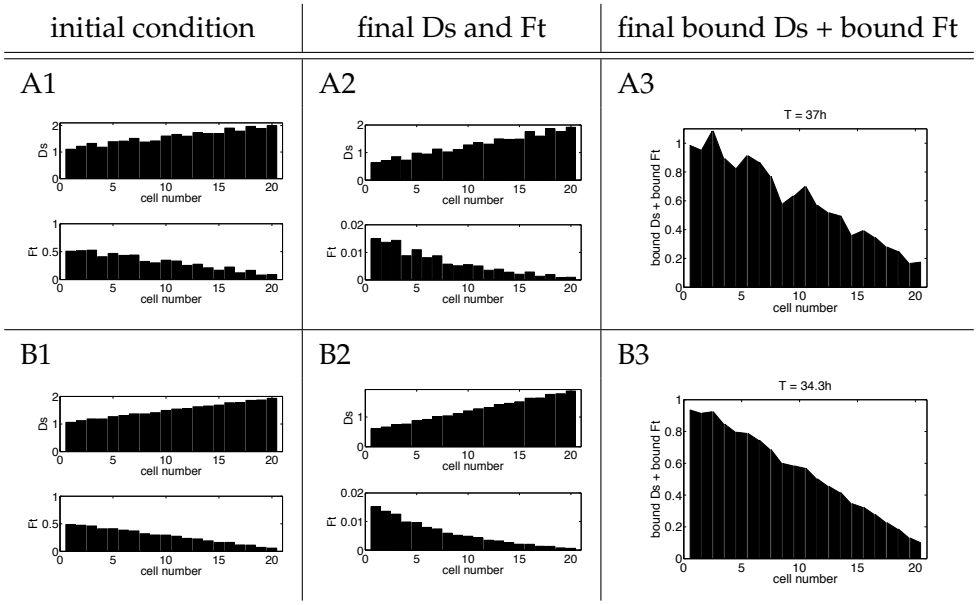

Figure 6.9: Initial conditions including anomalies and corresponding final distributions for system (6.1), each cell counts both its bound Ds and bound Ft; the parameter values are $\delta = 0, R = 5, \lambda = 0.1$ and $\mu_1 = \mu_2 = 0.5$; changing R, λ or the diffusion parameters does not alter the final direction of polarisation; Row A: initial Ft and Ds gradients plus random disturbances, the left and right side of each cell have the same value, in the final state several cells point the wrong way; row B: initial conditions with smaller disturbances than in row A, left and right side of each cell have the same protein amounts, in B3 cell 2 is polarised the wrong way.

In Figure 6.9 A1 we again added random values in [0,0.2] to the Ds gradient and random values in [0,0.1] to the Ft gradient, such that the left and the right side of each cell have the same value. In A3 we see that these anomalies cannot be corrected. Several cells point the wrong way. In B1 the disturbance in the initial conditions are significantly smaller and both sides of the cell still have the same values. The final distribution of the bridging complexes shows that one cell is pointing to the right. Varying R, λ, μ_1 or μ_2 does not alter the final direction of polarisation. The results suggest that if each cell orients according to the sum of bound Ds and bound Ft on its membrane the model is less capable of correcting errors in the initial conditions. This is an important issue since biological systems are known to include certain levels of fluctuations.

Analysis of clones

We include clones in the row of cells by changing the initial amount of a protein in a group of cells. First we consider clones which differ from the wild-type cells in the level of one protein. In Figure 6.10 we assume the distribution of bound Ds determines the polarity of the cells. Column 1 shows the initial conditions and column 2 and 3 the corresponding final distributions of Ds, Ft and DsFt. The direction of the effects of the clones on the wild-type cells are consistent with the experimental findings we presented in Section 1.2; clones lacking Ds or with a high level of Ft disturb the polarity in front of the clone (see A3 and D3) while clones lacking Ft or with a high level of Ds disrupt polarity behind the clone (see B3 and C3). Within the clone we see no polarity in A3 and the cells at the boundaries of the clones in B3-D3 are polarised. In experiments the hairs in clones lacking Ds show a swirling pattern within the clone and hairs in clones lacking Ft do not show any orientation [8]. Cells in clones with higher levels of Ds do not grow any hairs, while the hairs in clones with higher levels of Ft do not show any orientation [7]. Hence, the behaviour within the clones in our simulations does not fully match the experimental results.
The range of the effect of the clones varies between one cell in B3, two cells in A3 and C3 and three cells in D3. This does not change if we choose different positive values for R, λ or the diffusion. If we set both diffusion coefficients to zero we see that for some cases the effect of the clone is affected by diffusion and for some it is not. For the clone lacking Ds in row A we do not see an effect if there is no diffusion as shown in Figure 6.11 row A. We find that choosing $\mu_1 = 0$ and $\mu_2 = 10^{-6}$ yields the same effect of the clone as in Figure 6.10 A3 but with weaker polarity in the wild-type cells. Tracing the evolution of the final DsFt distribution we see that first all wild-type cells are polarised to the left and then the two cells to the left of the clone start to tend to the right and the strength of the polarity of

the cells to the right of the clone increases. During the whole process the amount of DsFt on the left side of cell 6 is greater than on the right side of cell 5 and the amount of DsFt on the right side of cell 12 is always less than on the left side of cell 13. This is due to the rapid polarisation at the beginning of the process and seems to be independent of parameter values. Therefore, the third cells from the clone boundary do not notice a difference and hence the clone never affects more than two cells.

The effect of a clone lacking Ft in Figure 6.10 row B is not driven by diffusion. For $\mu_1 = \mu_2 = 0$ we get the same distribution as in B3 with a weaker polarity in the wild-type cells. The Ds proteins in the clonal cell 8 and the wild-type cell 7 at the clone boundary do not have any Ft proteins to bind to in the cell to their right. Therefore, the DsFt level on the right side of these cells is zero. The DsFt level on their left sides is not disturbed. A similar argument can be applied to cells 10 and 11. Hence, the clone affects only one cell on each boundary and this is independent of the parameter values.

The effect of a clone with a higher Ds level in Figure 6.10 C3 is due to diffusion. Without diffusion we get wild-type polarity with higher total DsFt levels in the clonal cells. Choosing $\mu_1 = 0$ and $\mu_2 = 10^{-5}$ yields the effect of the clone on the wild-type cells. During the polarisation process we first get the wild-type polarity which subsequently changes to the DsFt distribution in C3. Due to the higher level of Ds in the clone, Ft is drawn from the two neighbouring cells. The range of two is independent of the parameter values.

Comparing Figure 6.10 D3 with Figure 6.11 B3 shows that the effect of a clone with a higher Ft level on the wild-type cells adjacent to the clone does not depend on diffusion. The effect on the second and third cell from the clone boundary is diffusion driven. In this case both Ds and Ft need to diffuse to get the effect. If we include diffusion and trace the polarisation process we see that at first the distribution in Figure 6.11 B3 arises and then the effect of the clone becomes obvious in the second and third cell from the clone boundary. The range of effect does not change if we change the parameter values. Similar to above, during the whole process $dsft_4^r < dsft_5^l$ and therefore cell 4 is not affected. The same argument explains why cell 14 is never affected.

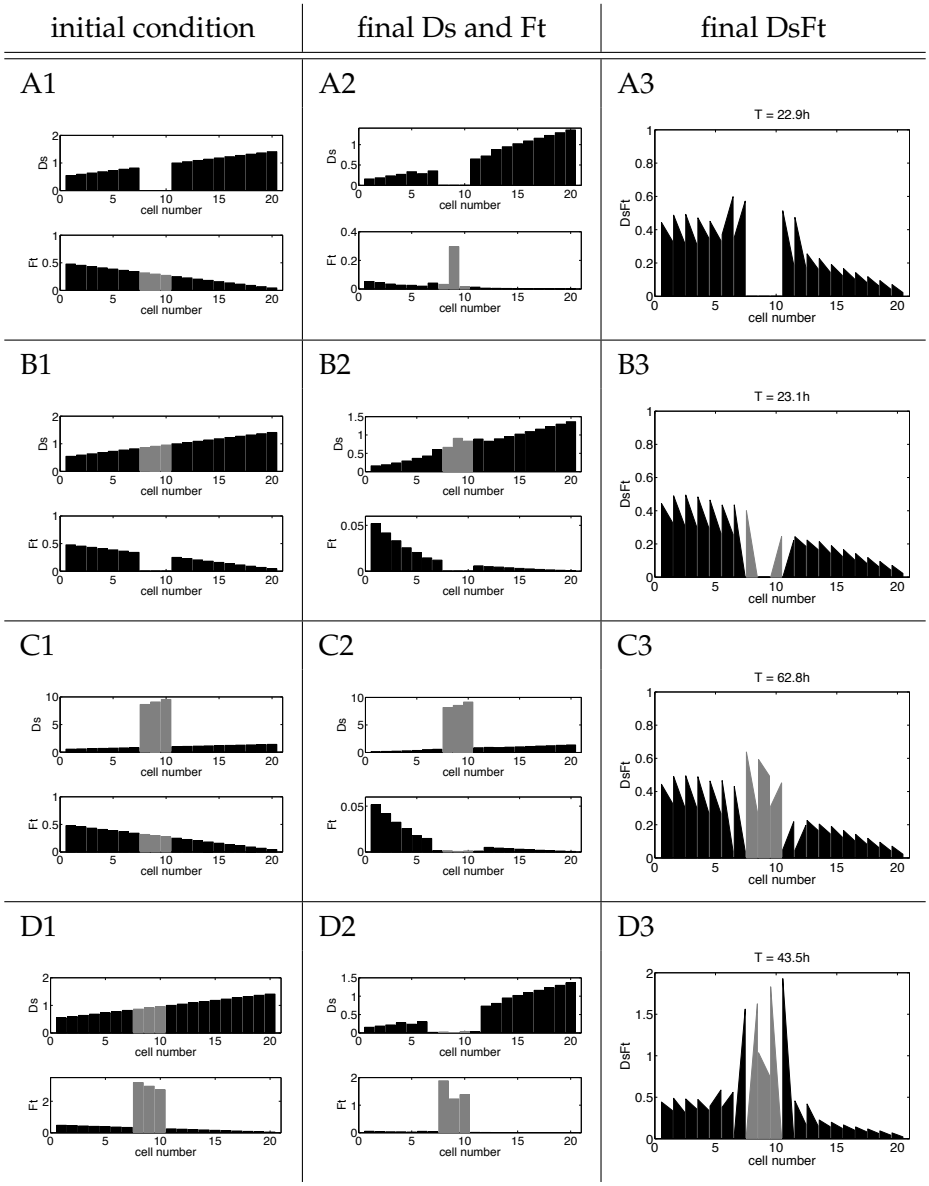

Figure 6.10: Simulations for system (6.1) for clones (in grey) which differ from the wild-type in the level of either Ds or Ft; in column 3 we show the distribution of bound Ds; the parameter values are $\delta = 0, R = 5, \lambda = 0.1$ and $\mu_1 = \mu_2 = 0.5$; Row A: a clone lacking Ds disrupts polarity in front of the clone; row B: a clone lacking Ft disrupts polarity behind the clone; row C: a clone with a high Ds level disrupts polarity behind the clone; row D: a clone with a high Ft level disrupts polarity in front of the clone.

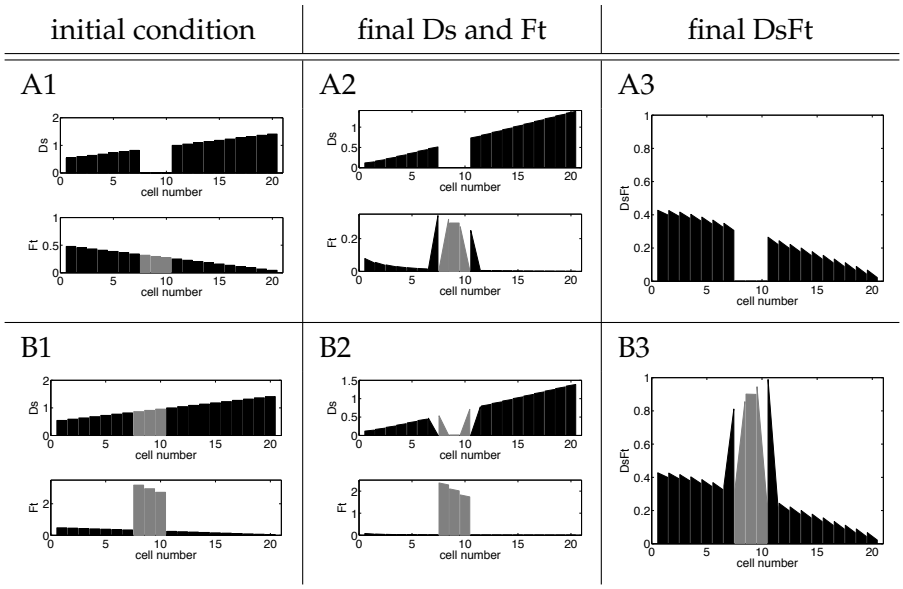

Figure 6.11: Simulations without diffusion, i.e. $\mu_1 = \mu_2 = 0$, for system (6.1) for clones (in grey) that differ from the wild type in the level of either Ds or Ft; each cell counts its bound Ds; the remaining parameter values are $\delta = 0, R = 5$ and $\lambda = 0.1$; The results intend to give insight into the interactions of the cells in our model but are biologically irrelevant. Therefore, the times to reach steady state are not stated. Row A: without diffusion a clone lacking Ds does not affect the wild-type cells around it, row B: without diffusion only part of the effect of a clone with a higher Ft level occurs.

Experiments for clones lacking both Ft and Ds have shown that the wild-type cells are not affected by the clone. A clone with higher levels of both Ft and Ds disrupts polarity in front of the clone [7]. Figure 6.12 shows that the result from our simulations for the case in which the cells polarise according to their distribution of bound Ds, do not match these experimental findings. For the clone lacking both Ft and Ds the proteins in the wild-type cells at the clone boundaries have nothing to bind to within the clone, so both of them point away from the clone. Setting the diffusion coefficients to zero has revealed that this effect in cells 7 and 11 is independent of diffusion while the effects in the second and third cell from the clone boundary are diffusion driven. They are initiated by the polarisation of cells 7 and 11 which offer their free Ft to these cells to form DsFt. Choosing $\mu_1 = 0$ and $\mu_2 = 10^{-6}$ yields the effect of the clone with weaker polarity in the wild-type cells. Increasing $\frac{R}{\lambda}$ increases the strength of the polarity but does not change the range of the effect of the clone. Comparing the results of our simulations to the experimental results suggests that this model lacks a component that represses the effect of the clone. This conclusion is mainly based on the finding that the effect on the two cells right next to the clone occurs rapidly and is independent of diffusion. One possible explanation would be

that the Fz system, which is assumed to act in parallel with the Ds system, hinders the effect of the clone. Peter Lawrence's group conducted an experiment with a clone lacking Ds and Ft in a fly lacking Fz; effects of this clone on the surrounding tissue could not be detected (personal correspondence with Peter Lawrence).

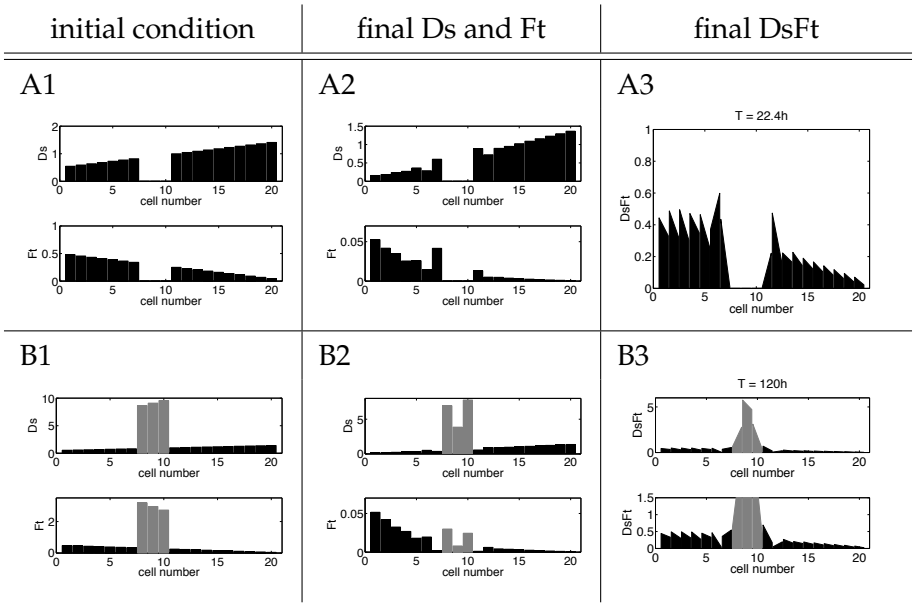

Figure 6.12: Simulations for system (6.1) for clones (in grey) which differ from the wild type in both protein levels, each cell counts its bound Ds, the parameter values are $\delta = 0, R = 5, \lambda = 0.1$ and $\mu_1 = \mu_2 = 0.5$; Row A: a clone lacking Ds and Ft has an effect on the wild-type cells on both sides of the clone, row B: a clone with high levels of Ds and Ft has an effect on the wild-type cells on both sides of the clone, the bottom figure in B3 shows an enlargement.

In our simulations, a clone with a higher level of Ds and Ft disturbs the polarity of the cells in front of the clone as well as the second cell behind the clone as shown in Figures 6.12 row B. This effect occurs because the proteins in cell 11 have so much to bind to in the clonal cell 10, that there are not enough binding partners for the proteins in cell 12. Hence, the distribution of DsFt in cell 12 is polarised to the right. This effect is driven by diffusion while the disturbance of cells 7 and 11 is independent of diffusion. Assuming that R, λ, μ_1 and μ_2 are positive, the range of the effect of the clone does not depend on the values of these parameters.

We will now investigate the behaviour around clones if the polarity of the cells is determined by the distribution of the sum of bound Ds and bound Ft. Figure 6.13 shows an initial condition with a clone that is lacking Ds and the final distributions of Ds, Ft and the cell bridging complexes. We see that polarity is affected in the same way on both sides of the clone. The same is true for the behaviour around the other clones we considered

in Figure 6.10. Assuming that R, λ, μ_1, μ_2 are positive, these results are independent of their values. As described in Section 1.2 experiments have revealed that the clones disrupt polarity either in front or behind the clone. Hence, our results do not agree with the experimental findings and therefore under our assumptions it is not reasonable to suggest that the cells orient due to the distribution of the sum of bound Ds and bound Ft.

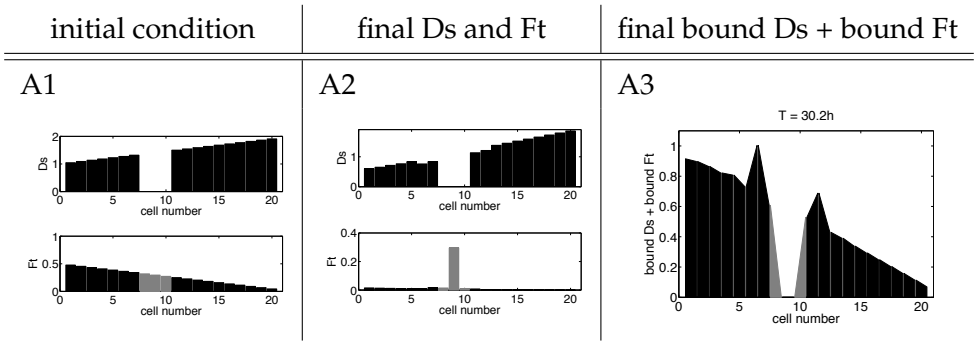

Figure 6.13: Simulations for system (6.1) for a clone (in grey) lacking Ds, the cells polarise according to the distribution of the sum of bound Ds and bound Ft, the parameter values are $\delta = 0, R = 5, \lambda = 0.1$ and $\mu_1 = \mu_2 = 0.5$.

In this section we have presented a conservative model for the Ds system based on the interactions of Ds and Ft as proposed by Casal *et al.* [7]. Our analysis clarified the difference between three different ways of determining the polarity of a cell. Under our assumptions, counting Ds seems the most suitable. However, there are still open questions remaining. We defer further discussion to Section 6.3.

6.2 Ds model including protein production and degradation

Steady states

In this section we determine the steady states for the Ds model (6.1), assuming a degradation rate $\delta > 0$. At steady state $\frac{\mathrm{d}DsFt_j^l}{\mathrm{d}t} = 0$ and $\frac{\mathrm{d}DsFt_j^r}{\mathrm{d}t} = 0$. Hence, we get

$$0 = \frac{\mathrm{d}Ds_j^l}{\mathrm{d}t} = \delta(\bar{D}_1 + a_j - Ds_j^l) + \mu_1(Ds_j^r - Ds_j^l), \tag{6.6}$$

$$0 = \frac{\mathrm{d}Ds_j^r}{\mathrm{d}t} = \delta(\bar{D}_1 + a_j - Ds_j^r) + \mu_1(Ds_j^l - Ds_j^r). \tag{6.7}$$

Reformulating (6.6) for $\mu_1 > 0$ yields

$$Ds_j^r = \frac{-\delta(\bar{D}_1 + a_j - Ds_j^l)}{\mu_1} + Ds_j^l. \tag{6.8}$$

Solving (6.7) for Ds_j^r we get

$$Ds_j^r = \frac{\mu_1 Ds_j^l + \delta(\bar{D}_1 + a_j)}{\delta + \mu_1}. \tag{6.9}$$

Since $\delta \neq 0$, equating (6.8) and (6.9) and solving for Ds_j^l yields

$$Ds_j^l = \bar{D}_1 + a_j.$$

Substituting this in (6.6), we get

$$Ds_j^r = \bar{D}_1 + a_j.$$

Analogous calculations for Ft with $\mu_2 > 0$ yield

$$Ft_j^r = Ft_j^l = \bar{F}_1 + b_j.$$

With these results we can calculate the steady states explicitly. Substitution yields

$$\begin{aligned} 0 &= \frac{\mathrm{d}DsFt_j^l}{\mathrm{d}t} = R(\bar{D}_1 + a_j)(\bar{F}_1 + b_{j-1}) - \lambda DsFt_j^l \\ 0 &= \frac{\mathrm{d}DsFt_j^r}{\mathrm{d}t} = R(\bar{D}_1 + a_j)(\bar{F}_1 + b_{j+1}) - \lambda DsFt_j^r, \end{aligned}$$

hence

$$\begin{aligned} DsFt_j^l &= \frac{R}{\lambda}(\bar{D}_1 + a_j)(\bar{F}_1 + b_{j-1}) \\ DsFt_j^r &= \frac{R}{\lambda}(\bar{D}_1 + a_j)(\bar{F}_1 + b_{j+1}). \end{aligned} \tag{6.10}$$

We see that the steady state depends on the ratio of the reaction parameters and the product of the production terms of the two proteins. Initial conditions, the degradation rate and diffusion do not influence it. Furthermore, the final amount of DsFt in a cell is independent of Ds in the neighbouring cells.

We consider the same three ways of determining the polarity of a cell as in Section 6.1. Counting bound Ds, the difference of the equations in (6.10) yields

$$DsFt_j^l - DsFt_j^r = \frac{R}{\lambda}(\bar{D}_1 + a_j)(b_{j-1} - b_{j+1}). \tag{6.11}$$

Thus, in this case the strength and direction of the polarisation depends on the difference in production of Ft between the cells. The model can overcome certain forms of anomalies in the production rates. Disturbance of the Ds production rate affects the strength of polarity but not the direction. Anomalies in the Ft production rate can influence the strength of polarity as well as the direction. The DsFt distribution is polarised to the left if $b_{j-1} - b_{j+1} > 0$ for all j; it is polarised to the right if $b_{j-1} - b_{j+1} < 0$ for all j. If the production rate

of Ft is the same in every cell, i.e. $b_j = 0$ for all j, we do not get polarity.
Counting bound Ft, (6.10) yields

$$DsFt^r_{j-1} - DsFt^l_{j+1} = \frac{R}{\lambda}(\bar{F}_1 + b_j)(a_{j-1} - a_{j+1}).$$

Here, the direction of polarisation depends on the production rate of Ds. If it decreases from left to right of the row of cells we get polarity to the left. Therefore, this approach seems to be suitable for the P compartment. Since in this work we focus on the A compartment, we omit this case.
If we assume that each cell orients with respect to the sum of bound Ds and bound Ft on its membrane, (6.10) yields

$$\begin{aligned}(DsFt^l_j + DsFt^r_{j-1}) - (DsFt^r_j + DsFt^l_{j+1}) = \frac{R}{\lambda}[(\bar{D}_1 + a_j)(b_{j-1} - b_{j+1}) \\ + (\bar{F}_1 + b_j)(a_{j-1} - a_{j+1})].\end{aligned} \tag{6.12}$$

We see that if the Ds production rate is the same in every cell, a decreasing Ft production rate will still yield polarity. If we assume the production rate of Ft is the same in every cell, the increasing Ds production rate will give polarity to the right. It is difficult to determine from equation (6.12) how the model will behave for anomalies in the production rates of the proteins. Therefore, we will analyse it numerically. For the same reasons as in Section 6.1, this model cannot reproduce the distribution proposed by Casal *et al.* [7] as shown in Figure 6.4.

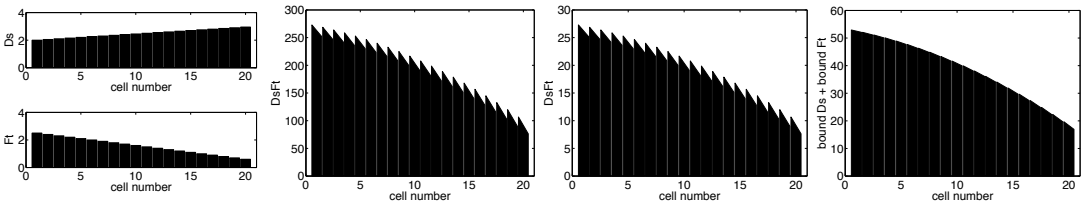

(a) (b) (c) (d)

Figure 6.14: Steady states derived from the analysis for system (6.1). We assume the following parameter values: $\bar{D}_1 = 2.1, \bar{F}_1 = 2.5, a_j = 0.05(j-1)$ and $b_j = -0.1(j-1)$, note the different scales in the different figures; (a) Steady state for free Ds and free Ft for any R and λ; (b) steady state for DsFt for $R = 5$ and $\lambda = 0.1$ assuming each cell counts its bound Ds; (c) steady state for DsFt for $R = 0.5$ and $\lambda = 0.1$, assuming each cell counts its bound Ds; (d) steady state for the cell bridging complexes for $R = 0.5$ and $\lambda = 0.1$, assuming each cell counts its bound Ds and bound Ft.

Figure 6.14 shows the steady states for Ds, Ft and the complexes for system (6.1). In Figure 6.14(a) we see the steady state for Ds and Ft which is independent of the parameter values

of R and λ. If we assume each cell polarises according to its distribution of bound Ds, the steady state for DsFt , $R = 5$ and $\lambda = 0.1$ is shown in Figure 6.14(b). The DsFt distribution is polarised to the left in all cells. Furthermore, the final amount of DsFt in each cell is much greater than the final Ds or Ft amounts. Decreasing R to 0.5 decreases the level of final DsFt but does not change the polarity as displayed in Figure 6.14(c). If we assume that every cell counts the sum of bound Ds and bound Ft on its membrane and choose $R = 0.5$ and $\lambda = 0.1$ we get the steady state in Figure 6.14(d). The distribution of the cell bridging complexes is polarised to the left in every cell and the amount of cell bridging complexes on the right side of cell j is the same as on the left side of cell $j + 1$.

Now we want to investigate the behaviour of the model if we include anomalies in the production rates of Ds and Ft. We have seen above that if polarity is determined by bound Ds, the system can overcome certain anomalies. If each cell counts both bound Ds and bound Ft we were not able to determine the effect of disturbed production rates from equation (6.12). Therefore, we consider the parameter values of Figure 6.14 and add random values to the production rates. Figure 6.15 shows the steady states for the system (6.1) if we assume $a_j = (0.05 + r_j)(j - 1)$ for all j for the Ds production rate and $b_j = -(0.1 + q_j)(j - 1)$ for all j for the Ft production rate, where r_j is a random number in $[0, 0.01]$ and q_j a random number in $[0, 0.02]$. We see in Figure 6.15(b) that the anomalies affect the strength of the polarity but not the direction. Increasing the level of disturbances in the production rate will eventually disrupt polarity (not shown). As expected from equation (6.12) the direction of polarity is independent of the values of R and λ.

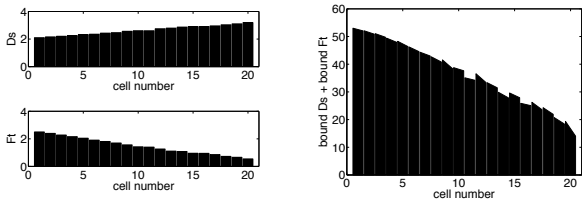

(a) (b)

Figure 6.15: Steady states for system (6.1) for anomalies in the production rates of Ds and Ft; we assume the following parameter values: $\bar{D_1} = 2.1, \bar{F_1} = 2.5, a_j = (0.05 + r_j)(j - 1)$ and $b_j = -(0.1 + q_j)(j - 1)$, with r_j a random number in $[0, 0.01]$ and q_j a random number in $[0, 0.02]$; (a) Steady states for Ds and Ft; (b) steady state for the sum of bound Ds and bound Ft, all cells point to the left, the anomalies in the production rate affect the strength of polarity but not the direction.

Analysis of clones

In this section we are interested in the effect of clones in the row of cells on the behaviour of the model. The clonal cells have a different production rate than the wild-type cells. Figure 6.16 shows the steady states of system (6.1) for Ds, Ft and the cell bridging complex, if we include three cells that do not produce Ds.

The final distributions of Ds and Ft are shown in Figure 6.16(a). Figure 6.16(b) displays the final distribution of bound Ds. Comparing the result to Figure 6.11 A3 we see that the two figures are qualitatively the same. Hence, if we include production in the model, the behaviour around a clone lacking Ds is the same as without production and without diffusion. Calculating the steady state for the clone lacking Ft and the clones with higher levels of Ds or Ft we get the same result; the final states if we include protein production and degradation are the same as in the conservative case if we have no diffusion (not shown). This is what we would expect from our analysis. The protein interactions are the same in both versions of the model. If we include production, the steady state is independent of diffusion, hence we do not expect diffusion driven effects. Figure 6.16(c) supports this result. It shows the final distribution of the bridging complexes if a cell counts both its bound Ds and bound Ft. The resulting behaviour is the same as in the case without production and without diffusion. In both cases (Figure 6.16(b) and (c)), changing the ratio $\frac{R}{\lambda}$ changes the final total amount of the bridging complex in each cell but not the pattern of polarisation.

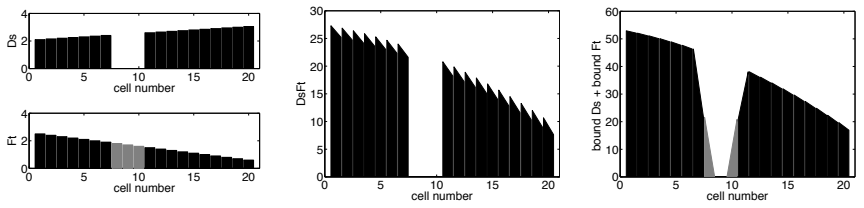

(a) (b) (c)

Figure 6.16: Steady states for systems (6.1); we consider $R = 0.5, \lambda = 0.1, \bar{D}_1 = 2.1, \bar{F}_1 = 2.5, a_j = 0.05(j-1)$ and $b_j = -0.1(j-1)$ and include a clone that does not produce Ds; (a) Steady states for Ds and Ft, (b) steady state for DsFt if we assume that each cell counts its bound Ds; (c) steady state for the sum of bound Ds and bound Ft.

In our simulations the wild-type cells on both sides of a clone show the same behaviour. Furthermore, the range of the effect of the clone is fixed. Hence, these results are different from the experimental observations described in Section 1.2.

The analysis in this section has shown that if we include constant production of the proteins the Ds model can generate wild-type polarity and correct certain anomalies in the initial conditions, but it cannot reproduce the behaviour around clones.

6.3 Discussion

In this chapter we presented a model for the Ds system in one spatial dimension for a row of cells. We considered several different cases. We distinguished between a conservative approach and including protein production and degradation. Furthermore, we assumed three different ways of determining the polarity of the cells. We focused on the A compartment of an abdominal segment and investigated how these different versions of the model behave for an increasing Ds gradient and a decreasing Ft gradient. In many cases we also analysed the potential to overcome anomalies and the behaviour around clones. We found out that if the cells polarise according to the distribution of bound Ft, we get polarity in the wrong direction both for the conservative approach and if we include protein production and degradation. Therefore, this method of determining polarity seems more suitable for the P compartment.
If we assume that each cell counts the sum of its bound Ds and bound Ft we get wild-type polarity for the conservative approach as well as if we include protein production and degradation. For a positive degradation rate this version of the model can correct small anomalies in the production rates; the initial conditions do not influence the final states. If we set the degradation rate to zero the model has difficulties correcting anomalies in the initial conditions. The effects around clones that differ from the wild-type cells in the level of either Ds or Ft are similar in both cases. The wild-type cells around a clone are affected in the same way on both sides of the clone. Furthermore, the range of the effect of the clone is fixed. These results do not agree with experimental observations.
Assuming the distribution of bound Ds determines the polarity of the cells, we get the wild-type polarity in the right direction for the conservative approach and if we choose a positive degradation rate. In addition, certain anomalies in the protein gradients can be overcome in both versions of the model. Considering clones in the row of cells that differ from the wild-type cells in the level of one protein, we found out that the behaviour of the model for a positive protein production rate is the same as for the conservative approach without diffusion. In most cases these results do not agree with the experimental findings. If we assume no protein production and positive diffusion the direction of the disturbance of the clones that are different concerning one protein agrees with the experimental find-

ings. The range of the effect of the clone varies between one and three cells depending on the type of the clone but independent of the parameter values. The behaviour of our model for clones that have either a higher level of Ds and Ft or lack both proteins does not match the experimental observations.

Out of the different cases we have analysed, the conservative approach combined with counting bound Ds to determine the polarity of the cells seems the best way to reproduce the experimental observations in the A compartment of an abdominal segment. However, it leaves many questions unanswered. The simulations for clones in the row of cells have shown that this model cannot yield longer-range propagation. The range of the effect of the clones is fixed for each type of clone. Experiments show a variability of the range of the effect of the clone. As mentioned above, Fj is assumed to inhibit Ds and activate Ft. Clones lacking either Ds or Ft show a longer-range effect if the surrounding tissue lacks Fj than in a wild-type background. A second issue is that in our simulations the clone lacking both Ds and Ft has an effect on the wild-type cells which is partly even independent of diffusion. Experiments have shown that such a clone does not affect the cells around it. This suggests that our model is missing a component that suppresses the effect of the clone. This problem together with the inability of the model to produce longer-range effects are the main issues to address when improving the model.

Apart from the abdomen the Ds system also occurs in the *Drosophila* wings and eyes. The idea of the mechanism in the eyes is essentially the same as in the abdomen. Experiments have shown that either the Ds or the Fj gradient are redundant [40]. A uniform Fj distribution combined with a Ds gradient or vice versa yield polarity. Reversing the directions of the gradients reverses polarity and if both proteins are distributed uniformly the cells do not polarise. To compare this result with our model we have to remember that Fj is assumed to enhance Ft, which yields a Ft gradient. Therefore, in our model this result would mean that either the Ds or the Ft gradient are redundant. Our results show that out of the cases we have studied, the approach without protein production and in which we count bound Ds to determine the polarity of the cells is the only version of the model that can reproduce these experimental findings.

In the *Drosophila* wing, Ft is distributed uniformly and the Ds and Fj gradients have opposite sign compared to the A compartment of an abdominal segment. A uniform Ds distribution can still yield polarity everywhere in the wing apart from the most proximal region and this is also true in the absence of a Fj gradient [31]. Together with further experiments analysing the role of Ds and Fj gradients in the wings [40], these findings suggest that the Ds system does not play an essential role in polarising the wing cells. This raises another question. It is still unclear whether the mechanism of the Ds system is common to

the different parts of the fruit fly. So far, evidence for the Ds system acting in parallel to the Fz system to generate PCP has only been found in the abdomen.

Chapter 7

Discussion

Planar cell polarity is an important feature of the development of vertebrates and invertebrates; its failure can lead to a variety of diseases like congenital deafness syndromes, neural tube closure defects, respiratory diseases and polycystic kidneys. In this work we focused on the fruit fly *Drosophila melanogaster*, particularly its wings and abdomen. There, PCP is detected by the orientation of hairs. The underlying mechanism of PCP is still mostly unknown. Experimentalists mainly focus on two protein networks, the Fz system – also referred to as the core proteins – and the Ds system. So far, two possibilities have been proposed of how these two systems interact; one idea is that the Fz system acts downstream of the Ds system while the second one is that the two systems act in parallel. The study of the behaviour of wild-type cells next to clones has provided most of the insight into the mechanism of PCP. The effects of clones are remarkably reproducible; in most cases one sees reorientation of the hairs in the wild-type tissue either in front or behind the clone, depending on which protein the clone is lacking.

Existing models of PCP consider the Fz system. Since the precise molecular interactions of the different proteins involved are mostly unknown, these models test various assumptions for the mechanism. We followed a different approach. We were interested in the features of whole classes of models that yield PCP. Therefore, we proposed two types of models, a non-conservative feedback and diffusion model and a conservative model, incorporating a minimum of biological detail. Furthermore, we considered two examples of the model class represented by the conservative model. These approaches were introduced by Amonlirdviman *et al.* [3] and Le Garrec *et al.* [29] to model the establishment of PCP in the *Drosophila* pupal wing. Concerning the Ds system we proposed a model for PCP in the *Drosophila* abdomen. It is based on the experimental findings by Casal *et al.* [7], which suggest that the Ds system can yield PCP on its own.

To investigate the properties of the five models, we analysed them in one spatial dimension for a row of cells, applying algebraic as well as numerical analysis of the steady states. For the feedback and diffusion model and the models by Amonlirdviman and Le Garrec we extended our analysis to two spatial dimensions. To numerically approximate the solutions of the full PDE systems of the two latter approaches we applied the finite element method, taking into account the different diffusive behaviour of the different proteins and protein complexes of the Fz system.

Our analysis of the feedback and diffusion model in Chapter 2 revealed that it can yield polarity as well as an unpolarised period two pattern. Both steady states are stable for strong feedback and weak diffusion. Polarity arises from homogeneous initial conditions. Increasing the inhomogeneity in the initial conditions yields the period two pattern. Robustness of the polarised steady state can be increased by increasing the strength of the feedback or decreasing the diffusion. Clones initiate the unpolarised period two pattern in the surrounding wild-type cells. This is inconsistent with experimental findings in which the direction of the hairs of cells next to a clone might be disturbed but they still have an orientation.

The conservative model in Chapter 3 shows different properties. This approach can yield polarity, either from an initial imbalance in every cell or via a wave. However, it cannot exhibit an inhomogeneous pattern in a row of cells. Therefore, the polarised steady state is more robust to anomalies in the initial conditions than in the feedback and diffusion model. Furthermore, cells next to a clone show polarity. The disturbance of the direction of those cells by clones lacking activity or with excessive activity resembles the effect of fz clones on the surrounding wild-type tissue in experiments.

For both models we have chosen a generic approach, omitting biological details to ensure that our results are relevant for whole classes of models. This course of action raises several questions. In both models, increasing the diffusion above a certain threshold, depending on the strength of the feedback, disrupts polarity. Therefore, the strength of intracellular diffusion is a key component, which affects the behaviour of the models. It would be interesting to investigate experimentally whether changing intracellular movement affects the overall pattern of planar polarity in a system such as the *Drosophila* wing. Another matter of interest would be to implement a specific type of protein transport into our models and investigate whether this changes the overall behaviour of the systems. A possible mechanism would be polarised transport along microtubules [39]. Furthermore, there is biochemical evidence which suggest the involvement of endocytosis in planar cell polarity. However, in *Drosophila* no genetic evidence for it has been found, yet [13].

In the two models we refer to the variables as amounts of "activity", leaving open the ques-

tion of what they represent in terms of specific molecular species. A concrete assignment of molecular identity to the activities in our models depends on the answer to a key question: what is it that polarises cells? In wild-type tissue of the *Drosophila* larval wing, the core PCP proteins become distributed asymmetrically in the membrane of cells shortly before the hairs start to grow. However, recently reported experiments show that *Drosophila* larval wings that are mutant for certain core proteins do not display asymmetric distribution of the core proteins, but nonetheless show normal hair development [45]. These results suggest that mechanisms other than asymmetric localisation of the core PCP proteins may be polarising the cells, such as asymmetric distribution of certain protein complexes or other intracellular components.

A third term that occurs in the analysis of these two models is the "strength of polarity". So far, in experiments polarity is detected by the orientation of structures like hairs or bristles. Therefore, only a direction but not a strength can be observed. In our models, however we see that the parameter values and initial conditions determine the direction as well as the strength of polarity. If we were able to assign a value to the strength of the polarity of a cell it would help to compare experimental findings with our results and give us the opportunity to rule out parameter sets, which again would give us a better idea of the underlying feedback mechanism.

The models by Amonlirdviman *et al.* [3] and Le Garrec *et al.* [29] are specific examples for the model class represented by the conservative model. These two approaches are based on the assumption that the distribution of the core proteins determines the polarity of a cell. In Chapter 4 we analysed the model by Amonlirdviman *et al.*. It consists of two main parts, a feedback loop and a persistent global bias. Our aim was to determine the relative importance of the two components to generate polarity. We found out that either of the two components is sufficient to obtain polarity. However, if we only rely on the feedback loop we need an initial cue that can be amplified. Furthermore, the analysis in two spatial dimensions for compartmentalised cells suggests that the desired polarised steady state is unstable and only arises from an initial cue that is symmetric with respect to the horizontal axis. Therefore, the system is very sensitive to any kinds of fluctuations, which are likely to occur in nature. Including clones in the field of cells yields an almost completely disordered behaviour of the wild-type cells in the field, which is inconsistent with experimental findings where the cells further away from the clone show normal polarity. Investigations of the full spatial model support this result. Therefore, the persistent global bias is not necessary to amplify polarity but without it the model cannot correct anomalies in the initial conditions. Furthermore, the results of the analysis of the full spatial model suggest that the proposed feedback loop might be more suitable to amplify an initial imbalance in Vang

than in Fz. However, this theory has yet to be investigated in more detail.

The model by Le Garrec *et al.* was analysed in Chapter 5. It consists of two feedback loops that amplify an initial global ligand gradient. Such a gradient has a similar effect to the persistent global bias in the model by Amonlirdviman *et al.*. Analogous analysis as in Chapter 4 showed that the gradient is not needed to generate polarity but that it is necessary to ensure robustness of the desired polarised steady state. For a row of cells in one spatial dimension we found different sets of parameter values for which the system polarises from an initial ligand imbalance in every cell. Investigations in two spatial dimensions for compartmentalised cells, however suggested that the desired polarised steady state is unstable and only arises from initial conditions that are symmetric with respect to the horizontal axis. Therefore, this steady state is very sensitive to fluctuations which are common in biological systems. A clone in the field of cells yields a completely disordered orientation of the surrounding cells, which does not match the experimental results. The analysis of the full spatial model supports these results; an initial ligand imbalance that is asymmetric with respect to the horizontal axis yields a similarly asymmetric final state, while for the same parameter values an initial condition that is symmetric with respect to the horizontal axis generates the desired polarity.

We see that both the model by Amonlirdviman *et al.* and the model by Le Garrec *et al.* need a global bias to ensure correct polarity. Considering the diffusion coefficient we found that for both models its value has to be below a certain threshold; otherwise the unpolarised steady state arises. The models differ mostly in their feedback mechanism. Amonlirdviman *et al.* assume that Vang, Pk and their complexes inhibit the binding of Dsh to Fz. Le Garrec *et al.* propose that Fz* and its complexes inhibit the binding of Vang to Fmi, while Dsh* complexes inhibit the binding of Pk to Vang. Hence the first feedback mechanism is driven by Vang and Pk while the second is driven by Fz* and Dsh*. It would be interesting to investigate in more detail whether the different feedback mechanisms have different effects on the final states of the models.

So far, we have discussed two approaches that represent certain classes of PCP models and two specific models that are examples for one of the model classes. All four approaches have shown that increasing the diffusion coefficient above a certain threshold leads to disruption of polarity. In all models we have calculated the times it takes to reach the polarised steady state. In many cases assuming the diffusion coefficients given in [22] led to simulation times that were in a reasonable range compared to the times measured in experiments. For the two-dimensional representations of the models by Amonlirdviman *et al.* and Le Garrec *et al.* however, we obtained simulation times that were far too short. A possible explanation is that the diffusion in the biological system is slower than as-

sumed. This idea is motivated by findings in yeast, which show that correct polarity relies on membrane diffusion being 1-2 orders of magnitude slower than the usually assumed speed [51].

The second key element of the four models is the feedback loop. We have seen that the model by Amonlirdviman *et al.* and the model by Le Garrec *et al.* have different feedback loops that both yield polarity. Together with the results of the analysis of the conservative model, this suggests that there is a wide range of feedback loops that can give the desired polarisation. Further theoretical as well as experimental analysis of the properties of the feedback loop would help to narrow the range of possible feedback loops.

An important finding in Chapters 4 and 5 is that in both specific models the biases are not necessary to amplify polarity but to ensure robustness of the models. Since the conservative model in Chapter 3 is a generalised form of these two models we would expect to see the same sensitivity to the initial conditions in two spatial dimensions. It would be interesting to investigate this matter further.

Overall, these results suggest that a feedback loop amplifying an initial imbalance in every cell cannot ensure robust polarisation of a field of cells. Therefore, the important question is whether nature uses some sort of global bias or a completely different mechanism. In the latter case we would have to start from scratch. If a global bias is imposed on the system further analysis of the amplifying mechanism would be of minimal interest, since finding the bias would be sufficient to explain the establishment of PCP. Recent work by Simons *et al.* [41] provides a first attempt at finding such a bias. Their results show that the interactions of Fz and Dsh are stabilised by pH and charge-dependent interactions of Dsh with the cell membrane. Hence, electrochemical cues could provide a bias.

Apart from the Fz system we also considered the Ds system. In Chapter 6 we proposed a model for the interactions of Ds and Ft in the *Drosophila* abdomen, based on the results of Casal *et al.* [7]. We analysed different versions of the model, with and without protein production and degradation. Furthermore, we considered three different ways of determining the polarity of a cell. We discovered that out of these different possibilities, the conservative version (without protein production and degradation) combined with polarisation of the cells according to their bound Ds distribution reproduces the experimental findings the best. However, it still leaves some uncertainties. Particularly, the behaviour around clones does not entirely match experimental findings. Contrary to observations in the *Drosophila* abdomen the range of the effect of the clones on the surrounding cells in our model is fixed; we do not get propagation. Furthermore, a clone lacking both Ft and Ds does not influence the neighbouring wild-type cells in experiments. Our model could not reproduce this result. It seems that our model is lacking a factor which can suppress or

override the effect of such a clone.

Further insight into the mechanism of the Ds system has been provided by experimental investigations in the *Drosophila* eye. Experiments in the *Drosophila* wing however, suggested that the Ds system is not essential to the polarisation of the wing cells. This indicates that the mechanisms polarising the cells in the different structures of the fruit fly might not be the same. Therefore, it is important to determine which protein interactions are common to the different structures of *Drosophila* and which are specific to certain parts. So far the findings that the Ds system can polarise the cells in the absence of the Fz system have only been obtained in the *Drosophila* abdomen. It has yet to be shown that they are valid in other parts of the fruit fly.

In summary, we have presented five models considering different aspects of the process of planar cell polarity. What is known so far can mainly be split into three modules. The first one includes the interactions of Fz, Fmi and Vang, which act cell non-autonomously. The second module describes the cell autonomous function of Dsh, Pk and Dgo to yield an asymmetric protein distribution. The third module covers the Ds system, i.e. the interactions of Ds, Ft and Fj. What remains unclear is how these modules are coordinated to ensure robust polarisation of the cells. The Ds system might act upstream of the Fz system or in parallel. Furthermore, it seems that the cell non-autonomous module of the Fz system already polarises the cells, while the cell-autonomously acting module just stabilises the polarity. In this context the feedback and diffusion model as well as the conservative model can be used to describe any of the three modules, depending on how we interpret the term "activity". The models by Amonlirdviman *et al.* and Le Garrec *et al.* mainly focus on the second module, while the model for the Ds system considers the third module. Considering the lack of models for the first module and the possibility that it polarises the cells on its own, in future work it would be interesting to investigate the interactions of Fz, Vang and Fmi further. Recent experimental papers have focused on this issue, raising the question whether Fmi acts actively to amplify polarity or passively by supporting the binding of Fz to Vang [9, 47, 55]. Theoretical studies might help to investigate this issue further.

We see that the work in this thesis has given some insight into the establishment of planar cell polarity while posing several new problems at the same time. It will be necessary to further investigate the raised questions both experimentally and theoretically.

Appendix A

Nelder-Mead algorithm

In Chapters 4 and 5 we apply a parameter search based on the Nelder-Mead algorithm. It was first introduced by Nelder and Mead [33] to solve unconstrained optimisation problems. It is a direct search method which relies on comparing the function values at the $n+1$ vertices x_i of a simplex. To find a point with a better function value the vertices of the simplex are changed by reflection, expansion, contraction and shrinkage. For our problem the vertices $x_1, \ldots, x_{n+1}$ are $n+1$ parameter sets. The objective function f is minimised. To obtain the value of $f(x_i)$ we calculate the homogeneous unpolarised steady state and the eigenvector with the largest real part λ_i of the given system for the parameter set x_i. Then $f(x_i) = -\lambda_i$. All our parameter values have to be positive. Hence, our problem is constrained. We need to adapt the Nelder-Mead method; whenever a component becomes negative we project it to the boundaries of our domain. Choosing α, β, γ and σ as the reflection, expansion, contraction and shrink coefficients we get the following algorithm:

Algorithm A.1

(S.0) *Choose* $\alpha > 0, \beta > 0, 0 < \gamma < 1$ *and* $0 < \sigma < 1$ *and get a starting simplex.*

(S.1) *Sort the vertices* $x_1, x_2, ..., x_{n+1}$ *of the current simplex so that their function values* $f_1, f_2, ..., f_{n+1}$ *are in ascending order.*

(S.2) *Compute the centroid of the n best points* $\bar{x} := \frac{1}{n}\sum_{i=1}^{n} x_i$ *and the reflection point* $x_r := \bar{x} + \alpha(\bar{x} - x_{n+1})$. *If* x_r *is out of the domain: projection to the boundary. Evaluate* $f_r = f(x_r)$.

(S.3) *If* $f_1 \leq f_r \leq f_n$, *set* $x_{n+1} := x_r$, *go to (S.7).*

(S.4) If $f_r < f_1$, calculate the expansion point $x_e := \bar{x} + \beta(x_r - \bar{x})$. If x_e is out of the domain: projection to the boundary. Evaluate $f_e = f(x_e)$. If $f_e < f_r$ set $x_{n+1} = x_e$ and got to (S.7); otherwise (if $f_e \geq f_r$) set $x_{n+1} := x_r$ and go to (S.7).

(S.5) If $f_r \geq f_n$ perform a contraction

- *(a) Inside: If $f_r \geq f_n$, perform an inside contraction, i.e. calculate $x_{ic} := \bar{x} + \gamma(x_{n+1} - \bar{x})$ and evaluate $f_{ic} = f(x_{ic})$. If $f_{ic} < f_{n+1}$, set $x_{n+1} := x_{ic}$ and go to (S.7); otherwise go to (S.6).*
- *(b) Outside: If $f_r < f_{n+1}$, perform an outside contraction , i.e. calculate $x_{oc} := \bar{x} + \gamma(x_r - \bar{x})$. If x_{oc} is out of the domain: projection to the boundary. Evaluate $f_{oc} = f(x_{oc})$. If $f_{oc} \leq f_r$, set $x_{n+1} := x_{oc}$ and go to (S.7); otherwise go to (S.6).*

(S.6) Perform a shrink step. Evaluate f at the n points $v_i = x_1 + \sigma(x_i - x_1), i = 2, ..., n+1$. The (unordered) vertices of the simplex at the next iteration consist of $x_1, v_2, ..., v_{n+1}$.

(S.7) If the stopping conditions are not satisfied go to (S.1).

As parameter values we use $\alpha = 1, \beta = 2, \gamma = 0.5$ and $\sigma = 0.5$. To generate the starting simplex we choose a point $x_0 \in \mathbb{R}^n_+$, where n is the number of parameters in our model. Setting $p = \frac{\sqrt{n+1}+n-1}{n\sqrt{2}}$ and $q = \frac{\sqrt{n+1}-1}{n\sqrt{2}}$, a vertex x_i of the starting simplex $\{x_0, ..., x_n\}$ is given by

$$x_i = x_0 + pe_i + \sum_{\substack{k=1 \\ k \neq i}}^{n} qe_k \quad \text{for all } i = 1, ..., n.$$

The parameter search is stopped if we have found a parameter set with a sufficiently large λ_i.

Appendix B

Systems of equations for the model by Amonlirdviman et al.

Here, we present the complete systems of equations for our analysis of the model by Amonlirdviman *et el.* [3] in Chapter 4. The reactions for the model are given in equations (4.1)-(4.10).

B.1 One-dimensional system

We assume a row of cells in which each cell has a left and a right side. Applying the law of mass action to (4.1)-(4.10) we get the corresponding system of ODEs. The subscripts indicate the cell number and the superscripts the side of the cell, l for left and r for right. The diffusion coefficients are included by μ_k for $k = 1, \ldots, 6$ and Δx denotes the extension of a cell from left to right. The square brackets indicate that we are dealing with concentrations. The scaling factor for the feedback loop is given by

$$\begin{aligned} B_i^l = 1 + K_b(K_{pk}\,[Pk]_i^l + [VangPk]_i^l + [FzVangPk]_i^l + [DshFzVangPk]_i^l \\ + K_{va}([Vang]_i^l + [FzVang]_i^l + [DshFzVang]_i^l))^{K_p} \\ B_i^r = 1 + K_b(K_{pk}\,[Pk]_i^r + [VangPk]_i^r + [FzVangPk]_i^r + [DshFzVangPk]_i^r \\ + K_{va}([Vang]_i^r + [FzVang]_r^i + [DshFzVang]_r^i))^{K_p}, \end{aligned}$$

and for the persistent global bias we have

$$M_1 < 1.$$

The resulting system of ODEs is

$$\begin{aligned}
\frac{\mathrm{d}[Dsh]_i^l}{\mathrm{d}t} &= -R_1\,[Dsh]_i^l\,[Fz]_i^l + \lambda_1 B_i^l\,[DshFz]_i^l - R_5\,[Dsh]_i^l\,[FzVang]_{i-1}^r \\
&\quad + \lambda_5\,B_i^l[DshFzVang]_{i-1}^r - R_8\,[Dsh]_i^l\,[FzVangPk]_{i-1}^r \\
&\quad + \lambda_8 B_i^l\,[DshFzVangPk]_{i-1}^r + \mu_1\,\frac{([Dsh]_i^r - [Dsh]_i^l)}{\Delta x^2}, \\
\frac{\mathrm{d}[Dsh]_i^r}{\mathrm{d}t} &= -R_1\,[Dsh]_i^r\,[Fz]_i^r + M_1\lambda_1 B_i^r\,[DshFz]_i^r - R_5\,[Dsh]_i^r\,[FzVang]_{i+1}^l \\
&\quad + M_1\lambda_5 B_i^r\,[DshFzVang]_{i+1}^l - R_8\,[Dsh]_i^r\,[FzVangPk]_{i+1}^l \\
&\quad + M_1\lambda_8 B_i^r\,[DshFzVangPk]_{i+1}^l + \mu_1\,\frac{([Dsh]_i^l - [Dsh]_i^r)}{\Delta x^2},
\end{aligned}$$

$$\begin{aligned}
\frac{\mathrm{d}[Pk]_i^l}{\mathrm{d}t} &= -R_3\,[Vang]_i^l\,[Pk]_i^l + \lambda_3\,[VangPk]_i^l - R_7[FzVang]_i^l\,[Pk]_i^l \\
&\quad + \lambda_7\,[FzVangPk]_i^l - R_{10}\,[DshFzVang]_i^l\,[Pk]_i^l \\
&\quad + \lambda_{10}\,[DshFzVangPk]_i^l + \mu_2\,\frac{([Pk]_i^r - [Pk]_i^l)}{\Delta x^2}, \\
\frac{\mathrm{d}[Pk]_i^r}{\mathrm{d}t} &= -R_3\,[Vang]_i^r\,[Pk]_i^r + \lambda_3\,[VangPk]_i^r - R_7\,[FzVang]_i^r\,[Pk]_i^r \\
&\quad + \lambda_7\,[FzVangPk]_i^r - R_{10}\,[DshFzVang]_i^r\,[Pk]_i^r \\
&\quad + \lambda_{10}\,[DshFzVangPk]_i^r + \mu_2\,\frac{([Pk]_i^l - [Pk]_i^r)}{\Delta x^2},
\end{aligned}$$

$$\begin{aligned}
\frac{\mathrm{d}[Fz]_i^l}{\mathrm{d}t} &= -R_1\,[Dsh]_i^l\,[Fz]_i^l + \lambda_1 B_i^l\,[DshFz]_i^l - R_2\,[Fz]_i^l\,[Vang]_{i-1}^r \\
&\quad + \lambda_2\,[FzVang]_{i-1}^r - R_6\,[Fz]_i^l\,[VangPk]_{i-1}^r + \lambda_6\,[FzVangPk]_{i-1}^r \\
&\quad + \mu_3\,\frac{([Fz]_i^r - [Fz]_i^l)}{\Delta x^2}, \\
\frac{\mathrm{d}[Fz]_i^r}{\mathrm{d}t} &= -R_1\,[Dsh]_i^r\,[Fz]_i^r + M_1\lambda_1 B_i^r\,[DshFz]_i^r - R_2\,[Fz]_i^r\,[Vang]_{i+1}^l \\
&\quad + \lambda_2\,[FzVang]_{i+1}^l - R_6\,[Fz]_i^r\,[VangPk]_{i+1}^l + \lambda_6\,[FzVangPk]_{i+1}^l \\
&\quad + \mu_3\,\frac{([Fz]_i^l - [Fz]_i^r)}{\Delta x^2},
\end{aligned}$$

$$\begin{aligned}
\frac{\mathrm{d}[Vang]_i^l}{\mathrm{d}t} &= -R_2\,[Fz]_{i-1}^r\,[Vang]_i^l + \lambda_2\,[FzVang]_i^l - R_3\,[Vang]_i^l\,[Pk]_i^l \\
&\quad + \lambda_3\,[VangPk]_i^l - R_4\,[DshFz]_{i-1}^r[Vang]_i^l + \lambda_4\,[DshFzVang]_i^l \\
&\quad + \mu_4\,\frac{([Vang]_i^r - [Vang]_i^l)}{\Delta x^2},
\end{aligned}$$

$$\frac{\mathrm{d}[Vang]_i^r}{\mathrm{d}t} = -R_2\,[Fz]_{i+1}^l\,[Vang]_i^r + \lambda_2\,[FzVang]_i^r - R_3\,[Vang]_i^r\,[Pk]_i^r + \lambda_3\,[VangPk]_i^r - R_4\,[DshFz]_{i+1}^l\,[Vang]_i^r + \lambda_4\,[DshFzVang]_i^r + \mu_4\,\frac{([Vang]_i^l - [Vang]_i^r)}{\Delta x^2},$$

$$\frac{\mathrm{d}[DshFz]_i^l}{\mathrm{d}t} = R_1\,[Dsh]_i^l\,[Fz]_i^l - \lambda_1\,B_i^l[DshFz]_i^l - R_4\,[DshFz]_i^l\,[Vang]_{i-1}^r + \lambda_4\,[DshFzVang]_{i-1}^r - R_9\,[DshFz]_i^l\,[VangPk]_{i-1}^r + \lambda_9\,[DshFzVangPk]_{i-1}^r + \mu_5\,\frac{([DshFz]_i^r - [DshFz]_i^l)}{\Delta x^2},$$

$$\frac{\mathrm{d}[DshFz]_i^r}{\mathrm{d}t} = R_1\,[Dsh]_i^r\,[Fz]_i^r - M_1\lambda_1 B_i^r\,[DshFz]_i^r - R_4\,[DshFz]_i^r\,[Vang]_{i+1}^l + \lambda_4\,[DshFzVang]_{i+1}^l - R_9\,[DshFz]_i^r\,[VangPk]_{i+1}^l + \lambda_9\,[DshFzVangPk]_{i+1}^l + \mu_5\,\frac{([DshFz]_i^l - [DshFz]_i^r)}{\Delta x^2},$$

$$\frac{\mathrm{d}[VangPk]_i^l}{\mathrm{d}t} = R_3\,[Vang]_i^l\,[Pk]_i^l - \lambda_3\,[VangPk]_i^l - R_6\,[Fz]_{i-1}^r\,[VangPk]_i^l + \lambda_6\,[FzVangPk]_i^l - R_9\,[DshFz]_{i-1}^r\,[VangPk]_i^l + \lambda_9\,[DshFzVangPk]_i^l + \mu_6\,\frac{([VangPk]_i^r - [VangPk]_i^l)}{\Delta x^2},$$

$$\frac{\mathrm{d}[VangPk]_i^r}{\mathrm{d}t} = R_3\,[Vang]_i^r\,[Pk]_i^r - \lambda_3\,[VangPk]_i^r - R_6\,[Fz]_{i+1}^l\,[VangPk]_i^r + \lambda_6\,[FzVangPk]_i^r - R_9\,[DshFz]_{i+1}^l\,[VangPk]_i^r + \lambda_9\,[DshFzVangPk]_i^r + \mu_6\,\frac{([VangPk]_i^l - [VangPk]_i^r)}{\Delta x^2},$$

$$\frac{\mathrm{d}[FzVang]_i^l}{\mathrm{d}t} = R_2\,[Fz]_{i-1}^r\,[Vang]_i^l - \lambda_2\,[FzVang]_i^l - R_5\,[Dsh]_{i-1}^r\,[FzVang]_i^l + M_1\lambda_5 B_{i-1}^r\,[DshFzVang]_i^l - R_7\,[FzVang]_i^l\,[Pk]_i^l + \lambda_7\,[FzVangPk]_i^l,$$

$$\frac{\mathrm{d}[FzVang]_i^r}{\mathrm{d}t} = R_2\,[Fz]_{i+1}^l\,[Vang]_i^r - \lambda_2\,[FzVang]_i^r - R_5\,[Dsh]_{i+1}^l[FzVang]_i^r + \lambda_5 B_{i+1}^l\,[DshFzVang]_i^r - R_7\,[FzVang]_i^r\,[Pk]_i^r + \lambda_7\,[FzVangPk]_i^r,$$

$$\begin{aligned}
\frac{\mathrm{d}[DshFzVang]_i^l}{\mathrm{d}t} &= R_4\,[DshFz]_{i-1}^r\,[Vang]_i^l - \lambda_4\,[DshFzVang]_i^l + R_5\,[Dsh]_{i-1}^r\,[FzVang]_i^l \\
&\quad - M_1\lambda_5 B_{i-1}^r\,[DshFzVang]_i^l - R_{10}\,[DshFzVang]_i^l\,[Pk]_i^l \\
&\quad + \lambda_{10}\,[DshFzVangPk]_i^l, \\
\frac{\mathrm{d}[DshFzVang]_i^r}{\mathrm{d}t} &= R_4\,[DshFz]_{i+1}^l[Vang]_i^r - \lambda_4\,[DshFzVang]_i^r + R_5\,[Dsh]_{i+1}^l\,[FzVang]_i^r \\
&\quad - \lambda_5\,B_{i+1}^l[DshFzVang]_i^r - R_{10}\,[DshFzVang]_i^r\,[Pk]_i^r \\
&\quad + \lambda_{10}\,[DshFzVangPk]_i^r,
\end{aligned}$$

$$\begin{aligned}
\frac{\mathrm{d}[FzVangPk]_i^l}{\mathrm{d}t} &= R_6\,[Fz]_{i-1}^r\,[VangPk]_i^l - \lambda_6\,[FzVangPk]_i^l + R_7\,[FzVang]_i^l\,[Pk]_i^l \\
&\quad - \lambda_7\,[FzVangPk]_i^l - R_8\,[Dsh]_{i-1}^r\,[FzVangPk]_i^l \\
&\quad + M_1\lambda_8 B_{i-1}^r\,[DshFzVangPk]_i^l, \\
\frac{\mathrm{d}[FzVangPk]_i^r}{\mathrm{d}t} &= R_6\,[Fz]_{i+1}^l\,[VangPk]_i^r - \lambda_6\,[FzVangPk]_i^r + R_7\,[FzVang]_i^r\,[Pk]_i^r \\
&\quad - \lambda_7\,[FzVangPk]_i^r - R_8\,[Dsh]_{i+1}^l\,[FzVangPk]_i^r \\
&\quad + \lambda_8\,B_{i+1}^l[DshFzVangPk]_i^r,
\end{aligned}$$

$$\begin{aligned}
\frac{\mathrm{d}[DshFzVangPk]_i^l}{\mathrm{d}t} &= R_8\,[Dsh]_{i-1}^r\,[FzVangPk]_i^l - M_1\lambda_8 B_{i-1}^r\,[DshFzVangPk]_i^l \\
&\quad + R_9\,[DshFz]_{i-1}^r\,[VangPk]_i^l - \lambda_9\,[DshFzVangPk]_i^l \\
&\quad + R_{10}\,[DshFzVang]_i^l\,[Pk]_i^l - \lambda_{10}\,[DshFzVangPk]_i^l, \\
\frac{\mathrm{d}[DshFzVangPk]_i^r}{\mathrm{d}t} &= R_8\,[Dsh]_{i+1}^l\,[FzVangPk]_i^r - \lambda_8\,B_{i+1}^l[DshFzVangPk]_i^r \\
&\quad + R_9\,[DshFz]_{i+1}^l\,[VangPk]_i^r - \lambda_9\,[DshFzVangPk]_i^r \\
&\quad + R_{10}\,[DshFzVang]_i^r\,[Pk]_i^r - \lambda_{10}\,[DshFzVangPk]_i^r.
\end{aligned}$$

B.2 Two-dimensional system for compartmentalised cells

Now we assume we have a field of hexagonal cells, which are subdivided into 6 triangular compartments. Applying the law of mass action to the reactions (4.1)-(4.10) we get the corresponding system of ODEs for the change of the protein concentrations in compartment $j \pmod 6$ of cell i. The superscript + indicates binding over the cell membrane. Note that cell bridging complexes are counted in the same cell as their Vang part. The square brackets indicate concentrations of the proteins and protein complexes. The parameters μ_k for $k = 1, \ldots, 6$ represent diffusion while Δx denotes the distance between two neigh-

bouring compartments in a cell. We omit the persistent global bias. The scaling factor B, representing the feedback, is given by

$$B_{i,j} = 1 + K_b(K_{pk}[Pk]_{i,j} + [VangPk]_{i,j} + [FzVangPk]_{i,j} + [DshFzVangPk]_{i,j} + K_{va}([Vang]_{i,j} + [FzVang]_{i,j} + [DshFzVang]_{i,j}))^{K_p}.$$

This yields the following system of equations

$$\begin{aligned}\frac{\mathrm{d}[Dsh]_{i,j}}{\mathrm{d}t} = &-R_1\,[Dsh]_{i,j}\,[Fz]_{i,j} + \lambda_1 B_{i,j}\,[DshFz]_{i,j} - R_5\,[Dsh]_{i,j}\,[FzVang]^+_{i,j} \\ &+ \lambda_5 B_{i,j}\,[DshFzVang]^+_{i,j} - R_8\,[Dsh]_{i,j}\,[FzVangPk]^+_{i,j} \\ &+ \lambda_8 B_{i,j}\,[DshFzVangPk]^+_{i,j} \\ &+ \mu_1\,\frac{([Dsh]_{i,j+1} + [Dsh]_{i,j-1} - 2[Dsh]_{i,j})}{\Delta x^2},\end{aligned}$$

$$\begin{aligned}\frac{\mathrm{d}[Pk]_{i,j}}{\mathrm{d}t} = &-R_3\,[Vang]_{i,j}\,[Pk]_{i,j} + \lambda_3\,[VangPk]_{i,j} - R_7\,[Pk]_{i,j}\,[FzVang]_{i,j} \\ &+ \lambda_7\,[FzVangPk]_{i,j} - R_{10}\,[Pk]_{i,j}\,[DshFzVang]_{i,j} \\ &+ \lambda_{10}\,[DshFzVangPk]_{i,j} + \mu_2\,\frac{([Pk]_{i,j+1} + [Pk]_{i,j-1} - 2[Pk]_{i,j})}{\Delta x^2},\end{aligned}$$

$$\begin{aligned}\frac{\mathrm{d}[Fz]_{i,j}}{\mathrm{d}t} = &-R_1\,[Dsh]_{i,j}\,[Fz]_{i,j} + \lambda_1 B_{i,j}\,[DshFz]_{i,j} - R_2\,[Fz]_{i,j}\,[Vang]^+_{i,j} \\ &+ \lambda_2\,[FzVang]^+_{i,j} - R_6\,[Fz]_{i,j}\,[VangPk]^+_{i,j} + \lambda_6\,[FzVangPk]^+_{i,j} \\ &+ \mu_3\,\frac{([Fz]_{i,j+1} + [Fz]_{i,j-1} - 2[Fz]_{i,j})}{\Delta x^2},\end{aligned}$$

$$\begin{aligned}\frac{\mathrm{d}[Vang]_{i,j}}{\mathrm{d}t} = &-R_2\,[Vang]_{i,j}[Fz]^+_{i,j} + \lambda_2\,[FzVang]_{i,j} - R_3\,[Vang]_{i,j}\,[Pk]_{i,j} \\ &+ \lambda_3\,[VangPk]_{i,j} - R_4\,[Vang]_{i,j}\,[DshFz]^+_{i,j} + \lambda_4\,[DshFzVang]_{i,j} \\ &+ \mu_4\,\frac{([Vang]_{i,j+1} + [Vang]_{i,j-1} - 2[Vang]_{i,j})}{\Delta x^2},\end{aligned}$$

$$\begin{aligned}\frac{\mathrm{d}[DshFz]_{i,j}}{\mathrm{d}t} = &\;R_1\,[Dsh]_{i,j}\,[Fz]_{i,j} - \lambda_1 B_{i,j}\,[DshFz]_{i,j} - R_4\,[DshFz]_{i,j}\,[Vang]^+_{i,j} \\ &+ \lambda_4\,[DshFzVang]^+_{i,j} - R_9\,[DshFz]_{i,j}\,[VangPk]^+_{i,j} \\ &+ \lambda_9\,[DshFzVangPk]^+_{i,j} \\ &+ \mu_6\,\frac{([DshFz]_{i,j+1} + [DshFz]_{i,j-1} - 2[DshFz]_{i,j})}{\Delta x^2},\end{aligned}$$

$$\begin{aligned}\frac{\mathrm{d}[VangPk]_{i,j}}{\mathrm{d}t} &= R_3\,[Vang]_{i,j}\,[Pk]_{i,j} - \lambda_3\,[VangPk]_{i,j} - R_6\,[VangPk]_{i,j}\,[Fz]^+_{i,j} \\ &\quad + \lambda_6\,[FzVangPk]_{i,j} - R_9\,[VangPk]_{i,j}\,[DshFz]^+_{i,j} \\ &\quad + \lambda_9\,[DshFzVangPk]_{i,j} \\ &\quad + \mu_5\,\frac{([VangPk]_{i,j+1} + [VangPk]_{i,j-1} - 2[VangPk]_{i,j})}{\Delta x^2},\end{aligned}$$

$$\begin{aligned}\frac{\mathrm{d}[FzVang]_{i,j}}{\mathrm{d}t} &= R_2\,[Vang]_{i,j}\,[Fz]^+_{i,j} - \lambda_2\,[FzVang]_{i,j} - R_5\,[FzVang]_{i,j}\,[Dsh]^+_{i,j} \\ &\quad + \lambda_5 B^+_{i,j}\,[DshFzVang]_{i,j} - R_7\,[Pk]_{i,j}\,[FzVang]_{i,j} + \lambda_7\,[FzVangPk]_{i,j},\end{aligned}$$

$$\begin{aligned}\frac{\mathrm{d}[DshFzVang]_{i,j}}{\mathrm{d}t} &= R_4\,[Vang]_{i,j}\,[DshFz]^+_{i,j} - \lambda_4\,[DshFzVang]_{i,j} + R_5\,[FzVang]_{i,j}\,[Dsh]^+_{i,j} \\ &\quad - \lambda_5 B^+_{i,j}\,[DshFzVang]_{i,j} - R_{10}\,[Pk]_{i,j}\,[DshFzVang]_{i,j} \\ &\quad + \lambda_{10}\,[DshFzVangPk]_{i,j},\end{aligned}$$

$$\begin{aligned}\frac{\mathrm{d}[FzVangPk]_{i,j}}{\mathrm{d}t} &= R_6\,[VangPk]_{i,j}\,[Fz]^+_{i,j} - \lambda_6\,[FzVangPk]_{i,j} + R_7\,[Pk]_{i,j}\,[FzVang]_{i,j} \\ &\quad - \lambda_7\,[FzVangPk]_{i,j} - R_8\,[FzVangPk]_{i,j}\,[Dsh]^+_{i,j} \\ &\quad + \lambda_8 B^+_{i,j}\,[DshFzVangPk]_{i,j},\end{aligned}$$

$$\begin{aligned}\frac{\mathrm{d}[DshFzVangPk]_{i,j}}{\mathrm{d}t} &= R_8\,[FzVangPk]_{i,j}\,[Dsh]^+_{i,j} - \lambda_8 B^+_{i,j}\,[DshFzVangPk]_{i,j} \\ &\quad + R_9\,[DshFz]^+_{i,j}\,[VangPk]_{i,j} - \lambda_9\,[DshFzVangPk]_{i,j} \\ &\quad + R_{10}\,[Pk]_{i,j}\,[DshFzVang]_{i,j} - \lambda_{10}\,[DshFzVangPk]_{i,j}.\end{aligned}$$

B.3 Full two-dimensional system

As a last step we consider the full system of PDEs for a hexagonal cell, which we get by applying the law of mass action to reactions (4.1)-(4.10). Different to the previous sections we now assume a continuous distribution of the protein and protein complex concentrations in the regions were they diffuse. For Dsh and Pk this region is the whole cell. Fz, Vang, DshFz and VangPk are restricted to the membrane and therefore the Laplacian in the corresponding equations is only applied in the membrane, indicated by the subscript

M. The cell bridging complexes FzVang, DshFzVang, FzVangPk and DshFzVangPk do not leave the edge of the membrane that is common to the two cells they connect. Hence, the Laplacian in the corresponding PDEs is only applied in this regime, indicated by the subscript S. We omit the persistent global bias. The superscript + indicates that the reactants are in different cells. The resulting cell bridging complex is counted in the same cell as its Vang part. The diffusion coefficients are given by μ_k for $k = 1, \ldots, 10$. The square brackets indicate protein and protein complex concentrations. For the feedback we introduce the scaling factor B by

$$\begin{aligned} B = 1 + K_b(K_{pk}[Pk] + [VangPk] + [FzVangPk] + [DshFzVangPk] \\ + K_{va}([Vang] + [FzVang] + [DshFzVang]))^{K_p}. \end{aligned}$$

Hence the full system of PDEs is given by

$$\begin{aligned} \frac{\partial\,[Dsh]}{\partial t} = &-R_1\,[Dsh][Fz] + \lambda_1 B\,[DshFz] - R_5\,[Dsh][FzVang]^+ \\ &+ \lambda_5 B\,[DshFzVang]^+ - R_8\,[Dsh][FzVangPk]^+ \\ &+ \lambda_8 B\,[DshFzVangPk]^+ + \mu_1\,\nabla^2[Dsh], \end{aligned}$$

$$\begin{aligned} \frac{\partial\,[Pk]}{\partial t} = &-R_3\,[Vang][Pk] + \lambda_3\,[VangPk] - R_7\,[FzVang][Pk] + \lambda_7\,[FzVangPk] \\ &- R_{10}\,[DshFzVang][Pk] + \lambda_{10}\,[DshFzVangPk] + \mu_2\,\nabla^2[Pk], \end{aligned}$$

$$\begin{aligned} \frac{\partial\,[Fz]}{\partial t} = &-R_1\,[Dsh][Fz] + \lambda_1 B\,[DshFz] - R_2\,[Fz][Vang]^+ + \lambda_2\,[FzVang]^+ \\ &- R_6\,[Fz][VangPk]^+ + \lambda_6\,[FzVangPk]^+ + \mu_3\,\nabla_M^2[Fz], \end{aligned}$$

$$\begin{aligned} \frac{\partial\,[Vang]}{\partial t} = &-R_2\,[Fz]^+\,[Vang] + \lambda_2\,[FzVang] - R_3\,[Vang][Pk] + \lambda_3\,[VangPk] \\ &- R_4\,[DshFz]^+\,[Vang] + \lambda_4\,[DshFzVang] + \mu_4\,\nabla_M^2[Vang], \end{aligned}$$

$$\begin{aligned} \frac{\partial\,[DshFz]}{\partial t} = &\;R_1\,[Dsh][Fz] - \lambda_1 B\,[DshFz] - R_4\,[DshFz][Vang]^+ \\ &+ \lambda_4\,[DshFzVang]^+ - R_9\,[DshFz][VangPk]^+ \\ &+ \lambda_9\,[DshFzVangPk]^+ + \mu_5\,\nabla_M^2[DshFz], \end{aligned}$$

$$\begin{aligned} \frac{\partial\,[VangPk]}{\partial t} = &\;R_3\,[Vang][Pk] - \lambda_3\,[VangPk] - R_6\,[Fz]^+\,[VangPk] + \lambda_6\,[FzVangPk] \\ &- R_9\,[DshFz]^+\,[VangPk] + \lambda_9\,[DshFzVangPk] + \mu_6\,\nabla_M^2[VangPk], \end{aligned}$$

$$\frac{\partial\,[FzVang]}{\partial t} = R_2\,[Fz]^+\,[Vang] - \lambda_2\,[FzVang] - R_5\,[Dsh]^+\,[FzVang] + \lambda_5 B^+\,[DshFzVang] - R_7\,[FzVang][Pk] + \lambda_7\,[FzVangPk] + \mu_7\,\nabla_S^2[FzVang],$$

$$\frac{\partial\,[DshFzVang]}{\partial t} = R_4\,[DshFz]^+\,[Vang] - \lambda_4\,[DshFzVang] + R_5\,[Dsh]^+\,[FzVang] - \lambda_5 B^+\,[DshFzVang] - R_{10}\,[DshFzVang][Pk] + \lambda_{10}\,[DshFzVangPk] + \mu_8\,\nabla_S^2[DshFzVang],$$

$$\frac{\partial\,[FzVangPk]}{\partial t} = R_6\,[Fz]^+\,[VangPk] - \lambda_6\,[FzVangPk] + R_7\,[FzVang][Pk] - \lambda_7\,[FzVangPk] - R_8\,[Dsh]^+\,[FzVangPk] + \lambda_8 B^+\,[DshFzVangPk] + \mu_9\,\nabla_S^2[FzVangPk],$$

$$\frac{\partial\,[DshFzVangPk]}{\partial t} = R_8\,[Dsh]^+\,[FzVangPk] - \lambda_8 B^+\,[DshFzVangPk] + R_9\,[DshFz]^+\,[VangPk] - \lambda_9\,[DshFzVangPk] + R_{10}\,[DshFzVang][Pk] - \lambda_{10}\;\,[DshFzVangPk] + \mu_{10}\nabla_S^2[DshFzVangPk].$$

Appendix C

Systems of equations for the model by Le Garrec et al.

We present the systems of equations used for the analysis of the approach by Le Garrec *et al.* [29], which we conduct in Chapter 5. The corresponding reactions are given by (5.1)-(5.8).

C.1 One-dimensional system

First we assume a row of cells in which every cell has a left and a right side. We get the system of ODEs by applying the law of mass action to (5.1)-(5.8). The superscripts l and r indicate the cell side, left and right, respectively. The subscript denotes the cell number. Diffusion is included in the equations by μ_k for $k = 1, \ldots, 9$ and Δx represents the intracellular distance between left and right side of a cell. To indicate that we are dealing with protein and protein complex concentrations we included square brackets. The inhibition scalings are given by

$$
\begin{aligned}
inh3_i^l &= \frac{1}{1 + A_3([Fz^*]_i^l + [Fz^*Fmi]_i^l + [Fz^*FmiFmiVang]_i^l + [Fz^*FmiFmiVangPk]_i^l)}, \\
inh3_i^r &= \frac{1}{1 + A_3([Fz^*]_i^r + [Fz^*Fmi]_i^r + [Fz^*FmiFmiVang]_i^r + [Fz^*FmiFmiVangPk]_i^r)}, \\
inh5_i^l &= \frac{1}{1 + A_5([Dsh^*FzFmiFmiVang]_i^l + [Dsh^*FzFmiFmiVangPk]_i^l)}, \\
inh5_i^r &= \frac{1}{1 + A_5([Dsh^*FzFmiFmiVang]_i^r + [Dsh^*FzFmiFmiVangPk]_i^r)}, \\
inh8_i^l &= \frac{1}{1 + A_8([Dsh^*FzFmiFmiVang]_i^l + [Dsh^*FzFmiFmiVangPk]_i^l)},
\end{aligned}
$$

$$inh8_i^r = \frac{1}{1 + A_8([Dsh^*FzFmiFmiVang]_i^r + [Dsh^*FzFmiFmiVangPk]_i^r)},$$

$$\begin{aligned}
en3_i^l &= 1 + B_3([Fz^*]_i^l + [Fz^*Fmi]_i^l + [Fz^*FmiFmiVang]_i^l + [Fz^*FmiFmiVangPk]_i^l),\\
en3_i^r &= 1 + B_3([Fz^*]_i^r + [Fz^*Fmi]_i^r + [Fz^*FmiFmiVang]_i^r + [Fz^*FmiFmiVangPk]_i^r),\\
en5_i^l &= 1 + B_5([Dsh^*FzFmiFmiVang]_i^l + [Dsh^*FzFmiFmiVangPk]_i^l),\\
en5_i^r &= 1 + B_5([Dsh^*FzFmiFmiVang]_i^r + [Dsh^*FzFmiFmiVangPk]_i^r),\\
en8_i^l &= 1 + B_8([Dsh^*FzFmiFmiVang]_i^l + [Dsh^*FzFmiFmiVangPk]_i^l),\\
en8_i^r &= 1 + B_8([Dsh^*FzFmiFmiVang]_i^r + [Dsh^*FzFmiFmiVangPk]_i^r).
\end{aligned}$$

This yields the following system of equations

$$\begin{aligned}
\frac{\mathrm{d}[Ld]_i^l}{\mathrm{d}t} &= -Kf_1\ [Fz]_i^l\ [Ld]_i^l + \mu_1\ \frac{([Ld]_i^r - [Ld]_i^l)}{\Delta x^2},\\
\frac{\mathrm{d}[Ld]_i^r}{\mathrm{d}t} &= -Kf_1\ [Fz]_i^r\ [Ld]_i^r + \mu_1\ \frac{([Ld]_i^l - [Ld]_i^r)}{\Delta x^2},
\end{aligned}$$

$$\begin{aligned}
\frac{\mathrm{d}[Fz]_i^l}{\mathrm{d}t} &= -Kf_1\ [Fz]_i^l\ [Ld]_i^l + \mu_2\ \frac{([Fz]_i^r - [Fz]_i^l)}{\Delta x^2},\\
\frac{\mathrm{d}[Fz]_i^r}{\mathrm{d}t} &= -Kf_1\ [Fz]_i^r\ [Ld]_i^r + \mu_2\ \frac{([Fz]_i^l - [Fz]_i^r)}{\Delta x^2},
\end{aligned}$$

$$\begin{aligned}
\frac{\mathrm{d}[Fz^*]_i^l}{\mathrm{d}t} &= -Kf_2\ [Fz^*]_i^l\ [Fmi]_i^l + Kd_2\ [Fz^*Fmi]_i^l + Kf_1\ [Fz]_i^l\ [ld]_i^l\\
&\quad + \mu_3\ \frac{([Fz^*]_i^r - [Fz^*]_i^l)}{\Delta x^2},\\
\frac{\mathrm{d}[Fz^*]_i^r}{\mathrm{d}t} &= -Kf_2\ [fz^*]_i^r\ [Fmi]_i^r + Kd_2\ [Fz^*Fmi]_i^r + Kf_1\ [Fz]_i^r\ [ld]_i^r\\
&\quad + \mu_3\ \frac{([Fz^*]_i^l - [Fz^*]_i^r)}{\Delta x^2},
\end{aligned}$$

$$\begin{aligned}
\frac{\mathrm{d}[Fmi]_i^l}{\mathrm{d}t} &= -Kf_2\ [Fz^*]_i^l\ [Fmi]_i^l + Kd_2\ [Fz^*Fmi]_i^l\\
&\quad - inh3_i^l Kf_3\ [Vang]_i^l\ [Fmi]_i^l + en3_i^l Kd_3\ [FmiVang]_i^l\\
&\quad + \mu_4\ \frac{([Fmi]_i^r - [Fmi]_i^l)}{\Delta x^2},
\end{aligned}$$

$$\begin{aligned}\frac{\mathrm{d}[Fmi]_i^r}{\mathrm{d}t} = &-Kf_2\ [Fz^*]_i^r\ [Fmi]_i^r + Kd_2\ [Fz^*Fmi]_i^r \\ &- inh3_i^r Kf_3\ [Vang]_i^r\ [Fmi]_i^r + en3_i^r Kd_3\ [FmiVang]_i^r \\ &+ \mu_4\ \frac{([Fmi]_i^l - [Fmi]_i^r)}{\Delta x^2},\end{aligned}$$

$$\begin{aligned}\frac{\mathrm{d}[Vang]_i^l}{\mathrm{d}t} = &-inh3_i^l Kf_3\ [Vang]_i^l\ [Fmi]_i^l + en3_i^l Kd_3\ [FmiVang]_i^l \\ &+ \mu_5\ \frac{([Vang]_i^r - [Vang]_i^l)}{\Delta x^2},\end{aligned}$$

$$\begin{aligned}\frac{\mathrm{d}[Vang]_i^r}{\mathrm{d}t} = &-inh3_i^r Kf_3\ [Vang]_i^r\ [Fmi]_i^r + en3_i^r Kd_3\ [FmiVang]_i^r \\ &+ \mu_5\ \frac{([Vang]_i^l - [Vang]_i^r)}{\Delta x^2},\end{aligned}$$

$$\begin{aligned}\frac{\mathrm{d}[Dsh]_i^l}{\mathrm{d}t} = &-Kf_6\ [Dsh]_i^l\ [Fz^*FmiFmiVang]_i^l \\ &+ Kd_6\ [Dsh^*FzFmiFmiVang]_i^l \\ &- Kf_7\ [Dsh]_i^l\ [Fz^*FmiFmiVangPk]_i^l \\ &+ Kd_7\ [Dsh^*FzFmiFmiVangPk]_i^l + \mu_6\ \frac{([Dsh]_i^r - [Dsh]_i^l)}{\Delta x^2},\end{aligned}$$

$$\begin{aligned}\frac{\mathrm{d}[Dsh]_i^r}{\mathrm{d}t} = &-Kf_6\ [Dsh]_i^r\ [Fz^*FmiFmiVang]_i^r \\ &+ Kd_6\ [Dsh^*FzFmiFmiVang]_i^r \\ &- Kf_7\ [Dsh]_i^r\ [Fz^*FmiFmiVangPk]_i^r \\ &+ Kd_7\ [Dsh^*FzFmiFmiVangPk]_i^r + \mu_6\ \frac{([Dsh]_i^l - [Dsh]_i^r)}{\Delta x^2},\end{aligned}$$

$$\begin{aligned}\frac{\mathrm{d}[Pk]_i^l}{\mathrm{d}t} = &-inh5_i^l Kf_5\ [Fz^*FmiFmiVang]_{i-1}^r\ [Pk]_i^l \\ &+ en5_i^l Kd_5\ [Fz^*FmiFmiVangPk]_{i-1}^r \\ &- inh8_i^l Kf_8\ [Dsh^*FzFmiFmiVang]_{i-1}^r\ [Pk]_i^l \\ &+ en8_i^l Kd_8\ [Dsh^*FzFmiFmiVangPk]_{i-1}^r \\ &+ \mu_7\ \frac{([Pk]_i^r - [Pk]_i^l)}{\Delta x^2},\end{aligned}$$

$$\begin{aligned}\frac{\mathrm{d}[Pk]_i^r}{\mathrm{d}t} = &-inh5_i^r Kf_5\ [Fz^*FmiFmiVang]_{i+1}^l\ [Pk]_i^r \\ &+ en5_i^r Kd_5\ [Fz^*FmiFmiVangPk]_{i+1}^l \\ &- inh8_i^r Kf_8\ [Dsh^*FzFmiFmiVang]_{i+1}^l\ [Pk]_i^r \\ &+ en8_i^r Kd_8\ [Dsh^*FzFmiFmiVangPk]_{i+1}^l \\ &+ \mu_7\ \frac{([Pk]_i^l - [Pk]_i^r)}{\Delta x^2},\end{aligned}$$

$$\begin{aligned}\frac{\mathrm{d}[Fz^*Fmi]_i^l}{\mathrm{d}t} = &\ Kf_2\ [Fz^*]_i^l\ [Fmi]_i^l - Kd_2\ [Fz^*Fmi]_i^l \\ &- Kf_4\ [Fz^*Fmi]_i^l\ [FmiVang]_{i-1}^r + Kd_4\ [Fz^*FmiFmiVang]_i^l \\ &+ \mu_8\ \frac{([Fz^*Fmi]_i^r - [Fz^*Fmi]_i^l)}{\Delta x^2},\end{aligned}$$

$$\begin{aligned}\frac{\mathrm{d}[Fz^*Fmi]_i^r}{\mathrm{d}t} = &\ Kf_2\ [Fz^*]_i^r\ [Fmi]_i^r - Kd_2\ [Fz^*Fmi]_i^r \\ &- Kf_4\ [Fz^*Fmi]_i^r\ [FmiVang]_{i+1}^l + Kd_4\ [Fz^*FmiFmiVang]_i^r \\ &+ \mu_8\ \frac{([Fz^*Fmi]_i^l - [Fz^*Fmi]_i^r)}{\Delta x^2},\end{aligned}$$

$$\begin{aligned}\frac{\mathrm{d}[FmiVang]_i^l}{\mathrm{d}t} = &\ inh3_i^l Kf_3\ [Vang]_i^l\ [Fmi]_i^l - en3_i^l Kd_3\ [FmiVang]_i^l \\ &- Kf_4\ [Fz^*Fmi]_{i-1}^r\ [FmiVang]_i^l + Kd_4\ [Fz^*FmiFmiVang]_{i-1}^r \\ &+ \mu_9\ \frac{([FmiVang]_i^r - [FmiVang]_i^l)}{\Delta x^2},\end{aligned}$$

$$\begin{aligned}\frac{\mathrm{d}[FmiVang]_i^r}{\mathrm{d}t} = &\ inh3_i^r Kf_3\ [Vang]_i^r\ [Fmi]_i^r - en3_i^r Kd_3\ [FmiVang]_i^r \\ &- Kf_4\ [Fz^*Fmi]_{i+1}^l\ [FmiVang]_i^r + Kd_4\ [Fz^*FmiFmiVang]_{i+1}^l \\ &+ \mu_9\ \frac{([FmiVang]_i^l - [FmiVang]_i^r)}{\Delta x^2},\end{aligned}$$

$$\begin{aligned}\frac{\mathrm{d}[Fz^*FmiFmiVang]_i^l}{\mathrm{d}t} = &\ Kf_4\ [Fz^*Fmi]_i^l\ [FmiVang]_{i-1}^r - Kd_4\ [Fz^*FmiFmiVang]_i^l \\ &- inh5_{i-1}^r Kf_5\ [Fz^*FmiFmiVang]_i^l\ [Pk]_{i-1}^r \\ &+ en5_{i-1}^r Kd_5\ [Fz^*FmiFmiVangPk]_i^l \\ &- Kf_6\ [Dsh]_i^l\ [Fz^*FmiFmiVang]_i^l \\ &+ Kd_6\ [Dsh^*FzFmiFmiVang]_i^l,\end{aligned}$$

$$\begin{aligned}\frac{\mathrm{d}[Fz^*FmiFmiVang]_i^r}{\mathrm{d}t} &= Kf_4\ [Fz^*Fmi]_i^r\ [FmiVang]_{i+1}^l - Kd_4\ [Fz^*FmiFmiVang]_i^r \\ &\quad - inh5_{i+1}^l Kf_5\ [Fz^*FmiFmiVang]_i^r\ [Pk]_{i+1}^l \\ &\quad + en5_{i+1}^l Kd_5\ [Fz^*FmiFmiVangPk]_i^r \\ &\quad - Kf_6\ [Dsh]_i^r\ [Fz^*FmiFmiVang]_i^r \\ &\quad + Kd_6\ [Dsh^*FzFmiFmiVang]_i^r,\end{aligned}$$

$$\begin{aligned}\frac{\mathrm{d}[Dsh^*FzFmiFmiVang]_i^l}{\mathrm{d}t} &= Kf_6\ [Dsh]_i^l\ [Fz^*FmiFmiVang]_i^l - Kd_6\ [Dsh^*FzFmiFmiVang]_i^l \\ &\quad - inh8_{i-1}^r Kf_8\ [Dsh^*FzFmiFmiVang]_i^l\ [Pk]_{i-1}^r \\ &\quad + en8_{i-1}^r Kd_8\ [Dsh^*FzFmiFmiVangPk]_i^l,\end{aligned}$$

$$\begin{aligned}\frac{\mathrm{d}[Dsh^*FzFmiFmiVang]_i^r}{\mathrm{d}t} &= Kf_6\ [Dsh]_i^r\ [Fz^*FmiFmiVang]_i^r - Kd_6\ [Dsh^*FzFmiFmiVang]_i^r \\ &\quad - inh8_{i+1}^l Kf_8\ [Dsh^*FzFmiFmiVang]_i^r\ [Pk]_{i+1}^l \\ &\quad + en8_{i+1}^l Kd_8\ [Dsh^*FzFmiFmiVangPk]_i^r,\end{aligned}$$

$$\begin{aligned}\frac{\mathrm{d}[Fz^*FmiFmiVangPk]_i^l}{\mathrm{d}t} &= inh5_{i-1}^r Kf_5\ [Fz^*FmiFmiVang]_i^l\ [Pk]_{i-1}^r \\ &\quad - en5_{i-1}^r Kd_5\ [Fz^*FmiFmiVangPk]_i^l \\ &\quad - Kf_7\ [Dsh]_i^l\ [Fz^*FmiFmiVangPk]_i^l \\ &\quad + Kd_7\ [Dsh^*FzFmiFmiVangPk]_i^l,\end{aligned}$$

$$\begin{aligned}\frac{\mathrm{d}[Fz^*FmiFmiVangPk]_i^r}{\mathrm{d}t} &= inh5_{i+1}^l Kf_5\ [Fz^*FmiFmiVang]_i^r\ [Pk]_{i+1}^l \\ &\quad - en5_{i+1}^l Kd_5\ [Fz^*FmiFmiVangPk]_i^r \\ &\quad - Kf_7\ [Dsh]_i^r\ [Fz^*FmiFmiVangPk]_i^r \\ &\quad + Kd_7\ [Dsh^*FzFmiFmiVangPk]_i^r,\end{aligned}$$

$$\begin{aligned}\frac{\mathrm{d}[Dsh^*FzFmiFmiVangPk]_i^l}{\mathrm{d}t} &= Kf_7\ [Dsh]_i^l\ [Fz^*FmiFmiVangPk]_i^l \\ &\quad - Kd_7\ [Dsh^*FzFmiFmiVangPk]_i^l \\ &\quad + inh8_{i-1}^r Kf_8\ [Dsh^*FzFmiFmiVang]_i^l\ [Pk]_{i-1}^r \\ &\quad - en8_{i-1}^r Kd_8\ [Dsh^*FzFmiFmiVangPk]_i^l,\end{aligned}$$

$$\begin{aligned}\frac{\mathrm{d}[Dsh^*FzFmiFmiVangPk]_i^r}{\mathrm{d}t} &= Kf_7\ [Dsh]_i^r\ [Fz^*FmiFmiVangPk]_i^r \\ &\quad - Kd_7\ [Dsh^*FzFmiFmiVangPk]_i^r \\ &\quad + inh8_{i+1}^l Kf_8\ [Dsh^*FzFmiFmiVang]_i^r\ [Pk]_{i+1}^l \\ &\quad - en8_{i+1}^l Kd_8\ [Dsh^*FzFmiFmiVangPk]_i^r.\end{aligned}$$

C.2 Two-dimensional system for compartmentalised cells

Now, we consider a field of hexagonal cells with 6 compartments each. Applying the law of mass action to (5.1)-(5.8) we get the ODEs for the change of the protein concentrations in compartment $j(\mathrm{mod}\ 6)$ of cell i. The distance between two neighbouring compartments within a cell is given by Δx, while μ_k for $k = 1, \ldots, 9$ represent diffusion. Binding over the cell membrane is indicated by the superscript +. Cell bridging complexes are counted in th same cell as their Fz part. The square brackets are included to indicate concentrations of the proteins and protein complexes. The inhibition scalings are given by

$$\begin{aligned}inh3_{i,j} &= \frac{1}{1 + A_3([Fz^*]_{i,j} + [Fz^*Fmi]_{i,j} + [Fz^*FmiFmiVang]_{i,j} + [Fz^*FmiFmiVangPk]_{i,j})}, \\ inh5_{i,j} &= \frac{1}{1 + A_5([Dsh^*FzFmiFmiVang]_{i,j} + [Dsh^*FzFmiFmiVangPk]_{i,j})}, \\ inh8_{i,j} &= \frac{1}{1 + A_8([Dsh^*FzFmiFmiVang]_{i,j} + [Dsh^*FzFmiFmiVangPk]_{i,j})},\end{aligned}$$

$$\begin{aligned}en3_{i,j} &= 1 + B_3([Fz^*]_{i,j} + [Fz^*Fmi]_{i,j} + [Fz^*FmiFmiVang]_{i,j} + [Fz^*FmiFmiVangPk]_{i,j}), \\ en5_{i,j} &= 1 + B_5([Dsh^*FzFmiFmiVang]_{i,j} + [Dsh^*FzFmiFmiVangPk]_{i,j}), \\ en8_{i,j} &= 1 + B_8([Dsh^*FzFmiFmiVang]_{i,j} + [Dsh^*FzFmiFmiVangPk]_{i,j}).\end{aligned}$$

Hence, we get the following system of equations

$$\frac{\mathrm{d}[Ld]_{i,j}}{\mathrm{d}t} = -Kf_1[Fz]_{i,j}[Ld]_{i,j} + \mu_1\ \frac{([Ld]_{i,j+1} + [Ld]_{i,j-1} - 2[ld]_{i,j})}{\Delta x^2},$$

$$\frac{\mathrm{d}[Fz]_{i,j}}{\mathrm{d}t} = -Kf_1[Fz]_{i,j}[Ld]_{i,j} + \mu_2\ \frac{([Fz]_{i,j+1} + [Fz]_{i,j-1} - 2[Fz]_{i,j})}{\Delta x^2},$$

$$\begin{aligned}\frac{\mathrm{d}[Fz^*]_{i,j}}{\mathrm{d}t} &= -Kf_2[Fz^*]_{i,j}[Fmi]_{i,j} + Kd_2[Fz^*Fmi]_{i,j} + Kf_1[Fz]_{i,j}[ld]_{i,j} \\ &\quad + \mu_3\ \frac{([Fz^*]_{i,j+1} + [Fz^*]_{i,j-1} - 2[Fz^*]_{i,j})}{\Delta x^2},\end{aligned}$$

$$\begin{aligned}\frac{\mathrm{d}[Fmi]_{i,j}}{\mathrm{d}t} &= -Kf_2[Fz^*]_{i,j}[Fmi]_{i,j} + Kd_2[Fz^*Fmi]_{i,j} \\ &\quad - inh3_{i,j}Kf_3[Vang]_{i,j}[Fmi]_{i,j} + en3_{i,j}Kd_3[FmiVang]_{i,j} \\ &\quad + \mu_4 \frac{([Fmi]_{i,j+1} + [Fmi]_{i,j-1} - 2[Fmi]_{i,j})}{\Delta x^2},\end{aligned}$$

$$\begin{aligned}\frac{\mathrm{d}[Vang]_{i,j}}{\mathrm{d}t} &= -inh3_{i,j}Kf_3[Vang]_{i,j}[Fmi]_{i,j} + en3_{i,j}Kd_3[FmiVang]_{i,j} \\ &\quad + \mu_5 \frac{([Vang]_{i,j+1} + [Vang]_{i,j-1} - 2[Vang]_{i,j})}{\Delta x^2},\end{aligned}$$

$$\begin{aligned}\frac{\mathrm{d}[Dsh]_{i,j}}{\mathrm{d}t} &= -Kf_6[Dsh]_{i,j}[Fz^*FmiFmiVang]_{i,j} + Kd_6[Dsh^*FzFmiFmiva]_{i,j} \\ &\quad - Kf_7[Dsh]_{i,j}[Fz^*FmiFmiVangPk]_{i,j} \\ &\quad + Kd_7[Dsh^*FzFmiFmiVangPk]_{i,j} \\ &\quad + \mu_6 \frac{([Dsh]_{i,j+1} + [Dsh]_{i,j-1} - 2[Dsh]_{i,j})}{\Delta x^2},\end{aligned}$$

$$\begin{aligned}\frac{\mathrm{d}[Pk]_{i,j}}{\mathrm{d}t} &= -inh5_{i,j}Kf_5[Fz^*FmiFmiVang]^+_{i,j}\,[Pk]_{i,j} \\ &\quad + en5_{i,j}Kd_5[Fz^*FmiFmiVangPk]^+_{i,j} \\ &\quad - inh8_{i,j}Kf_8[Dsh^*FzFmiFmiVang]^+_{i,j}\,[Pk]_{i,j} \\ &\quad + en8_{i,j}Kd_8[Dsh^*FzFmiFmiVangPk]^+_{i,j} \\ &\quad + \mu_7 \frac{([Pk]_{i,j+1} + [Pk]_{i,j-1} - 2[Pk]_{i,j})}{\Delta x^2},\end{aligned}$$

$$\begin{aligned}\frac{\mathrm{d}[Fz^*Fmi]_{i,j}}{\mathrm{d}t} &= Kf_2[Fz^*]_{i,j}[Fmi]_{i,j} - Kd_2[Fz^*Fmi]_{i,j} \\ &\quad - Kf_4[Fz^*Fmi]_{i,j}[FmiVang]^+_{i,j} + Kd_4[Fz^*FmiFmiVang]_{i,j} \\ &\quad + \mu_8 \frac{([Fz^*Fmi]_{i,j+1} + [Fz^*Fmi]_{i,j-1} - 2[Fz^*Fmi]_{i,j})}{\Delta x^2},\end{aligned}$$

$$\begin{aligned}\frac{\mathrm{d}[FmiVang]_{i,j}}{\mathrm{d}t} &= inh3_{i,j}Kf_3[Vang]_{i,j}[Fmi]_{i,j} - en3_{i,j}Kd_3[FmiVang]_{i,j} \\ &\quad - Kf_4[Fz^*Fmi]^+_{i,j}\,[FmiVang]_{i,j} \\ &\quad + Kd_4[Fz^*FmiFmiVang]^+_{i,j} \\ &\quad + \mu_9 \frac{([FmiVang]_{i,j+1} + [FmiVang]_{i,j-1} - 2[FmiVang]_{i,j})}{\Delta x^2},\end{aligned}$$

$$\begin{aligned}\frac{\mathrm{d}[Fz^*FmiFmiVang]_{i,j}}{\mathrm{d}t} &= Kf_4[Fz^*Fmi]_{i,j}[FmiVang]^+_{i,j} - Kd_4[Fz^*FmiFmiVang]_{i,j}\\ &\quad - inh5^+_{i,j}Kf_5[Fz^*FmiFmiVang]_{i,j}[Pk]^+_{i,j}\\ &\quad + en5^+_{i,j}Kd_5[Fz^*FmiFmiVangPk]_{i,j}\\ &\quad - Kf_6[Dsh]_{i,j}[Fz^*FmiFmiVang]_{i,j}\\ &\quad + Kd_6[Dsh^*FzFmiFmiVang]_{i,j},\end{aligned}$$

$$\begin{aligned}\frac{\mathrm{d}[Dsh^*FzFmiFmiVang]_{i,j}}{\mathrm{d}t} &= Kf_6[Dsh]_{i,j}[Fz^*FmiFmiVang]_{i,j}\\ &\quad - Kd_6[Dsh^*FzFmiFmiVang]_{i,j}\\ &\quad - inh8^+_{i,j}Kf_8[Dsh^*FzFmiFmiVang]_{i,j}[Pk]^+_{i,j}\\ &\quad + en8^+_{i,j}Kd_8[Dsh^*FzFmiFmiVangPk]_{i,j},\end{aligned}$$

$$\begin{aligned}\frac{\mathrm{d}[Fz^*FmiFmiVangPk]_{i,j}}{\mathrm{d}t} &= inh5^+_{i,j}Kf_5[Fz^*FmiFmiVang]_{i,j}[Pk]^+_{i,j}\\ &\quad - en5^+_{i,j}Kd_5[Fz^*FmiFmiVangPk]_{i,j}\\ &\quad - Kf_7[Dsh]_{i,j}[Fz^*FmiFmiVangPk]_{i,j}\\ &\quad + Kd_7[Dsh^*FzFmiFmiVangPk]_{i,j},\end{aligned}$$

$$\begin{aligned}\frac{\mathrm{d}[Dsh^*FzFmiFmiVangPk]_{i,j}}{\mathrm{d}t} &= Kf_7[Dsh]_{i,j}[Fz^*FmiFmiVangPk]_{i,j}\\ &\quad - Kd_7[Dsh^*FzFmiFmiVangPk]_{i,j}\\ &\quad + inh8^+_{i,j}Kf_8[Dsh^*FzFmiFmiVang]_{i,j}[Pk]^+_{i,j}\\ &\quad - en8^+_{i,j}Kd_8[Dsh^*FzFmiFmiVangPk]_{i,j}.\end{aligned}$$

C.3 Full two-dimensional system

As a last step we consider the full system of PDEs for a hexagonal cell, which we get by applying the law of mass action to (5.1)-(5.8). All the proteins and protein complexes are restricted to the membrane. Different to the previous sections we now assume their concentrations are distributed continuously. Cell bridging complexes do not diffuse. The remaining proteins and protein complexes diffuse in the whole membrane and therefore the Laplacian in the corresponding PDEs is only applied in this regime. The diffusion coefficients are μ_k with $k = 1, \ldots, 9$. The superscript + indicates binding over the cell

membrane. The resulting cell bridging complexes are counted in the same cell as their Fz part. The square brackets indicate that we are dealing with concentrations. The inhibition parameters are given by

$$inh3 = \frac{1}{1 + A_3([Fz^*] + [Fz^*Fmi] + [Fz^*FmiFmiVang] + [Fz^*FmiFmiVangPk])},$$
$$inh5 = \frac{1}{1 + A_5([Dsh^*FzFmiFmiVang] + [Dsh^*FzFmiFmiVangPk])},$$
$$inh8 = \frac{1}{1 + A_8([Dsh^*FzFmiFmiVang] + [Dsh^*FzFmiFmiVangPk])},$$

$$en3 = 1 + B_3([Fz^*] + [Fz^*Fmi] + [Fz^*FmiFmiVang] + [Fz^*FmiFmiVangPk]),$$
$$en5 = 1 + B_5([Dsh^*FzFmiFmiVang] + [Dsh^*FzFmiFmiVangPk]),$$
$$en8 = 1 + B_8([Dsh^*FzFmiFmiVang] + [Dsh^*FzFmiFmiVangPk]).$$

Therefore, we get the following system of equations

$$\frac{\partial [Ld]}{\partial t} = -Kf_1[Fz][Ld] + \mu_1 \nabla^2 [Ld],$$

$$\frac{\partial [Fz]}{\partial t} = -Kf_1[Fz][Ld] + \mu_2 \nabla^2 [Fz],$$

$$\frac{\partial [Fz^*]}{\partial t} = -Kf_2[Fz^*][Fmi] + Kd_2[Fz^*Fmi] + Kf_1[Fz][ld] + \mu_3 \nabla^2 [Fz^*],$$

$$\begin{aligned}\frac{\partial [Fmi]}{\partial t} = &-Kf_2[Fz^*][Fmi] + Kd_2[Fz^*Fmi] - inh3\ Kf_3[Vang][Fmi] \\ &+ en3\ Kd_3[FmiVang] + \mu_4 \nabla^2 [Fmi],\end{aligned}$$

$$\frac{\partial [Vang]}{\partial t} = -inh3\ Kf_3[Vang][Fmi] + en3\ Kd_3[FmiVang] + \mu_5 \nabla^2 [Vang],$$

$$\begin{aligned}\frac{\partial [Dsh]}{\partial t} = &-Kf_6[Dsh][Fz^*FmiFmiVang] + Kd_6[Dsh^*FzFmiFmiVang] \\ &- Kf_7[Dsh][Fz^*FmiFmiVangPk] \\ &+ Kd_7[Dsh^*FzFmiFmiVangPk] + \mu_6 \nabla^2 [Dsh],\end{aligned}$$

$$\begin{aligned}\frac{\partial\,[Pk]}{\partial t} &= -inh5\ Kf_5[Fz^*FmiFmiVang]^+\ [Pk]\\ &\quad + en5\ Kd_5[Fz^*FmiFmiVangPk]^+\\ &\quad - inh8\ Kf_8[Dsh^*FzFmiFmiVang]^+\ [Pk]\\ &\quad + en8\ Kd_8[Dsh^*FzFmiFmiVangPk]^+ + \mu_7\nabla^2[Pk],\end{aligned}$$

$$\begin{aligned}\frac{\partial\,[Fz^*Fmi]}{\partial t} &= Kf_2[Fz^*][Fmi] - Kd_2[Fz^*Fmi] - Kf_4[Fz^*Fmi][FmiVang]^+\\ &\quad + Kd_4[Fz^*FmiFmiVang] + \mu_8\nabla^2[Fz^*Fmi],\end{aligned}$$

$$\begin{aligned}\frac{\partial\,[FmiVang]}{\partial t} &= inh3\ Kf_3[Vang][Fmi] - en3\ Kd_3[FmiVang]\\ &\quad - Kf_4[Fz^*Fmi]^+\ [FmiVang]\\ &\quad + Kd_4[Fz^*FmiFmiVang]^+ + \mu_9\nabla^2[FmiVang],\end{aligned}$$

$$\begin{aligned}\frac{\partial\,[Fz^*FmiFmiVang]}{\partial t} &= Kf_4[Fz^*Fmi][FmiVang]^+ - Kd_4[Fz^*FmiFmiVang]\\ &\quad - inh5^+\ Kf_5[Fz^*FmiFmiVang][Pk]^+\\ &\quad + en5^+\ Kd_5[Fz^*FmiFmiVangPk]\\ &\quad - Kf_6[Dsh][Fz^*FmiFmiVang] + Kd_6[Dsh^*FzFmiFmiVang],\end{aligned}$$

$$\begin{aligned}\frac{\partial\,[Dsh^*FzFmiFmiVang]}{\partial t} &= Kf_6[Dsh][Fz^*FmiFmiVang] - Kd_6[Dsh^*FzFmiFmiVang]\\ &\quad - inh8^+\ Kf_8[Dsh^*FzFmiFmiVang][Pk]^+\\ &\quad + en8^+\ Kd_8[Dsh^*FzFmiFmiVangPk],\end{aligned}$$

$$\begin{aligned}\frac{\partial\,[Fz^*FmiFmiVangPk]}{\partial t} &= inh5^+\ Kf_5[Fz^*FmiFmiVang][Pk]^+\\ &\quad - en5^+\ Kd_5[Fz^*FmiFmiVangPk]\\ &\quad - Kf_7[Dsh][Fz^*FmiFmiVangPk]\\ &\quad + Kd_7[Dsh^*FzFmiFmiVangPk],\end{aligned}$$

$$\frac{\partial\,[Dsh^{*}FzFmiFmiVangPk]}{\partial t} = Kf_7[Dsh][Fz^{*}FmiFmiVangPk] - Kd_7[Dsh^{*}FzFmiFmiVangPk] + inh8^{+}\ Kf_8[Dsh^{*}FzFmiFmiVang][Pk]^{+} - en8^{+}\ Kd_8[Dsh^{*}FzFmiFmiVangPk].$$

References

[1] P. N. Adler, R. E. Krasnow, and J. Liu. Tissue polarity points from cells that have higher Frizzled levels towards cells that have lower Frizzled levels. *Curr. Biol.*, 7:940–949, 1997.

[2] J. Alberty, C. Carstensen, and S. A. Funken. Remarks around 50 lines of matlab: short finite element implementation. *Numerical Algorithms*, 20:117–137, 1999.

[3] K. Amonlirdviman, N. A. Khare, D. R. P. Tree, W.-S. Chen, J. D. Axelrod, and C. J. Tomlin. Mathematical modeling of planar cell polarity to understand domineering nonautonomy. *Science*, 307:423–426, 2005.

[4] J. D. Axelrod. Progress and challenges in understanding planar cell polarity signaling. *Sem. Cell Dev. Biol.*, doi:10.1016/j.semcdb.2009.08.001, 2008.

[5] R. Bastock, H. Strutt, and D. Strutt. Strabismus is asymmetrically localised and binds to Prickle and Dishevelled during *Drosophila* planar polarity patterning. *Development*, 130:3007–3014, 2003.

[6] A. Belle, A. Tanay, L. Bitincka, R. Shamir, and E. O'Shea. Quantification of protein half-lives in the budding yeast proteome. *PNAS*, 103:13004–13009, 2006.

[7] J. Casal, P. A. Lawrence, and G. Struhl. Two separate molecular systems, Dachsous/Fat and Starry Night/Frizzled, act independently to confer planar cell polarity. *Development*, 133:4561–4572, 2006.

[8] J. Casal, G. Struhl, and P. A. Lawrence. Developmental compartments and planar polarity in *Drosophila*. *Curr. Biology*, 12:1189–1198, 2002.

[9] W.-S. Chen, D. Antic, M. Matis, C. Y. Logan, M. Povelones, G. A. Abderson, R. Nusse, and J. D. Axelrod. Asymmetric homotypic interactions of the atypical cadherin Flamingo mediate intercellular polarity signaling. *Cell*, 133:1093–1105, 2008.

[10] J. R. Collier, N. A. M. Monk, P. K. Maini, and J. H. Lewis. Pattern formation by lateral inhibition with feedback: A mathematical model of Delta-Notch intercellular signalling. *J. Theor. Biol.*, 183:429–446, 1996.

[11] C. E. Elmer and E. S. Van Vleck. Analysis and computation of travelling wave solutions of bistable differential-difference equations. *Nonlinearity*, 12:771–798, 1999.

[12] B. Ermentrout. *Simulating, Analyzing and Animating Dynamical Systems, A guide to XPPAUT for researchers and students*. SIAM, 2002.

[13] M. Gagliardi, E. Piddini, and J.-P. Vincent. Endocytosis: A positive or a negative influence on Wnt signalling? *Traffic*, 9:1–9, 2008.

[14] S. Ganguly, P. Singh, R. Manoharlal, R. Prasad, and A. Chattopadhyay. Differential dynamics of membrane proteins in yeast. *Bioch. and Bioph. Res. Com,*, 387:661–665, 2009.

[15] N. Guo, C. Hawkins, and J. Nathans. Frizzled6 controls hair patterning in mice. *Proc. Natl. Acad. Sci. USA*, 101:9277–9281, 2004.

[16] P. Houston. *Lecture Notes: Variational Methods*. 2007/2008.

[17] A. Jenny, J. Reynolds-Kenneally, G. Das, M. Burnett, and M. Mlodzik. Diego and Prickle regulate Frizzled planar cell polarity signalling by competing for Dishevelled binding. *Nature Cell Biol.*, 7:691–697, 2005.

[18] C. Johnson. *Numerical solutions of differential equations by the finite element method*. Cambridge University Press, 1987.

[19] T. Kacmarczyk and E. M. Craddock. Cell size is a factor in body size variation among Hawaiian and nonHawaiian species of *Drosophila*. *Dros. Inf. Serv.*, 83:144–148, 2000.

[20] J. P. Keener. Propagation and its failure in coupled systems of discrete excitable cells. *SIAM J. Appl. Math.*, 47:556–572, 1987.

[21] M. Kerszberg and J.-P. Changeaux. A simple molecular model of neurulation. *BioEssays*, 20:758–770, 1998.

[22] B. N. Kholodenko, J. B. Hoek, and H. V. Westerhoff. Why cytoplasmic signalling proteins should be recruited to cell membranes. *Cell Biology*, 10:173–178, 2000.

[23] T. J. Klein and M. Mlodzik. Planar cell polarization: An emerging model points in the right direction. *Ann. Rev. Cell Dev. Biol.*, 21:155–176, 2005.

[24] J. C. Lagarias, J. A. Reeds, M. H. Wright, and P. E. Wright. Convergence properties of the Nelder-Mead simplex algorithm in low dimensions. *SIAM J. Opt.*, 9:112–147, 1998.

[25] P. A. Lawrence. Gradients in the insect segment: the orientation of hairs in the milkweed bug *Oncopeltus fasciatus*. *J. Exp. Biol.*, 44:607–620, 1966.

[26] P. A. Lawrence, J. Casal, and G. Struhl. Cell interactions and planar polarity in the abdominal epidermis of *Drosophila*. *Development*, 131:4651–64, 2004.

[27] P. A. Lawrence, G. Struhl, and J. Casal. Planar cell polarity: one or two pathways? *Nature Reviews Genetics*, 8:555–563, 2007.

[28] J.-F. Le Garrec and M. Kerszberg. Modeling polarity buildup and cell fate decision in the fly eye: insight into the connection between the PCP and Notch pathways. *Dev. Genes Evol.*, 218:413–426, 2008.

[29] J.-F. Le Garrec, P. Lopez, and M. Kerszberg. Establishment and maintenance of planar epithelial cell polarity by asymmetric cadherin bridges: A computer model. *Dev. Dyn.*, 235:235–246, 2006.

[30] D. Ma, C.-h. Yang, H. McNeil, M. A. Simon, and J. D. Axelrod. Fidelity in planar cell polarity signalling. *Nature*, 421:543–547, 2003.

[31] H. Matakatsu and S. S. Blair. Interactions between Fat and Dachsous and the regulation of planar cell polarity in the *Drosophila* wing. *Development*, 131:3785–3794, 2004.

[32] J. D. Murray. *Mathematical Biology*. Springer-Verlag, 1989.

[33] J. A. Nelder and R. Mead. A simplex method for function minimization. *Comput. J.*, 7:308–313, 1965.

[34] M. R. Owen. Waves and propagation failure in discrete space models with nonlinear coupling and feedback. *Physica D*, 173:59–76, 2002.

[35] M. R. Owen, J. A. Sheratt, and H. J. Wearing. Lateral induction by juxtacrine signaling is a new mechanism for pattern formation. *Dev. Biol.*, 217:54–61, 2000.

[36] E. Plahte and L. Øyehaug. Pattern-generating travelling waves in a discrete multicellular system with lateral inhibition. *Physica D*, 226:117–128, 2007.

[37] R. L. Raffard, K. Amonlirdviman, J. D. Axelrod, and C. J. Tomlin. An adjoint-based parameter identification algorithm applied to planar cell polarity signaling. *IEEE Trans. Autom. Control*, 53 (Special Issue on Systems Biology):109–121, 2008.

[38] S. Schamberg, P. Houston, N. A. M. Monk, and M. R. Owen. Modelling and analysis of planar cell polarity. *submitted to Bull. of Math. Biol.*

[39] Y. Shimada, S. Yonemura, H. Ohkura, D. Strutt, and T. Uemura. Polarized transport of Frizzled along the planar microtubule arrays in *Drosophila* wing epithelium. *Dev. Cell.*, 10:209–222, 2006.

[40] M. A. Simon. Planar cell polarity in the *Drosophila* eye is directed by graded Four-Jointed and Dachsous expression. *Development*, 131:6175–6184, 2004.

[41] M. Simons, W. J. Gault, D. Gotthardt, R. Rohatgi, T. J. Klein, Y. Shao, H.-J. Lee, A.-L. Wu, Y. Fang, L. M. Satlin, J. T. Dow, J. Chen, J. Zheng, M. Boutros, and M. Mlodzik. Electrochemical cues regulate assembly of the Frizzled/Dishevelled complex at the plasma membrane during planar epithelial polarization. *Nature Cell Biol.*, 11:286–294, 2009.

[42] M. Simons and M. Mlodzik. Planar cell polarity signaling: From fly development to human disease. *Ann. Rev. Genetics*, 2008.

[43] G. Struhl, D. A. Barbash, and P. A. Lawrence. Hedgehog organises the pattern and polarity of epidermal cells in the *Drosophila* abdomen. *Development*, 124:2143–2154, 1997.

[44] D. Strutt. The asymmetric subcellular localisation of components of the planar polarity pathway. *Sem. Cell Dev. Biol.*, 13:225–231, 2002.

[45] D. Strutt and H. Strutt. Differential activities of the core planar polarity proteins during *Drosophila* wing patterning. *Dev. Biol.*, 302:181–194, 2007.

[46] H. Strutt and D. Strutt. Nonautonomous planar polarity patterning in *Drosophila*: Dishevelled-independent functions of frizzled. *Dev. Cell*, 3:851–863, December 2002.

[47] H. Strutt and D. Strutt. Differential stability of Flamingo protein complexes underlies the establishment of planar polarity. *Curr. Biology*, 18:1–10, 2008.

[48] D. R. Tree, D. Ma, and J. D. Axelrod. A three-tired mechanism for regulation of planar cell polarity. *Sem. Cell Dev. Biol.*, 13:217–224, 2002.

[49] D. R. Tree, J. M. Shulman, R. Rousset, M. P. Scott, D. Gubb, and J. D. Axelrod. Prickle mediates feedback amplification to generate asymmetric planar cell polarity signaling. *Cell*, 109:371–381, 2002.

[50] T. Usui, Y. Shima, Y. Shimada, S. Hirano, R. W. Burgess, T. L. Schwarz, M. Takeichi, and T. Uemura. Flamingo, a seven-pass transmembrane cadherin, regulates planar cell polarity under the control of Frizzled. *Cell*, 98:585–595, 1999.

[51] J. Valdez-Taubas and H. R. B. Pelham. Slow diffusion of proteins in the yeast plasma membrane allows polarity to be maintained by endocytic cycling. *Curr. Biology*, 13:1636–1640, 2003.

[52] G. Von Dassow, E. Meir, E. M. Munro, and G. M. Odell. The segment polarity network is a robust developmental module. *Nature*, 406:188–192, 2000.

[53] S. D. Webb and M. R. Owen. Oscillations and patterns in spatially discrete models for developmental intercellular signalling. *J. Math. Biol.*, 48:444–476, 2003.

[54] S. D. Webb and M. R. Owen. Intra-membrane ligand diffusion and cell shape modulate juxtacrine patterning. *J. Theor. Biol.*, 230:99–117, 2004.

[55] J. Wu and M. Mlodzik. The Frizzled extracellular domain is a ligand for Van Gogh/Stbm during nonautonomous planar cell polarity signaling. *Dev. Cell*, 15:462–469, 2008.

[56] J. Wu and M. Mlodzik. A quest for the mechanism regulating global planar cell polarity of tissues. *Trends in Cell Biol.*, 19:295–305, 2009.

[57] T. Xu and G. M. Rubin. Analysis of genetic mosaics in developing and adult *Drosophila* tissues. *Development*, 117:1223–1237, 1993.

[58] J. A. Zallen. Planar polarity and tissue morphogenesis. *Cell*, 129:1051–1063, 2007.